# Rock Physics Modelling and Seismic Inversion for Reservoir Characterisation

Thesis

*submitted in partial fulfilment of the requirements for the degree of*

**Doctor of Philosophy**

By

**Siddharth Garia**

166104013

Under the supervision of

**Dr. Ravi K and Dr. Archana M Nair**

Department of Civil Engineering

Indian Institute of Technology Guwahati

March 2022

**Dedicated to**
**My Parents**

**For their support, encouragement and love**

# DECLARATION

I, Siddharth Garia, declare that this PhD thesis entitled "Rock Physics Modelling and Seismic Inversion for Reservoir Characterisation" is carried out by me under the guidance of my supervisors.

I certify that:

1. This thesis is a presentation of my own original research work.
2. Any part of this thesis has not been submitted for any degree or diploma or any other qualification either in this institute or in any other university.
3. Whenever I have referred to any published things or quotes from other resources, every effort has been clearly accredited by citing them in the text of the thesis work.
4. Wherever contributions of others are involved, I have acknowledged to indicate this clearly.
5. I confirm that the present thesis is free from plagiarism to the best of my knowledge and I take the whole responsibility if any complaint arises.
6. I also affirm that my supervisors are not in a position to check for any possible instance of plagiarism within this submitted work.

Signature: 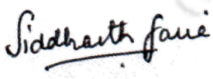

Date: 24/03/2022

भारतीय प्रौद्योगिकी संस्थान गुवाहाटी

# Indian Institute of Technology Guwahati

## CERTIFICATE

This is to certify that the thesis entitled **"Rock Physics Modelling and Seismic Inversion for Reservoir Characterisation"** submitted by **Siddharth Garia,** in partial fulfilment of the requirements for the award of the degree of Doctor of Philosophy, to the Indian Institute of Technology Guwahati, Assam, India, is a record of the original bonafide research work carried out by him under our supervision and guidance at the Department of Civil Engineering, Indian Institute of Technology Guwahati, Assam, India. The thesis work, in our opinion, is worthy of consideration for the award of the degree of Doctor of Philosophy in Civil Engineering of the Institute. The work presented in this thesis has not been submitted in part or full to any other university or institute for the award of any degree/diploma.

Date: 24/03/2022

Place: Guwahati

Dr. Ravi K
Associate Professor, Geotechnical Engineering
Department of Civil Engineering, IIT Guwahati

24/03/2022

Dr. Archana M Nair
Associate Professor, Earth Systems Science and Engineering
Department of Civil Engineering, IIT Guwahati

# Acknowledgements

The journey of my thesis was definitely a unique learning experience and it would not have been possible without the support and contribution of several people.

First and foremost, I am thankful to my supervisors Dr. Ravi K and Dr. Archana M Nair, Associate Professor, Department of Civil Engineering, IIT Guwahati for giving me the opportunity to work with them and for their relentless support and commitment. I particularly thank them for imparting interest towards the field of academic research and training me continuously towards it. Throughout this journey, they gave me all of the necessary guidance, assistance, constructive recommendations, enthusiasm, and patience. Their guidance was invaluable during the research and writing of this thesis. Besides my supervisors, I wholeheartedly thank my doctoral committee panel members, Dr. Arindam Dey, Dr. Rishikesh Bharti and Dr. Pankaj Kalita for their insightful ideas, comments, and recommendations at various phases of this study. I want to convey my sincere appreciation to my former doctoral committee member Dr. A Murali Krishna, Professor, Department of Civil and Environmental Engineering, IIT Tirupati. I also express my sincere thanks to all the faculty members of the Indian Institute of Technology, Guwahati (IITG), for their assistance and help.

I would like to acknowledge Keshava Deva Malaviya Institute of Petroleum Exploration (KDMIPE), Oil and Natural Gas Corporation (ONGC) for the core samples, Oil India Limited (OIL), Duliajan and Department of Geology, Guwahati University for the analytical support. I am also thankful to Mr. B.M. Tripathy, DGM, KDMIPE for the support given for this study. I also acknowledge dGB Earth Sciences, Netherlands for providing academic license for seismic data interpretation software, National Data Repository (NDR), Directorate General of Hydrocarbons (DGH), India for the seismic and well log data. I also acknowledge the support of Central Instruments Facility, IITG for providing facilities for using FESEM (field emission scanning electron microscope) and Mechanical Engineering Workshop, IITG for fabrication related work. I am also thankful to Mr. Upen Gohain, Technical Superintendent, IITG, Mr. Dipak Sarkar and Mr. Himmat Jain for their help related to the setup development. I am also grateful to Dr. Jayanta Laskar, Associate Professor, Department of Geological Sciences, Gauhati University for his valuable suggestions and encouragement.

I owe great thanks to the staff of Department of Civil Engineering, particularly Mr. Nripen Kalita, Mr. Hari Ram Upadhyaya, Ms. Reshima Begum, Mr. Balen Kalita, Mr. Susanta Kumar

Sarma, Mr. Madhab Rajbongshi, Mr. Pranab Hazarika, Mr. Saurabh Mudoi, Mr. Soroj Patowary and technical officers Dr. Arun Borsaikia, Mr. Samarjyoti Kalita for extending their support and cooperation for laboratory related works.

A special thanks to Arnab Kumar Pal, Adnan Ahmad, Ande Bhuvaneswari Devi, Shreya Katre, Dhritilekha Deka, Uma Narayan, Sourav Kumar, Lahit Mushahary, Abhishek Dixit for their consistent assistance, support and help. Completing this work would have been more challenging without the support and friendship provided by my friends, Dr. Rohini Kale, Anant Dubey, Saroj Sahu, Arnab Sinha, Subhra Pal, Argha Guha, Deepak Patwa, Rojimul Hussain, Ankan Hazra, Rituraj Devrani, Abhishek Saha, Sagar Sen, Vistar Gupta, Nitish Mason, Goutom Sarkar, Shailesh Yadav, Nikhilesh Dey, Bismoy Chowdhury, Suman Haldar, Sanjukta Dutta, Aindrila Ghoshal, Dr. Saswati Ray and Dr. Ashutosh Sharma. I express my thanks to them for their unconditional friendship, care, support, and patience throughout this study. I would also like to extend my gratitude to my parents and younger brother Sarthak Garia, for their support, prayers, and sacrifices, without which the work would not have been accomplished.

Finally, I would like to thank Ministry of Education, Government of India for providing the financial assistance and Indian Institute of Technology, Guwahati for all the necessary facilities for successful completion of this work. Beyond all, I owe it all to the Almighty for providing me with the health, wisdom, and strength to carry out this research successfully.

March 2022

## Table of Contents

# Abstract

Rock physics modelling is vital in various stages of exploration and production to comprehend the fluctuations in the seismic response to variations in the physical and fluid properties of rock. Rock physics explores the quantitative relationships of seismic, sonic or ultrasonic velocities to the petrophysical properties so as to predict beyond the existing data range facilitating the initial phase of seismic interpretation. This can be achieved through a forward or an inverse rock physics model, with the primary aim being linking the elastic properties of rocks to porosity, lithology etc. Therefore, rock physics is an integral part of reservoir characterisation, seismic reservoir monitoring and lithology discrimination.

An extensive study based on the data generated in the laboratory under ambient conditions as available in the literature indicates that mineralogy and fluid content are vital factors in altering acoustic velocities of sedimentary rocks like sandstones. However, in rock physics, studies incorporating mineralogical effects on rock behaviour along with petrophysical properties are limited to a few. Accordingly, this study attempts to investigate the effects of petrophysical properties of core plugs along with mineralogical properties on compressional wave velocity ($V_p$) in combination rather than separately with a multivariate statistical approach. The core plugs are from the two most prolific hydrocarbon producing regions of India. All parameters were measured in the laboratory using standard and well-established laboratory methods, i.e., $V_p$ by ultrasonic transducers, porosity by helium gas porosimeter, permeability by nitrogen gas permeameter, grain and pore diameters were calculated from FESEM images, petrographic analysis was carried out using optical microscopy and the mineral content by X-ray diffraction. The multivariate regression analysis has been used in the present study to establish single and multi-parameter correlations highlighting the importance of mineralogy in rock physics by incorporating laboratory-derived $V_p$, petrophysical and mineralogical data. Subsequently, generalised models were developed for carbonates and sandstones.

Generally, well log data are used in the rock physics workflow for quantitative seismic data interpretation. However, it is widely accepted that laboratory-based estimation of different parameters is essential to corroborate data obtained from the well logs. Therefore, to validate the efficacy of the laboratory-based rock physics model, seismic inversion was performed on the seismic section belonging to the Upper Assam basin on which the laboratory-based model was developed. Integrating the laboratory-derived rock physics model with the conventional seismic inversion workflow, the density varied between 2.23 to 2.73 g/cc, while porosity varied

between 7 to 27%. These generated models were compared with well log data, and there was a reasonable agreement between them. The results indicated that prospective exploration potential exists in the northwestern region of the study area due to the increasing thickness as well as reservoir quality of the hydrocarbon-bearing zone. Hence, the present research provides a framework for reservoir characterisation using integrated seismic, well and laboratory-based approaches. Such a workflow may facilitate an improvement in the assessment and prediction of productive reservoir zones during the exploration stage.

**Keywords**: rock physics; density; porosity; acoustic; laboratory; sandstones; carbonates; seismic inversion

## List of Figures

## List of Tables

## List of Abbreviations

| Abbreviation | Description |
|---|---|
| FESEM | Field Emission Scanning Electron Microscope |
| XRD | X Ray Diffraction |
| PUNDIT | Portable Ultrasonic Non-destructive Digital Indicating Tester |
| ASTM | American Society for Testing and Materials |
| ISRM | International Society for Rock Mechanics |
| IS | Indian Standard |
| CR | Carbonates |
| BO | Bombay Offshore basin |
| GD | Grain density |
| SD | Standard deviation |
| Max. | Maximum |
| Min. | Minimum |
| Avg. | Average |
| DIA | Digital Image Analysis |
| ONGC | Oil and Natural Gas Corporation |
| UA | Upper Assam |
| SS | Sandstone |
| UPV | Ultrasonic Pulse Velocity |
| AR | Aspect Ratio |
| IUPAC | International Union of Pure and Applied Chemistry |
| BET | Brunauer–Emmett–Teller |
| LOM | Light Optical Microscope |
| SEM | Scanning Electron Microscope |
| MICP | Mercury Injection Capillary Pressure |
| HGP | Helium Gas Porosimeter |
| NN | Neural Network |
| MLFN | Multi-layer Feed-forward Neural Network |
| PNN | Probabilistic Neural Network |
| 2D | Two Dimensional |
| 3D | Three Dimensional |

| | |
|---|---|
| TWT | Two-way Travel Time |
| AI | Acoustic Impedance |
| O | Operator |
| S | Seismic Traces |
| Z | Impedance |
| RMSE | Root Mean Square Error |
| $V_{shale}$ | Volume of Shale |
| GR | Gamma Ray |
| $GR_{log}$ | Gamma Ray Log |
| $GR_{min}$ | Minimum of Gamma Ray Log |
| $GR_{max}$ | Maximum of Gamma Ray Log |
| NPHI | Neutron Log |
| RHOB | Density Log |
| DT | Sonic Log |
| HDRS | Deep Resistivity Log |
| PHID | Density Porosity Log |
| API | American Petroleum Institute |

## List of Symbols

| Symbols | Description |
|---|---|
| $V_p$ | P-wave velocity |
| $V_s$ | S-wave velocity |
| $\rho$ | Bulk density |
| $\phi$ | Porosity |
| $\phi'$ | Effective porosity |
| $\rho_{dry}$ | Dry density |
| $\rho_{sat}$ | Saturated density |
| $\rho_{bulk}$ | Bulk density |
| $W_a$ | Water absorption |
| C | Clay content |
| L | Length of Specimen |
| k | Permeability |
| $w_{sat}$ | Saturated weight |
| $w_{dry}$ | Dry weight |
| $w_{sub}$ | Submerged weight |
| A | Area of specimen |
| $D_e$ | Effective diameter |
| E | Elastic modulus (GPa) |
| G | Shear modulus (GPa) |
| $I_s$ | Point load strength (MPa) |
| K | Bulk modulus (GPa) |
| P | Breaking load |
| $S_r$ | Degree of saturation (%) |
| t | Transit time |
| V | Loss of volume on wear ($cm^3$ /50 $cm^2$) |
| $\tau$ | Shear strength (MPa) |
| $\upsilon$ | Poisson's ratio |
| $\lambda$ | Lame's parameter |
| $\sigma_t$ | Indirect tensile strength (MPa) |
| mD | Millidarcy |
| km/s | Kilometre per second |

| | |
|---|---|
| $R^2$ | Coefficient of determination |
| MPa | Megapascal |
| GPa | Gigapascal |
| kHz | Kilohertz |
| m | Metre |
| mm | Milimetre |
| % | Percentage |
| K | Mode pore size |
| m/s | Metre per second |
| g/cc | Gram per cubic centimetre |
| r | Correlation coefficient |
| µm | Micrometre |
| $UPV_{54\ kHz}$ | Ultrasonic Pulse Velocity using 54 kHz |
| $UPV_{500\ kHz}$ | Ultrasonic Pulse Velocity using 500 kHz |
| $V_b$ | Bulk Volume |
| nm | Nanometre |
| psi | Pound per square inch |
| $V_{ref}$ | Volume of the Reference Chamber |
| $V_{sam}$ | Volume of the Sample Chamber |
| $P_{calculated}$ | Calculated Pressure |
| $P_{observed}$ | Observed Pressure |
| cm | Centimetre |
| cc | Cubic Centimetre |
| Q | Volumetric Flow Rate |
| dp/dx | Pore Pressure Gradient |
| µ | Viscosity |
| A | Cross-Sectional Area |
| kV | Kilo Volt |
| $V_{pquartz}$ | Compressional Wave Velocity of Quartz |
| $V_{pfeldspar}$ | Compressional Wave Velocity of Feldspar |
| $V_{pcalcite}$ | Compressional Wave Velocity of Calcite |
| $V_{pdolomite}$ | Compressional Wave Velocity of Dolomite |
| $K^{HS+}$ | Hashin-Shtrikman-Walpole Upper bound Bulk Moduli |

| | |
|---|---|
| $K^{HS-}$ | Hashin-Shtrikman-Walpole Lower bound Bulk Moduli |
| $G^{HS+}$ | Hashin-Shtrikman-Walpole Upper bound Shear Moduli |
| $G^{HS-}$ | Hashin-Shtrikman-Walpole Lower bound Shear Moduli |
| $V_{pmatrix}$ | Compressional Wave Velocity of Matrix |
| $\upsilon_{calcite}$ | Poisson's Ratio of calcite |
| $\upsilon_{dolomite}$ | Poisson's Ratio of dolomite |
| $S_w$ | Water Saturation |
| $R_w$ | Resistivity of Formation Water |
| $R_t$ | True Resistivity of Formation |
| a | Tortuosity Factor |

# Chapter 1
# Introduction

## 1.1 Overview

Subsurface modelling and characterisation is critical in assessing productive reservoir zones during the exploration and production of a hydrocarbon field (Avseth et al., 2010). The natural heterogeneities of the subsurface geology have a significant impact on the performance of a reservoir. Heterogeneities can occur at various scales due to the variations in porosity, clay content, lithology, pore fluids, temperature and pressure (Mukerji et al., 2001). Seismic data, ultrasonic and petrophysical measurements of core plugs, and usage of different types of well log data are the methods of subsurface modelling and characterisation. Seismic data provide a structural image of the reservoir zone that depends on lithology, porosity, type of fluid, temperature and pressure (Mavko et al., 2009). Therefore, seismic data is considered the most significant source of information for hydrocarbon reservoirs and sedimentary basin studies (Seyyedattar et al., 2020). It is used to extract information about the subsurface rock and fluid information, which would help identify potential prospective hydrocarbon reservoirs (Yu et al., 2016).

An extensive understanding about the close association among key reservoir properties such as porosity, permeability and seismic wave velocities is suitable for applications related to seismic modelling, fluid substitution and rock physics diagnostics (Sang and Sun, 2014; Panizza and Ravazzoli, 2019; Jiang et al., 2020). Investigations on the propagation of seismic waves ($V_p$, Vs) through rocks provide valuable information regarding the estimation of petrophysical properties (Vilhelm et al., 2016). To predict the physical properties, it is necessary to establish relations between wave propagation attributes and petrophysical and lithological properties. This can be achieved by transforming seismic data into elastic attributes and subsequently into the different petrophysical properties through statistically derived relationships or a rock physics model (Aleardi, 2018).

Rock physics addresses the relationships between rock properties, such as porosity, lithology, fluid saturations and elastic properties such as velocities or impedances (Grana, 2014). These models can be used in quantitative seismic interpretation and reservoir characterisation. The model can be a set of simple empirical equations or sophisticated theoretical models (Mavko et al., 2009). Rock physics deals with the interpretation of seismic, sonic and ultrasonic velocities with respect to the petrophysical properties to predict beyond the existing data range facilitating the initial phase of seismic interpretation (Avseth et al., 2010). Rock physics based

quantitative interpretation has been instrumental in seismic reservoir monitoring and seismic lithology discrimination because it links seismic data and reservoir properties (Bachrach, 2006). Therefore, rock physics modelling is vital to comprehend the variations in physical and fluid properties due to the fluctuations in the seismic response during various stages of exploration and production (Makarynska et al., 2010; Mirkamali et al., 2020).

The different rock physics models can be categorised into different sub-classes such as theoretical, empirical and heuristic (Avseth et al., 2010). The theoretical models are mainly mechanics based estimates of the rock's elastic properties. These elastic models may be inclusion models, contact models, computational models, bounds and transformations. An efficient rock physics model must consider the different geological factors or environments that may affect the acoustic properties (Xu and Payne, 2009; Avseth et al., 2010). There exists a wide variety of velocity-porosity relations and rock physics models in the reference literature. Also, statistical rock physics is widely used in hydrocarbon reservoir studies for modelling the acoustic, petrophysical and geomechanical properties of rocks (Grana and Rossa, 2010; Rafik and Kamel, 2017). Statistical rock physics integrates physical models with statistics to account for and predict scenarios beyond the available data range (Grana and Rossa, 2010). These techniques facilitate the prediction and estimation of hydrocarbon resources beyond the well data.

The amalgamation of mineralogical and petrographical knowledge is essential for better approximation and analysis of rock behaviour (Ündül, 2016). Researchers have observed the mineralogy and fluid content are vital factors in altering acoustic velocities in the case of sedimentary rocks like sandstones (Li and Gu, 2015; Dentith et al., 2020). However, in rock physics modelling, such studies incorporating mineralogical and petrographical effects on rock behaviour along with petrophysical properties are limited to a few. Therefore, this study is intended to understand the effects of petrophysical properties along with mineralogical and petrographical properties on $V_p$ in combination rather than separately with a multivariate statistical approach.

Several studies in the literature suggest correlations between the seismic velocities ($V_p$, $V_s$) and the important rock petrophysical and geomechanical properties (Vernik, 1994). Correlating bulk mineralogy of rock may not be a standalone factor; however, it has an effect on compressional wave velocity ($V_p$) along with density and porosity. The characteristics of the reservoir are used as input to make predictions of the effective elastic properties. Several factors have an interdependency and an integrated analysis is required to understand the undercovered trend. A forward rock physics model attempts to predict the elastic behaviour (e.g., elastic

moduli, seismic velocities) of rocks from reservoir properties (e.g., porosity, constituent properties, saturation) (Bredesen, 2012). Figure 1 depicts the conceptual framework on how the different parameters are linked together by rock physics and seismic modelling. Therefore, this study used a workflow that applied geological principles coupled with analytical and digital image analysis techniques. Such a generalised predictive model will behave more realistic since it contains all the components that capture $V_p$ variations.

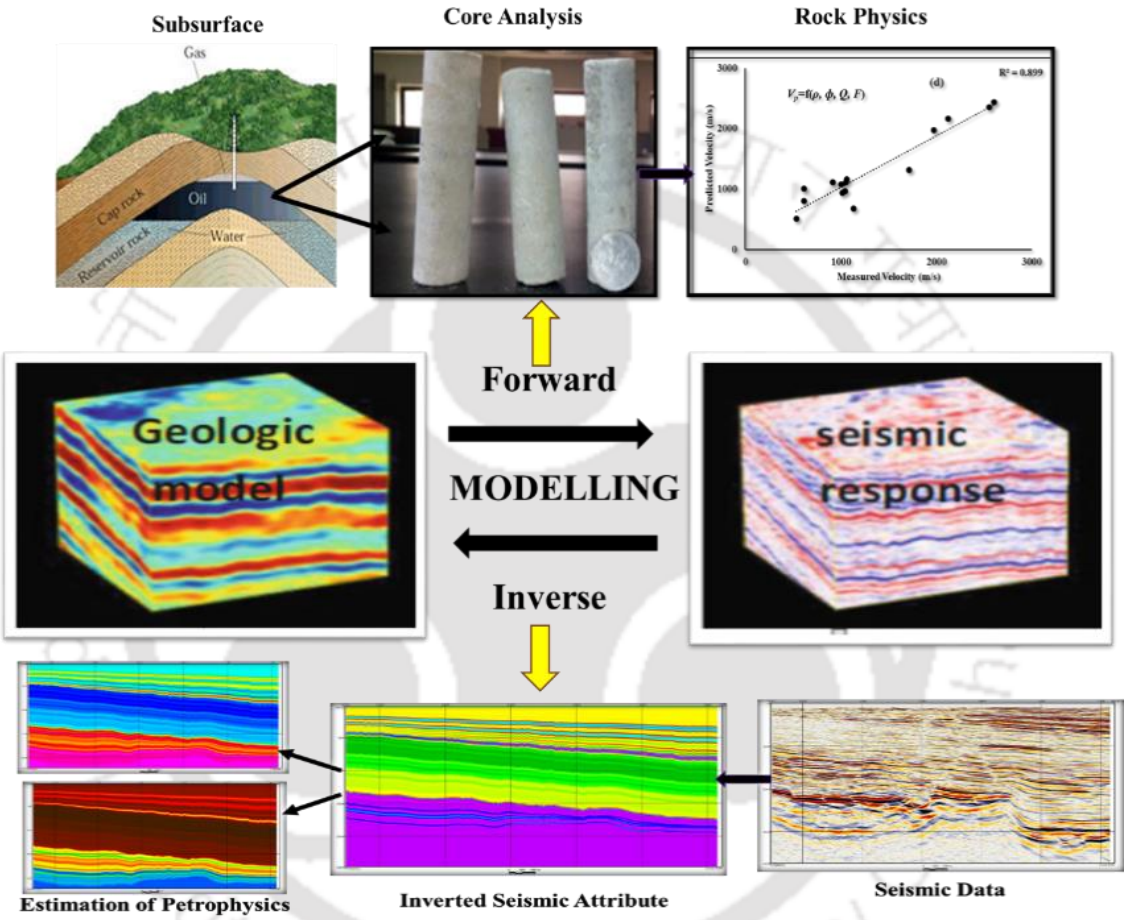


Figure 1.1 Interrelationships among different parameter domains linked together by rock physics and seismic modelling

## 1.2 Motivation

In the context of reservoir characterisation, reservoir properties are predicted and modelled from seismic data by the inversion process. The inversion process transforms the seismically derived parameters (such as $V_p$, $V_s$, acoustic impedance, elastic impedance, seismic attributes) into rock properties that describe the lithology and petrophysical properties such as porosity, permeability and saturation. However, the estimation of reservoir properties from seismic data suffers from a highly underdetermined problem with non-unique solutions (Oliver et al., 2008).

A workflow based on the numerical reformulation of a laboratory-based rock physics model may reduce the non-uniqueness. It is essential to understand the geological trend and reservoir distribution to build a suitable rock physics workflow (Ali et al., 2020). Generally, well log data are used in the rock physics workflow for quantitative interpretation. However, it is widely accepted that laboratory-based estimation of petrophysical, geomechanical and mineralogical parameters is essential to corroborate data obtained from the well logs (Ambati et al., 2021). For laboratory studies, core plugs collected from multiple wells of the same basin is essential. Analysis of the core plugs, collected from multiple wells of the same basin, tend to be more representative of a broader lithologic unit (Zhang et al., 2020a). Therefore, the key process in the inversion workflow is the integration of well logs and laboratory-based models for the transformation of seismic-to-reservoir properties.

India has a vast stretch of sedimentary cover, offshore and onshore, and 26 basins have been recognized (Bastia, 2006). These basins are divided into 5 different categories (category I to V), based on hydrocarbon prospectivity. In the present study, an integrated analysis is carried out considering the petrophysical and mineralogical properties with the ultrasonic measurements for the Bombay offshore and Upper Assam basin. These basins are known to be prolific hydrocarbon producing regions in India. Bombay offshore basin is a category I sedimentary basin in India, that is known for commercial hydrocarbon production (Bastia, 2006). The Bombay offshore basin is considered to have around 50% of India's total oil reserves (Mohan, 1985). This formation belongs to the early Miocene age (Guha and Pandey, 1974; Mohan, 1978; Basu et al., 1980). This basin consists of approximately 70% carbonates (Wandrey, 2004a). Several researchers reported values of petrophysical and acoustic properties for studies pertaining to this basin in the literature. Sharma et al., (2020) reported an average porosity range of 14.1% to 16.9% and permeability less than 5mD. As per Wandrey (2004a) and Schön (2015), average porosity and permeability ranges from 15-20% and 100-250 mD, respectively. The log values reported by Roy and Chatterjee (2020) varies from: Vp=3811 to 4193 m/s, bulk density = 2.51 to 2.66 g/cc and porosity = 14 to 22%. Similarly, Chandrasekhar and Rao (2012) reported velocity log data in the range of 983 to 1352 m/s. The other basin, of which datasets are considered in the present study, is the Upper Assam basin in India. The Upper Assam basin is a tertiary sub-basin (Mathur, 2014), and it is surrounded by the Himalayan orogenic belt in the north, Mishmi Thrust in the east, Schuppen Belt in the south (Mandal and Dasgupta, 2013). As per Bastia (2006), this basin is also classified as a category I sedimentary basin, and it is the first known hydrocarbon province (Pahari et al., 2008) in India. Hydrocarbons are being produced for more than a century from the Upper Assam basin

(Pahari et al., 2008; Mandal et al., 2011). As per Wandrey (2004b), the reservoir rocks are interbedded sandstones of the Kopili formation, sandstones of Barail, Surma and Tipam groups. Several researchers investigated the petrophysical and acoustic properties of this basin in the literature. Wandrey (2004b) reported a porosity range of 7-30% and a permeability range of 8-800 mD. Zaei and Rao (2019) reported average density as 2.40 g/cc and porosity as 13% for Tipam sandstones. The log derived porosity ranges from 27-30% (Ishwar and Bharadwaj, 2013) and 15-30% (Bharali and Borgohain, 2013). Similarly, Gogoi and Chatterjee (2019) reported log derived porosity for Tipam sandstones as 30-36% and for Barail sandstones as 18-30%. Mandal et al. (2011) reported a regional velocity trend in the range of 1600- 2900 m/s. Similarly, Gogoi and Chatterjee (2018), reported seismic velocity in the range of 2500-4000 m/s. With reference to the Indian context, Upper Assam basin has been identified as one of the 76 priority provinces by USGS (Wandrey, 2004b) and hydrocarbon exploration opportunity still exists in this basin (Mandal and Dasgupta, 2013) parallel to Naga thrust fault and north of Brahmaputra river (Wandrey, 2004b; Pahari et al., 2008).

Hence, the aim of this study is the incorporation of laboratory-derived petrophysical and mineralogical data in the quantitative interpretation of compressional wave velocity (Vp) to enhance the capability of rock physics models in reservoir characterization. The present research deals with the laboratory based assessment on factors controlling the acoustic properties of carbonates from Bombay offshore and sandstones from the Upper Assam basin. Subsequently, seismic data and well logs from the Upper Assam basin were used to first invert the seismic data to obtain acoustic impedance, from which the interpretations were made for the spatial distributions of different parameters such as porosity, density, shale volume and water saturation. In totality, this work deals with rock physics laboratory measurements, statistical correlations between various petrophysical properties and applications of laboratory and well log data to interpret seismic inversion in terms of petrophysical properties.

## 1.3 Objectives of the Study

Based on the above discussion, the following objectives are outlined for the present research study.

I. To measure the compressional wave velocity of different types of sedimentary rocks using laboratory-based measurements and study its association with-

   (a) the petrophysical properties

   (b) the mechanical properties

II. To study the effect of mineralogy on the compressional wave velocity of different types of sedimentary rocks.

III. To develop a rock physics model integrating petrophysical variables and mineralogical variables with the velocity model.

IV. To validate the efficacy of the rock physics model in the quantitative interpretation of geophysical data for the exploration of conventional energy sources.

## 1.4 Organisation of the Thesis

Having identified the objectives, the thesis is organised chapter-wise as follows:

- **Chapter 1** gives a general overview of the thesis, motivation behind this research work and its importance. The objectives of the study are also listed in this chapter.
- **Chapter 2** reviews the literature comprehensively on the background research and identifies the gap areas.
- **Chapter 3** describes the laboratory methods and techniques for the estimation of acoustic and petrophysical properties.
- **Chapter 4** deals with the assessment of factors controlling the acoustic properties of carbonates.
- **Chapter 5** presents a multivariate statistical approach in correlating the acoustic properties with petrophysics and mineralogy on sandstones.
- **Chapter 6** presents the mapping of petrophysical properties by integrating well log data and laboratory-based rock physics model through seismic inversion.
- **Chapter 7** summarises the major findings and conclusions of the study. The limitations of the study and recommendations for future work are also presented in this chapter.

# Chapter 2
# Literature Review

## 2.1 Introduction

This chapter presents the literature background leading to motivation for the objectives of the thesis. Along with the literature background, limitations in the current state of the art are identified. Section 2.2 covers a comprehensive analysis of the relationships between elastic wave velocities and petrophysical properties of sedimentary rocks based on laboratory measurements. Section 2.4 presents an overview of elastic wave velocities as indicators of lithology-based geomechanical behaviour of sedimentary rocks.

## 2.2 Variation of $V_p$ with the Petrophysical Properties of Sedimentary Rocks

An attempt is made to correlate the variation in compressional and shear wave velocities ($V_p$ and $V_s$) of different sedimentary rocks with respect to different petrophysical parameters such as porosity, density, water absorption, clay content and permeability. In order to include a wide range of datasets for a comprehensive analysis, datasets used in this study are generated by various researchers from laboratory experiments conducted on sandstones, carbonates and other sedimentary rocks such as mudstone and shale under ambient conditions. The present study used only reported datasets generated from experimental measurements under ambient conditions so as to have a common reference condition. Literature reported datasets generated from experimental measurements under stressed conditions were found to be derived under a range of stress values rather than a common standard value. As a result, it will be challenging to establish a common reference condition to correlate velocity values with petrophysical parameters. Moreover, samples might undergo mechanical alteration during pressurisation under stressed conditions (alter sample microstructure) (Baechle et al., 2005). Therefore, the datasets developed under stressed conditions in the laboratory have been excluded from this literature review study.

The dataset comprises ultrasonic velocity measurements conducted on different types of sandstone, mudstone, wackestone, limestone, marlstone, siltstone, conglomerate, claystone, marl, dolomite, shale, shaly sands and dolomitic limestone. Table 2.1 summarises the details about the ultrasonic technique used for measuring $V_p$ and $V_s$ on different rock types by different researchers in their respective studies. During the data generation process, it was found that high-quality data are scarce, and hence we have adopted a much-generalised approach in consideration of geographic location, stratigraphy or geochronology of the rocks. The location

of rocks from which the datasets have been generated for this particular study has been plotted in global map as shown in Figure 2.1 and it indicates that datasets from all across the world have been taken for this study. The datasets used for the present study comprises $V_p$ and $V_s$ measured for various sedimentary rock samples in the laboratory using different ultrasonic techniques, as discussed in the subsequent paragraphs. However, it was found that experimental datasets available for measured values of shear wave velocity ($V_s$) are very rare. The reason for fewer datasets available for the relationship between $V_s$ and petrophysical properties in the literature may be due to several reasons, including the fact that $V_s$ is commonly calculated from $V_p$ values that are already established method followed by researchers. Many empirical relations are suggested in the literature, such as $V_p/V_s$ = 1.65 to 2 (Johnston and Christensen, 1993), $V_p/V_s$ = 1.5 to 1.7 for quartzose sandstones, $V_p/V_s$ = 1.9 for pure limestones (Assefa et al., 2003). Hence, more studies were focused on relating $V_p$ with the petrophysical properties such as porosity, permeability, density, clay content etc. Using the correlation between $V_p$ and $V_s$ ($V_p$, $V_s$ ratio), the relationship between $V_s$ and other petrophysical properties can be evaluated.

The different ultrasonic techniques, namely pulse-echo (Gaviglio, 1989; Klimentos, 1991; Assefa et al., 2003) and through transmission (Han et al., 1986; Yasar and Erdogen, 2004; Kahraman and Yeken, 2008; Kilic and Teymen, 2008; Moradian and Behnia, 2009; Sarkar et al., 2012; Madhubabu et al., 2016) were used by various researchers to measure the compressional (longitudinal) and shear (transverse) wave velocities in different rock samples. In the pulse-echo technique, only one transducer (acting as both transmitter and receiver) is used to measure velocity. For through transmission technique, a pair of transducers (one transmitter and one receiver) are used for measuring the velocity and hence the measured velocity ($V_p$ or $V_s$) may not be affected by the type of measurement. The velocity of the rock samples has been determined either by using PUNDIT- Portable Ultrasonic Non-destructive Digital Indicating Tester (Kilic and Teymen, 2008; Karakul and Ulusay, 2013; Yasar and Erdogen, 2004; Moradian et al., 2009; Brotons et al., 2016), or by using a combination of the pulse generator, transducers (transmitter and receiver) of varying frequencies (54 kHz to 1 MHz) and oscilloscope (Kahraman and Yeken, 2008; Mueller, 2013; Vilhelm et al., 2016). The PUNDIT consists of a pulse generator, transducers and an electronic counter for time interval measurements. Two different kinds of transducers have been used: a longitudinal transducer for measuring the P-wave velocity and a shear transducer for measuring the S-wave velocity. The velocity values determined do not appear to be frequency-dependent as long as the wavelength is significantly greater than the grain size (ISRM, 1978, ASTM, D2845). ISRM

(1978) recommends the minimum lateral dimension should not be less than ten times the wavelength while ASTM stipulates five times the wavelength.

Several test techniques and procedures have been employed in the literature for determining the different petrophysical properties. Table 2.2 tabulates the different standards/codes that have been used for the determination of different physical parameters, while Table 2.3 tabulates the instruments/tests used/conducted to derive datasets that are used for this study. We have not carried out any standardisation or normalisation on the datasets though it may be important to have one such as we are using datasets generated from different methods or process. However, such an approach can propagate some bias in the analysis and hence we used original data as such.

To understand the relationship between compressional wave velocity ($V_p$) and porosity, a combined graphical representation was generated from the given datasets of Kahraman et al. (2008), Kilic and Teymen (2008), Kurtulus et al. (2016), Kassab and Weller, (2015), Madhubabu et al. (2016). For datasets that are not in a table format, graphical values were taken and plotted along with other datasets (Soroush et al., 2011; Pappalardo, 2015; Parent et al., 2015 and Sayed et al., 2015). Similarly, the bulk density-$V_p$ graph was plotted from values obtained by Kahraman et al. (2008), Moradian and Behnia (2009) and Kurtulus et al. (2016) and from graphical values given by Soroush et al. (2011); Parent et al. (2015) and Sayed et al. (2016). Water absorption- $V_p$ relationship was obtained from the dataset of Kahraman et al. (2008) and Kurtulus et al. (2015) and graphical values from Soroush et al. (2011). Permeability-$V_p$ relationship was derived from studies conducted by Kassab et al. (2015), Al-Dousari et al. (2016), Sayed et al. (2016).

From the available data, a linear plot is considered to illustrate the relationship between the compressional velocities (km/s) with porosity (%), bulk density (g/cc) and water absorption (%). A semi-log plot is used between compressional wave velocities and permeability (mD). It is important to understand the fact that a combined graphical representation of two parameters taken from studies conducted by various researchers across the world could lead to a general or universal trend that could nullify the effect of many other less important factors underlying in it. For this purpose, we first analysed existing trends or relationships in the form of equations (empirical relations) established by various researchers. From such an analysis, it was found that empirical relationships derived by various researchers are applicable only to the datasets on which it was derived and is not useful as a general trend for extrapolation or interpolation. In another way, it means the correlation between the two parameters is poor. Although a general

positive or negative trend is shown between the plotted parameters, it cannot be generalised in the form of a mathematical equation.

An effort is made to exclusively understand the relationship between $V_p$ and porosity and the underlying effect of density on it. This is achieved by plotting velocity ratio (ratio of actual $V_p$ and $V_p$ obtained through proposed general trend for density) and porosity for those particular datasets for which density, porosity and compressional velocity were measured in the laboratory and available. These datasets include the studies of Kahraman et al. (2008), Soroush et al. (2011), Kurtulus et al. (2015), Kassab et al. (2015). This attempt is made to nullify the density effect by removing the effect of density from the porosity-velocity relationship.

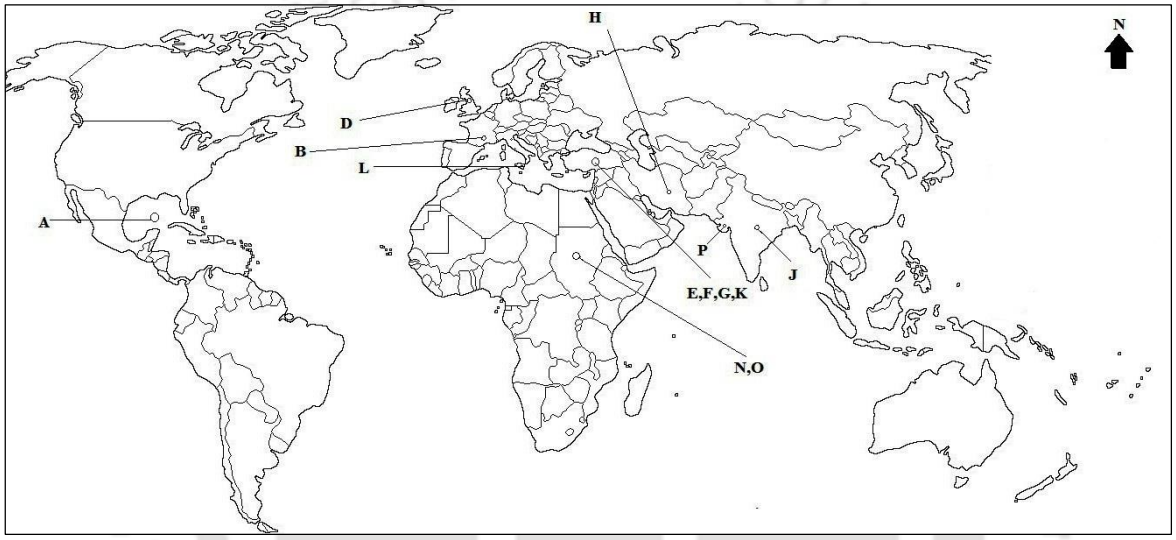


**LEGENDS**

**A**- Gulf of Mexico, **B**-Western Provence, France, **D**- Southern England, **E**- Adana, Turkey, **F**- Nigde, Kayseri, Konya & Antalya, Turkey, **G**- Southern Anatolia, **H**- Iran, **J**- Jutogh, Lower Shiwalik & Lower Gondwana, India, **K**- Cebecikoy, Hereke, Akveren, Soguck & Bakirkoy, Turkey, **L**- Peloritani Mounts, NE Sicily, **N**- Tushka, Egypt, **O**- North Sinai, Egypt, **P**- Kutch, Gujrat, India

Figure 2.1 Locations of study area appropriate to the sedimentary rock samples relevant to this literature review study

Table 2.1 Compilation of different studies generated by various researchers relevant to this literature review study

| **Label Number** | **Rock Type** | **Lab Technique Used** | **Reference** |
|---|---|---|---|
| A | Sandstone | Through transmission, | Han et al. (1986) |

| | | | | |
|---|---|---|---|---|
| | | | P wave frequency 1 MHz and S wave 0.6 MHz, $V_p$ measured on water-saturated rocks under varying confining pressures (upto 40 MPa) | |
| B | B1 | Mudstone | Pulse echo method, transducer frequency 2.25 MHz | Gaviglio (1989) |
| | B2 | Wackestone | | |
| C | | Sandstone | Pulse echo method, ultrasonic frequency (0.5-1.5 MHz), $V_p$ measured on water-saturated rocks under varying confining pressures (upto 40 MPa) | Klimentos (1991) |
| D | | Limestone | Pulse echo method, $V_p$ frequency 0.85 MHz and $V_s$ frequency 0.7 MHz measured under 50 MPa hydrostatic pressure | Assefa et al. (2002) |
| E | | Carbonate rocks | Through transmission method | Yasar and Erdogan (2004) |
| F | | Carbonate rocks | Through transmission, transducer frequency 54 kHz | Kahraman and Yeken (2008) |
| G | G1 | Limestone | Through transmission | Kilic et al. (2008) |
| | G2 | Sandstone | | |

| | | | | |
|---|---|---|---|---|
| H | H1 | Limestone | Through transmission, transducer frequency 1 MHz | Moradian et al. (2009) |
| | H2 | Sandstone | | |
| | H3 | Marlstone | | |
| I | I1 | Sandstone | Ultrasonic pulse technique | Soroush et al. (2011) |
| | I2 | Siltstone | | |
| | I3 | Conglomerate | | |
| | I4 | Claystone | | |
| | I5 | Limestone | | |
| | I6 | Marl | | |
| | I7 | Micro-conglomerate | | |
| J | J1 | Limestone | Through transmission | Sarkar et al. (2012) |
| | J2 | Sandstone | | |
| | J3 | Dolomitic limestone | | |
| | J4 | Dolomite | | |
| | J5 | Shale | | |
| K | | Limestone | Ultrasonic pulse generator operating at 54 kHz | Kurtulus et al. (2015) |
| L | | Dolostone | High Emission MAE device with probes of frequency 53 kHz | Pappalardo (2015) |
| M | | Limestone | Not mentioned | Parent et al. (2015) |
| N | | Sandstone | USLT 2000 device with 500kHz frequency | Kassab et al. (2015) |
| O | | Carbonate rocks | Through transmission, $V_p$ measured at 63 kHz and $V_s$ at 33 kHz frequency | Sayed et al. (2015) |
| P | | Carbonate rocks | Through transmission | Madhubabu et al. (2016) |

| | | | | |
|---|---|---|---|---|
| Q | Q1 | Sandstone | Obtained at 1 MHz frequency, $V_p$, $V_s$ measured under effective stress of 4000psig | Al-Dousari et al. (2016) |
| | Q2 | Shaly sands | | |
| | Q3 | Carbonate rocks | | |

Table 2.2 Standards for determination of different physical parameters of rock samples

| **Parameter** | **Standard** | **Formula** |
|---|---|---|
| Density | ISRM 1977, IS 13030 - 1991 | $\rho_{dry} = \frac{w_{sat} * \rho_{fluid}}{w_{sat} - w_{sub}}$ |
| Porosity | ISRM 1977, IS 13030-1991 | $\phi = \frac{w_{sat} - w_{dry}}{w_{sat} - w_{sub}}$ |
| P wave velocity | ASTM D2845, IS 13311, Part 1: 1992 | $v = \frac{L}{t}$ |

Table 2.3 Instruments/Tests used/conducted related to petrophysical properties to derive datasets relevant to this study

| **S No** | **Parameters analysed** | **Instruments used** | **Reference** |
|---|---|---|---|
| 1 | Porosity | Helium Gas Porosimeter | Klimentos (1991)<br>Assefa et al. (2003) |
| | | Water Saturation Technique | Kahraman et al. (2008)<br>Kurtulus et al. (2015)<br>Madhubabu et al. (2016) |
| 2 | Permeability | Nitrogen Gas Permeameter | Klimentos (1991)<br>Assefa et al. (2003)<br>Kassab et al. (2015)<br>Sayed et al. (2015) |
| 3 | Grain density | Helium pycnometer | Gegenhuber (2016) |

| | | | |
|---|---|---|---|
| 4 | Mineralogy | XRD | Klimentos (1991) |
| | | Thin section studies | Klimentos (1991)<br>Karakul et al. (2013)<br>Pappalardo et al. (2015)<br>Madhubabu et al. (2016) |

## 2.3 Results and Discussion

In the present study, we tried to analyse the change in the compressional and shear wave velocities of various sedimentary rock samples with respect to a number of petrophysical parameters such as porosity, bulk density, water saturation, permeability etc. in ambient conditions. Among the datasets analysed, datasets labelled as D, E, F, K, L, M, O, P represent carbonate rocks while A, C, N represent sandstones, as referred to in Table 2.1. Datasets labelled as B, G, H, I, J, Q represents a combination of different rock types as summarised in Table 2.1. The relations between petrophysical properties and compressional and shear wave velocities for reservoir rocks have been analysed and plotted, and all the empirical relations existing between them have been tabulated.

### 2.3.1 Density and Porosity

One of the important petrophysical properties analysed in this study is bulk density. The bulk density takes into account the total volume (solid and pore space) of the rock specimen, including the natural voids. Several researchers, in their studies, have related $V_p$, $V_s$ with the bulk density since these values are relatively easy to measure in the field as well as in the laboratory. A combined graphical representation of all the datasets (Figure 2.2(a)) were generated to analyse the existing relationships and derive a general trend. The range of bulk density found from the graph is between 1.85g/cc to 2.75g/cc, and $V_p$ ranges from 2 km/s to 7.1 km/s. In general, it can be said that there is a linear relationship between $V_p$ and bulk density for all rock types. Figure 2.2(b) is an alternative representation of Figure 2.2 (a) along with empirical equations derived by various researchers relating bulk density and P-wave velocity (Label No. F, I, K, H, M, O, N are plotted as datasets, empirical equations are plotted as lines, Label M is logarithmic variation, Label I is polynomial variation while the rest labels are linearly varying as reported in their respective studies). It is obvious from Figure 2.2(b) that all the empirical relationships given are valid to only the datasets from which it was derived, and none of the existing empirical equations can be used as a general trend. Table 2.4 enlists all the empirical relations existing between density (bulk, saturated and dry density) and $V_p$. We tried

to fit a general trend for the entire dataset plotted, and Figure 2.2(c) shows the general (proposed) linear trend bounding the maximum and minimum range of bulk density and compression wave velocity. General trends or global trends should be independent of the type of rock under study, which is not applicable in this case.

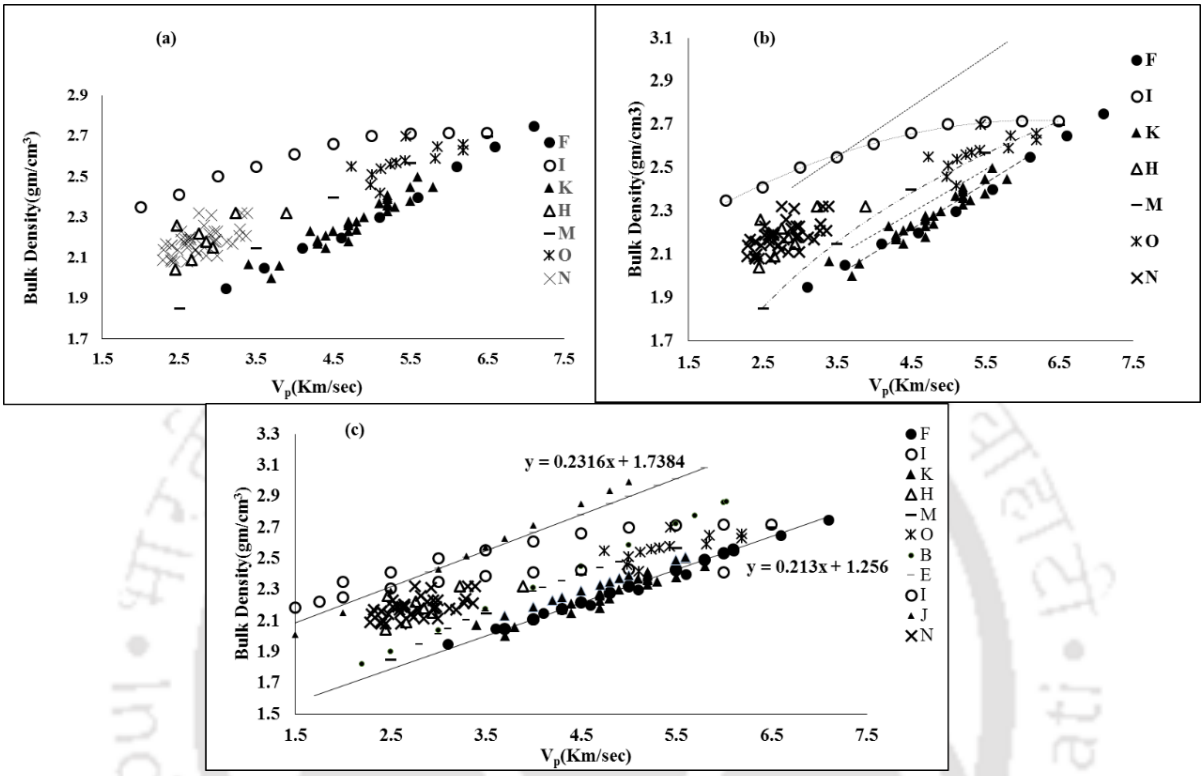


Figure 2.2 Graphical representation of bulk density versus $V_p$, (a) as reported by different researchers, (b) including empirical equations generated by different researchers and, (c) including general trend derived from this study (where Y is Bulk density (g/cc), and X is $V_p$ (km/s))

Table 2.4 Compilation of empirical equations derived for velocity ($V_p$, $V_s$) and density as reported by various researchers

| S. No. | Parameters | Empirical relation | Coefficient of determination ($R^2$) | Reference |
|---|---|---|---|---|
| 1 | $\rho_{dry}$ (g/cc) - $V_p$ (km/s) | $V_P = 3.661\rho_{dry} - 4.461$ | 0.78 | B (Gaviglio, 1989) |
| 2 | $\rho_{bulk}$ (g/cc) - $V_p$ (km/s) | $V_P = 4.3183\rho_{bulk} - 7.5071$ | 0.81 | E (Yasar and Erdogan, 2004) |

| | | | | |
|---|---|---|---|---|
| 3 | **ρbulk** (g/cc) - **Vp** (km/s) | $\rho_{bulk} = 0.213V_P + 1.256$ | 0.821 | F (Kahraman and Yeken, 2008) |
| 4 | **ρbulk** (g/cc) - **Vp** (m/s) | $\rho_{bulk} = -2X10^{-8}V_P^2 + 0.0002V_P + 1.93$ | 0.71 | I (Soroush et al., 2011) |
| 5 | **ρbulk** (g/cc) – **Vs** (m/s) | $\rho_{bulk} = -6X10^{-8}V_S^2 + 0.0004V_S + 1.94$ | 0.73 | I (Soroush et al., 2011) |
| 6 | **ρdry** (g/cc) - **Vp** (m/s) | $\rho_{dry} = 0.00028V_P + 1.59$ | 0.934 | J (Sarkar et al., 2012) |
| 7 | **ρdry** (g/cc) - **Vp** (m/s) | $\rho_{dry} = .0003V_P + 0.9815$ | 0.8794 | K (Kurtulus et al., 2016) |
| 8 | **ρsat** (g/cc) - **Vp** (m/s) | $\rho_{sat} = 1.8771e^{5E-0.5V_P}$ | 0.8182 | K (Kurtulus et al., 2016) |
| 9 | **ρbulk** (g/cc) - **Vp** (m/s) | $\rho_{bulk} = 0.0002V_P + 1.339$ | 0.8996 | K (Kurtulus et al., 2016) |
| 10 | **ρbulk** (kg/m$^3$) - **Vp** (m/s) | $\rho_{buik} = 946\ln(V_P) - 5561$ | 0.84 | M (Parent et al., 2015) |

A detailed analysis of the relationship between $V_p$ and porosity ($\phi$) is presented in this study. For this purpose, three graphs have been plotted, which highlights the correlation between $\phi$ and $V_p$. In Figure 2.3(a), only the datasets as reported by different researchers for their respective reservoir rock types have been plotted. In Figure 2.3(b), data representing the empirical equations as studied across the literature for the respective reservoir rocks, along with the datasets combined is plotted. Figure 2.3(c) shows the general (proposed) trend, that is, an exponential decrease in porosity with an increase in $V_p$. Such a type of general trend is independent of the type of rock under study, which may be important for identifying an accurate relationship among the two parameters ($\phi$ and $V_p$). On closer scrutiny, the range of porosity found from the plotted graph is 0.40% to 37.81% for all the different rock types, for $V_p$ varying between 1.47 km/s to 6.75 km/s. However, the porosity values for carbonates and sandstones are scattered over the entire graph. Thus, it is clear that a negative correlation exists between $V_p$ and porosity, which is valid for rock types for different porosity ranges. The dominant variables affecting the compressional wave velocity ($V_p$) include bulk density and porosity. In

order to account for its dependency, $V_p$ has been plotted with a bulk density as the primary axis and porosity as a secondary axis for a common set of data available Kahraman et al. (2008), Soroush et al. (2011), Kurtulus et al. (2015), Kassab et al. (2015), as shown in Figure 2.4 (b). It is evident from the highlighted circle in the graph that, for a lower value of $V_p$, lower is the bulk density and higher is the porosity, thereby showing the generality in the correlations that relate the petrophysical properties of rocks with $V_p$.

Table 2.5 enlists all the empirical relations that exist between porosity and $V_p$ as reported across the literature. Various researchers have developed several empirical relationships from their datasets, and after plotting these datasets, it is evident that those empirical relationships are not valid in a general form, and a one-to-one correlation is not possible. Hence, an attempt is made to establish a one-to-one relationship by removing the influence of the density factor. The sole purpose of plotting Figure 2.5(b) is to understand the direct relationship between $V_p$ and porosity by removing the density effect (for datasets of Kahraman et al. (2008), Soroush et al. (2011), Kurtulus et al. (2015), Kassab et al. (2015)). Figure 2.5(c) shows the combined representation of porosity with respect to compressional wave velocity measured ($V_p$) to the ratio between $V_p$ and $V_p$ (Density) calculated from the general trend observed between bulk density and $V_p$ (for datasets of Kahraman et al. (2008); Soroush et al. (2011); Kurtulus et al. (2015); Kassab et al. (2015)). Previous studies provide limited information about how density has an effect on porosity and velocity. The plot so generated shows a decrease in porosity with an increase in $V_p$.

Detailed analysis on the relationship between $V_s$ and Bulk Density is not possible due to scarcity of data. Figure 2.6 depicts a graphical representation of Bulk Density with respect to $V_s$ obtained with a poorly fitted general trend derived from studies conducted by three different literatures, namely Moradian et al. (2009); Soroush et al. (2011) and Sayed et al. (2015). The range of bulk density found from the plotted graph is 2.04 g/cc to 2.73 g/cc for all the different rock types, for $V_s$ varying between 1.2 km/s to 3.1 km/s. In his study, Soroush et al. (2011), (legend I) suggested a quadratic (increasing trend) correlation between both the parameters, which is also evident from Figure 2.6. In general, $V_s$ increases with an increase in bulk density. However, in totality, a scattered plot is observed but cannot be generalised due to data scarcity. No clear trend is observed between bulk density and $V_s$ (Figure 2.6).

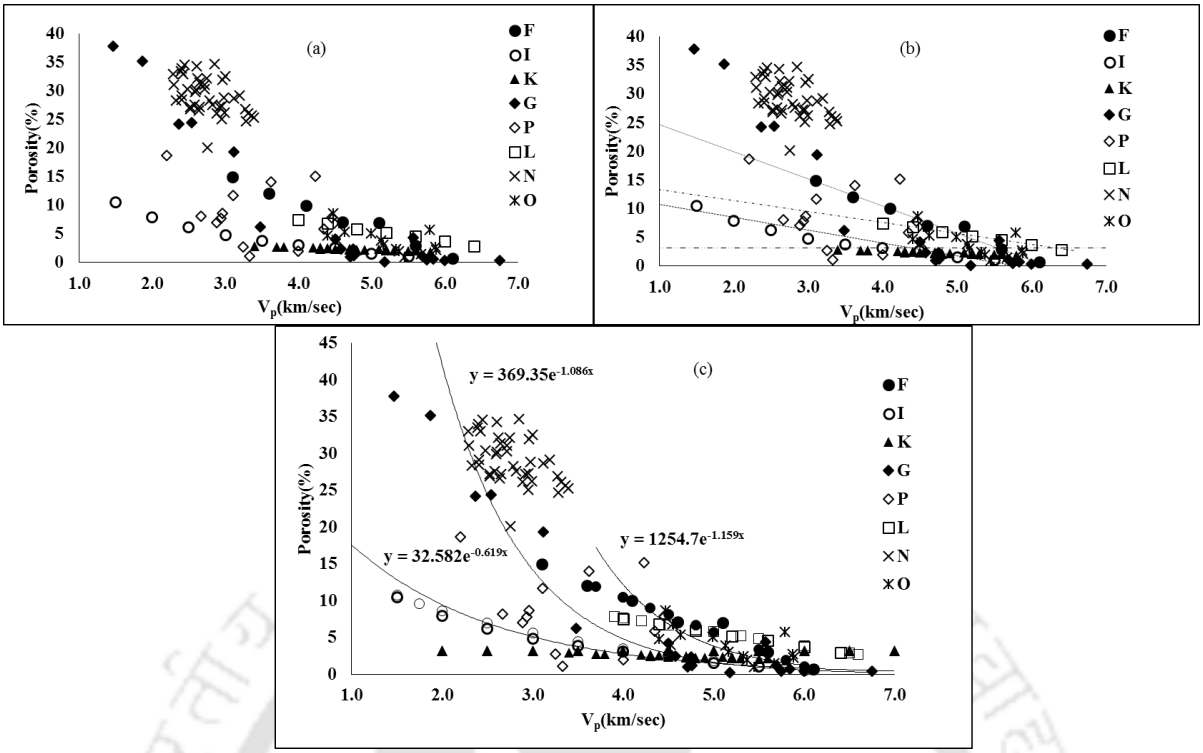


Figure 2.3 $V_p$ versus Porosity (a) as reported by different researchers, (b) including empirical relationships generated by various researchers (datasets plotted as symbols while lines represent empirical equation) and, (c) including general trends derived from this study (datasets plotted as symbols while solid lines represent proposed general trends)

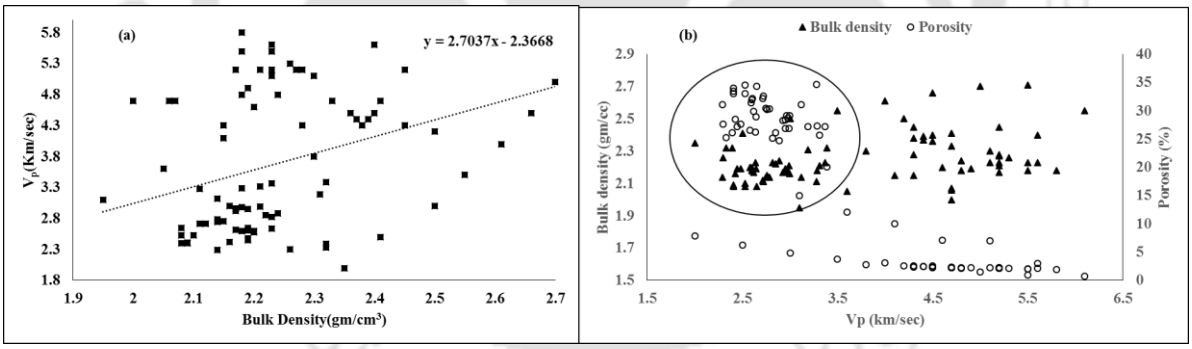


Figure 2.4 $V_p$ versus Bulk Density (a) as reported by different researchers along with general trend used to calculate $V_p$ (Density) in this study (where Y axis is $V_p$ (km/s) and X is Bulk density (g/cc)), and (b) $V_p$ versus porosity and bulk density (the datasets falling in the circle shows a porosity value more than 20% with a low bulk density and comparatively lower $V_p$ values)

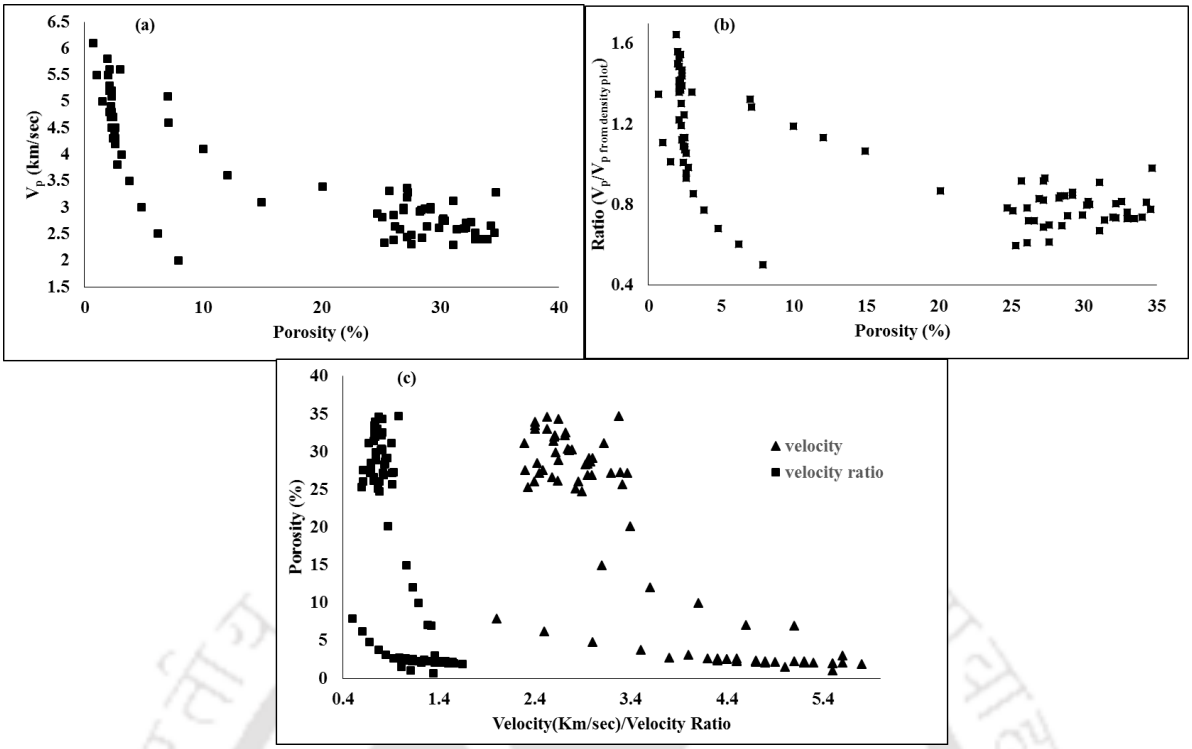


Figure 2.5 $V_p$ versus Porosity, (a) as reported by different researchers (where Y is $V_p$ (km/s) and X is Porosity (%), (b) including ratio of $V_p$ and $V_p$ obtained from density plot, and porosity, as reported by different researchers, (c) including $V_p$ and ratio of $V_p$ and $V_p$ obtained from density plot, with porosity as reported by different researchers

Table 2.5 Compilation of empirical equations derived for velocity ($V_p$, $V_s$) and porosity as reported by various researchers

| S. No. | Parameters | Empirical relation | Coefficient of determination ($R^2$) | Reference |
|---|---|---|---|---|
| 1 | $\phi$ (fraction)-$V_p$ (km/s) | $V_P = 5.02 - 5.63\phi$ | 0.840 | A (Han et al. 1986) |
| 2 | $\phi$ (fraction)-$V_s$ (km/s) | $V_S = 3.03 - 3.78\phi$ | 0.754 | A (Han et al. 1986) |
| 3 | $\phi$ (%)-$V_p$ (m/s) | $V_P = 5317 - 89\phi$ | 0.46 | D (Assefa et al. 2003) |
| 4 | $\phi$ (%)-$V_s$ (m/s) | $V_S = 2844 - 49\phi$ | 0.44 | D (Assefa et al. 2003) |

| | | | | |
|---|---|---|---|---|
| 5 | $\phi$ (%)-$V_p$ (km/s) | $\phi = -4.733V_P + 29.377$ | 0.844 | F (Kahraman and Yeken, 2008) |
| 6 | $\phi$ (%)-$V_p$ (m/s) | $\phi = -7.415\ln(V_P) + 64.96$ | 0.63 | I (Soroush et al. 2011) |
| 7 | $\phi$ (%)-$V_s$ (m/s) | $\phi = -8.61\ln(V_S) + 69.45$ | 0.60 | I (Soroush et al. 2011) |
| 8 | $\phi$ (%)-$V_p$ (km/s) | $\phi = 15.24 - 1.899V_P$ | 0.74 | L (Pappalardo 2015) |
| 9 | $\phi$ (%)-$V_p$ (km/s) | $\phi' = 6.377 - 0.719V_P$ | 0.60 | L (Pappalardo 2015) |
| 10 | $\phi$ (%)-$V_p$ (m/s) | $\phi = -0.004V_P + 3.1465$ | 0.85 | K (Kurtulus et al. 2016) |

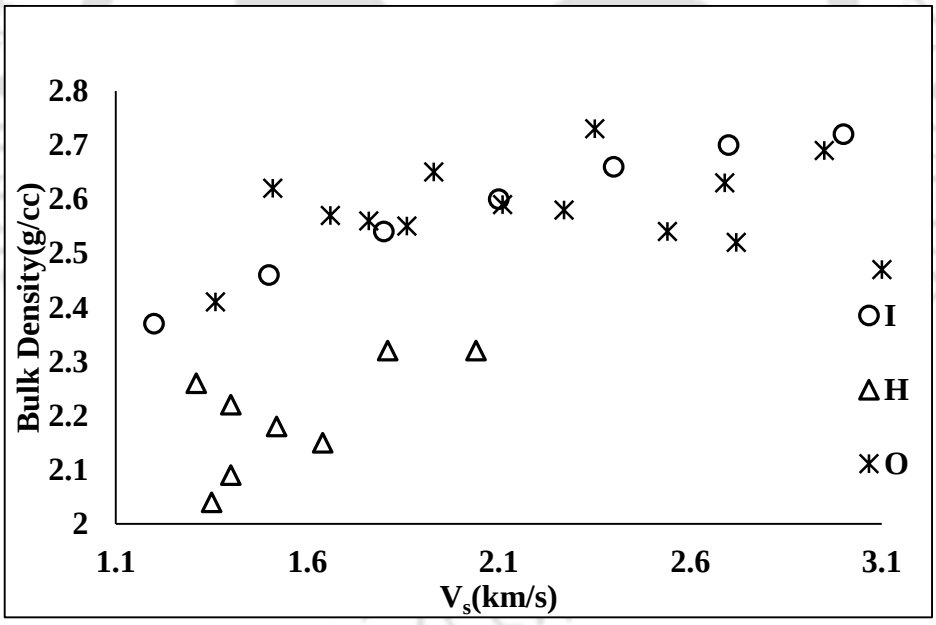


Figure 2.6 $V_s$ (Shear wave velocity) versus Bulk Density as reported by different researchers

### 2.3.2 Water Absorption and Saturating Fluid

The plotted graph, as well as the results reported in the literature, indicate that there is a negative correlation between $V_p$ and water absorption. Thus, $V_p$ may be used as an objective parameter for the estimation of water absorption characteristics (Kurtulus et al., 2016). From the graph, as shown in Figure 2.7, the range of water absorption found from the graph is 0.1 % to 6.45% and $V_p$ range is 2 km/s to 6.1 km/s. However, water absorption being an important

rock index depends on the mineralogy and porosity of rock (Soroush et al., 2011). Table 2.6 shows the empirical relations between water absorption and $V_p$ and $V_s$.

Also, the type of the saturating fluid also has an effect on the compressional and shear wave velocities. A rock may be saturated with water, oil, brine or gas. The velocity of the P-wave is highest for brine saturated, intermediate for kerosene and lowest for the dry rock at all pressures, whereas the shear wave velocities are highest for the dry rock and lowest for the brine saturated rock. Moreover, the effect of saturating fluid is more in compressional velocities than in shear wave velocities (Toksoz et al., 1976).

Table 2.6 Compilation of empirical equations derived for velocity ($V_p$, $V_s$) and water absorption as reported by various researchers

| S. No. | Parameters | Empirical relation | Coefficient of determination ($R^2$) | Reference |
|---|---|---|---|---|
| 1 | $W_a$ (%)- $V_p$ (km/s) | $W_a = -2.248V_P + 13.76$ | 0.90 | F (Kahraman and Yeken, 2008) |
| 2 | $W_a$ (%)- $V_p$ (m/s) | $W_a = -4.184\ln(V_P) + 36.56$ | 0.81 | I (Soroush et al., 2011) |
| 3 | $W_a$ (%)- $V_s$ (m/s) | $W_a = -4.390\ln(V_S) + 35.28$ | 0.75 | I (Soroush et al., 2011) |

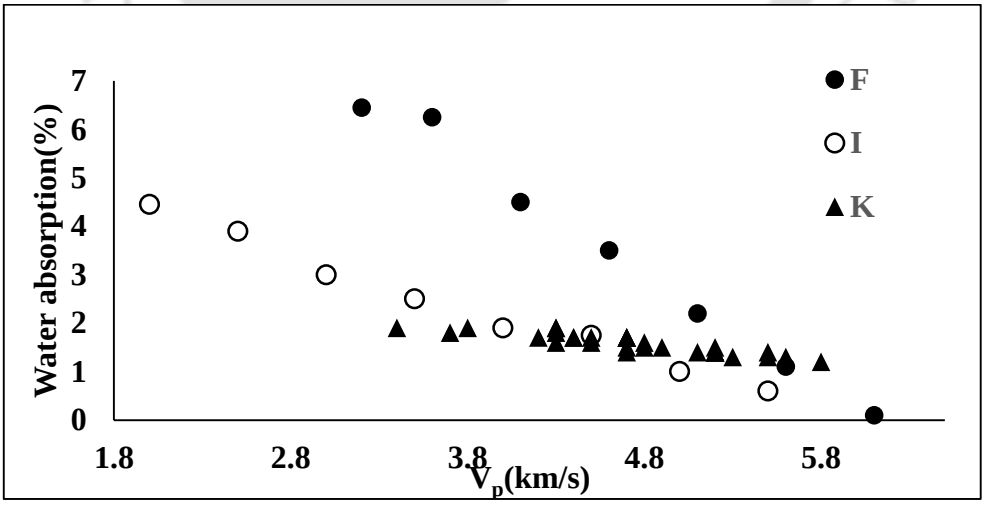


Figure 2.7 $V_p$ versus water absorption as reported by different researchers

### 2.3.3 Permeability

Very few studies have been conducted considering the effect of permeability on the compressional and shear wave velocity. Kassab et al. (2015) illustrated that there is no clear trend between $V_p$ and permeability, while Sayed et al. (2015) observed a weak relationship between the two. Also, Al-Dousari et al. (2016) observed a weak relation between the two properties measured under effective stress of 4000 psig. But, Klimentos (1991), through his study under confining pressure, indicated that there is a minor increasing trend of P-wave velocity with increasing permeability, thereby suggesting that the effect of permeability alone is negligible. In other words, the effect of permeability on P-wave velocity is minimal compared to that of porosity and clay content. However, it is to be noted that there is an interdependency of permeability with porosity, density and a combined analysis is required to understand the undercovered trend of permeability clearly. In other words, the misleading permeability-velocity relationship may be attributed to the influence of the clay content-velocity relationship. From the plotted semi-log graph as shown in Figure 2.8, the range of permeability found is 1.15 mD to 4969.19 mD and $V_p$ range is 3.12 km/s to 6.33 km/s.

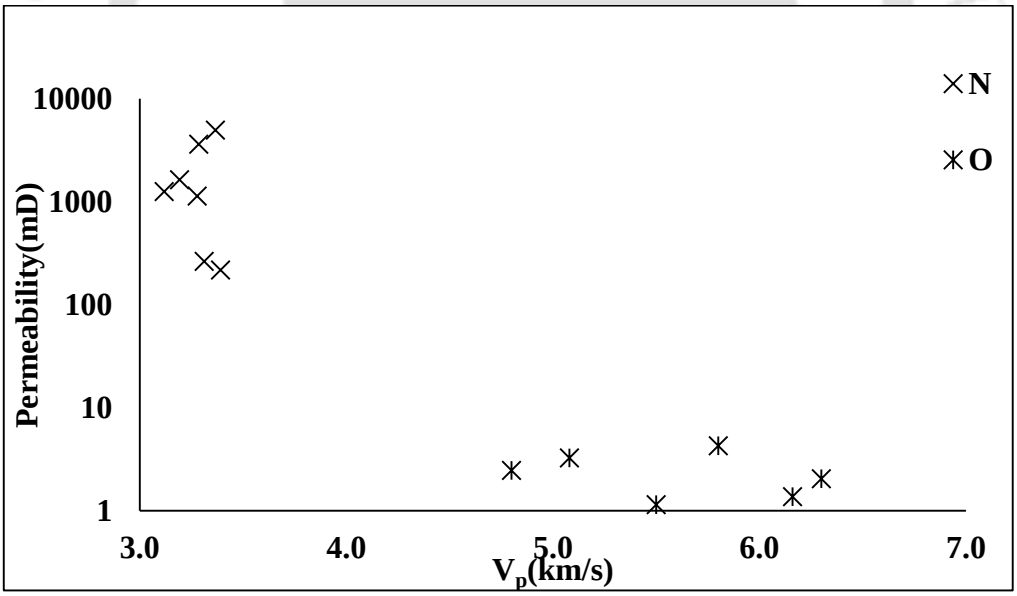


Figure 2.8 $V_p$ versus Permeability as reported by different researchers

### 2.3.4 Clay Content

Most of the researchers have investigated the relationship between clay content and $V_p$ and $V_s$ under confining pressures (Han et al., 1986; Klimentos, 1991) and observed that there is a clear linear trend of decreasing P-wave velocity with an increase in the clay content in both poor and well-consolidated rock samples. The reason for the effect being the higher compressibility of

the clay minerals significantly affects the ultrasonic waves travelling through the rocks. Even small amounts of clay content may have a larger effect on decreasing the velocity since clays can alter the petrophysical properties by reducing the pore size or increasing the specific surface area. However, Al-Dousari et al. (2016) studied the relationship between clay content and $V_p$ measured at effective stress of 4000 psi on sandstone/shaly sands/carbonate rocks and observed scattering of data indicating no clear trend. Hence, it can be concluded that clay content has a dominant effect on $V_p$, and a small variation in its amount can result in a change in $V_p$. There is a lack of study on the influence of clay content on $V_p$ as well as $V_s$ under ambient conditions. It is predictable that $V_p$ and $V_s$ will be affected by the amount of clay present in the rock sample. The effect of clay can already be sighted by its effect in other petrophysical parameters, especially density, porosity and permeability.

## 2.4 Variation of $V_p$ with the Geomechanical Properties of Sedimentary Rocks

Different geomechanical properties such as elastic modulus/deformation modulus, Poisson's ratio (υ), uniaxial compressive strength (UCS), shear strength properties, tensile strength, point load index are widely used for rock mass characterisation in geological and geotechnical engineering. However, there are no direct methods by which these properties can be obtained in the laboratory or in-situ without following a time-consuming and laborious procedure. Thus, the ultrasonic technique, an indirect method, were found reliable to determine these properties in rocks. Many researchers have studied the correlation between the compressional wave velocity ($V_p$) and the geomechanical properties of sedimentary rocks such as sandstones and carbonates. $V_p$, $V_s$ have been correlated with different mechanical properties from the dataset available in the literature to understand the existing association between the two and its importance in reservoir characterisation. Researchers have obtained a strong correlation between geomechanical properties (UCS, indirect tensile strength, E, υ, slake durability, point load strength) and $V_p$, $V_s$ (longitudinal and shear wave) for different rocks (sandstone, shale, limestone, coal, marlstone, siltstone, conglomerate, marl, dolomitic limestone, dolomite, argillaceous limestone, claystone). Table 2.7 presents the summary of techniques used by various researchers on different rocks reported in the literature. Different empirical relations have also been reported in literature correlating these geomechanical properties with $V_p$, $V_s$ for different rock types. These correlations were achieved based on numerous testings from different types of formations with different lithology and different parts of the world (Figure 2.9). The use of such empirical correlations is sometimes the only method to evaluate the

strength under certain conditions where rock cores cannot be obtained for conducting laboratory tests. The datasets in this review are based on mainly sandstones and carbonate rocks under ambient conditions. The datasets have been plotted together, and graphs of variation of compressional wave velocity with UCS, indirect tensile strength ($\sigma_t$), Young's modulus (E), Poisson's ratio (υ), slake durability and point load strength have been shown. Due to the scarcity of available data, the rocks considered in this study, namely sandstones and carbonate rocks, are neither from any particular geological time period nor any preference of a geographical region has been taken. The map (Figure 2.9) shows the locations of the rock types considered, and it illustrates all the available datasets from the entire world have been considered for this literature review. The datasets reported in this study belongs to tests conducted on dry rocks. The literature reference regarding laboratory techniques used by different researchers is summarised in Table 2.7. The test procedures for determining $V_p$, point load index, UCS, E have been standardised by IS and ASTM (Table 2.8).

Table 2.7 Summarised data details reported in the literature

| Designation | Rock Type | Lab Technique Used | Reference |
|---|---|---|---|
| A | Limestone, mudstones, psammite, greenstones, granites | - | D'Andrea et al. (1965) and extended by McCann et al. (1990) |
| B | Sandstone | - | Freyburg (1972) |
| C | Sandstone | - | Fjaer (1999) |
| D | Sandstone | Through transmission, P wave frequency 1 MHz and S wave 0.6 MHz, $V_p$ measured on water-saturated rocks at different confining pressures (up to 40 MPa) | Han et al. (1986) |
| E | Sandstone | - | Moos et al. (1948) |
| F | Limestone | Through transmission, transducer frequency 54 kHz | Kahraman (2001) |
| G | Carbonates | Through transmission | Yasar and Erdogan. (2004) |

| | | | |
|---|---|---|---|
| H | Sandstone<br>Shale<br>Limestone<br>Dolomite | Not mentioned | Chang et al. (2006) |
| I | Limestone<br>Sandstone | Through transmission | Kilic and Teymen (2008) |
| J | Limestone<br>Sandstone | Not mentioned | Cobanoglu and Celik (2008) |
| L | Carbonate rocks | Through transmission transducer frequency 54 kHz | Kahraman and Yeken (2008) |
| M | Sandstone<br>Coal<br>Shaly rock | Through transmission | Sharma and Singh (2008) |
| N | Limestone<br>Sandstone<br>Marlstone | Through transmission, transducer frequency 1 MHz | Moradian and Behnia (2009) |
| O | Sandstone<br>Siltstone<br>Conglomerate<br>Limestone<br>Marl | Ultrasonic pulse technique | Soroush et al. (2011) |
| P | Limestone<br>Sandstone<br>Dolomitic limestone<br>Dolomite<br>Coal<br>Shale | Through transmission | Sarkar et al. (2012) |
| Q | Marl<br>Sandstone<br>Argillaceous limestone<br>Limestone | Through transmission | Karakul and Ulusay (2013) |

| | | | |
|---|---|---|---|
| | Sandstone<br>Clay stone | | |
| R | Limestone | Not mentioned | Parent et al. (2015) |
| S | Dolostone | High Emission MAE device with probes of frequency 53 kHz | Pappalardo (2015) |
| T | Limestone | Ultrasonic pulse generator operating at 54 kHz | Kurtulus et al. (2016) |
| U | Carbonate rocks | Through transmission | Madhubabu et al. (2016) |

Table 2.8 Standards for determination of different parameters of rocks

| Parameter | Standard |
|---|---|
| Point Load Index | ASTM D5731, IS 8764-1998 |
| UCS | IS 9143-1979, ASTM D2938-2002 |
| Brazilian tensile strength | IS 10082-1981, ASTM D3967-08 |
| Durability (slake durability) | IS 10050-1981 |

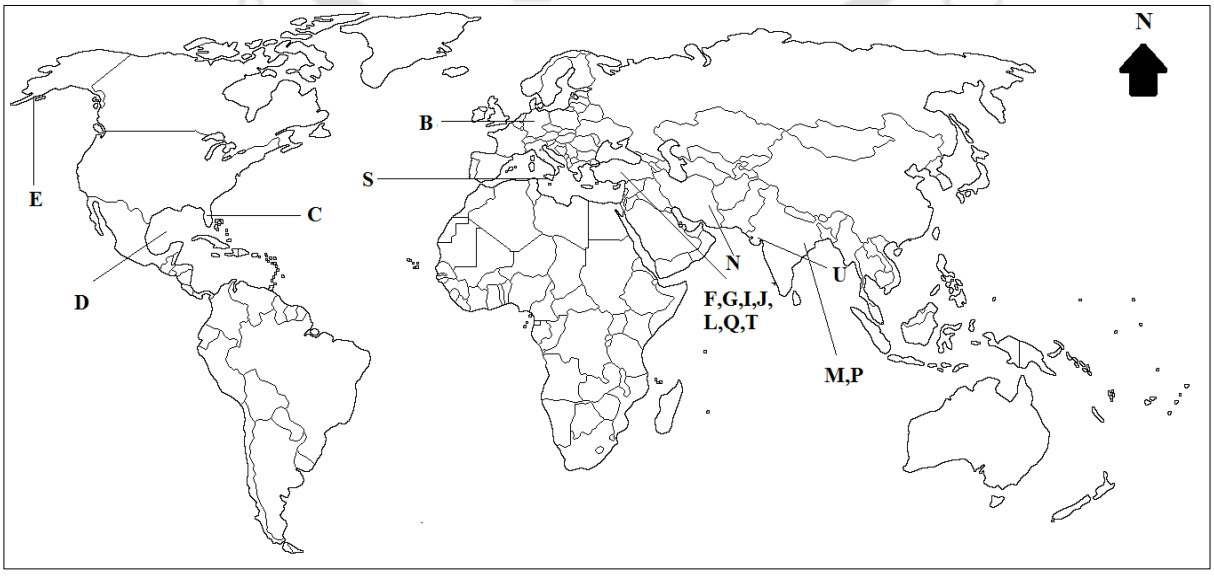

| LEGENDS |
| --- |
| B-Thuringia, Germany, C- Gulf Coast, USA, D- Gulf of Mexico, E- Cook Inlet, Alaska, USA, F- Turkey,<br>G- Adana, Turkey, I- Southern Anatolia, Turkey, J- Turkey,<br>L- Nigde, Kayseri, Konya & Antalya, Turkey, M- Lower Shiwalik & Lower Gondwana (Singrauli & Jharia), India, N- Iran, P- Jutogh, Lower Shiwalik & Lower Gondwana, India, Q- Turkey, S- Peloritani Mounts, NE Sicily, T- Cebecikoy, Hereke, Akveren, Soguck & Bakirkoy, Turkey, U- Kutch, Gujarat, India |

Figure 2.9 Location map of different sedimentary rock samples reported in this literature review study

## 2.5 Results and Discussion

The different mechanical properties of rocks, $V_p$ and $V_s$, reported in this literature review were based on laboratory measurements under ambient conditions. Amongst the different literature data analysed, datasets labelled as B, C, D, E represent sandstones, datasets labelled as A, F, G, L, S, T, U represent carbonates, while datasets labelled as H, I, J, N, O, P, Q consists of a combination of different rocks (Table 2.7).

### 2.5.1 Rock Strength

The rock strength, categorised as compressive and tensile, is one of the most crucial geomechanical properties. A suitable core for testing is not always available, and in the absence of cores, correlations can be used to estimate strength. Moos et al. (1948); D'Andrea et al. (1964); Freyburg (1972); McCann et al. (1990); Fjaer (1992); Vernik et al. (1993); Moos et al. (2001); Kahraman (2001); Yasar and Erdogan (2004); Entwisle et al. (2005); Sharma and Singh (2008); Cobanoglu and Celik (2008); Kilic and Teymen (2008); Moradian and Behnia (2009); Soroush et al.(2011); Sarkar et al. (2012); Karakul and Ulusay (2013); Pappalardo (2015); Parent et al. (2015); Kurtulus et al. (2016) established empirical correlations between UCS, tensile strength and $V_p$. Tables 2.9 and 2.10 present the instrument used to evaluate UCS and indirect tensile strengths in the literature and Tables 2.11 and 2.12 depict the relationships between UCS, indirect tensile strength, and $V_p$ as reported in the literature.

Table 2.9 Instrument used for evaluating UCS in the literature

| Instrument used | Associated Literature | Sample | Location |
| --- | --- | --- | --- |
| UCS Instrument | 1. Madhubabu et al. (2016) | Carbonate rocks | Gujarat, India |

| | | | |
|---|---|---|---|
| | 2. Kilic and Teymen (2008) | Sandstone | Turkey |
| | 3. Pappalardo (2015) | Sandstone | Sicily |
| | 4. Sarkar et al. (2012) | Sandstone | Jutogh, India |
| | 5. Kurtulus et al. (2016) | Limestone | Turkey |
| | 6. Moradian and Behnia (2009) | Sandstone & Limestone | Iran |

Table 2.10 Instrument used for evaluating indirect tensile strength in the literature

| Instrument used | Associated Literature | Sample | Location |
|---|---|---|---|
| Brazilian Tensile strength instrument | 1. Kilic and Teymen (2008) | Sandstones | Turkey |
| | 2. Kurtulus et al. (2016) | Limestones | Turkey |

Table 2.11 Summary of correlation laws between ultrasonic velocity ($V_p$) and UCS available in the literature

| S No. | Parameters | Empirical Relation | $R^2$ | Reference |
|---|---|---|---|---|
| 1 | UCS (MPa)-$V_p$ (km/s) | $UCS = 35.4V_P - 55$ | 0.80 | A (D'Andrea et al., 1965) |
| 2 | UCS (MPa)-$V_p$ (m/s) | $UCS = 0.035V_P - 31.5$ | - | B (Freyburg, 1972) |
| 3 | UCS (MPa)-$V_p$ (m/s) | $UCS = 3.3X10^{-20}\rho^2V_P^4[(1+\upsilon)/(1-\upsilon)]^2(1-2\upsilon)[1+0.78V_{clay}]$ | - | C (Fjaer, 1992) |
| 4 | UCS (MPa)-$V_p$ (m/s) | $UCS = 1.745X10^{-9}\rho V_P^2 - 21$ | - | E (Moos et al., 1999) |
| 5 | UCS (MPa)-$V_p$ (km/s) | $UCS = 9.95V_P^{1.21}$ | 0.83 | F (Kahraman, 2001) |

| | | | | |
|---|---|---|---|---|
| 6 | UCS (MPa)-$V_p$ (m/s) | $V_P = 0.0317UCS + 2.0195$ | - | G (Yasar and Erdogan, 2004) |
| 7 | UCS (MPa)-$V_p$ (km/s) | $UCS = 56.71V_P - 192.93$ | 0.67 | J (Cobanoglu and Celik, 2008) |
| 8 | UCS (MPa)-$V_p$ (km/s) | $UCS = 2.304V_P^{2.4315}$ | 0.94 | I (Kilic and Teymen, 2008) |
| 9 | UCS (MPa)-$V_p$ (m/s) | $UCS = 165.05e^{(-4451.07/V_P)}$ | 0.70 | N (Moradian and Behnia, 2009) |
| 10 | UCS (MPa)-$V_p$ (m/s) | $UCS = 43V_P + 1000$ | - | O (Soroush et al., 2011) |
| 11 | UCS (MPa)-$V_p$ (m/s) | $UCS = 0.038V_P - 50$ | 0.934 | P (Sarkar et al., 2012) |
| 12 | UCS (MPa)-$V_p$ (km/s) | $UCS = 7.812V_P^{1.6}$ for $S_r$=0 | - | Q (Karakul and Ulusay, 2013) |
| 13 | UCS (MPa)-$V_p$ (km/s) | $UCS = 6.070V_P^{1.633}$ for $S_r$=0.2 | - | Q (Karakul and Ulusay, 2013) |
| 14 | UCS (MPa)-$V_p$ (km/s) | $UCS = 4.937V_P^{1.673}$ for $S_r$=0.5 | - | Q (Karakul and Ulusay, 2013) |
| 15 | UCS (MPa)-$V_p$ (km/s) | $UCS = 4.401V_P^{1.684}$ for $S_r$=0.7 | - | Q (Karakul and Ulusay, 2013) |
| 16 | UCS (MPa)-$V_p$ (m/s) | $UCS = 5.61*10^{-9}V_P^{2.75}$ | 0.86 | R (Parent et al., 2015) |
| 17 | UCS (MPa)-$V_p$ (km/s) | $V_P = 3.110 + 0.0289UCS$ | 0.88 | S (Pappalardo, 2015) |
| 18 | UCS (MPa)-$V_p$ (m/s) | $UCS = 0.018V_P - 18.405$ | 0.93 | T (Kurtulus et al., 2016) |

Table 2.12 Summary of correlation laws between velocities ($V_p$, $V_s$) and indirect tensile strength available in the literature

| S. No. | Parameters | Empirical Relation | $R^2$ | Reference |
|---|---|---|---|---|
| 1 | $\sigma_t$ (MPa)-$V_p$ (km/s) | $\sigma_t = 0.4935V_P^{1.8723}$ | 0.9216 | I (Kilic and Teymen, 2008) |

| | | | | |
|---|---|---|---|---|
| 2 | $\sigma_t$ (MPa)-$V_p$ (m/s) | $\sigma_t = 0.348e^{0.0004V_P}$ | 0.53 | O (Soroush et al., 2011) |
| 3 | $\sigma_t$ (MPa)-$V_s$ (m/s) | $\sigma_t = 0.277e^{0.0008V_S}$ | 0.52 | O (Soroush et al., 2011) |
| 4 | $\sigma_t$ (MPa)-$V_p$ (km/s) | $\sigma_t = 1.050V_P^{1.389}$ for $S_r$=0 | - | Q (Karakul and Ulusay, 2013) |
| 5 | $\sigma_t$ (MPa)-$V_p$ (km/s) | $\sigma_t = 0.919V_P^{1.416}$ for $S_r$=0.2 | - | Q (Karakul and Ulusay, 2013) |
| 6 | $\sigma_t$ (MPa)-$V_p$ (km/s) | $\sigma_t = 0.767V_P^{1.444}$ for $S_r$=0.5 | - | Q (Karakul and Ulusay, 2013) |
| 7 | $\sigma_t$ (MPa)-$V_p$ (km/s) | $\sigma_t = 0.694V_P^{1.447}$ for $S_r$=0.7 | - | Q (Karakul and Ulusay, 2013) |
| 8 | $\sigma_t$ (MPa)-$V_p$ (km/s) | $\sigma_t = 0.583V_P^{1.473}$ for $S_r$=1 | - | Q (Karakul and Ulusay, 2013) |

Yasar and Erdogan (2004) conducted studies relating UCS and ultrasonic tests on 13 samples of numerous carbonate rock types around Antara/Turkey and correlated using simple linear relations, reported $R^2$ of 0.80, while Moradian and Behnia (2009) in their study in three different sedimentary rock types (sandstone, limestone and marlstone) around various dam sites in Iran, reported $R^2$ =0.70. However, velocity values were multiplied by density values to obtain a better regression coefficient between UCS and $V_p$. The correlation coefficient improved to 0.75 as against 0.70. Sharma and Singh (2008) found a relation with $R^2$ =0.9022 on tests carried on seven types of rock (1 igneous, three sedimentary and three metamorphic). Kahraman (2001) reported an empirical correlation between $V_p$ and UCS with $R^2$ =0.83. Cobanoglu and Celik (2008) described a correlation with $R^2$ 0.67 for two rock types only. Sarkar et al. (2012), in this study, reported $R^2$ =0.934. Kurtulus et al. (2016) reported a strong linear dependence on UPV with an $R^2$ =0.93. In his study, Kilic and Teymen (2008) carried on 19 rock types comprising ten igneous rocks (seven of which were volcanic), seven sedimentary and two metamorphic of Southern Anatolia location, correlated the $V_p$ and the indirect tensile strength and reported a strong correlation with an $R^2$ =0.9216. Karakul and Ulusay (2013) gave empirical equations between $V_p$ and the indirect tensile strength for different degree of saturation values.

The variation of UCS and $\sigma_t$ with $V_p$ observed by various researchers are presented in Figures 2.10 and 2.11. It is observed from Figure 2.10 that the UCS value of limestone from Turkey

location (label T in Table 2.7) varies from 19 MPa to 46 MPa with a change in $V_p$ from 3.4 km/s to 5.8 km/s. Comparatively, the UCS value of limestone from the Paris location (label R in Table 2.7) varies from 20 MPa to 135 MPa with a change in $V_p$ from 3 km/s to 6 km/s. The percentage increase, thus observed in UCS from the Turkey location (label T), is 142%, while the percentage increase in UCS from the Paris location (label R) is 575%. The indirect tensile strength values, as observed from Figure 2.11, varies from 0.7 MPa to 19.7 MPa and $V_p$ range is 1.47 km/s to 6.75 km/s. Significant results presented by McCann et al. (1990) showed wide variability in the velocity values for individual rock types as against a limited range of UCS values. They obtained a correlation coefficient of 0.94, $R^2$ value of 0.88. for a multiplicative model of the form $y = ax^b$. In spite of obtaining a good correlation between UCS and $V_p$, McCann et al. (1990) suggested caution in deriving strength values and vice-versa owing to the scattering of data points (large variation in $V_p$ values for a limited range of UCS values) indicating non-linear nature of the relationship. However, to improve the accuracy of deriving strength values from velocity measurements, the mineralogy of the rock needs to be investigated. For instance, the dependency of velocity measurements on an increase or decrease in quartz or feldspar content for sandstones and calcite or dolomite content for carbonates, may be examined. Nevertheless, velocity measurements may be utilised to give a varied indication of disparity in rock mass strength.

To understand the link between the strength properties and $V_p$, the combined graphical representation of the variation of UCS and tensile strength (indirect tensile strength) with $V_p$ is plotted in Figure 2.10, and 2.11 respectively, where Figure 2.10, 2.11 (a) illustrates data as reported by different researchers; Figure 2.10, 2.11 (b) illustrates data including general trend derived from this study using simple regression analysis and confidence interval; Figure 2.10, 2.11 (c) illustrates data plotted on a log-log scale indicating non-linear relationship. The confidence intervals were set at 95%, as most of the raw data are within the confidence intervals. Hence, from the plotted graphs, it is observed that both UCS and tensile strength increases with an increase in $V_p$. However, there is a wide variation in the strength values and for a particular value of $V_p$ there exist two values of rock strength (UCS and tensile strength). This scattering of data results may be due to some other influential factors like mineralogical composition or higher clay content leading to an alteration in mechanical and elastic properties of rocks, thereby showing the dispersion of data points in the graph. Moreover, it is observed that carbonate rocks have a higher value of UCS as compared to sandstones which can be attributed to a greater value of density, thereby resulting in a higher value of $V_p$ for carbonate rocks.

An attempt is made to present the non-linear relationship between UCS and indirect tensile strength with $V_p$, as shown in Figures 2.10 (c) and 2.11 (c). A log-log graph is plotted since a reasonable straight-line relationship is obtained; however, obtained $R^2$ is 0.28 (presented in the form of $y = ax^b$) for UCS-$V_p$ and $R^2$ is 0.49 (of the form $y = ax^b$) for indirect tensile strength-$V_p$ plot. The scatter is observed due to the presence of outliers. For the UCS-$V_p$ plot, the variation in $V_p$ is observed to be as low as 2 km/s to 6.5 km/s. Similarly, for the tensile strength-$V_p$ plot, the variation in $V_p$ is observed to be as low as 2.2 km/s to 6.75 km/s. Ideally, a major mineral present in sandstone has a $V_p$ of 6.057 km/s (quartz's grain density is 2.65 g/cc) (Domenico, 1984), while, for the case of carbonates, $V_p$ is 6.259 km/s corresponding to major mineral calcite with a grain density 2.71 g/cc) (Domenico, 1984). However, these $V_p$ values are the maximum (for zero porosity). Thus, any variation in the $V_p$ value corresponds to an alteration in porosity value. For instance, the minimum value of $V_p$ obtained from the study is 2 km/s, maybe indicating high porosity of the same sample. This is because an increase in porosity is always associated by an equivalent decrease in $V_p$, since seismic velocity in the pores is less than the grains of which the rocks is composed of.

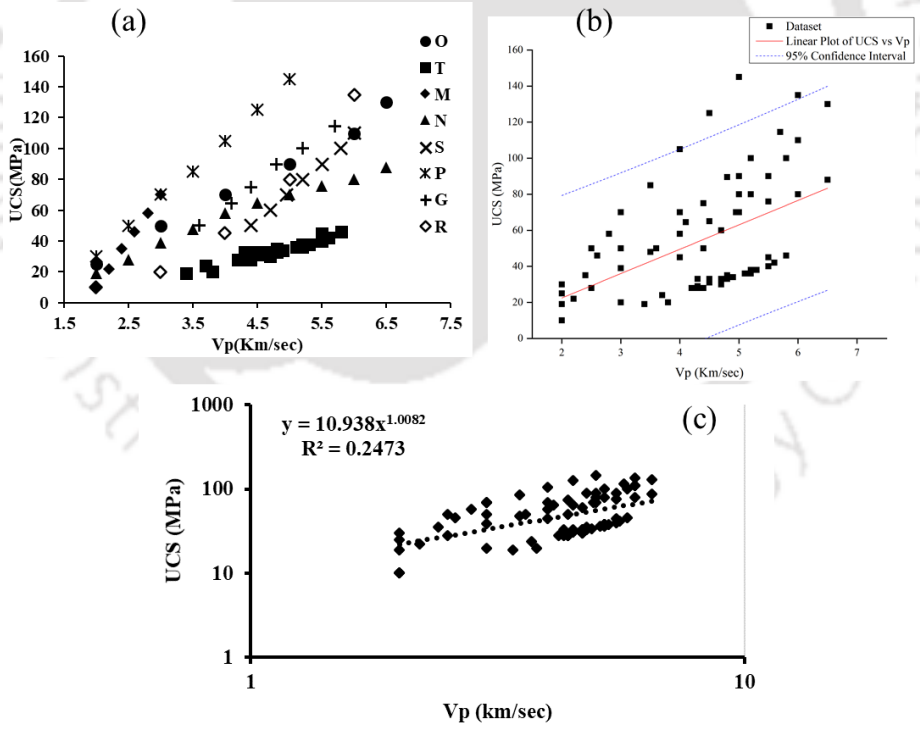


Figure 2.10 Variation of uniaxial compressive strength with the compressional wave velocity (a) as per studies of several researchers (b) including general trend derived from this study using simple regression analysis and confidence interval (c) data plotted on a log-log scale indicating non-linear nature of the relationship

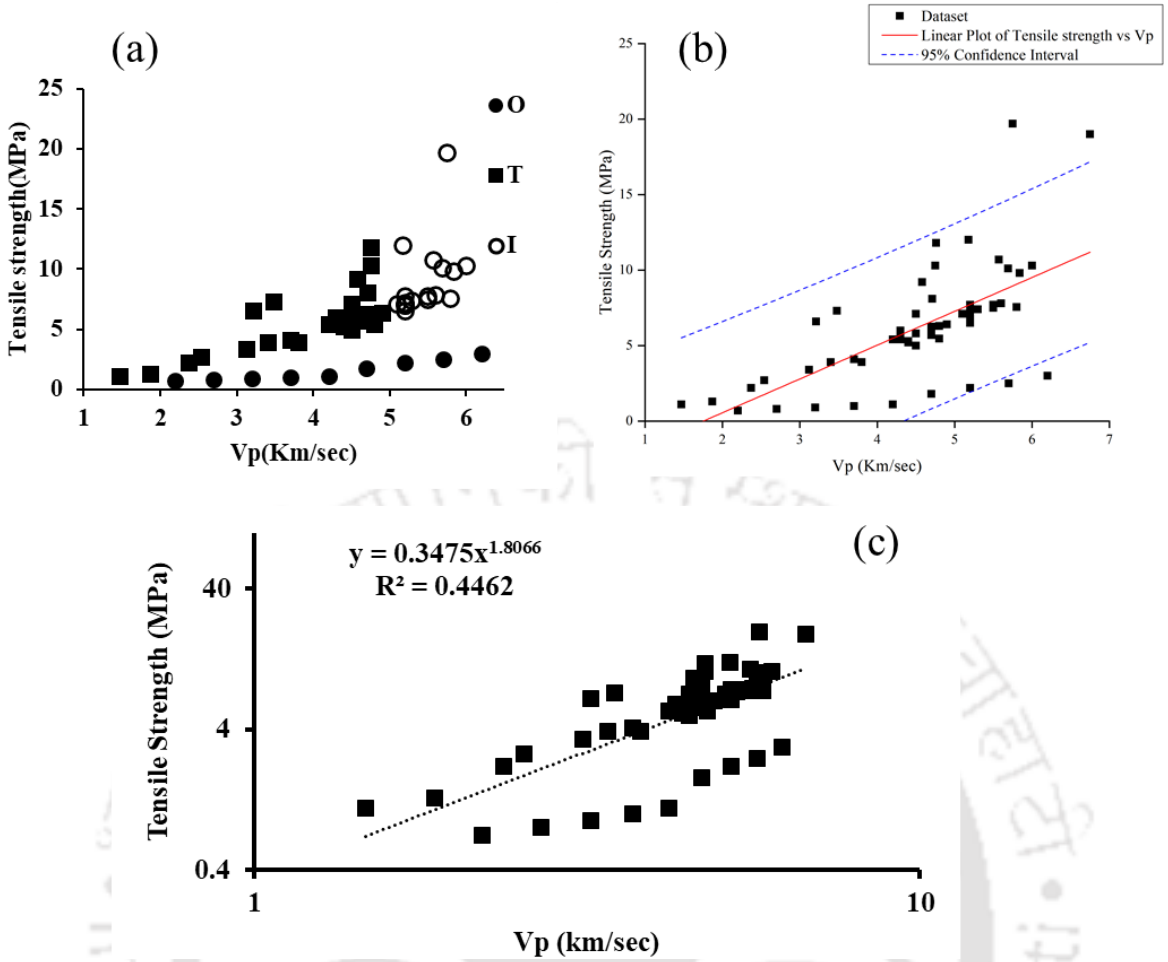


Figure 2.11 Variation of indirect tensile strength with the compressional wave velocity (a) as per studies of several researchers (b) including general trend derived from this study using simple regression analysis and confidence interval (c) data plotted on a log-log scale indicating non-linear nature of the relationship

### 2.5.2 Modulus of Elasticity

The prediction of elastic modulus (E) can be made from the measurement of $V_p$ and $V_s$ since E is an important parameter for intact rock classification and criteria for rock failure. The laboratory determination of E involves rigorous, time-consuming and destructive testing. Hence, ultrasonic techniques can be utilised to provide a direct evaluation of the rock mass. Thus, studies by Yasar and Erdogan (2004), Moradian and Behnia (2009), Parent et al. (2015), Pappalardo (2015), Kurtulus et al. (2015) were conducted to establish a relationship between the two as shown in Figure 2.12. Many correlations have been reported as shown in Table 2.13. The range of Young's modulus values found from the graph is 2 GPa to 69.14 GPa and $V_p$ range is 1.47 km/s to 6.75 km/s. Yasar and Erdogan (2004) found a regression coefficient of 0.86 for studies conducted on carbonate rocks, Parent et al. (2015) and Kurtulus et al. (2016) found 0.77 and 0.76 respectively for limestones, Pappalardo (2015) observed a value of 0.80

for dolostone, while Moradian and Behnia (2009) reported the highest regression coefficient value of 0.92.

Table 2.13 Summary of correlation laws between ultrasonic velocities ($V_p$, $V_s$) and Young's Modulus available in the literature

| S. No. | Parameters | Empirical Relation | $R^2$ | Reference |
|---|---|---|---|---|
| **1** | E (GPa)-$V_p$ (km/s) | $V_P = 0.0937E + 1.7528$ | 0.86 | G (Yasar and Erdogan, 2004) |
| **2** | E (GPa)-$V_p$ (m/s) | $E = 0.965V_P^{0.810}$ | 0.77 | R (Parent et al., 2015) |
| **3** | E (GPa)-$V_p$ (m/s) | $E = 2.06V_P^{2.78}$ | 0.92 | N (Moradian and Behnia, 2009) |
| **4** | E (MPa)-$V_p$ (km/s) | $E = -15718.21 + 5075.79V_P$ | 0.80 | S (Pappalardo, 2015) |
| **5** | E (GPa)-$V_p$ (m/s) | $E = 0.0114V_P + 3.7059$ | 0.76 | T (Kurtulus et al., 2016) |

To understand the correlation between E and $V_p$, different datasets were compiled from the literature, and a combined graphical representation of its variation is plotted in Figure 2.12, where Figure 2.12 (a) illustrates datasets as reported by different researchers; Figure 2.12 (b) illustrates datasets including general trend derived from this study using simple regression analysis and confidence interval; Figure 2.12 (c) illustrates data plotted on a log-log scale indicating non-linear relationship (of the form $y = ax^b$, with $R^2 = 0.55$). The confidence intervals were set at 95%. From the plotted graph, the modulus of elasticity increases with an increase in $V_p$. However, for a particular value of $V_p$, there exist two values of E. Such a wide variation may be due to the change in mineralogical composition (rock composition and texture, clay content, anisotropy etc.), leading to an alteration in mechanical and elastic properties of rocks.

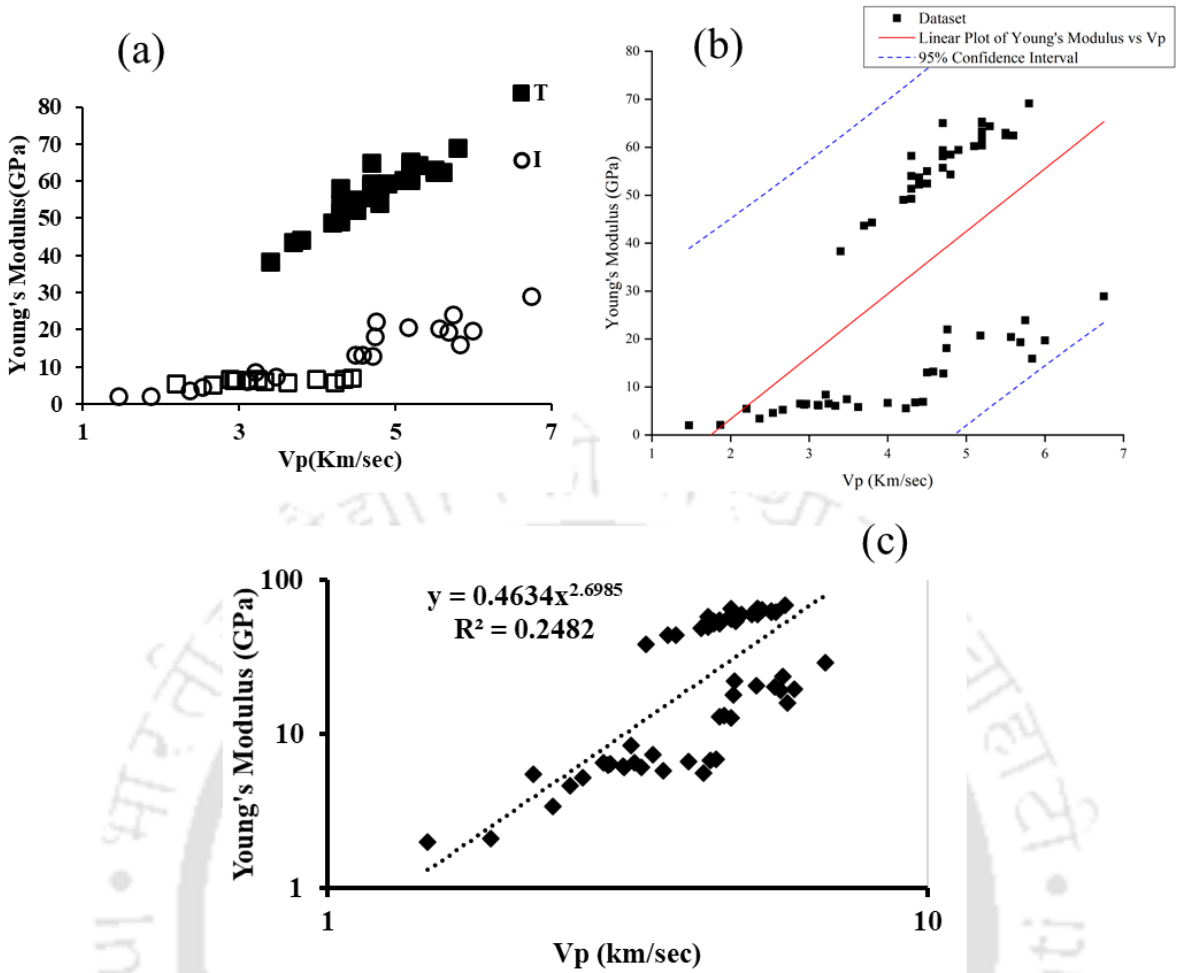


Figure 2.12 Variation of Young's Modulus with the compressional wave velocity (a) as per studies of several researchers (b) including general trend derived from this study using simple regression analysis and confidence interval (c) data plotted on a log-log scale indicating non-linear nature of the relationship

### 2.5.3 Poisson's Ratio

Among the elastic properties, Poisson's ratio (υ) is the least studied but, at the same time, the most interesting (Gercek, 2007). υ is defined as the ratio of decrease in transverse dimension to that of increase axial dimension when subjected to uniaxial stress for an isotropic material. At a given temperature and a given pressure, υ is constant for an isotropic material and its values lie between -1 to 0.5. Empirical equations were reported by Parent et al. (2015), Kurtulus et al. (2015) as shown in Table 2.14. Parent et al. (2015) and Kurtulus et al. (2016) gave empirical equations with regression coefficient values of 0.67 and 0.85 respectively for limestone. To understand the association between υ and $V_p$, combined graphical representation of its variation is presented in Figure 2.13, where Figure 2.13 (a) illustrates data as reported by different researchers; Figure 2.13 (b) illustrates data including general trend derived from this study using simple regression analysis and confidence interval; Figure 2.13 (c) illustrates data

plotted with calcite mineral values showing alteration. The confidence intervals were set at 95%. The range of Poisson's ratio values found from the graph is 0.23 to 0.4 and $V_p$ range is 2.2 km/s to 5.8 km/s. From the plotted graph, it is observed that as $V_p$ increases, υ decreases or there is a negative linear correlation between them. Hence, a decrease in υ is linked with an increase in $V_p$, which further leads to an increase in E. Ideally, for limestone samples, the major mineral present would be calcite with a value of Poisson's ratio 0.316 and $V_p$ 6.259 km/s. However, as explained earlier, due to the influence of several factors (mineralogy, porosity, saturation), there occurs a deviation from these values.

Table 2.14 Summary of correlation laws between ultrasonic velocity ($V_p$) and Poisson's ratio available in the literature

| S. No. | Parameters | Empirical Relation | $R^2$ | Reference |
|---|---|---|---|---|
| 1 | υ -$\mathbf{V_p}$ (m/s) | $\upsilon = 0.152V_p^{\,0.126}$ | 0.67 | R (Parent et al., 2015) |
| 2 | υ -$\mathbf{V_p}$ (m/s) | $\upsilon = -5E - 0.5V_P + 0.6$ | 0.85 | T (Kurtulus et al., 2016) |

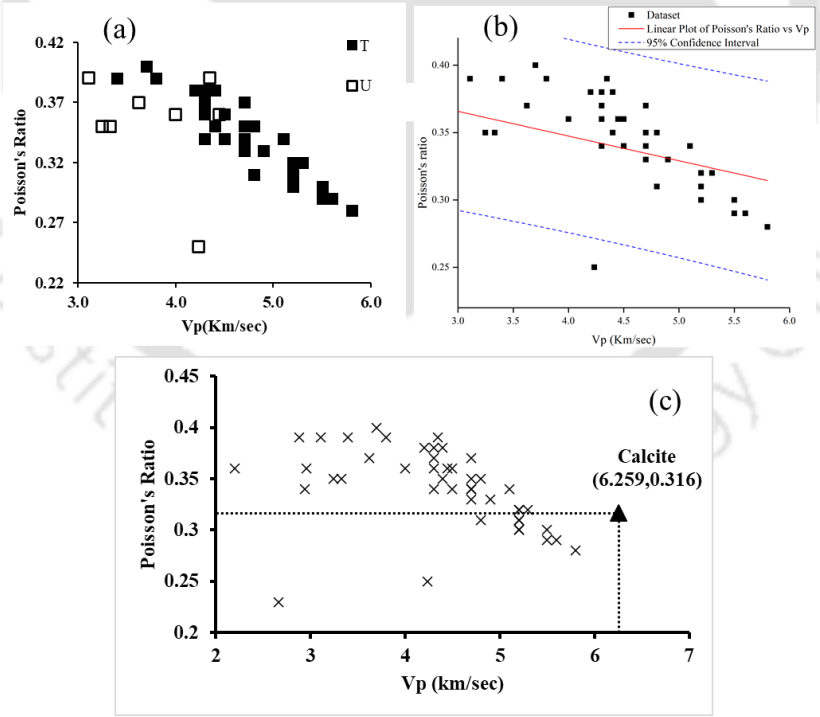


Figure 2.13 Variation of Poisson's Ratio with the compressional wave velocity (a) as per studies of several researchers (b) including general trend derived from this study using simple regression analysis and confidence interval (c) data plotted with calcite mineral values showing alteration

### 2.5.4 Other Parameters

Some of the other parameters that can be predicted using ultrasonic velocity include slake durability index (SDI) and point load strength (Sharma and Singh, 2008). The slake durability test estimates the resistance of rock samples to weakening and breakdown resulting from a standard cycle of wetting and drying (Sharma and Singh, 2008). In this study, the data corresponding to slake durability is limited (low number of datasets available). A probable reason may be since slake durability is partially controlled by strength, indicating a coherent relation amongst them, and studies related to $V_p$ –strength (UCS, indirect tensile strength) correlation were already studied by different researchers, as also discussed in the earlier sections. The presence of clay minerals would also play a major role in slake durability studies. To understand the association between SDI and $V_p$, a combined graphical representation of its variation is presented in Figure 2.14, where Figure 2.14 (a) illustrates data as reported by different researchers; Figure 2.14 (b) illustrates data including general trend derived from this study using simple regression analysis and confidence interval; Figure 2.14 (c) illustrates data plotted showing linear nature of the relationship (in the form y=ax+b with $R^2$ = 0.64). The confidence intervals were set at 95%. The range of slake durability values found from graph is 93.1 % to 99.6 % and $V_p$ range is 2 km/s to 5 km/s. From the plotted graph, it is observed that slake durability increases with an increase in $V_p$. Sarkar et al. (2012) found a linear correlation between $V_p$ and SDI, with a regression coefficient of 0.903. Sharma and Singh (2008) also reported a similar linear correlation, but they found a low correlation coefficient of 0.7831. Table 2.15 presents the summary of correlation laws between ultrasonic velocity ($V_p$) and SDI as proposed by researchers.

The other parameter, i.e. point load strength, is also a measure for the determination of rock strength. Point load test is an alternate method to estimate UCS since it is a reliable, economical and easy technique (Madhubabu et al., 2016). The combined graphical representation of the change of point load strength with $V_p$ is presented in Figure 2.15, where Figure 2.15 (a) illustrates data as reported by different researchers; Figure 2.15 (b) illustrates data including general trend derived from this study using simple regression analysis and confidence interval; Figure 2.15 (c) illustrates data plotted on a log-log scale (since a reasonable straight line is obtained on doing so), indicating non-linear nature relationship (of the form $y = ax^{b,}$ with $R^2$ = 0.59). The confidence intervals were set at 95%. Table 2.16 presents the summary of correlation laws between ultrasonic velocity ($V_p$) and point load strength, along with $V_p$-$V_s$, $V_p$-shear strength and $V_p$-V (loss of volume on wear, $cm^3/50\ cm^2$) as proposed by researchers.

The range of point load strength values found from the graph is 0.35 MPa to 8.6 MPa and $V_p$ range is 1.47 km/s to 6.75 km/s. From the plotted graph, it is noted that point load strength increases proportionately with $V_p$.

Table 2.15 Summary of correlation laws between ultrasonic velocity ($V_p$) and Slake Durability Index available in the literature

| S. No. | Parameters | Empirical Relation | $R^2$ | Reference |
|---|---|---|---|---|
| 1 | SDI (%)- $V_p$ (m/s) | $SDI = 0.0069V_P + 78.577$ | 0.7831 | M (Sharma and Singh, 2008) |
| 2 | SDI (%)- $V_p$ (m/s) | $SDI = 0.0014V_P + 92.98$ | 0.904 | P (Sarkar et al., 2012) |

Table 2.16 Summary of correlation laws between ultrasonic velocities ($V_p$, $V_s$) and other parameters available in the literature

| S. No. | Parameters | Empirical Relation | $R^2$ | Reference |
|---|---|---|---|---|
| 1 | $V_p$ (km/s)-$V_s$ (km/s) | $V_P / V_S = 1.55 + 0.56n + 0.43C$ | - | D (Han et al., 1986) |
| 2 | $V_p$ (km/s)-$V_s$ (km/s) | $V_P = 1.26V_S + 1.07$ | - | D (Han et al., 1986) |
| 3 | V(cc/50 $cm^2$)-$V_p$(km/s) | $V = 57997V_P^{-2.4279}$ | 0.8452 | I (Kilic and Teymen, 2008) |
| 4 | $V_s$ (m/s)-$V_p$ (m/s) | $V_S = 0.456V_P + 264.3$ | 0.90 | O (Soroush et al., 2011) |
| 5 | $\tau$ (MPa)-$V_p$ (m/s) | $\tau = 0.0019V_P - 2.6545$ | 0.90 | T (Kurtulus et al., 2016) |
| 6 | $I_S$ (MPa)-$V_p$ (m/s) | $I_S = 0.0005V_P + 0.659$ | 0.83 | T (Kurtulus et al., 2016) |
| 7 | $I_S$ (MPa)-$V_p$ (m/s) | $I_S = 0.022V_P + 30.631$ | 0.70 | T (Kurtulus et al., 2016) |

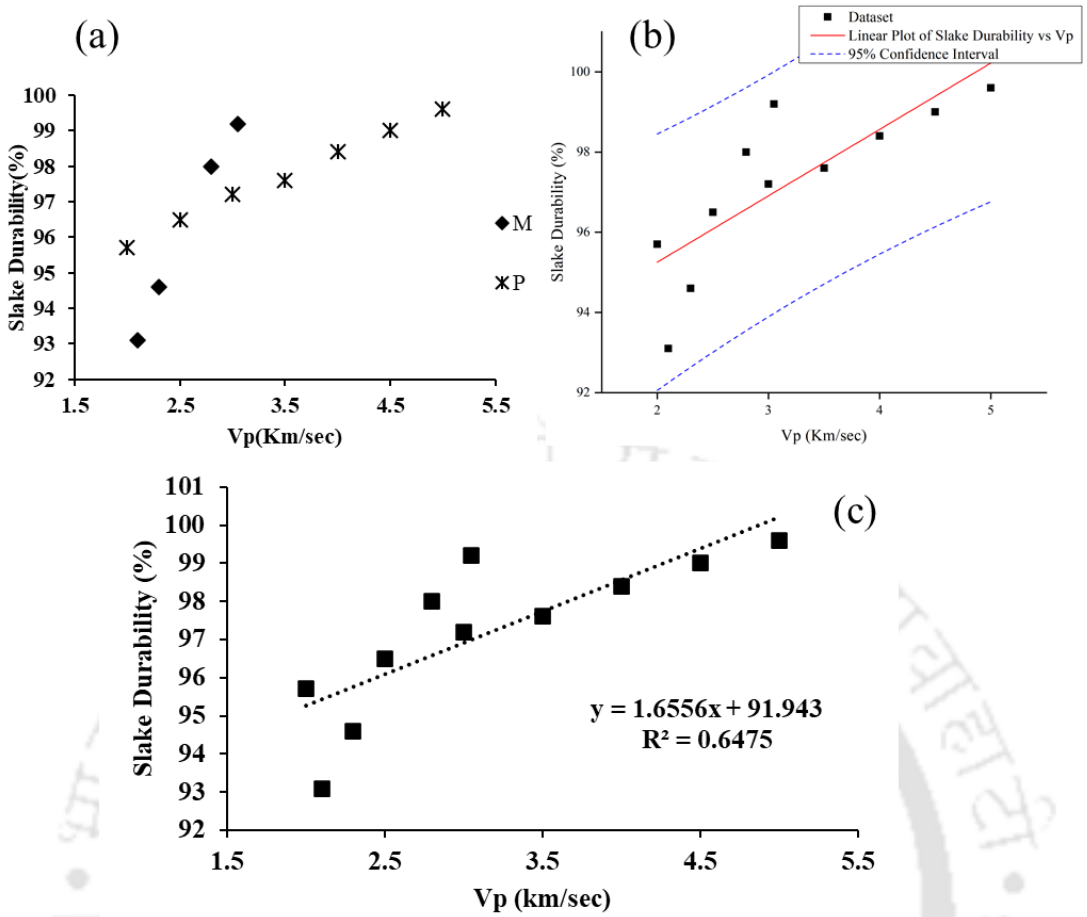


Figure 2.14 Variation of slake durability with the compressional wave velocity (a) as per studies of several researchers (b) including general trend derived from this study using simple regression analysis and confidence interval (c) data plotted showing linear nature of the relationship

Several theoretical velocity models were also reported in the literature (Assefa et al., 2003; Karakul and Ulusay, 2013) to predict $V_p$. In their study, Karakul and Ulusay (2013) reported that for rocks with high effective clay content, the utilisation of theoretical velocities is not favourable since the comparison between the theoretical Gassmann-Biot velocities and the experimental results showed inconsistency when calculated at varying degrees of saturation. Similarly, Assefa et al. (2003) reported that, for low porosity rocks, the theoretical velocities (predicted by both Gassmann and Biot theories) overestimated the measured velocities due to the negligence of rock-fluid interaction. Also, when compared to Biot- Gassmann velocity model, time average and Raymer's relationships overestimated $V_p$ (Assefa et al., 2003). Thus, it can be concluded that the use of theoretical models may yield over or under predictions.

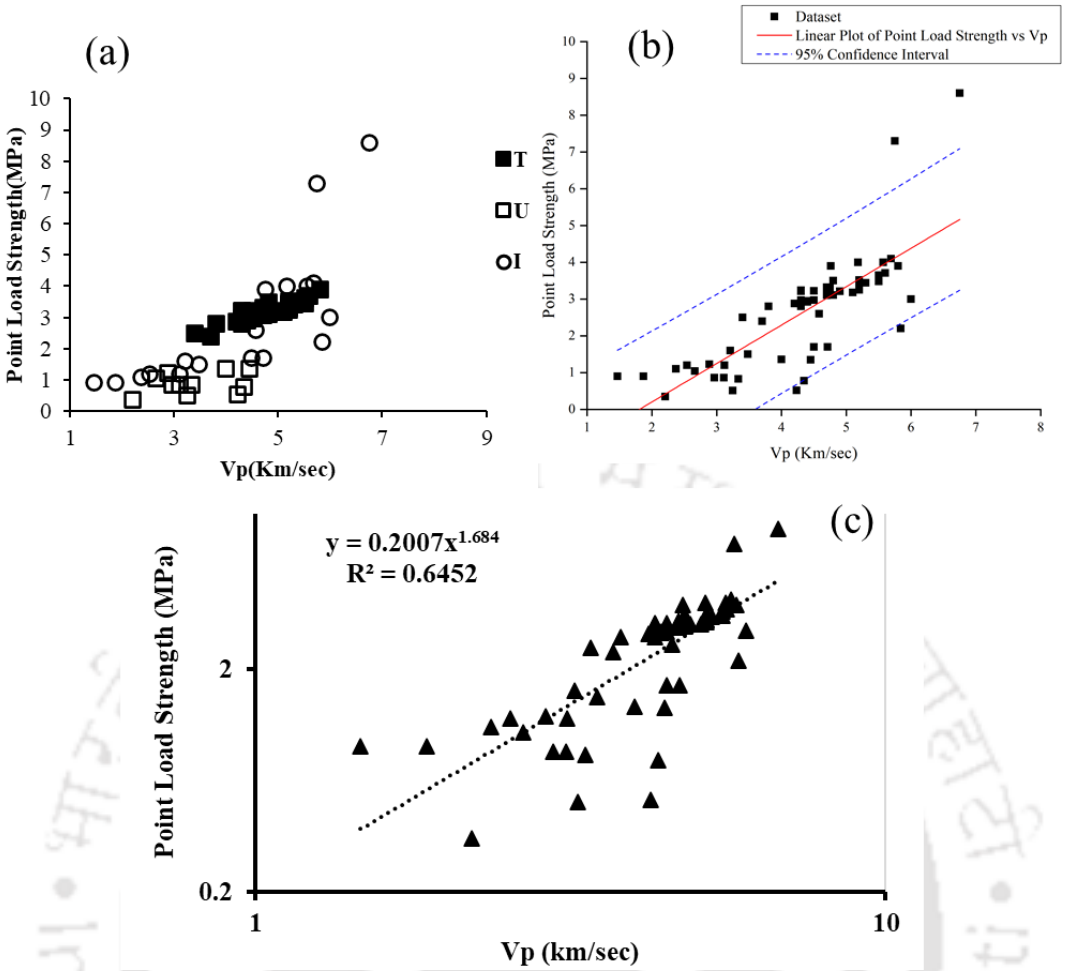


Figure 2.15 Variation of point load strength with the compressional wave velocity (a) as per studies of several researchers (b) including general trend derived from this study using simple regression analysis and confidence interval (c) data plotted on a log-log scale indicating non-linear nature of the relationship

## 2.6 Conclusions

Based on the comprehensive scrutiny from the available literature, it can be concluded that it is extremely important to focus the research towards an inclusive study incorporating the petrophysical, geological and mechanical factors so as to identify and address all the scenarios that lead to an alteration in the petrophysical, geomechanical and elastic properties of rocks. With the use of this geophysical technique, information related to exploration studies can be increased since rock types can be assessed qualitatively. The following conclusions are made from the comprehensive analysis of available datasets from the literature:

- The empirical relationships derived by various researchers are valid only to the particular dataset for which the relationship was derived. An effort is made to propose a general trend (global trends) for Porosity versus $V_p$ and Bulk density versus $V_p$, which is independent of the type of datasets. The influence of other factors like mineralogy, rock framework, pore

geometry has not been studied by the researchers in their respective studies. The factors such as chemical and mineralogical composition, the structure and geometry of the pores and the grain size also need to be taken care of while assessing the relationship between the different petrophysical properties with compressional and shear wave velocities.

- It is evident from the literature that there exists a definite link among $V_p$, $V_s$ with mechanical properties of rocks and hence, it can be considered as a dependable parameter to provide a link with these properties. It is observed that UCS, Brazilian tensile strength, point load index and E increases with an increase in $V_p$, but υ decreases. The correlation listed in this review study may be generalised for almost all types of rock and help to identify the different alterations in rock mass strength.
- The development of empirical or semi-analytical equations/models needs attention. The empirical relations established in the literature are mere site-specific (lack generalisation) and may lead to misclassification. The datasets exhibit wide ranges for velocities and geomechanical parameters. This is because there are several other parameters such as mineralogy, pore geometry, rock framework, saturation, porosity that influence these geomechanical properties. Furthermore, several trends of petrophysical, geomechanical parameters conclude that there is an undercovered trend that affects these parameters and a combined analysis involving the integration of geological, petrophysical and engineering properties (geomechanical properties) is required to understand this undercovered trend. In order to widen the acceptability of the empirical equations and to improve the existing ones, the influential parameters such as degree of saturation, effective clay content, the rock's composition (matrix), mineral constituents and void space (pore geometry/pore structure/pore architecture/pore size distribution) of the rock also need to be taken into account. Such studies should be undertaken in future research so as to understand the effects which would be favourable in interpreting the overall picture.
- The modulus obtained from ultrasonic testing only provides the modulus in the very low strain elastic range (dynamic modulus), whereas for most design purposes, modulus values are from much higher strains (static modulus), often with a strain of a percent or more. The method of testing can also have a significant effect depending on whether the strain is measured over the length and diameter of the sample or from local strain gauges such as direct contact strain gauges. The static modulus is generally lesser than the dynamic modulus, and literature establishing the correlations among the static and dynamic modulus of various varieties of rock is available.

Extensive combined analysis involving the integration of geological, petrophysical and engineering properties (mechanical properties) are presently scarce. Much attention is required to further understand and develop standard guidelines/predictions for field experimentation so as to reinforce the technique as an equally important, complementary technique.

# Chapter 3
# Laboratory Methods and Techniques for Estimation of Acoustic and Petrophysical Properties

## 3.1 Introduction

This chapter discusses the different methods and techniques used to estimate the acoustic, petrophysical and mineralogical variables in the laboratory. Sedimentary rock core plugs obtained from two different hydrocarbon-producing basins of India belonging to category I basins were used for the study. The core plugs consist of carbonates of the Bombay Offshore basin and sandstones of the Upper Assam basin, India. Figure 3.1 shows the geographical location of the sedimentary basins from where core plugs were obtained.

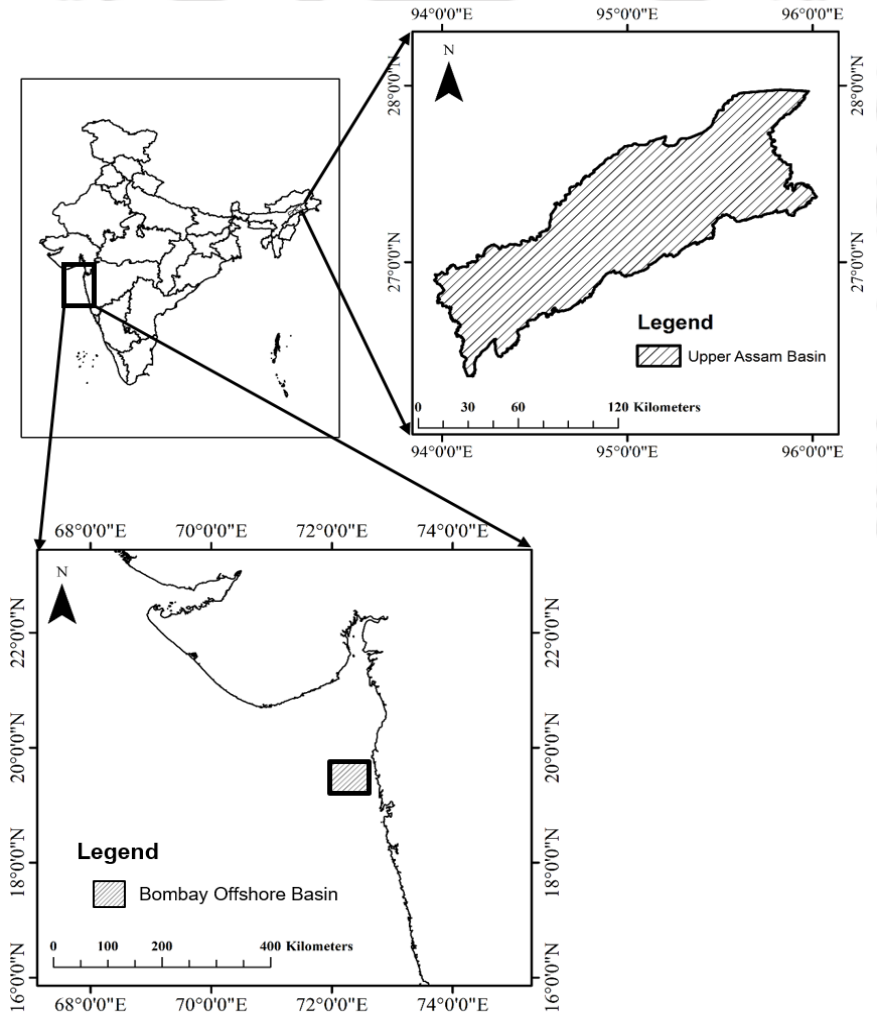


Figure 3.1 Geographical location of the Upper Assam Basin and the Bombay offshore basin (Sandstone samples are from Upper Assam Basin and Carbonates from Bombay offshore basin)

The acoustic property, $V_p$ was measured with the help of ultrasonic transducers in the laboratory, while porosity was measured with the help of a helium gas porosimeter (HGP). An in-house fabricated, semi-automated, cost-effective setup of the well-established and widely used HGP instrument was also developed to evaluate porosity for different rock types such as sandstones, carbonates and shale at a laboratory scale. Permeability was measured with the help of a nitrogen gas permeameter. The mineral content of the plugs was determined by powder XRD (X-ray Diffraction), while grain and pore diameter were quantified from digitally acquired FESEM images. The subsequent sections discuss in detail the methodology adopted for measuring the different parameters.

## 3.2 Materials and Methods

Before carrying out any analysis, all the rock core plugs were cleaned using a soxhlet extractor apparatus. The extractor helps to remove the organic content from the core plugs since a meagre amount of presence of organic compounds may alter the properties of rocks (Love et al., 2005; Matthiesen et al., 2014, 2017). The cleaned plugs would yield a more accurate analysis of the different petrophysical properties. Methanol, toluene and dichloromethane were used as chemicals. Methanol and dichloromethane were used to remove the polar and non-polar organic compounds, while toluene was used to remove the resistant, non-polar molecules (Jelavic et al., 2018). These samples were then analysed for thin section, FESEM (Field Emission Scanning Electron Microscope) and XRD analysis. In the following sections, we briefly explain the experimental procedures and data acquisition parameters by each technique.

### 3.2.1 Ultrasonic Velocity Measurements

The seismic wave propagation was reproduced in the laboratory by using the ultrasonic velocity measurement technique. Several studies conducted by Han et al. (1986), Gaviglio (1989), Klimentos (1991), Yasar et al. (2004), Kahraman and Yeken (2008), Kilic and Teymen (2008), Sarkar et al. (2012), Karakul and Ulusay (2013), Madhubabu et al. (2016) have utilised this ultrasonic velocity measurement technique to measure $V_p$ (compressional wave velocity), Vs (shear wave velocity) of different rocks in the laboratory.

In this study, ultrasonic transducers were used to measure the compressional wave velocity of the dry core specimens utilising the through transmission technique by using the PUNDIT (Portable Ultrasonic Nondestructive Digital Indicating Tester) device (Figure 3.2), by complying with the ASTM and ISRM standard guidelines. The procedure involves the following steps. Rock cores that are free of weathering, visible cracks or joints were analysed.

The length of the specimen was measured with the help of a vernier caliper and this value is fed into the device. Both the ends of the rock core plug were made flat and subsequently smoothened. Coupling gel was applied to the two opposite ends of the specimen to establish a direct contact between the specimen and the transducers by removing the air gap. The transducers were then placed on the two opposite sides of the specimen to measure the transit time and $V_p$. Transducers of varying frequencies are available ranging from 54 kHz to 1 MHz. The range of frequency of the ultrasonic transducers to be used in the laboratory or field may also influence the velocity measurement, although it is not yet highlighted in the literature. The standards (ASTM and ISRM codes) stipulate that as long as the wavelength is significantly greater than the grain size, the velocity values determined do not appear to be frequency-dependent. Additionally, the travel distance through the rock samples should be ten times the average grain size of the rock sample (ISRM 1981; Kahraman and Yeken, 2008; Fener, 2011; Karaman et al., 2015). The measurements were conducted in accordance with these guidelines. However, in the present study, it was observed that measurements with transducers of 500 kHz frequency was unable to measure velocity for coarse-grained core plugs. Therefore, for the present study, transducers of 54 kHz frequency was used for ultrasonic velocity measurements at laboratory scale.

In order to explore the influence of frequency on velocity measurements, measurements were conducted using 54 kHz and 500 kHz frequency transducers on dry rock cores of varying dimensions at ambient conditions in the laboratory. A variety of samples with different lengths and diameters were taken for analysis (Figure 3.3). The description of the analysed rock core samples that include lithology, length and diameter of all the core plugs were measured and tabulated in Table 3.1.

Figure 3.2 Determination of $V_p$ in laboratory for rock core plugs by PUNDIT setup

Figure 3.3 Core samples collected for performing ultrasonic pulse velocity measurement (A1 to A11 from left to right)

Table 3.1 Description of the rock cores used for the UPV test

| S. No | Rock Code | Lithology | Length (mm) | Diameter (mm) | Length to diameter ratio (Aspect Ratio, AR) |
|---|---|---|---|---|---|
| 1 | A1 | Sandstone | 51 | 54.6 | 0.93 |
| 2 | A2 | Sandstone | 32 | 54 | 0.59 |
| 3 | A3 | Sandstone | 33.76 | 54.6 | 0.62 |
| 4 | A4 | Sandstone | 30.4 | 54.9 | 0.55 |
| 5 | A5 | Sandstone | 55.7 | 56 | 0.99 |
| 6 | A6 | Sandstone | 30 | 54.5 | 0.55 |
| 7 | A7 | Sandstone | 70.4 | 48.3 | 0.77 |
| 8 | A8 | Sandstone | 37.45 | 25.14 | 1.49 |
| 9 | A9 | Sandstone | 56.11 | 25.45 | 2.20 |
| 10 | A10 | Carbonate | 73.05 | 25.29 | 2.89 |
| 11 | A11 | Carbonate | 47.33 | 25.41 | 1.86 |

The range of $V_p$ values obtained for different samples by using transducers of two different frequencies were plotted in the form of a histogram, as shown in Figure 3.4. The highest and lowest recorded $V_p$ was 3174 m/s (for sample A11) and 1920 m/s (for sample A5) for 54 kHz transducer, while 3371 m/s (for sample A11) and 2126 m/s (for sample A5) for 500 kHz transducer, respectively. Bulk density was also measured for all the samples, as shown in Figure 3.5, and it ranges from 1.89 to 2.54 g/cc.

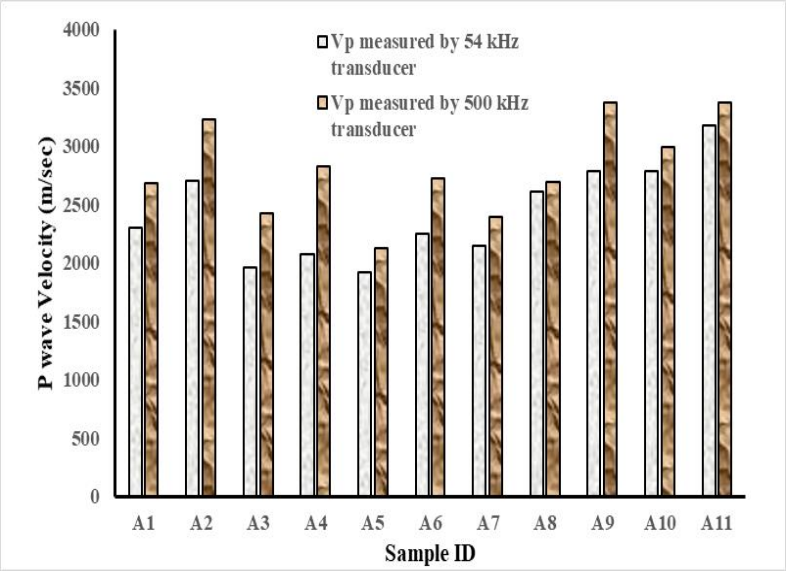


Figure 3.4 Ultrasonic pulse velocity values of the sandstone and carbonate samples used in the study measured by 54 kHz and 500 kHz transducers

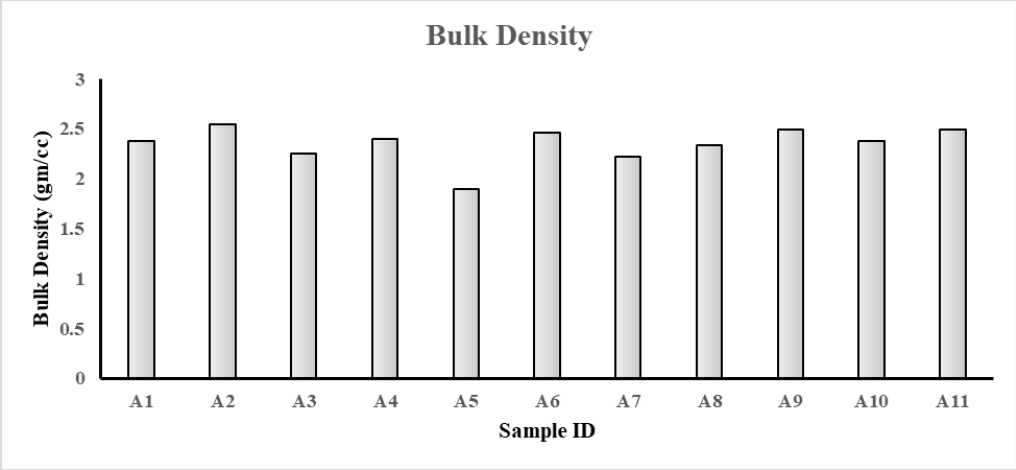


Figure 3.5 Bulk density of the sandstone and carbonate samples used in the study

Velocity measurements could not be obtained for all the core plugs by transducers of 500 kHz frequency. Hence, rock samples were selected, which gave velocity measurements by 500 kHz frequency transducer (Figure 3.5). Obtained data through both 54 kHz and 500 kHz frequency transducers were statistically analysed using a least square regression method. $UPV_{54kHz}$ and $UPV_{500kHz}$ were correlated using regression analysis, and it was observed that $R^2$ obtained was 0.76 (Figure 3.6). The measurements done by using 500 kHz transducers gave higher velocity measurement values than 54 kHz transducers, and the percentage increase varied from 3 to 36%.

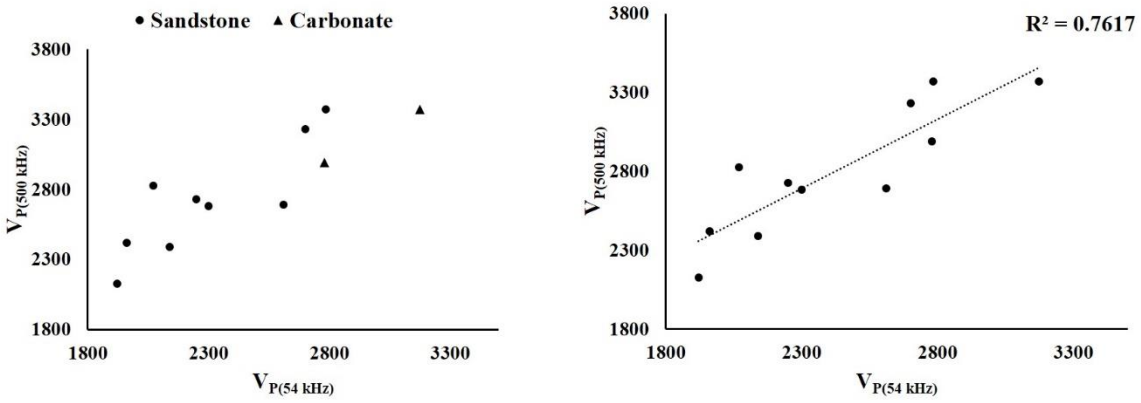


Figure 3.6 Correlated ultrasonic pulse velocity values of the sandstone and carbonate samples used in the study measured through 54kHz and 500 kHz transducer

The 500 kHz frequency transducers were not capable of measuring velocity for coarse-grained samples only, however, this aspect may further be investigated with velocity measurements on a large dataset of samples of varying grain sizes. Therefore, for the present study, transducers of 54 kHz frequency was used for ultrasonic velocity measurement at laboratory scale since it was capable of measuring Vp for all the available carbonate and sandstone rock core plugs.

### 3.2.2 Measurement of Petrophysical Properties

The petrophysical properties of the specimens, which include bulk density, porosity, permeability, mineral content and pore diameter, were evaluated by established standard laboratory methods. The bulk volume was obtained by vernier caliper measurements. Mass of the specimen was measured with the help of a weighing balance sensitive to 0.001 g. Pore diameters were calculated with the help of FESEM images. With the help of a helium gas porosimeter, parameters such as grain volume, grain density and porosity were measured. Permeability was measured with the help of a nitrogen gas permeameter. The subsequent sections describe in brief the methodology adopted for the measurement of different properties.

### 3.2.3 Porosity Measurement

Helium gas porosimeter, a widely known conventional method, was used to measure the porosity of rock core plugs in the laboratory. This method is based on the principle of Boyle's law. Gas volume changes within a known volume of the sample chamber can be monitored with respect to pressure changes. By equilibrating the pressure of the sample chamber to that of the reference chamber, it is the helium gas volume that is equilibrated. Therefore, the setup measures the grain volume of the rock core placed in the sample chamber. Bulk volume is

measured by other methods like vernier caliper. Thereafter porosity ($\phi$) is measured as the ratio of pore volume to bulk volume.

$$\phi = \frac{V_b - V_s}{V_b} \tag{3.1}$$

where $V_b$ is the bulk volume and $V_s$ is the grain volume of the rock samples.

## 3.3 Development and Optimisation of In-House Fabricated, Semi-Automated Helium Gas Porosimeter

Porosity in petroleum reservoirs is considered to be one of the most significant petrophysical properties since it is used to determine hydrocarbon reserves and also used for reservoir description (Korte et al., 2017; Pal et al., 2018, 2020). Knowledge of the porosity of porous mediums such as sandstones and carbonates is substantial in understanding their structural stability and efficiency as petroleum reservoirs on account of their economic potential. Porosity and pore size distribution plays a vital role in assessing the formation, its structure, and potential of any reservoir since it affects the physical properties of a reservoir and influences significantly other properties such as elastic wave velocities, elastic moduli, permeability, dielectric constant (Yu et al., 2016; Garia et al., 2019), geo-mechanical behaviour, fluid transport, and controls its interaction with the surrounding rocks (Sarkar et al., 2012; Garia et al., 2020). For studies related to the hydrocarbon industry involving economic and scientific inferences, porosity plays a central role in assessing the ability of reservoir rock to estimate its capability of storing and transmitting hydrocarbons (Assefa et al., 2003; Fusi and Martinez-Martinez, 2013). An analytical understanding is required in order to estimate reservoir volume and to evaluate its producibility. The hydrocarbons are stored in these microscopic void spaces (pores) and flow out of the rock through the connected pore structure. Therefore, precise porosity measurement is significant for resource evaluation and reserve calculations, especially in petroleum reservoirs. This becomes essentially important considering the high heterogeneity and complex pore structure of the rocks, especially in the case of carbonates. Moreover, mere perception or qualitative understanding is not sufficient, and it needs to be quantified. For scientific and engineering purposes, precise quantitative assessment of the pore structure is an elementary prerequisite for a wide variety of fields varying from materials engineering to earth sciences (Yu et al., 2016).

According to IUPAC (International Union of Pure and Applied Chemistry), the pore space in the rock is categorised into three scales, namely micro-pores, meso-pores and macro-pores (Sing, 1985). The pore space is classified as micro-pores if the pore diameter is less than 2 nm,

meso-pores if the pore diameter ranges between 2-50 nm, and macro-pores if the pore diameter is greater than 50 nm (Sing, 1985). Due to the existence of these multiple scales of pore types in rocks, a range of different testing methods has been developed to address the complexity and investigate the pore spaces. These methods can be broadly classified as- adsorption or expansion technique comprising of Boyle's Law porosimetry and BET (Brunauer–Emmett–Teller) analysis; Archimedian porosimetry comprising of fluid saturation/impregnation; mercury porosimetry comprising of mercury intrusion porosimetry; and Image analysis method comprising of analysis of LOM (Light Optical Microscope) and SEM (Scanning Electron Microscope) images (Anovitz and Cole, 2015; Zou and Malzbender, 2016). These different methods depend on completely different physical principles, which lead to different advantages and limitations in applications. Some methods, namely gas expansion, water saturation, mercury intrusion, measure the effective porosity (open or connected pores) while some, namely image analysis, gas adsorption, measures both the ineffective porosity (isolated/closed pores) and effective porosity part of the rock (Zou and Malzbender, 2016). Different authors utilised these different methods or techniques in the literature for porosity or pore volume calculation or pore size distribution of geological samples. For instance, Kahraman and Yeken (2008), Karakul and Ulusay (2013), Zargari et al. (2015), Kurtulus et al. (2016) used water saturation techniques for calculating porosity. This method, based on Archimedes' principle, is an inexpensive and simple method in operation to measure effective porosity. However, such a method fails to furnish any information regarding pore space distribution. One of the major shortcomings of the water saturation method is that the measurements may be inconsistent if clay content is present in the rock since water may react with the clay. However, other fluids like kerosene and ethanol may be used to eliminate this shortcoming (Kuila, 2013; Zou and Malzbender, 2016). Mercury porosimetry method is another technique that detects effective porosity and also measures the pore size distribution. Bakke and Øren (1997), Haines et al. (2015), Gaboreau et al. (2016), Zargari et al. (2015), Hemes et al. (2015) utilised mercury injection capillary pressure (MICP) analysis in their respective studies. However, this method is destructive to samples (Zou and Malzbender, 2016). Also, the mercury intrusion porosimetry technique does not measure the porosity associated below the minimum pore throat diameter of 3.6 nm accessible by mercury (Kuila 2013). Another method that measures the pore size distribution is the $N_2$ and $CO_2$ adsorption and BET surface area analysis. Zargari et al. (2015), Gaboreau et al. (2016) and Wei et al. (2016) used the BET surface area analysis in their respective studies. Nitrogen adsorption is a reliable technique but with a pore size limitation of 1.7-200 nm (Kuila, 2013). An alternative method to measure both the connected (effective)

and isolated (ineffective) porosity is the image analysis method; however, this method fails to discriminate between these two isolated and effective type porosity. Desbois et al. (2011), Haines et al. (2015), Liu et al. (2017), Korte et al. (2017) and Jin et al. (2017), used this digital image analysis technique in their respective studies. Another well-established and widely used method for estimating porosity is the helium gas porosimeter method. Han et al. (1986), Phillips et al. (1989), Klimentos (1991), Assefa et al. (2003), Haines et al. (2015), Archilha et al. (2015), Sayed et al. (2015) and Kassab and Weller (2015) used helium gas porosimeter method for estimating the effective porosity in their respective studies. This method is based on Boyle's law gas transfer technique that involves filling the pores of the porous material with helium gas under specific gas pressure. Such a method is useful since helium gas is inert in nature and has high diffusivity (Anovitz and Cole, 2015). As a result, its tiny molecules rapidly penetrate the small pores of the rock core samples and do not adsorb on rock surfaces as air may do (Beeson, 1950). The other advantages are that the samples remain contamination-free after testing, unlike in other test techniques like mercury intrusion porosimetry, where the sample recovery to its original state is difficult or lost, i.e., the sample may become non-reusable. Also, the duration to conduct this test is very short compared to other fluid saturation or impregnation methods where indifferent saturation or impregnation period may vary and thus result in a variation in results since full saturation time (complete impregnation of the pore network) is ambiguous. Hence, these advantages of the helium gas porosimeter make it a well-established and widely used method for performing porosity measurements on different porous geological samples. Figure 3.7 presents a summary of different methods along with the applicability ranges of each of these methods. Each technique has its applicability, advantage and limitation when assessing porosity values for a wide range of geological samples, as already discussed earlier.

In this study, we demonstrate an in-house fabricated, semi-automated, cost-effective setup of the well-established and widely used helium gas porosimeter (HGP) instrument to evaluate porosity for different rock types such as sandstones, carbonates and shale at a laboratory scale. The need to fabricate a well-established porosimeter aroused due to the highly inflamed cost of existing commercial helium gas porosimeters. The setup was calibrated by using four different steel cylinders of known volume. These steel cylinders are used to ensure that the known volume is of the steel with 0% porosity. Hence, the porosity measurements obtained were standardised on the basis of these steel cylinders with 0% porosity. The other salient features of the existing setup involve its ability to perform measurements on samples of different dimensions up to NX (54 mm) core size, thereby increasing the applicability without

requiring any extra sample holder as required in an industry-based porosimeter. When compared to other contemporary methods and techniques, the existing setup is developed and fabricated at a relatively lower cost. The results obtained by this fabricated setup gave satisfactory results when compared with industry-based porosimeter. The samples remain contamination-free even after testing. It is thereby suggested that by virtue of its cost-effectiveness and adaptability in measuring different ranges of samples of known volume, the current setup is best suited for applications involving conventional reservoir characterisation based on porosity values.

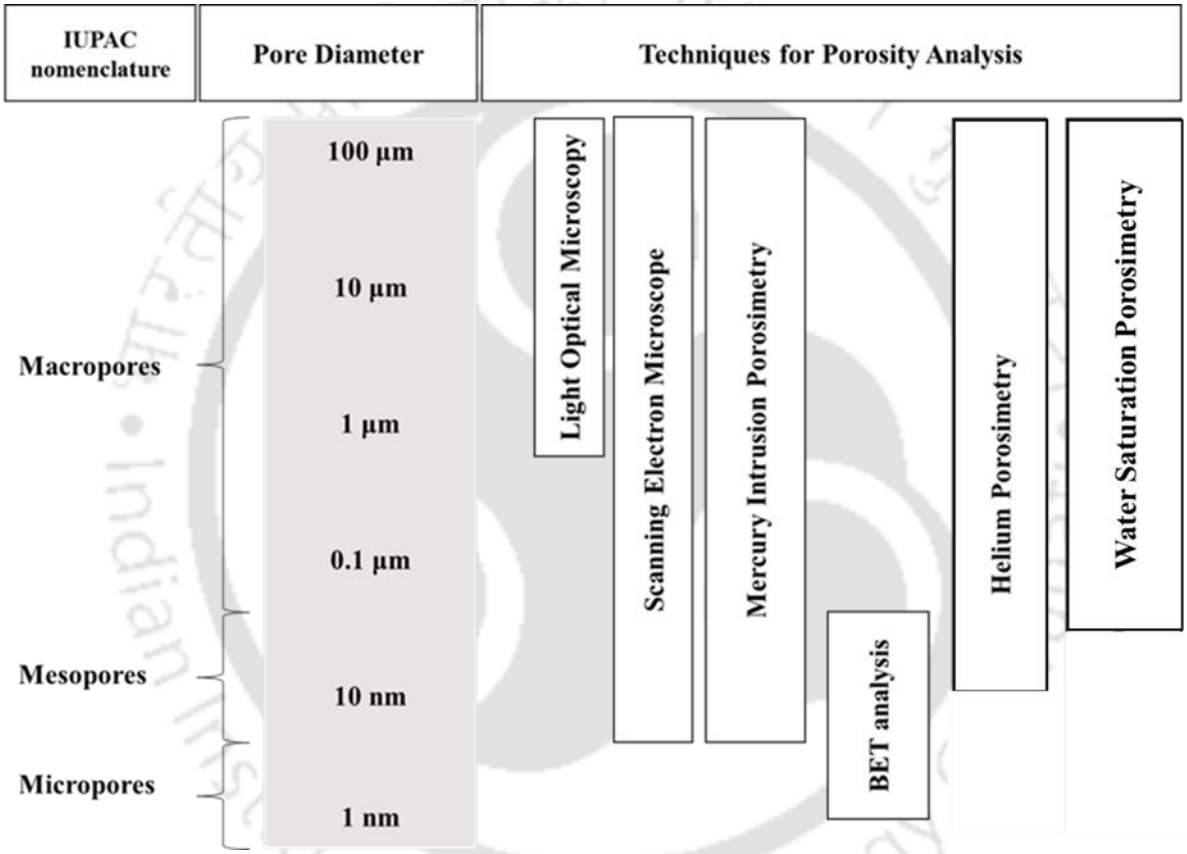


Figure 3.7 Different methods used for the determination of porosity with their applicability ranges (modified from Anovitz and Cole, 2015)

### 3.3.1 Instrument Setup

The helium gas porosimeter setup comprises two chambers, namely the reference chamber and sample chamber made up of stainless steel. The rock specimen for the porosity measurement is kept in the sample chamber. Both the chambers have 58 mm diameter and 107 mm height and are connected by a SS pipe of 12 mm diameter. Two metal valves are placed, one at the beginning and another in between both the chambers, to control the flow of gas. The two manometers are attached at two ends, i.e. one at the entry-level and the other one adjacent to

the sample chamber. The two stationed manometers can read pressure values up to 150 psi and 60 psi, respectively.

Figure 3.8 presents the schematic diagram of the helium gas porosimeter setup. The volume of the reference chamber ($V_{ref}$) and the sample chamber ($V_{sam}$) are kept identical. $P_1$ is the manometer reading at the beginning (reference pressure) (kept constant at 100 psi), while $P_2$ is the manometer reading after the stabilisation of pressure (equilibrated pressure reading) after opening the second valve. Figure 3.9 shows the actual working helium gas porosimeter setup as elaborated in this study.

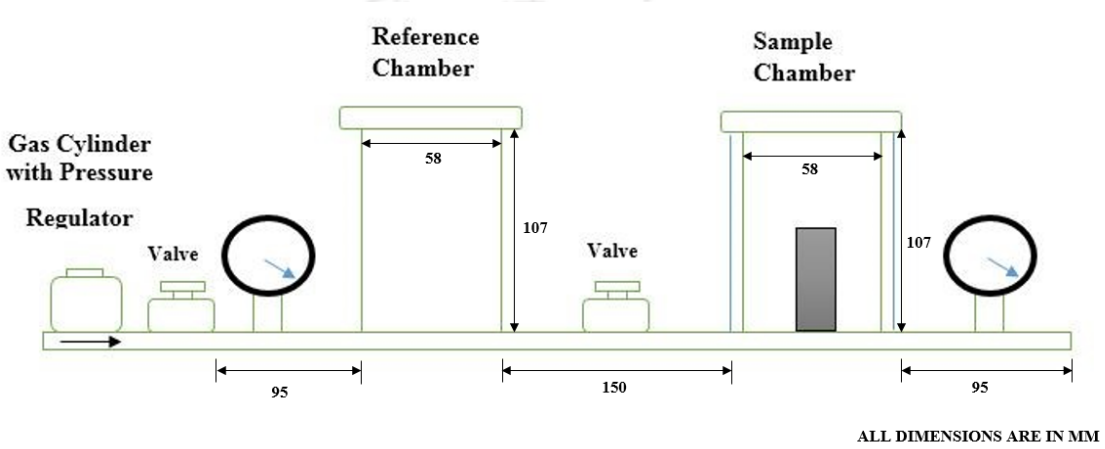


Figure 3.8 Schematic diagram showing the working of Helium Gas Porosimeter (HGP) setup

Figure 3.9 Helium Gas Porosimeter (HGP) setup as elaborated in this study

### 3.3.2 Operating Scientific Principle

The operating scientific principle of the helium gas porosimeter (HGP) setup is based on Boyle's law. The current setup measures porosity on the basis of the measurement of grain volume. This grain volume is evaluated based on the drop in pressure, which in turn is due to the change in volume. The volume of the reference chamber is denoted as $V_{ref}$ and the volume of the sample chamber is denoted as $V_{sam}$. The helium gas is allowed to enter these chambers at controlled pressure through the steel pipe connecting the gas cylinder, reference chamber and sample chamber. The pressure of the helium gas before entering the reference chamber is denoted as $P_1$ and the pressure at the end of the sample chamber is denoted as $P_2$. When a porous specimen is kept in the sample chamber, the pressure drop (difference in the pressure $P_1$ and $P_2$) is a measure of the pore volume of the specimen. Equations (3.2) and (3.3) demonstrate the methodology to estimate porosity as per Boyle's law.

$$P_1 V_{ref} = P_2 (V_{ref} + V_{sam} - V_s) \tag{3.2}$$

$$V_s = \frac{(P_2 V_{ref} + P_2 V_{sam} - P_1 V_{ref})}{P_2} \tag{3.3}$$

where $V_s$ is the volume of grains (solids) in the rock, $V_{ref}$ is the reference chamber volume, $V_{sam}$ is the sample chamber volume, $P_1$ and $P_2$ are the pressure before and after (at equilibrium) opening the valve. Therefore, the above-described technique gives the solid volume of the sample. However, it is to be noted that the gas penetrates only into the open (effective) volume of the rock. A vernier caliper may be used to calculate the bulk volume ($V_b$). Porosity ($\phi$) can therefore be calculated as follows-

$$\phi = \frac{V_b - V_s}{V_b} \tag{3.4}$$

### 3.3.3 Experimental Procedure

Based on the principle discussed above, the helium gas is initially contained in a reference chamber with known $P_1$ and $V_{ref}$. This chamber is connected to a sample chamber through a valve that, when opened, allows the helium gas to expand into this sample chamber, which contains the sample, allowing the pressure to equilibrate to a new value $P_2$ ($P_2$ is noted when it equilibrates). This equilibration in pressure depends upon the available space in the sample chamber, which in turn depends on how much of the sample chamber is filled with solid rock particles. For each plug sample, the measurements were repeated three times, and the pressure

readings were the same (no fluctuations from the obtained value were observed). The pressure readings did not change as and when the test was repeated for the particular sample. The measurement procedure is summarised in the flowchart (Figure 3.10).

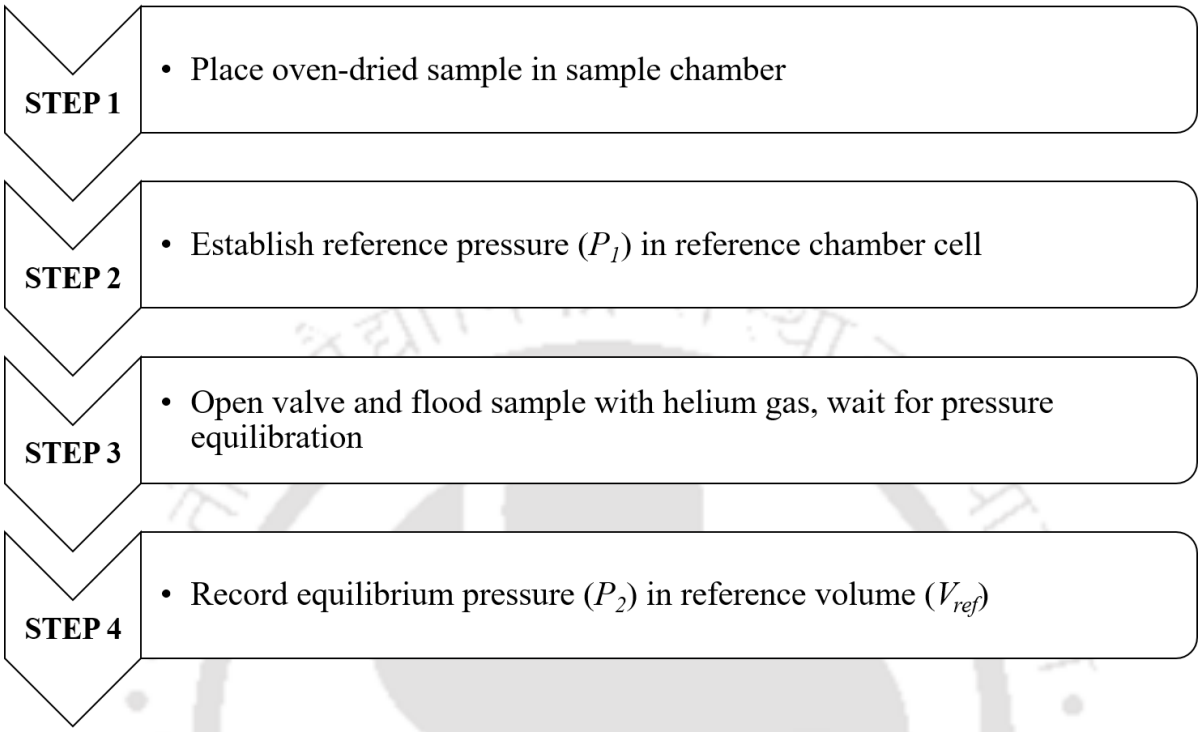


Figure 3.10 Flowchart showing the measurement procedure for the HGP setup

The HGP setup is intended to perform grain volume and porosity measurements for porous geological materials like sandstone, carbonate and shale rocks. However, to obtain results with a higher degree of accuracy and precision, certain controls are maintained in the setup. These include pressure control, leakage control and temperature control. These controls are discussed below in the subsequent sections.

The measurement conducted by the current HGP setup had to be compared with that of a commercial HGP used in the industry for validation and for checking the accurateness of the results generated by the setup. Hence, all the measurements were conducted at 100 psi with the current HGP setup for the present study. The instrument is capable to perform measurements up to 150 psi. Moreover, a higher pressure may introduce leakages (slow leaks) from the joints, which are presently controlled in the setup.

The second control is related to leakage. The pressure control and duration of the test do not introduce the leakage factor into account. The joints remained intact during the course of the experiment.

The third control, i.e., temperature control factor, is not accounted for since all the experiments were conducted at ambient conditions in the laboratory.

For precise and accurate working of the setup, the components essential include- a high precision gas pressure manometer, a zero displacement volume valve and an ideal gas medium. The first two components are a part of the structural design details. The sensitivity of the results largely depends upon the precision of the manometer readings. By making repeated measurements of pressure readings, the precision limits were reduced, and the uncertainty of porosity measurement was, thus, significantly lowered. The other component, that is, the gas medium, is a crucial part of the porosimeter. Stable composition and density, negligible reactivity (especially for adsorption) with porous material are the essential characteristics of the gas medium. Helium gas satisfies the following criteria. The porosimeter setup has been used for analysis on carbonates of the Bombay offshore basin and sandstones of the Upper Assam basin. Both these basins are known to be prolific hydrocarbon producers for decades in India (Rao and Talukdar, 1980; Mathur, 2014).

### 3.3.4 Calibration

For calculating porosity based on grain volume from the setup, four steel cylinders of known volume were used for calibration of the setup. Figure 3.11 shows the reference cylindrical samples of 35 mm diameter, each with varying lengths of 25 mm, 50 mm, 75 mm and 90 mm. These steel cylinders are used so as to ensure that the known volume (Table 3.2) is of the steel with 0% porosity. Each of these steel cylinders was placed in the sample chamber one by one, and the manometer readings were noted for an initial pressure of 100 psi till the pressure equilibrates. Considering the grain volume to be equal to bulk volume, i.e. $V_s=V_b$ (0% porosity) for steel cylinders, the pressure $P_2$ was calculated as per equation (3.3). This calculated pressure ($P_{calculated}$) obtained from equation (3.3) is plotted against observed pressure ($P_{observed}$) readings for an initial pressure of 100 psi as shown in the calibration curve (Figure 3.12). This calibration curve is used for correcting the pressure readings obtained for different porous rock core plugs to obtain the actual pressure values, which would indicate the actual grain volume and porosity of the samples under investigation. A python-based code was also developed for obtaining straightforward results by the use of this setup, which makes it semi-automated, rapid and convenient to operate.

Table 3.2 Reference steel cylinder details used for calibration purpose in this study

| Name | Dimensions, cm | | Mass, g | Volume, cc | Density, g/cc |
|---|---|---|---|---|---|
| | Diameter | Length | | | |
| A | 3.5 | 2.5 | 188.401 | 24.04 | 7.836 |
| B | 3.5 | 5.0 | 376.555 | 48.081 | 7.831 |
| C | 3.5 | 7.5 | 565 | 72.121 | 7.833 |
| D | 3.5 | 9.0 | 678 | 86.546 | 7.834 |

Figure 3.11 Reference steel cylinders used for calibration purpose in this study

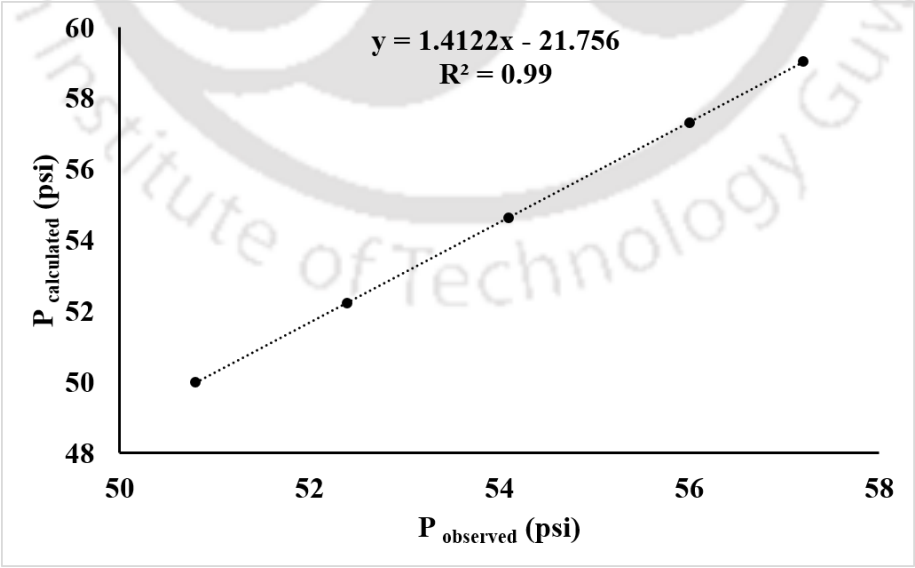


Figure 3.12 Calibration curve generated for the setup by pressure equilibration for an initial pressure of 100 psi with varying grain volume

### 3.3.5 Sources of Error in the Setup

The sources of error in the setup may be due to the error associated with the measurement of bulk volume of the specimen. To account for these errors, caliper measurement was taken at three different locations of the core plug, i.e. at the top, middle and bottom portion. The average of these dimensions was done to minimise this source of error. Calibration, as discussed earlier, was also performed.

### 3.3.6 Pressure Sensitivity Analysis

The pressure sensitivity analysis was performed for the setup by calculating the grain volume of different steel cylinders subjected to a range of initial pressures from 50 to 150 psi (50, 60, 70, 100, 110, 120, 130, 150 psi). The calibration procedure was adopted as explained earlier. Based on this analysis, a generalised trend was derived for the setup, as shown in Figure 3.13.

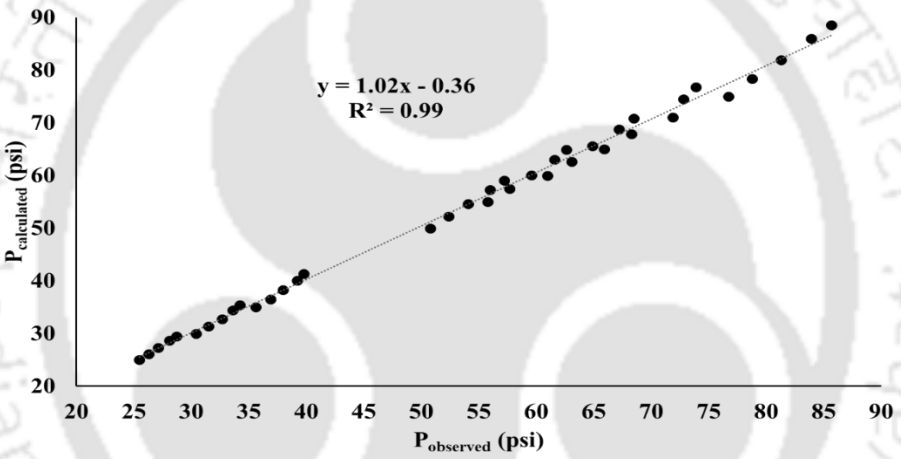


Figure 3.13 Sensitivity analysis for different range of initial pressures including general trend derived for the setup

## 3.4 Porosity Measurements by In-House Fabricated Helium Gas Porosimeter

The fabricated setup should be capable of measuring porosity accurately for all the range of samples of different grain volume, i.e., the effect of grain volume should not affect the porosity calculation. The grain volume of the steel cylinders was calculated by subjecting the different steel cylinders to the same initial pressure of 100 psi. The plot between calculated and observed pressure (Figure 3.12) shows a high coefficient of determination ($R^2$=0.99), indicating better accuracy of the fabricated setup. Moreover, the sensitivity of the instrument to varying initial pressures was also analysed and $R^2$ was observed to be 0.99 (Figure 3.13). Considering the calibration curve for an initial pressure of 100 psi (Figure 3.12), the grain volume, bulk volume

and the porosity of carbonate and sandstone rock core plugs, measured using the HGP setup, are presented in Tables 3.2 and 3.3. The range of porosity values for carbonates vary from a minimum value of 3.22% to a maximum value of 29.383%, whereas for sandstones, porosity values vary from a minimum value of 4.777% to a maximum value of 28.438%.

Table 3.3 Compilation of different parameters obtained for carbonate rock core plugs by the setup

| S. No. | Sample ID | $P_2$, psi | Grain Volume, cc | Bulk Volume, cc | Corrected | | |
|---|---|---|---|---|---|---|---|
| | | | | | $P_2$, psi | Grain Volume, cc | Porosity, % |
| 1 | C1 | 53 | 32.004 | 36.7 | 53.089 | 32.903 | 10.345 |
| 2 | C2 | 51.8 | 19.647 | 20.51 | 51.394 | 15.345 | 25.180 |
| 3 | C3 | 51.8 | 19.647 | 19.83 | 51.394 | 15.341 | 22.614 |
| 4 | C4 | 53.2 | 34.009 | 36.91 | 53.371 | 35.721 | 3.220 |
| 5 | C5 | 52.3 | 24.864 | 24 | 52.100 | 22.801 | 4.999 |
| 6 | C6 | 51.7 | 18.591 | 17.32 | 51.253 | 13.831 | 20.150 |
| 7 | C7 | 52.8 | 29.983 | 37.65 | 52.807 | 30.055 | 20.171 |
| 8 | C8 | 52.5 | 26.924 | 36.43 | 52.383 | 25.725 | 29.383 |
| 9 | C9 | 53.1 | 33.008 | 35.89 | 53.230 | 34.316 | 4.385 |
| 10 | C10 | 52.1 | 22.789 | 25.11 | 51.818 | 19.842 | 20.977 |

Table 3.4 Compilation of different parameters obtained for sandstone rock core plugs by the setup

| S. No. | Sample ID | $P_2$, psi | Grain Volume, cc | Bulk Volume, cc | Corrected | | |
|---|---|---|---|---|---|---|---|
| | | | | | $P_2$, psi | Grain Volume, cc | Porosity, % |
| 1 | S1 | 52.3 | 24.864 | 29.03 | 52.101 | 22.801 | 21.46 |

| | | | | | | | |
|---|---|---|---|---|---|---|---|
| 2 | S2 | 52 | 21.746 | 24.9 | 51.677 | 18.352 | 26.298 |
| 3 | S3 | 52.1 | 22.789 | 25.6 | 51.818 | 19.843 | 22.489 |
| 4 | S4 | 51.9 | 20.698 | 23.55 | 51.536 | 16.853 | 28.438 |
| 5 | S5 | 52.7 | 28.967 | 36.85 | 52.665 | 28.619 | 22.334 |
| 6 | S6 | 52.4 | 25.896 | 31.01 | 52.242 | 24.266 | 21.745 |
| 7 | S7 | 52.2 | 23.829 | 25.35 | 51.959 | 21.325 | 15.876 |
| 8 | S8 | 52 | 21.746 | 20.5 | 51.677 | 18.351 | 10.479 |
| 9 | S9 | 52.3 | 24.864 | 28.52 | 52.101 | 22.801 | 20.055 |
| 10 | S10 | 52 | 21.746 | 23.49 | 51.677 | 18.351 | 21.874 |
| 11 | S11 | 51.8 | 19.647 | 19.32 | 51.395 | 15.346 | 20.571 |
| 12 | S12 | 52.6 | 27.948 | 28.54 | 52.525 | 27.177 | 4.777 |
| 13 | S13 | 51.9 | 20.699 | 18.59 | 51.536 | 16.853 | 9.344 |
| 14 | S14 | 53.1 | 33.009 | 36.11 | 53.231 | 34.316 | 4.968 |

From the porosity values obtained, it is observed that sandstone core plugs have higher porosity values than carbonate rock core plugs. Figures 3.14 and 3.15 show the porosity and grain density measurement results obtained for carbonates and sandstones by the setup, respectively, in the form of histogram plots.

To check the accuracy of the porosity measurements, all the samples were also tested in a commercial helium gas porosimeter used in the petroleum industry. A cross-plot between the two measurements showed a strong coefficient of determination $R^2 = 0.98$ for carbonates and $R^2=0.95$ for sandstones, as shown in Figure 3.16.

For estimating the error involved in the grain volume measurement of the rock sample by the setup, a statistical method was used. The error analysis involved taking into consideration the cumulative effect of (i) change in manometer pressure reading (least count of 0.1 psi) and (ii) change in volume of the sample measured by a vernier caliper (least count of 0.02 mm). The error was measured by repeatedly doing the same experiment by varying the readings in accordance with the least count (considering both positive and negative fluctuations from the

actual value). This accommodates all combinations of errors associated with the measurement. Based on this analysis, carbonate and sandstone samples show an error of 0.37% and 0.55%, respectively, as shown in Figure 3.17.

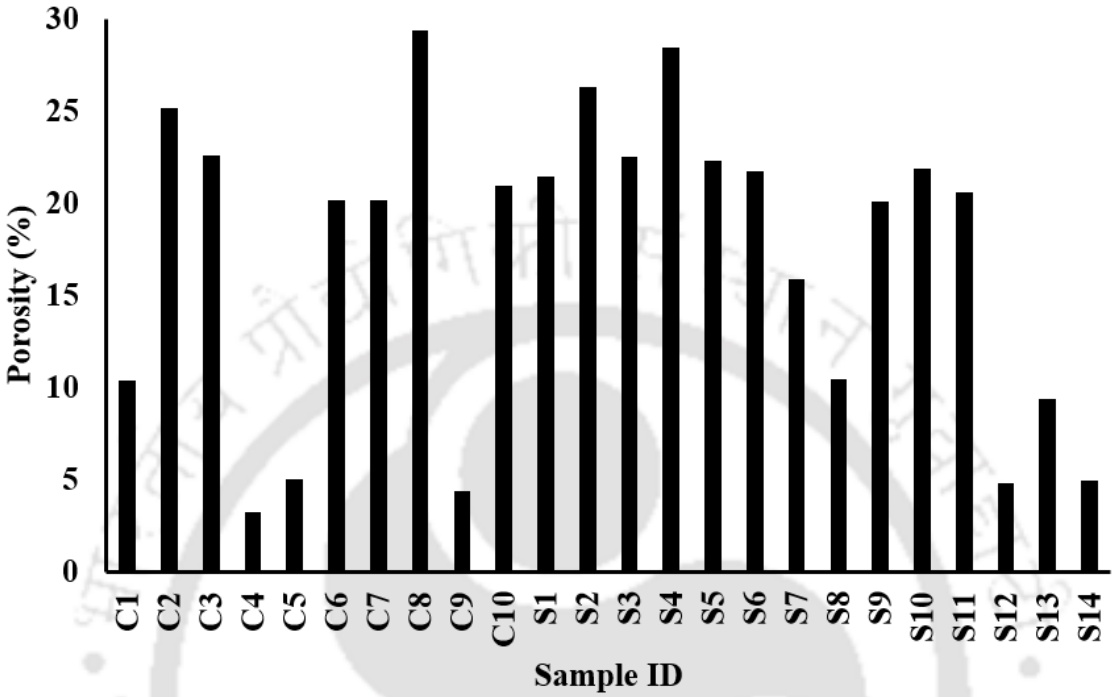


Figure 3.14 Porosity measurement results obtained for carbonates and sandstones by the setup

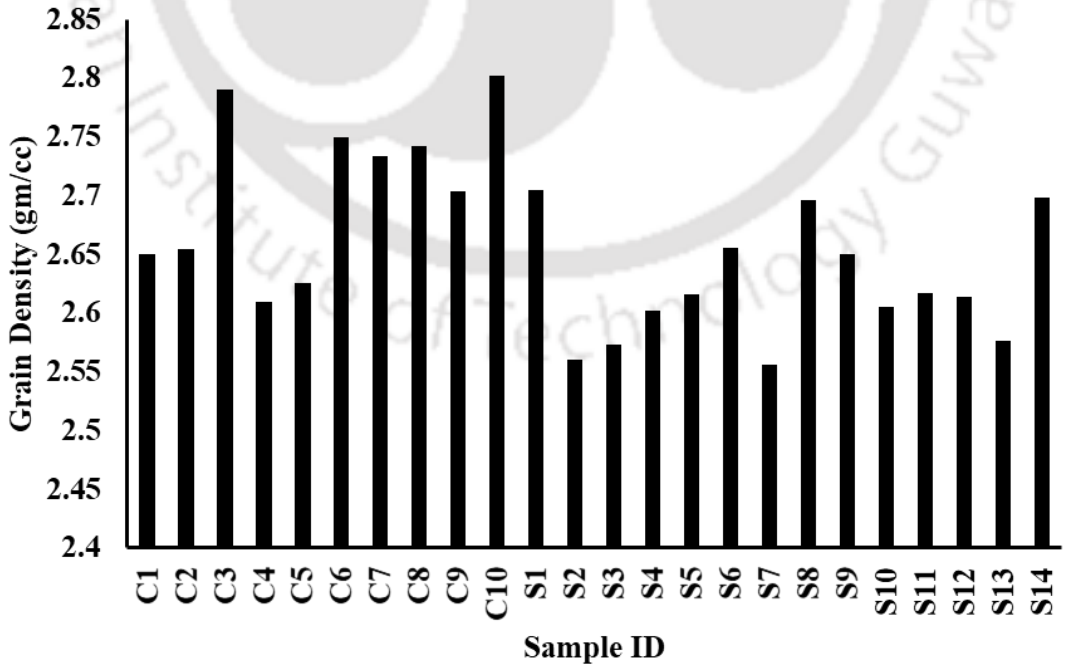


Figure 3.15 Grain density measurement results obtained for carbonates and sandstones by the setup

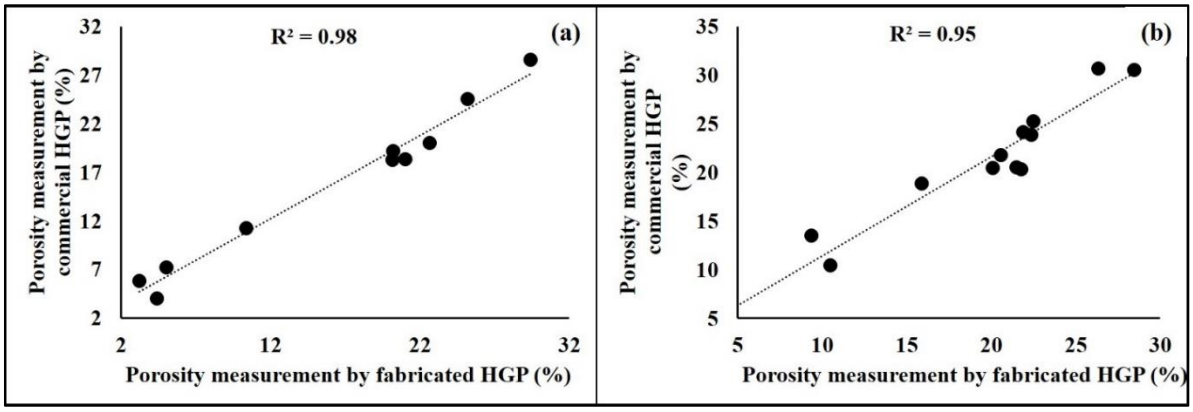


Figure 3.16 Plot showing the relationship between porosity measurements obtained from commercial helium gas porosimeter and the fabricated Helium Gas Porosimeter (HGP) setup for (a) carbonates and (b) sandstones

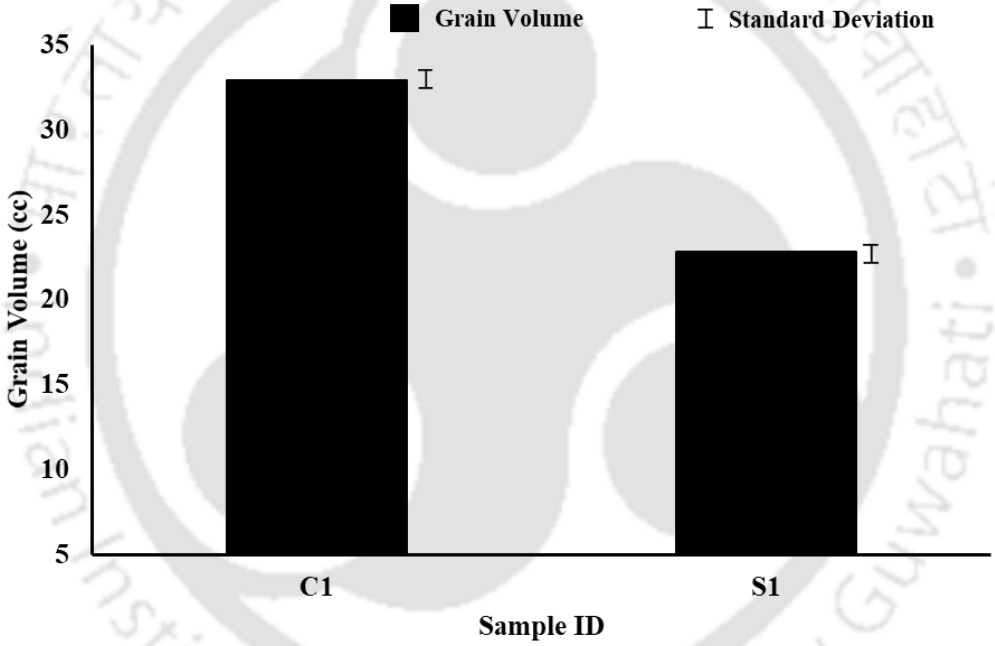


Figure 3.17 Grain volume measurements obtained for carbonates and sandstones by the setup and its associated error (0.37 % for carbonate and 0.55 % for sandstone)

Two dominant petrophysical variables, porosity measured through the setup and bulk density, were plotted together. For estimating bulk density, the mass of the sample was measured by a weighing balance with a least count of 0.001 g and the volume was measured by a vernier caliper with a least count of 0.02 mm. Bulk density was thus obtained by dividing the mass and the volume. A graph is plotted between porosity (%) and bulk density (g/cc) as shown in Figure 3.18. The plot so generated shows a decrease in porosity with an increase in bulk density, with $R^2$= 0.96, for both carbonate (Figure 3.18a) and sandstone samples (Figure 3.18c). This trend thus shows the generality in the correlations that relate these two petrophysical variables, i.e.,

an inverse relationship between these two. Similarly, a graph is plotted between porosity (%) and grain density (g/cc) for carbonate (Figure 3.18b) and sandstone samples (Figure 3.18d). However, it is to be noted that the influence of other factors such as mineralogy also affects the petrophysical properties of sedimentary rocks. The porosity values so obtained from the apparatus is in range with the porosity ranges obtained by other researchers for the same sedimentary basins. For the Bombay offshore sedimentary basin, the porosity values for carbonate rocks were observed to be 15-20% (Schön, 2015), while for the Upper Assam basin, the values were between 7-30% (Wandrey, 2004b).

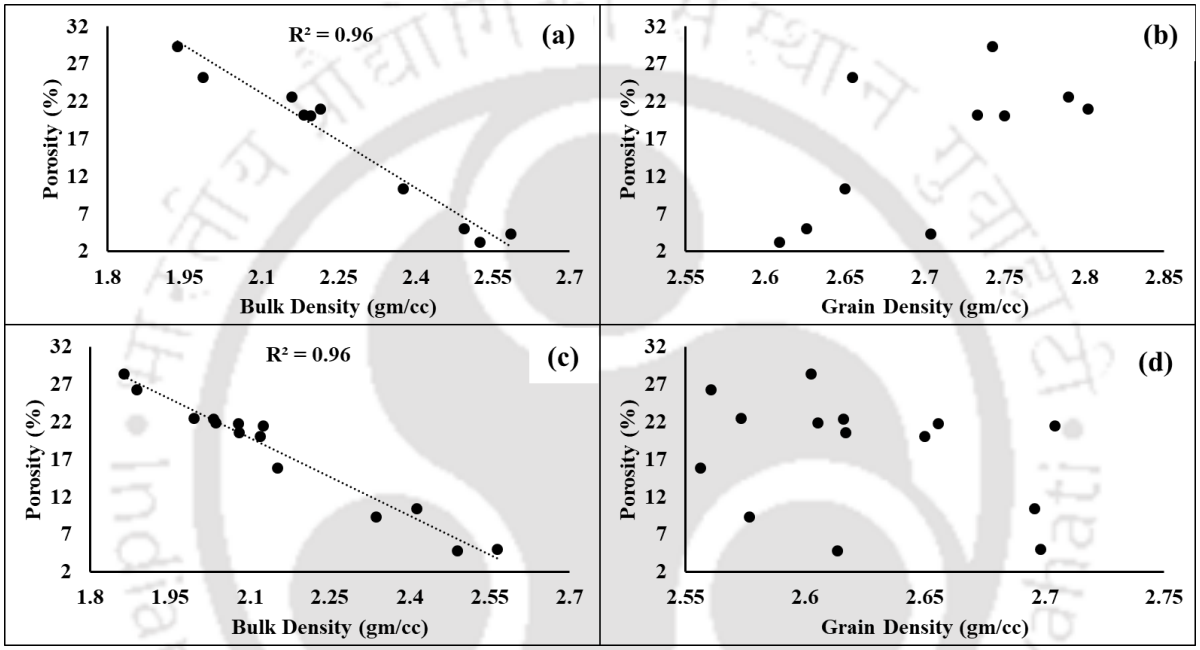


Figure 3.18 Cross plot depicting the relationship between bulk density, grain density with porosity obtained by the setup for (a) carbonates and (b) sandstones

The experimental results generated by the use of this HGP setup provides satisfactory results when compared with the industry-based commercial instrument with a strong coefficient of determination $R^2$ = 0.98 for carbonates and $R^2$=0.95 for sandstones. It is to be noted that under ideal conditions, the measurements conducted by the fabricated HGP setup and industry-based porosimeter should be similar with $R^2$ = 1. However, a study conducted by Dotson et al. (1951) investigated a porosity check program for porosity measurements conducted by five different laboratories on ten different samples and observed variations within the same measurement method. The variations in porosity measurements may occur, however, these are expected to agree within the same order of magnitude (Dotson et al., 1951). For the present study, this criterion is fulfilled by the existing setup with a strong coefficient of determination obtained on the analysis of a comprehensive dataset of carbonate and sandstone rocks.

The equipment can be used for estimating grain volume and porosity measurements for any size of sandstone, carbonate and shale rock core samples, provided the volume of the sample under investigation is known. Apart from being economical, the semi-automated setup reduces the time of conducting laboratory measurements, and the sample remains free from any contamination. This makes the setup suitable for research purposes. These samples may further be used for other petrophysical, geomechanical examinations.

## 3.5 Permeability Measurement

The steady-state method has been recognised as the standard method to evaluate permeability in the laboratory of intact rock cores/plugs (Li et al., 2009; Amann-Hildenbrand et al., 2012, 2013). This method, based on Darcy's law, is found to be an accurate and reliable technique for conventional rock samples (Sander et al., 2017). Steady-state permeability is a permeability measured when fluid passing through the core sample has a steady flow rate for some constant pressure difference applied across the core sample. Darcy's law can be described as:

$$Q = \frac{kA}{\mu}\frac{dp}{dx} \tag{3.5}$$

where Q is volumetric flow rate, dp/dx is pore pressure gradient, μ is viscosity, k is intrinsic permeability (sometimes referred as absolute or true permeability) and A is cross-sectional (flow-through) area.

## 3.6 Image Analysis

For investigating the pore architecture of rocks, FESEM analysis was performed. A small, clean and dry chip of the rock core plug was taken and then coated with gold to improve the electron emission. A beam voltage of 10kV was used when acquiring FESEM images under the backscattered electron mode for all samples (make- Zeiss and model- Sigma). The obtained FESEM images for all the samples were further analysed to measure the pore, grain diameter and aspect ratio.

The pore diameter values were quantified from digitally acquired FESEM images using Fiji – ImageJ, an open-source image-processing and analysis software for multiple platforms (Kuva et al., 2012). The representative FESEM image was thresholded to identify the mineral matrix and pores accurately by setting appropriate threshold values (Shen et al., 2015). The optimal threshold value was achieved by comparing the binary image with the actual image. The pore diameter of every pores visible inside the image has been quantified, taking all the pore area and assuming the pores as cylindrical (Torskaya et al., 2014). The built-in standard

measurement of ImageJ's "Analyze particles", such as the diameter of a circle of equal projection area (Mazzoli and Favoni, 2012), was chosen, on the basis of previous papers found in the literature (Walton, 1948; Al-Thyabat and Miles, 2006; Igathinathane et al., 2009). The proposed method is precise, rapid and reproducible (Mazzoli and Favoni, 2012).

## 3.7 Mineralogical Study

The petrographic analysis was carried on all the samples using optical microscopy. Optical microscopy in transmitted light was performed on thin sections of carbonates. A polarised light microscope (Make: Olympus, Model: BX51) equipped with a camera and dedicated image analysis software (stream start) for evaluating the microfabric parameters were employed.

## 3.8 X-Ray Powder Diffraction Analysis

The mineral content of the plugs was determined by powder XRD (X-ray diffraction) using Rigaku TTRAX III diffractometer with Ni-filtered CuKα radiation. Specimens were prepared by grinding and sieving of the samples with sieve size 75 microns. Powders obtained from each sample were analysed with a PANanalytical diffractometer. The mineral phases were determined by using the X'Pert Highscore Plus software based on the ICDD powder diffraction file of PDF 2 (Abouelresh, 2017; Nikolakopoulos et al., 2018). The semi-quantitative analysis obtained through interpretation software X'Pert high score gave information on the relative amount of different minerals present based on the peak intensities.

## 3.9 Regression Analysis

The results obtained by performing different analyses on samples required regression analysis to determine meaningful interrelationships among the variables and build predictive models. The petrophysical properties, mineralogical content, $V_p$ were plotted to predict and understand the relationship among these properties by using multivariate regression analysis. It is a statistical approach that integrates supplementary independent variables in the predictive equation (Balan et al., 1995). In a general sense, multivariate regression analysis can be adopted to formulate a mathematical model between input and output variables. Hence, the multivariate statistics technique was employed to achieve the best-fit relationships amongst different properties that have a coherent relationship. Since a one-to-one correlation would have either under-estimated or over-estimated the results, therefore, this approach of analysing the data set by means of multivariate analysis was adopted. Mathematically, it can be expressed as –

$$Y = a_0 + a_1X_1 + a_2X_2 + ..... + a_nX_n \quad (3.6)$$

where Y is the dependent or output variable, $X_1$ to $X_n$ are independent, or input variables and $a_0$ to $a_n$ are the regression coefficients.

Equation (3.6) can also be illustrated as [Response] = [mean (depending on $X_1$, $X_2$, …., $X_n$)]. The least-square method was used to fit the equation (Johnson and Wichern, 2002; Montgomery et al., 2012). The regression coefficients $a_0$, $a_1$,…, $a_n$ can be estimated by minimising the sum of squares of differences: $\sum (Y_i - a_0 - a_1 X_1 - a_2 X_2 - \ldots - a_n X_n)^2$ (Johnson and Wichern, 2002). There are several accessible software packages that solve such problems (Balan et al., 1995), and R software was employed in the present study (R Core Team (2013)).

## 3.10 Fragmented Analysis of Major Mineral Constituents and Saturation Conditions for Rock Mass Classification Based on $V_p$

Since there are multiple parameters that alter the elastic and mechanical properties of sedimentary rocks, an attempt is made to introduce and then analyse its variability with some of the mechanical properties. Since rock is composed of multiple minerals, so varying the amount of these major minerals would reflect the change in $V_p$, and this change in $V_p$ could thereby be related to get an inference on a certain property under investigation. For instance, in sandstones, the major minerals present include quartz and feldspar, while for carbonates, the major minerals present include calcite and dolomite. These minerals have certain parameter values such as $V_{p\ quartz}$ = 6.057 km/s, $V_{p\ feldspar}$ = 4.68 km/s, $V_{p\ calcite}$ = 6.259 km/s, $V_{p\ dolomite}$ = 6.93 km/s (Simmons, 1965; Nur and Simmons, 1969; Domenico, 1984; Mavko et al., 2009). These values are the maximum, i.e. for zero porosity. Similarly, the other parameter values such as Vs, density, υ, K, G and E for these minerals are tabulated in Table 3.5 (References- Simmons 1965; Nur and Simmons 1969; Domenico 1984; Mavko et al., 2009).

For changing $V_p$, the density of material was varied by changing the mineralogy of the rock as well as the saturation of pores. Thus, we assume several volume percentages of these minerals so as to change the density of the material. For sandstones, the volume percentage was varied from 75% quartz and 25% feldspar to 100% quartz and 0% feldspar content. Similarly, for carbonates, volume percentage was varied from 75% calcite and 25% dolomite to 100% calcite and 0% dolomite content. Based on these varying volume mineral percentages, $V_p$ was calculated as-

$$(V_{Quartz}) \times (Vp_{Quartz}) + (V_{Feldspar}) \times (Vp_{Feldspar}) = Vp \tag{3.7}$$

$$(V_{Calcite}) \times (Vp_{Calcite}) + (V_{Dolomite}) \times (Vp_{Dolomite}) = Vp \tag{3.8}$$

where, $V_{Quartz}$, $V_{Feldspar}$, $V_{Calcite}$ and $V_{Dolomite}$ are the volume percentage (in fraction) of these minerals.

These equations are based on the Voigt averaging (isostrain conditions) (Brocher, 2005), which may overestimate the velocities of the mixtures. At any given volume fraction of constituents, $V_p$ will fall between the bounds, but its precise value depends on the geometric details. Since the geometric details of the datasets in the literature are not known, hence allowable theoretical range of seismic velocity values or the upper bound values were computed by using Voigt averaging method. Other methods like Voigt–Reuss–Hill average can also be used. Moreover, various studies (Ji et al., 2006; Ji et al., 2007; Johnston and Toksoz, 1980) may be referred to estimate the different parameters based on phenomenological approach.

The tabulated datasets of $V_p$ obtained by varying the volume percentage of major minerals for sandstones and carbonates are presented in Table 3.7. Doing such an exercise would provide the range of $V_p$ values for different proportions of quartz and feldspar content for sandstones, calcite and dolomite content for carbonates, which would help in understanding the variability of major minerals with $V_p$. The common aim is to construct a template that honours the data (known data) and extends the interpretation to unknown situations in different exploration cases. Table 3.6 compiles $V_p$ and Bulk Moduli values for some fluids (Schön, 2015)).

In order to forecast the effective elastic moduli of a mixture of grains and pores, Hashin-Shtrikman-Walpole bounds (Berryman, 1995; Walpole, 1966) was used for evaluating bulk and shear moduli (K and G, refer equations 3.9- 3.12). Thereafter, E was calculated by using equation 3.16. The range of datasets of E and $V_p$ obtained by varying the volume percentage of major minerals for sandstones and carbonates, with a porosity variation from 2% to 40% for different geological scenarios (fluid saturations - water, gas, brine and oil-saturated) is provided as an annexure (Table S1). The formulation of Hashin-Shtrikman-Walpole bounds (Berryman 1995) are presented in the form of equations -

$$K^{HS+} = \wedge(G_{max}), \tag{3.9}$$

$$K^{HS-} = \wedge(G_{max}), \tag{3.10}$$

$$G^{HS+} = \Gamma(£(K_{max}, G_{max})), \tag{3.11}$$

$$G^{HS-} = \Gamma(£(K_{min}, G_{min})) \tag{3.12}$$

Where,

$$\wedge(z) = \left\{ \frac{1}{K(r) + \frac{4}{3}z} \right\}^{-1} - \frac{4}{3}z \tag{3.13}$$

$$\Gamma(z) = \left\{ \frac{1}{G(r) + z} \right\}^{-1} - z \tag{3.14}$$

$$£(K,G) = \frac{G}{6}\left\{ \frac{9K + 8G}{K + 2G} \right\} \tag{3.15}$$

$$E = \frac{9KG}{G + 3K} \tag{3.16}$$

The brackets {.} in equations 3.13-3.15 specify an average over the medium (which is similar to average over the constituents weighted by their volume fractions).

Based on the obtained values of K and G, the £ parameter was calculated {£($K_{max}$, $G_{max}$) and £($K_{min}$, $G_{min}$)}. Since $G_{min}$=0, hence, theoretically lower bound E=0. If the low Hashin-Shtrikman bound is zero for Young's modulus, it does not mean that this bound does not exist. This means that the bounds are wide, and the modulus may vary within 200%. Hence, the upper bound is plotted in Figure 4(d). Different clusters or trends of data can be interpreted or classified based on this plot. The plot may also be useful for understanding or extracting values for similar geological conditions as well as to understand the variability for conditions that are yet to be explored for interpreting potential moduli values or $V_p$ values.

To analyse the effect of mineralogy on Poisson's ratio (υ), the volume percentage of major minerals were varied, and $V_p$ was calculated based on equation 3.8. Thereafter υ was calculated as-

$$(V_{Calcite}) \times (\upsilon_{Calcite}) + (V_{Dolomite}) \times (\upsilon_{Dolomite}) = \upsilon \tag{3.17}$$

The tabulated datasets of υ and $V_p$ obtained by varying the volume percentage of major minerals for sandstones and carbonates are presented in Table 3.7. A theoretical model represented in the form of equation 3.17 was used to analyse the effect of mineralogy on Poisson's ratio. The limitation of this model is that it does not take into account the effect of porosity and pore geometry.

Table 3.5 Table illustrating different parameter values for different minerals (these values are the maximum (zero porosity)) (References- Simmons 1965; Nur and Simmons 1969; Domenico 1984; Mavko et al., 2009)

| **Minerals** | **$V_p$ (km/s)** | **Vs (km/s)** | **Density (g/cc)** | **Poisson's Ratio** | **Bulk Modulus K (GPa)** | **Shear Modulus G (GPa)** | **Young's Modulus E (GPa)** |
|---|---|---|---|---|---|---|---|
| Quartz | 6.057 | 4.153 | 2.65 | 0.08 | 37 | 44 | 95 |
| Calcite | 6.259 | 3.243 | 2.71 | 0.316 | 76.8 | 32 | 84.2 |
| Dolomite | 6.93 | 4.23 | 2.87 | 0.202 | 76.4 | 49.7 | 119.4 |
| Feldspar | 4.68 | 2.39 | 2.56 | 0.32 | 37.5 | 15 | 39.6 |
| *$V_p$ variation* | | | | | | | |
| $V_p$ order | Mineralogy | | *Dolomite > Calcite > Quartz > Feldspar* | | | | |
| $V_p$ order | Fluids | | *Brine>Water >Oil>Gas* | | | | |

Table 3.6 Compressional wave velocity and Bulk Moduli values for some fluids (Schön, 2015)

| **Fluids** | **$V_p$ (km/s)** | **Bulk Modulus K (GPa)** |
|---|---|---|
| Brine | 1.635 | 2.6 |
| Water | 1.5 | 2.2 |
| Oil | 1.2 | 1.1 |
| Gas | 0.6 | 0.1 |

Table 3.7 Tabulated datasets of Poisson's ratio and $V_p$ obtained by varying the volume percentage of major minerals for sandstones and carbonates

| **SANDSTONES** | | | | **CARBONATES** | | | |
|---|---|---|---|---|---|---|---|
| **Fraction of Quartz** | **Fraction of Feldspar** | **$V_p$ (=$V_{pmatrix}$)** | **Poisson's ratio (υ)** | **Fraction of Calcite** | **Fraction of Dolomite** | **$V_p$ (=$V_{pmatrix}$)** | **Poisson's ratio (υ)** |
| 0.75 | 0.25 | 5.71275 | 0.14 | 0.75 | 0.25 | 6.42675 | 0.2875 |
| 0.8 | 0.2 | 5.7816 | 0.128 | 0.8 | 0.2 | 6.3932 | 0.2932 |
| 0.85 | 0.15 | 5.85045 | 0.116 | 0.85 | 0.15 | 6.35965 | 0.2989 |
| 0.9 | 0.1 | 5.9193 | 0.104 | 0.9 | 0.1 | 6.3261 | 0.3046 |

| | | | | | | | |
|---|---|---|---|---|---|---|---|
| 0.95 | 0.05 | 5.98815 | 0.092 | 0.95 | 0.05 | 6.29255 | 0.3103 |
| 1 | 0 | 6.057 | 0.08 | 1 | 0 | 6.259 | 0.316 |

As discussed above, by using the formulation of Hashin-Shtrikman-Walpole bounds (Berryman, 1995), it was found that an upper bound is prevailing. Based on this, the variation of E with $V_p$ is analysed, and the template is presented in Figure 3.19. This template can be used to predict the elastic properties for different geological scenarios that include water-saturated, gas saturated, brine saturated, and oil saturated conditions for sandstones and carbonates along with the literature dataset (Kurtulus et al., 2016 – label T (refer Table 2.7), Kilic and Teymen, 2008 – label I (refer Table 2.7) and Madhubabu et al., 2016 – label U (refer Table 2.7)).

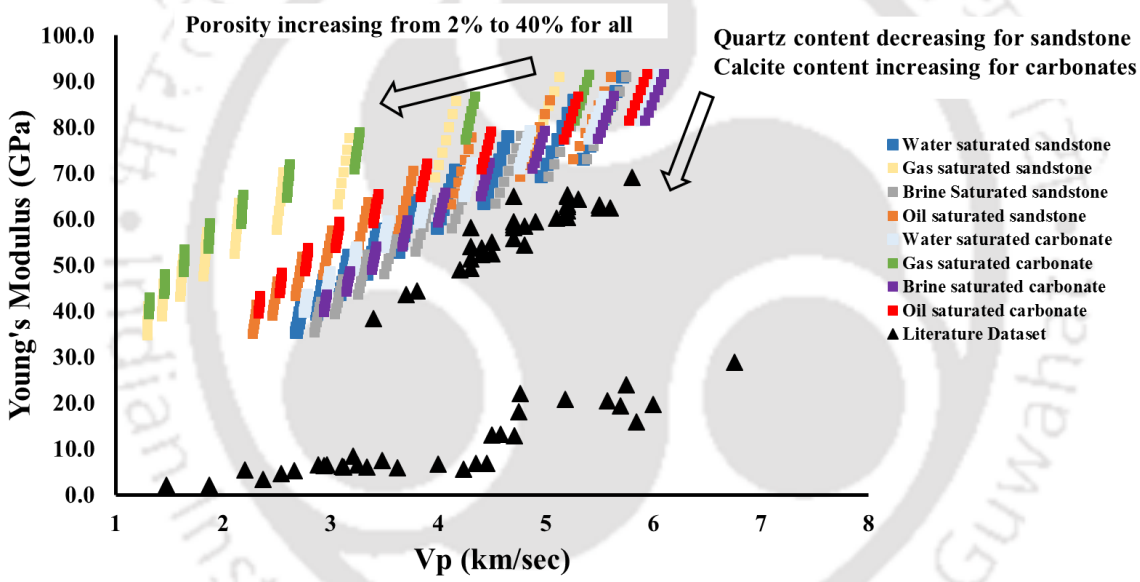


Figure 3.19 Graphical representation of E versus $V_p$ for different geological scenarios along with incorporating the effect of varying porosity and mineral composition, including literature dataset

The plotted datasets highlight several salient features-

- With an increase in porosity from 2 to 40%, there is a decrease in E and $V_p$ values for all types of saturation scenarios for sandstones and carbonates.
- With an increase in quartz content and subsequent decrease in feldspar content in sandstones, E and $V_p$ increases (owing to the higher density of quartz mineral as compared to feldspar mineral); while for carbonates, with an increase in calcite content and

subsequent decrease in dolomite content, E and $V_p$ decreases (owing to the higher density of dolomite mineral as compared to calcite mineral).

- Carbonates have a higher value of E and $V_p$ than sandstones (higher density of minerals found in carbonates than sandstones) for all particular set of saturation conditions.
- More or less, there is an approximate 50% reduction in $V_p$ and E values for a porosity increase from 2 to 40%.

Similarly, the $V_p$ values, so obtained by the fragmented analysis were plotted in Figure 3.20 for literature dataset of UCS-$V_p$ plot (Kurtulus et al., 2016; Moradian and Behnia, 2009; Pappalardo, 2015; Parent et al., 2015; Sarkar et al., 2012; Sharma and Singh, 2008; Soroush et al., 2011; Yasar and Erdogan, 2004) and Figure 3.21 for indirect tensile strength- $V_p$ plot (Kilic and Teymen, 2008; Kurtulus et al., 2016; Soroush et al., 2011). The marked rectangles show the range of $V_p$ values for sandstones (5.7 km/s to 6 km/s – Table 3.7) and carbonates (6.25 km/s to 6.43 km/s – Table 3.7) when considering the effect of varying mineral contents.

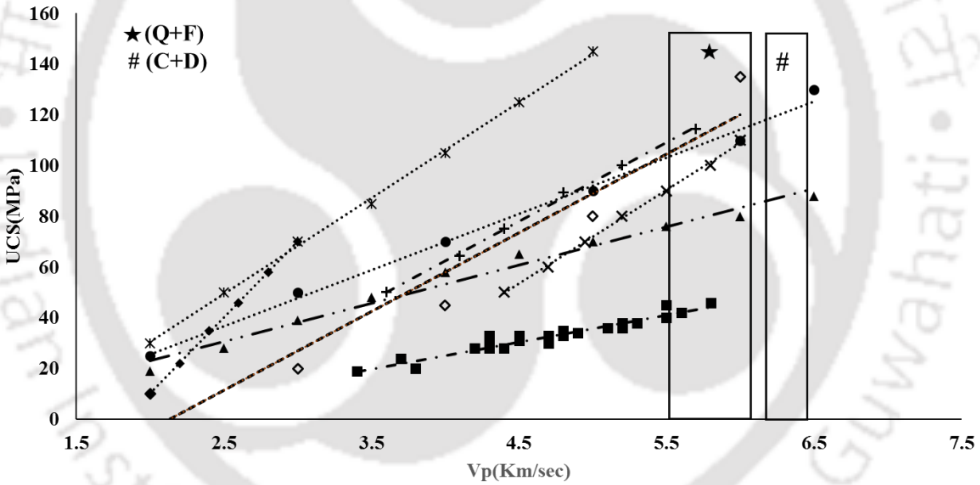


Figure 3.20 Graphical representation of UCS versus $V_p$, as reported by different researchers along with their trend line. The marked rectangle shows the range of $V_p$ values for sandstones (5.7 km/s to 6 km/s) when considering the effect of varying mineral contents (* major minerals Q-quartz and F- feldspar with varying proportions (75 % Q,25 % F, 80 % Q,20 % F, till 100 % Q, 0 % F), while for carbonates, $V_p$ varies from 6.25 km/s to 6.43 km/s for varying major minerals (# C- calcite and D- dolomite) proportions (100 % C, 0 % D till 75 % C,25 % D)

Additionally, to account for the mineralogy effect on $V_p$, the generated dataset of $V_p$- υ were plotted with the existing dataset from the literature (Kurtulus et al., 2016; Mavko et al., 2009), as shown in Figure 3.22. The circled part depicts the decrease in Poisson's ratio values with a decrease in calcite and an increase in dolomite content, thereby highlighting the effect of mineral content on $V_p$ values and thus on Poisson's ratio (Table 3.7). Moreover, the effect of

porosity, clay content (if present) was not considered, which may also add to the dispersion in the values. The influence of porosity on υ of natural rocks are limited due to the lack of experimental data over different porosity and pore geometry ranges (Yu et al., 2016). However, studies (Dunn and Ledbetter, 1995; Wang et al., 2009; Yu et al., 2016) provide a comprehensive review on υ and may be referred for further study.

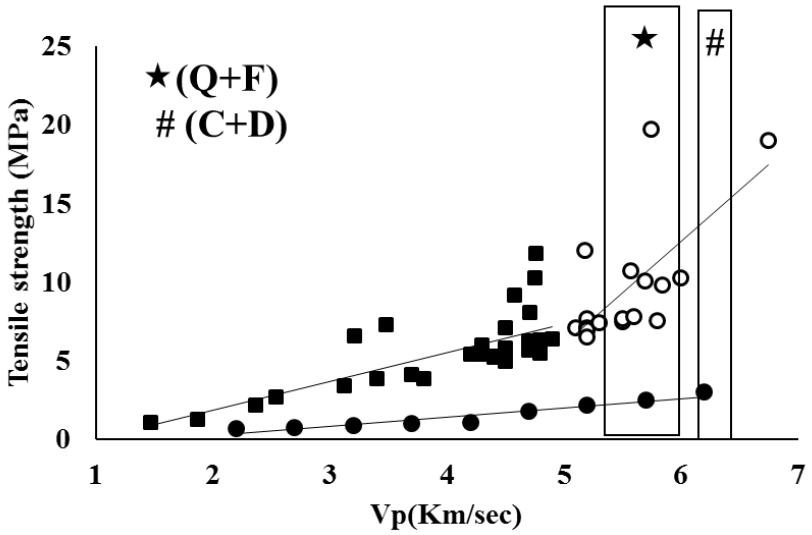


Figure 3.21 Graphical representation of indirect tensile strength versus $V_p$, as reported by different researchers along with their trend line. The marked rectangles show the range of $V_p$ values for sandstones (5.7 km/s to 6 km/s) when considering the effect of varying mineral contents (* major minerals Q-quartz and F- feldspar with varying proportions (75 % Q,25 % F till 65 % Q, 35 % F), while for carbonates, $V_p$ varies from 6.25 km/s to 6.43 km/s for varying major minerals (# C- calcite and D- dolomite) proportions (100 % C, 0 % D till 75 % C,25 % D)

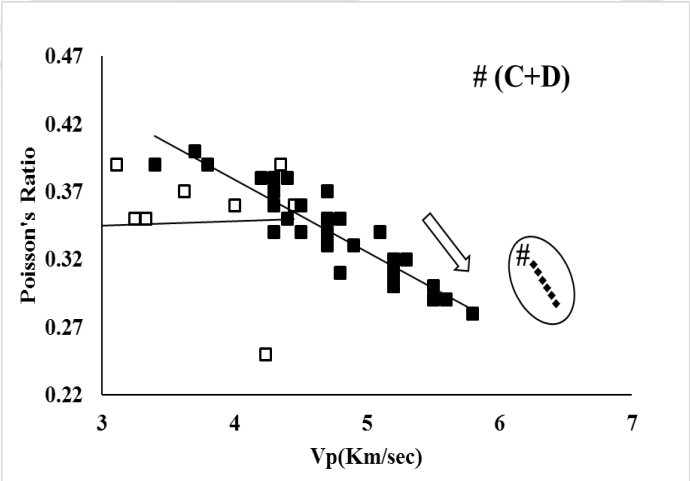


Figure 3.22 Graphical representation of Poisson's ratio versus $V_p$, as reported by different researchers along with their trend line. Label # represents limestone major minerals (C- calcite and D- dolomite) different proportions (75 % C, 25 % D, 80 % C, 20 % D, till 100 % C, 0 %

D). The circled part depicts the decrease in Poisson's ratio values with a decrease in calcite and an increase in dolomite content, thereby highlighting the effect of mineral content on $V_p$ values and thus on Poisson's ratio

However, apart from mineralogy, porosity, saturation also has an influence on the alteration of the geomechanical properties. The presence of clay minerals could also lead to a deviation in $V_p$ values. Also, $V_p$ increases with increasing saturation and also depends on the type of fluid (Table 3.6). Hence, to be more precise when assessing rock mass conditions, this inclusive study (considering all influential parameters) may be carried out so as to be more reliable when dealing in different stages of an investigation. However, it is important here to mention that it is improbable that $V_p$ values may ever substitute the mechanically derived parameters, although a suggestion of the variation can be noted or a comparative study of different geomechanical properties of various lithological units can be investigated. These seismic measurements can be viewed as complementary and equally important for studies related to the evaluation of rock mass performance (geomechanical classification system).

## 3.11 Summary and Conclusions

In the present study, the seismic wave propagation was reproduced in the laboratory by using the ultrasonic velocity measurement technique to measure the $V_p$ of different rocks. Ultrasonic transducers of 54 kHz frequency were used to measure $V_p$ utilising the through-transmission technique. The porosity of sandstones and carbonates was measured using cost-effective, semi-automated, in-house fabricated helium gas porosimeter setup. The need to fabricate a well-established porosimeter aroused due to the highly inflamed cost of existing commercial helium gas porosimeters. This setup allows measurement of grain volume and subsequently porosity of sandstone, carbonate and shale rocks at laboratory scale. The setup was calibrated by using four different steel cylinders of known volume. These steel cylinders are used to ensure that the known volume is of the steel with 0% porosity. Hence, the porosity measurements obtained were standardised on the basis of these steel cylinders with 0% porosity. The primary purpose of constructing the helium gas porosimeter is its wide applicability (range) for performing porosity measurements on conventional reservoir rocks, thereby making it a well-established and widely used method. An accurate porosimeter operating on Boyle's law principle is of considerable value in analysing cores for either routine or research purposes. Comparatively, the dominancy of this instrument over other porosity measurement techniques or methods can be illustrated from the fact that it takes into consideration the wide applicability in the sample dimensions without contaminating the sample. In an industry-based commercial porosimeter,

the core sample holder is of a specific size, i.e., either 1 inch or 1.5-inch diameter. This makes the sample preparation an essential step in order to perform porosity measurements. However, this disadvantage is taken care of in the existing setup. This setup offers measurement of rock samples up to NX (54 mm) core size of known volume with ease. There is no requirement for a sample holder for performing measurements for samples of different diameters.

Particularly for conventional reservoir rocks, this method is the most suited method due to the non-destructive nature and reusability of the core plugs for other petrophysical and geomechanical examinations. The use of helium gas in Boyle's law porosimeter reduces the error due to gas adsorption to negligible proportions (Beeson 1950). Helium gas poses no threat for interaction or reaction with the rock grains. This makes it possible to construct instruments that permit the determination of porosity with a high degree of accuracy, with great rapidity and without contamination. As compared to other contemporary techniques, the advantage of Boyle's law instrument is most outstanding when the determination time is compared with that required in obtaining porosity by evacuation of the core followed by saturation with a liquid of known density. The results obtained by this setup were compared with industry-based commercial porosimeter and found to be satisfactory with $R^2 = 0.98$ for carbonates, $R^2 = 0.95$ for sandstones. It is thereby suggested that by virtue of its cost-effectiveness and adaptability in measuring different ranges of samples of known volume, the current setup is best suited for applications involving conventional reservoir characterisation based on porosity values.

An attempt was made to understand the variation of E with $V_p$ with the help of a fragmented analysis of major mineral constituents and saturation conditions for rock mass classification based on $V_p$. This will help to understand the variability of $V_p$ values associated with the change in saturation conditions for a reservoir rock under investigation. Such a template would aid in the interpretation of the geomechanical behaviour of rocks on the basis of $V_p$ values, even in the absence of well log data. However, the present template considers the effect of only major minerals and porosity. Other factors such as the presence of other minor minerals, clay content may also alter the properties, which may be one of the reasons for the literature dataset falling below the modelled template dataset. Thus, it can be inferred that material with higher E will have a higher $V_p$ due to higher density and presence of lower pores (lower porosity).

# Chapter 4
# Laboratory Assessment on Factors Controlling the Acoustic Properties of Carbonates

## 4.1 Introduction

Carbonate reservoirs are one of the most significant sources of hydrocarbon with about 50-60% of the world's oil reserve (Vanorio et al., 2008; Xu and Payne, 2009; Payne et al., 2010; Burchette, 2012; Mousavi et al., 2012; de Ceia et al., 2015; Madhubabu et al., 2016; Sun et al., 2017). The potential for the additional gas reserve is huge (Vanorio et al., 2008), thereby suggesting the economic significance of carbonate rocks. However, the rocks that constitute these reservoirs are heterogeneous, fractured and described by textural variations, leading to complicated relations between petrophysical properties and geophysical data (Vanorio et al., 2008). Carbonates often are more heterogeneous than sandstones due to a more complex distribution of grains and pore space. The natural discontinuities and inhomogeneity of the rocks can create internal and external uncertainties when estimating petrophysical and geo-mechanical properties (Misaghi et al., 2010). This uncertainty is due to the complexity in the method of formation of these rocks and dissolution. The major factors that cause the heterogenetic behaviour of carbonates compared to sandstones are- (i) carbonates are autochthonous while sandstones are allochthonous and (ii) higher reactivity of carbonates (Choquette and Pray, 1970; Moore and Wade, 2013; Ehrenberg and Nadeau, 2005). The latter difference has a higher significance for diagenesis and reservoir quality (Ehrenberg and Nadeau, 2005). The higher reactivity subjects the carbonates to several alterations within the pore system, leading to a change in pore architecture, thereby taking a toll on the pore space that may destroy/alter porosity. Chemical effects prone to chemical reactions pose difficulties in acoustic modelling by inducing variations in the rock frame properties (Vanorio et al., 2008). Few studies (Regnet et al., 2015; Husseiny and Vanorio, 2015, 2017) have highlighted that micrite content and macroporosity are also important when interpreting and modelling petrophysical relations.

As stipulated earlier, due to the mutual influence of changes in depositional facies and diagenetic alterations occurring over a period due to several geological processes, carbonates tend to develop varied pore types, i.e., a variety of pore types may be present in carbonates (Lucia, 2007). As per Mousavi et al., 2012, the different types of pores considered in the classification of pores are - (i) interparticle porosity, (ii) intercrystalline porosity, (iii) intraparticle porosity, (iv) moldic porosity, (v) vuggy porosity, (vi) touching vug and (vii)

microporosity. Pore types control fluid flow and hence are very important for transport properties (Mousavi et al., 2012). For instance, as per Baechle et al. (2009), rock dominated by intraparticle porosity and rock dominated by interparticle porosity has a velocity variation of almost 1500 m/s. One of the main geometric features is the pore aspect ratio, which is defined as the ratio between the major and the minor axes of an ellipse that encloses the pore and describes the elongation of the pore bounding ellipsoid (Anselmetti and Eberli, 1993; Eberli et al., 2003; Assefa et al., 2003; Kumar and Han, 2005; Weger et al., 2009). To counter the heterogeneity existing due to the complexity in the pore geometry, pore distribution and pore arrangement within the rock matrix, recent advances in technology have provided a more decisive basis for assessing a more reliable estimation of the pore-scale modelling (Wildenschild and Sheppard, 2013). In reality, there will be changes in porosity and permeability even at the micro-level, which in turn will result in huge uncertainty in the estimation of both parameters. The high diagenetic potential of carbonate rock results in changes in the pore structure, making the whole pore structure more complex to analyse. The advent of new techniques, such as digital rock methods/digital image analysis (DIA), can be used to understand the role of pore geometry and pore size distribution in porosity and permeability estimation. The advantage of digital image analysis (DIA) is that it can be used for pore network extraction/modelling with less computing time to obtain different parameters (Suicmez and Touati, 2007). Besides, it can also take into account all types of pore microstructure and help in characterisation, which may be necessary for studies related to digital rock physics modelling. Such studies may help to develop digital rock typing that can be used for subsurface geological modelling. Hence, to address the heterogeneity, an extensive and comprehensive study incorporating all the pore features is fundamental for assessing the diverse nature of carbonates. Such pore-scale study in amalgamation with the conventional rock analysis and incorporating the wider-ranging geological and engineering studies with the laboratory data would help establish a consistent relationship with the acoustic properties that would provide a more realistic rock physics model.

The most basic and classical rock physics models are the Gassmann equation (Gassmann, 1951), the Wyllie time average equation (Wyllie et al., 1956) and the Kuster-Toksoz model (Kuster and Toksoz, 1974). However, these models lack suitability when considering the pore geometry's effect on elastic wave velocities because of the assumptions of these models (Wang et al., 2011). The limitation of the Gassmann equation lies in the applicability to predict velocities with various secondary storage spaces in carbonate reservoirs (for example, caves, cracks etc.) (Wang et al., 2011). Wyllie time average equation works best for primary porosity

and assumes single homogeneous mineralogy (Mavko and Mukerji, 1998). The Kuster-Toksoz model assumes isotropic, linear, elastic media and is found suitable for ultrasonic laboratory conditions. However, in low-frequency bands, velocities predicted by this model and the seismic wave velocities generally exhibit differences (Mavko and Mukerji, 1998; Wang et al., 2011). Other models of velocity prediction are extended models of these three models. Therefore, this study attempts to undertake a comprehensive laboratory study to address the gap and understand how petrophysical and geological properties like mineralogy, pore geometry etc. affect the acoustic properties of carbonates.

This study aims to evaluate and understand the factors that contribute to the heterogeneity of carbonates and thereafter establish their association with the acoustic properties. It is based on applying geological principles coupled with analytical and digital image analysis techniques. Hence, for the purpose of the analysis, carbonate samples of the Bombay Offshore basin, India, were investigated in the laboratory at ambient conditions. Thereafter, multivariate analysis is performed to understand different factors that affect $V_p$. The high correlation signifies the importance of pore scale parameters. Moreover, the effect of saturation on $V_p$ considering variation in major mineral constituents and porosity for different saturating fluids is also evaluated. With this approach, this study maximises the use of experimentally derived laboratory data that are usually inhibited by realistic geological information.

## 4.2 Materials and Methods

### 4.2.1 Geology of the Study Area and Sample Description

Carbonate rock core plugs are from the Bombay offshore Category I sedimentary basin in India, known for commercial production (Bastia, 2006). The Bombay offshore basin is considered to have around 50% of India's total oil reserves (Mohan, 1985). This formation belongs to the early Miocene age (Guha and Pandey, 1974; Mohan, 1978; Basu et al., 1980). Figure 4.1 shows the geographical location of the sedimentary basin from where representative core plugs were obtained. Due to the confidentiality of the provided core plugs by ONGC Limited, only depth information of the obtained core plugs is provided. The generalized stratigraphic column of the Bombay offshore basin is shown in Figure 4.2. Prior to detailed microscopic analysis, megascopic analysis and visual inspection, which included colour and texture identification, were carried out on all the carbonate samples. All the tests, physical, petrological and acoustic measurements were carried out by following the ISRM (International Society for Rock Mechanics) suggested methods, ASTM (American Society for Testing and Materials) specifications and IS (Indian Standard) Codes.

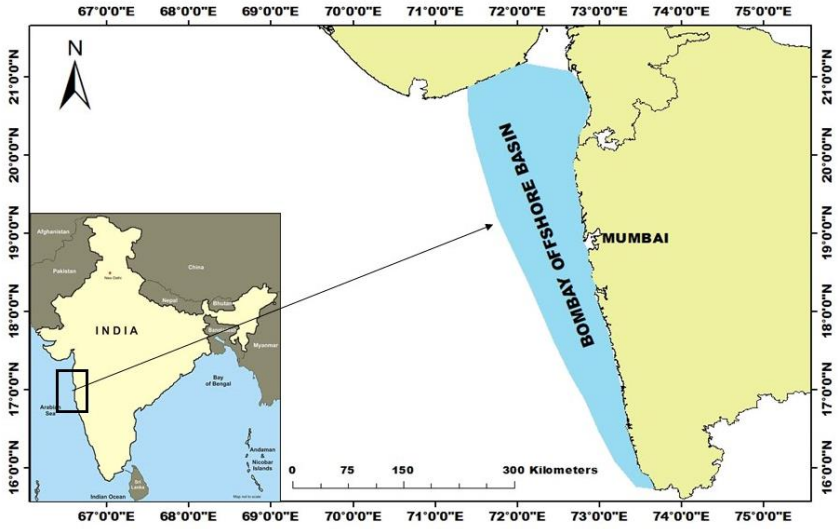


Figure 4.1 Geographical map of the study area with an inset highlighting the location of the sampled rocks (Carbonates from Bombay Offshore)

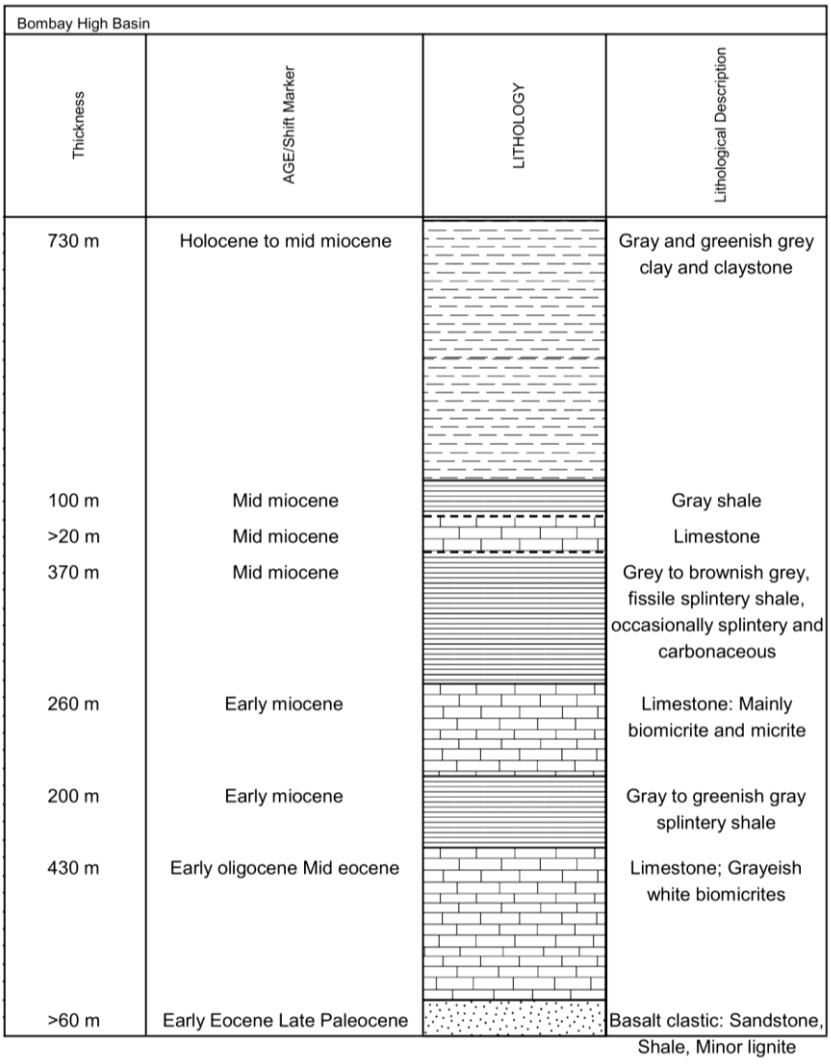


Figure 4.2 Stratigraphic column of Bombay offshore basin (modified from Basu et al., 1980)

### 4.2.2 Methodology

Carbonate rock core plugs, ten in number (Figure 4.3), from the Bombay offshore basin were used to measure parameters that include acoustic, petrophysical and mineralogical variables in the laboratory. Before carrying out any analysis, all the rock core plugs were cleaned using the soxhlet extractor apparatus to remove any organic content. The rock samples were then used for evaluating different parameters. Compressional wave velocity ($V_p$) was measured in the laboratory using piezoelectric transducers of 54 kHz by employing the ultrasonic-through transmission technique. Porosity was measured by using a helium gas porosimeter, while permeability was measured by using a nitrogen gas permeameter. The grain and pore diameters were calculated with the help of FESEM images. The petrographic analysis was carried out using optical microscopy. The mineral content of the rock core plugs was determined by XRD (X-ray Diffraction). The procedure of determining each parameter is discussed and elaborated in Chapter 3.

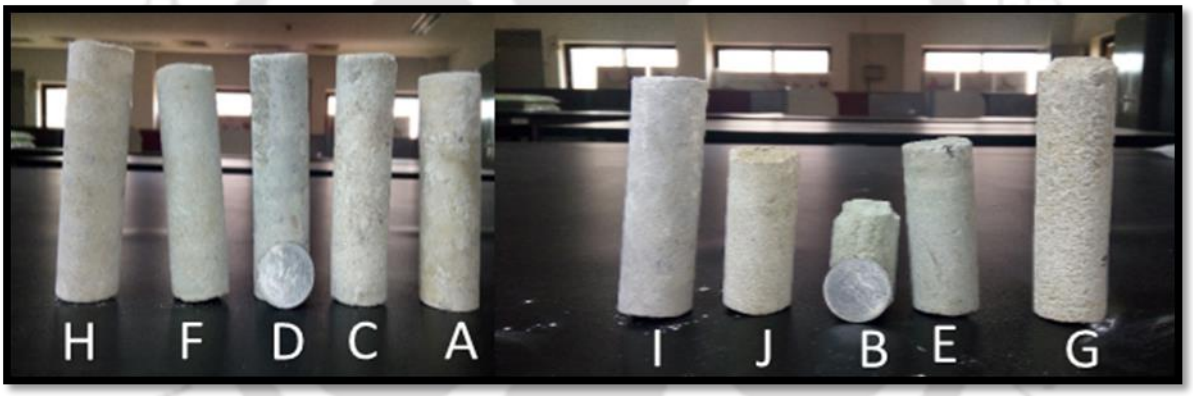


Figure 4.3 Carbonate rock samples considered in this study obtained from Bombay offshore basin

## 4.3 Results and Discussion

### 4.3.1 General Petrographic Description

For petrological analysis, the rocks were investigated using visual inspection techniques. It was observed that carbonate samples are pale white to grey-white in colour and fine to coarse in texture. The thin-section images of carbonates (Figure 4.4) show an abundance of fossils (shell fragments of foraminifera) in carbonate samples. The presence of fossils was reported in the literature (Basu et al., 1982) for carbonates of this basin. As per Basu et al. (1982), limestone is primarily biomicrite, fossiliferous micrite and mostly contains a large bioclastic element.

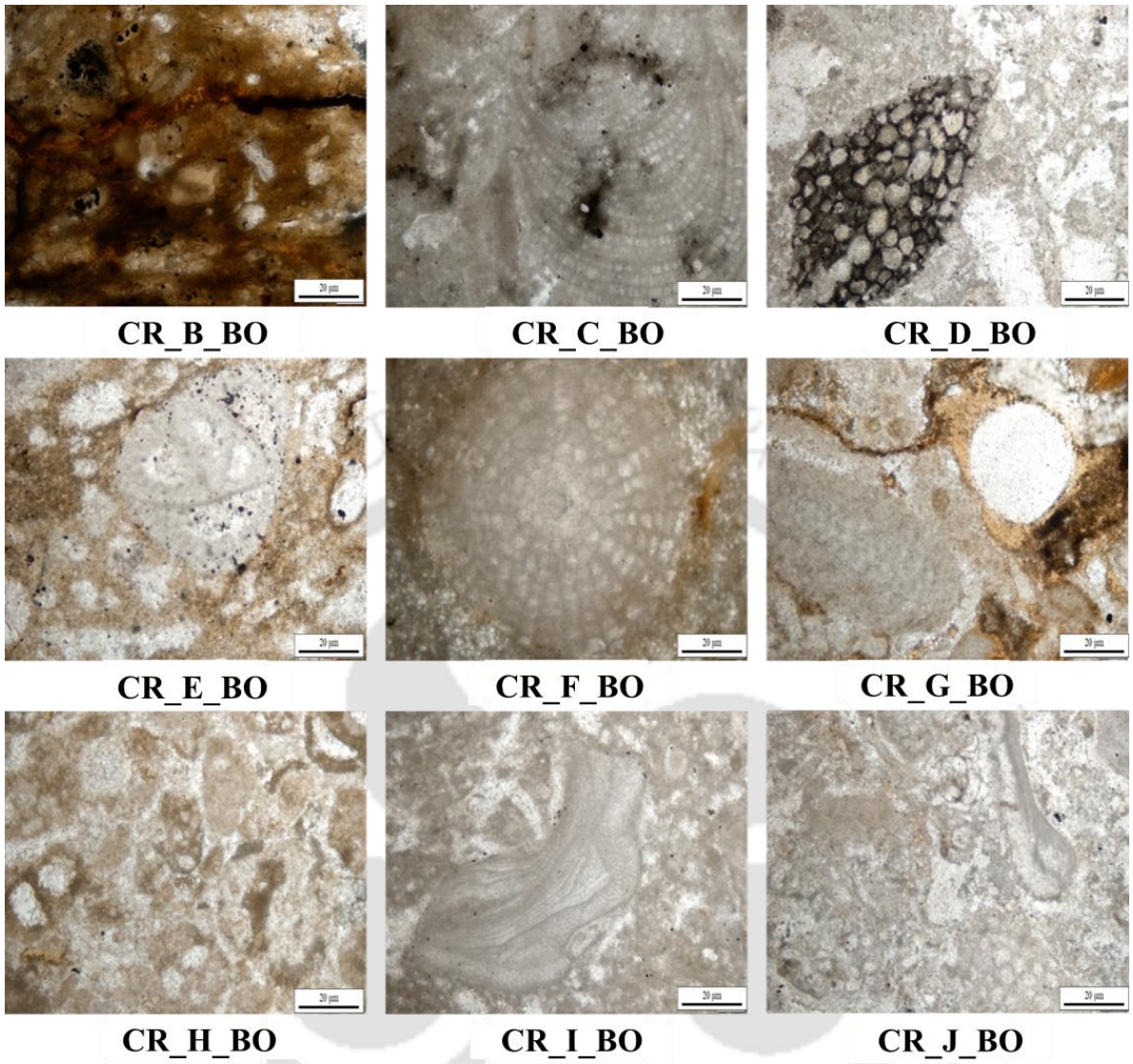


Figure 4.4 Optical Photomicrographs of the carbonate samples (Magnification: 10X, Scale:20µm) (Photomicrograph showing the abundance of fossil in the sample)

The mineral content of the rock specimen was confirmed by XRD analysis. The results revealed that dolomite was the dominant mineral in carbonates. However, quartz was present as a minor mineral in carbonates. Its presence may indicate that siliceous deposits have precipitated during diagenesis, where they partially filled the pores. XRD spectra show the presence of different minerals for carbonates, as shown in Figure 4.5. Results obtained from semi-quantitative XRD analysis of carbonates are tabulated in Table 4.1.

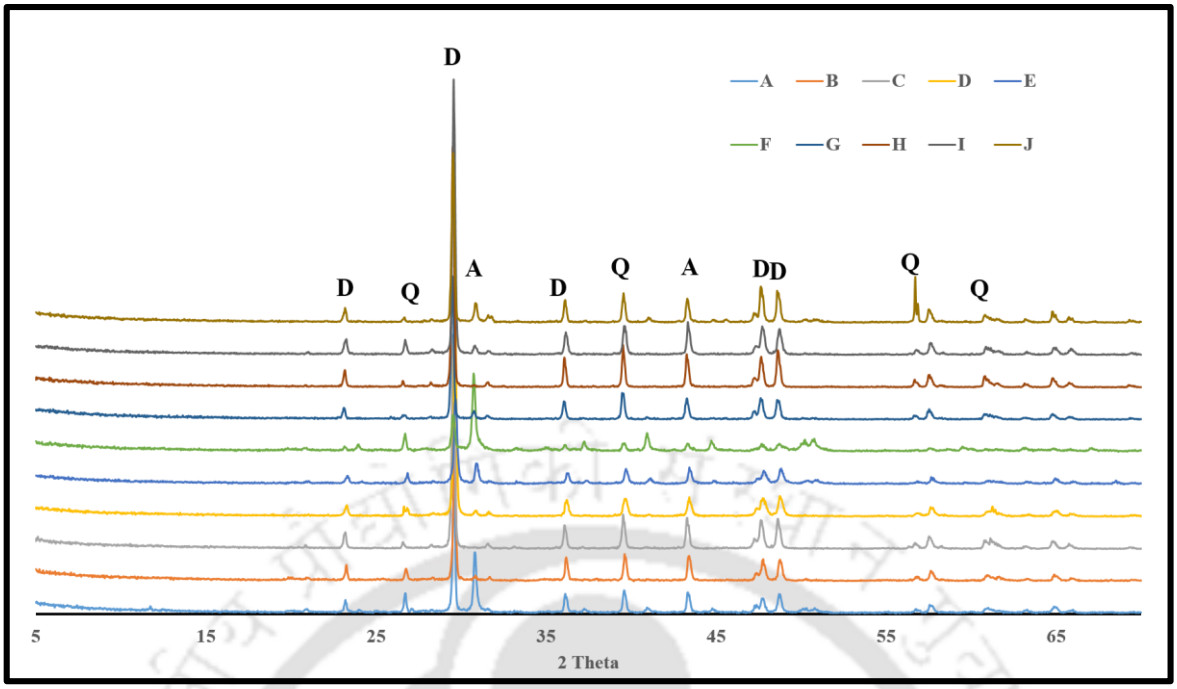


Figure 4.5 X-ray diffraction pattern of carbonate samples (legends showing the sample ID) showing presence of different peaks for different minerals (D- Dolomite, Q- Quartz, A- Ankerite)

Table 4.1 Results obtained from semi-quantitative XRD (X-ray diffraction) analysis of carbonates

| Sample ID | Mineral Composition (%) | | | | |
|---|---|---|---|---|---|
| | Quartz | Dolomite | Gypsum | Ankerite | Calcite |
| CR_A_BO | 19 | 58 | 5 | 18 | 0 |
| CR_B_BO | 9 | 90 | 0 | 1 | 0 |
| CR_C_BO | 6 | 82 | 0 | 0 | 12 |
| CR_D_BO | 5 | 91 | 0 | 4 | 0 |
| CR_E_BO | 30 | 58 | 0 | 11 | 0 |
| CR_F_BO | 5 | 27 | 0 | 67 | 0 |
| CR_G_BO | 7 | 89 | 0 | 4 | 0 |
| CR_H_BO | 2 | 92 | 0 | 0 | 6 |
| CR_I_BO | 2 | 95 | 0 | 3 | 0 |
| CR_J_BO | 2 | 93 | 0 | 0 | 4 |

### 4.3.2 Acoustic and Petrophysical Properties

Table 4.2 summarises the description of the obtained samples, including the depth of the drilled core samples (below ground level), length and diameter of carbonates, respectively. The designation used for the studied samples highlights the type of sample (CR for carbonates), followed by the name of the sample (A, B, C etc.) and lastly, the location of the obtained sample (BO for Bombay Offshore basin). The measured petrophysical and acoustic properties for carbonates are presented in histograms, as shown in Figure 4.6. The different parameters vary as: length = 39.19 mm to 74.19 mm, diameter = 25.29 mm to 25.45 mm, $V_p$ = 1760 m/s to 4560 m/s, bulk density ( $\rho$ ) = 1.94 g/cc to 2.59 g/cc, grain density (GD) = 2.63 g/cc to 2.72 g/cc, porosity ( $\phi$ ) = 4.09% to 28.58% and permeability (k) = 0.2083 mD to 112.317 mD. The standard deviation in $V_p$ measurement for all samples, i.e., CR_A_BO till CR_J_BO are 5.77, 15.27, 25.33, 17.32, 30.33, 17.32, 11.54, 15.27, 23.09, 10.77 m/s respectively. The summary of measured petrophysical and acoustic properties with standard deviations (SD) for the studied carbonate rock core plugs is presented in Table 4.3. It is to be noted that permeability of carbonates CR_D_BO, CR_E_BO, CR_F_BO, CR_I_BO is below the detectable limit, less than 0.01mD.

Table 4.2 Details of the studied carbonate rock core plugs

| S. No | Sample ID | Depth (below Ground level) of core samples (m) | Length (mm) | Diameter (mm) |
|---|---|---|---|---|
| 1 | CR_A_BO | 1190-1208 | 73.05 | 25.29 |
| 2 | CR_B_BO | 772-780.5 | 40.54 | 25.38 |
| 3 | CR_C_BO | 1709-1727 | 39.19 | 25.38 |
| 4 | CR_D_BO | 1336-1347.5 | 72.95 | 25.38 |
| 5 | CR_E_BO | 1386-1397 | 47.33 | 25.41 |
| 6 | CR_F_BO | 1423.6-1430.1 | 70.37 | 25.45 |
| 7 | CR_G_BO | 7064-7081.5 | 74.19 | 25.42 |

| | | | | |
|---|---|---|---|---|
| 8 | CR_H_BO | 1829-1840 | 72.35 | 25.32 |
| 9 | CR_I_BO | 2058-2064.5 | 71.06 | 25.36 |
| 10 | CR_J_BO | 2337-2355 | 49.72 | 25.36 |
| | | **Max.** | **74.19** | **25.45** |
| | | **Min.** | **39.19** | **25.29** |
| | | **Avg.** | **61.075** | **25.375** |

The Bombay offshore basin consists of approximately 70% carbonates (Wandrey, 2004a). Different researchers reported values of petrophysical and acoustic properties for studies pertaining to this basin in the literature. Sharma et al. (2020) reported an average porosity range of 14.1% to 16.9% and permeability less than 5mD. As per Wandrey (2004a) and Schön (2015), average porosity and permeability ranges from 15-20% and 100-250 mD, respectively. The log values reported by Roy and Chatterjee (2020) varies from: $V_p$=3811 to 4193 m/s, bulk density = 2.51 to 2.66 g/cc and porosity = 14-22%. Similarly, Chandrasekhar and Rao (2012) reported velocity log data in the range of 983 to 1352 m/s. Observing the variation of properties in the literature, the core plugs were so selected and investigated such that they cover the maximum variability of the different properties. Hence, analysis on ten number of carbonate core plugs was performed. Moreover, sample acquisition/collection is difficult and not a straightforward task.

### 4.3.3 Regression Analysis

The subsequent sections deal with evaluating and analysing the different relationships such as $V_p$-bulk density, $V_p$-porosity, $V_p$–permeability, $V_p$-mineral content and porosity-permeability correlations one by one, i.e., in isolation/separately.

#### 4.3.3.1 Bulk Density, Porosity and Permeability Relations

Regression analysis was performed to predict and understand the relationships between bulk density, porosity, permeability and $V_p$. Bulk density control on $V_p$ was checked, and a correlation was obtained as shown in Figure 4.7(a) with $R^2$=0.73. Similarly, porosity control on $V_p$ was checked, and a correlation was obtained as shown in Figure 4.7(b) with $R^2$=0.72. The relationship between permeability and $V_p$ was also checked, and a correlation was obtained as shown in Figure 4.7(c) with $R^2$= 0.68.

### 4.3.3.2 Mineralogy Relation

This section presents the dependability of $V_p$ with the mineral content for carbonate rock core plugs. The major mineral present in carbonates includes dolomite, while quartz was present as a minor mineral. In order to investigate whether mineralogical parameters control acoustic properties, the mineral composition was plotted against $V_p$ for all the carbonate samples, as shown in Figure 4.8. Moreover, since $V_p$ and porosity are inversely related to each other, any dispersion in $V_p$ values will be reflected in the porosity values. Subsequently, the mineral composition was also plotted with porosity, as shown in Figure 4.9.

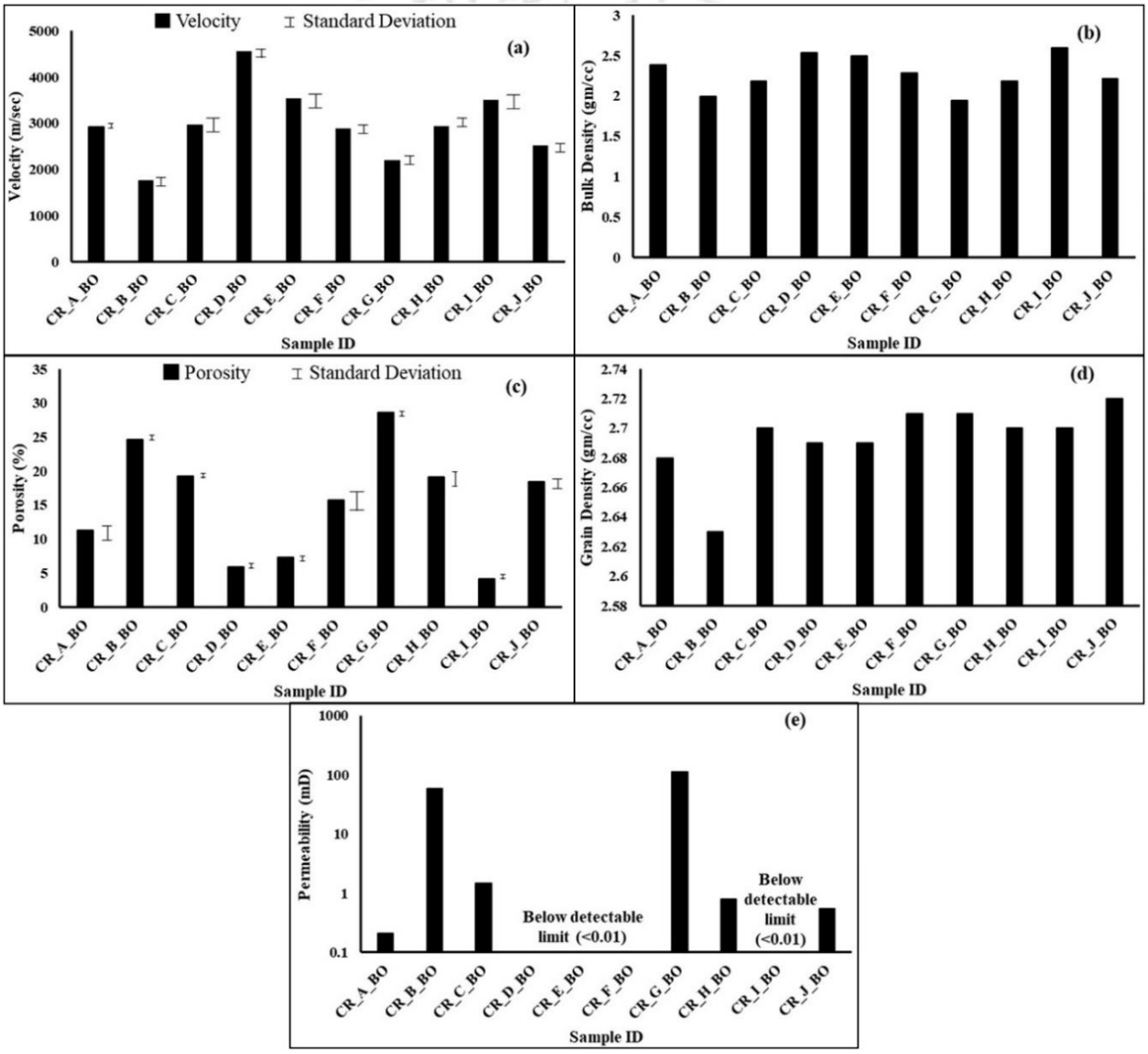


Figure 4.6 Measured petrophysical and acoustic properties of the studied carbonate rock core plugs [(a) Velocity, (b) Bulk density, (c) Porosity, (d) Grain density, (e) Permeability]

The plotted Figures 4.8, 4.9 highlight the importance of mineralogical composition on $V_p$ and porosity. When samples are analysed in isolation/separately, the following observations can be

noted. For instance, ankerite mineral present in sample F (67%) may contribute to an increase in $V_p$ value (2880 m/s), despite the porosity of sample F (15.77%) being on the higher side. Moreover, quartz, being the secondary mineral in the case of carbonates, tend to reduce porosity. This is evident from sample E (quartz content is 30%, porosity is 7.25%). Another observation from the cross-plots indicates that for samples H, I, J and D, with similar dolomite and quartz contents, $V_p$ fluctuates. This may infer that dolomite content may not be a criterion for low or high $V_p$.

Table 4.3 Summary of measured petrophysical and acoustic properties with standard deviations (SD) for the studied carbonate rock core plugs

| **Sample ID** | **Velocity (m/s)** | | **Bulk Density (g/cc)** | | **Porosity (%)** | | | **Grain Density (g/cc)** | | **Permeability (mD)** |
|---|---|---|---|---|---|---|---|---|---|---|
| | $V_p$ | SD | $\rho$ | SD | $\phi$ | SD | % Change | GD | SD | k |
| CR_A_BO | 2920 | 5.77 | 2.38 | 0.0017 | 11.33 | 0.284 | 2.508 | 2.68 | 0.0086 | 0.208 |
| CR_B_BO | 1760 | 15.27 | 1.99 | 0.0008 | 24.6 | 0.014 | 0.057 | 2.63 | 0.0001 | 58.966 |
| CR_C_BO | 2976 | 25.33 | 2.18 | 0.001 | 19.2 | 0.071 | 0.368 | 2.7 | 0.0028 | 1.4595 |
| CR_D_BO | 4560 | 17.32 | 2.53 | 0.002 | 5.9 | 0.064 | 1.079 | 2.69 | 0.0021 | Below detectable limit <0.01 |
| CR_E_BO | 3530 | 30.33 | 2.49 | 0.0008 | 7.25 | 0.093 | 1.282 | 2.69 | 0.0023 | |
| CR_F_BO | 2880 | 17.32 | 2.28 | 0.0014 | 15.77 | 0.459 | 2.913 | 2.71 | 0.0146 | |
| CR_G_BO | 2200 | 11.54 | 1.94 | 0.0014 | 28.58 | 0.014 | 0.049 | 2.71 | 0.0007 | 112.317 |
| CR_H_BO | 2940 | 15.27 | 2.18 | 0.0008 | 19.19 | 0.211 | 1.101 | 2.7 | 0.007 | 0.791 |
| CR_I_BO | 3500 | 23.09 | 2.59 | 0.002 | 4.09 | 0.04 | 0.988 | 2.7 | 0.0015 | Below detectable limit <0.01 |
| CR_J_BO | 2510 | 10.77 | 2.21 | 0.0004 | 18.4 | 0.11 | 0.599 | 2.72 | 0.0035 | 0.538 |

#### 4.3.3.3 Pore Size Controls

To analyse the pore heterogeneity present in carbonates, the pore characteristics were closely investigated with the help of digital rock methods, namely FESEM analysis. The samples were analysed to capture all the wide-ranging pores of varying sizes varying from micro to

nanometer. Figure 4.10 shows the obtained FESEM image for carbonate A. Similarly, FESEM images were procured for all the samples and pore sizes were measured.

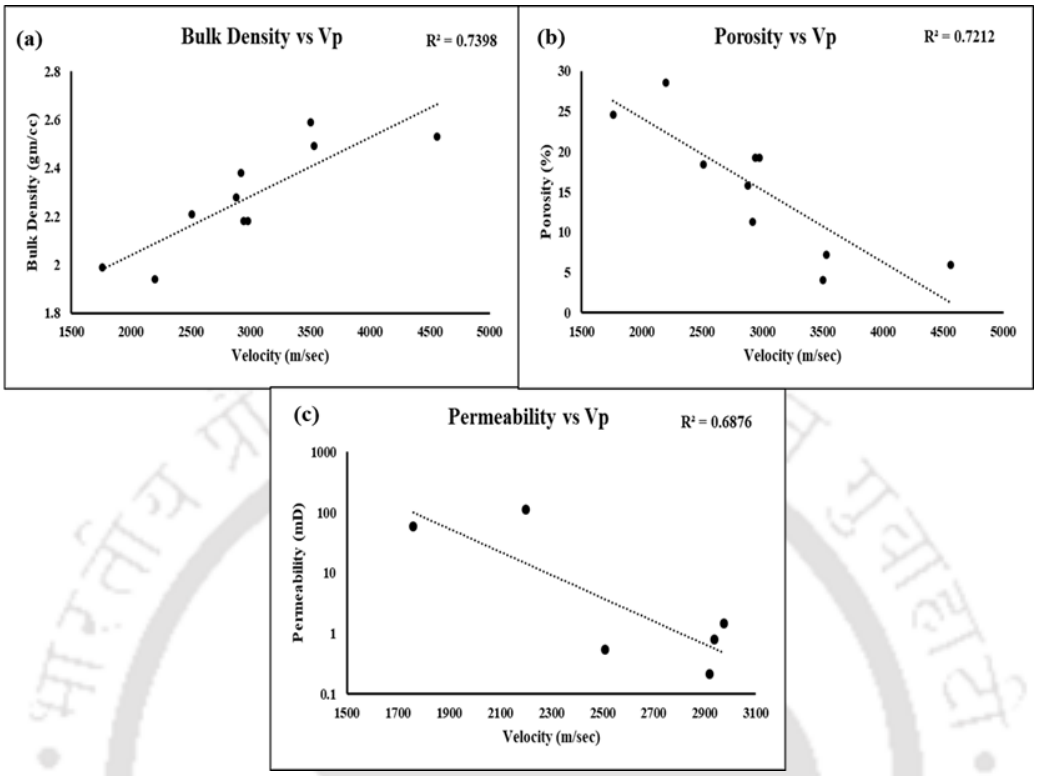


Figure 4.7 Interrelationships between various properties for carbonates [(a) Bulk density - Velocity modelling, (b) Porosity- Velocity modelling, (c) Permeability – Velocity modelling]

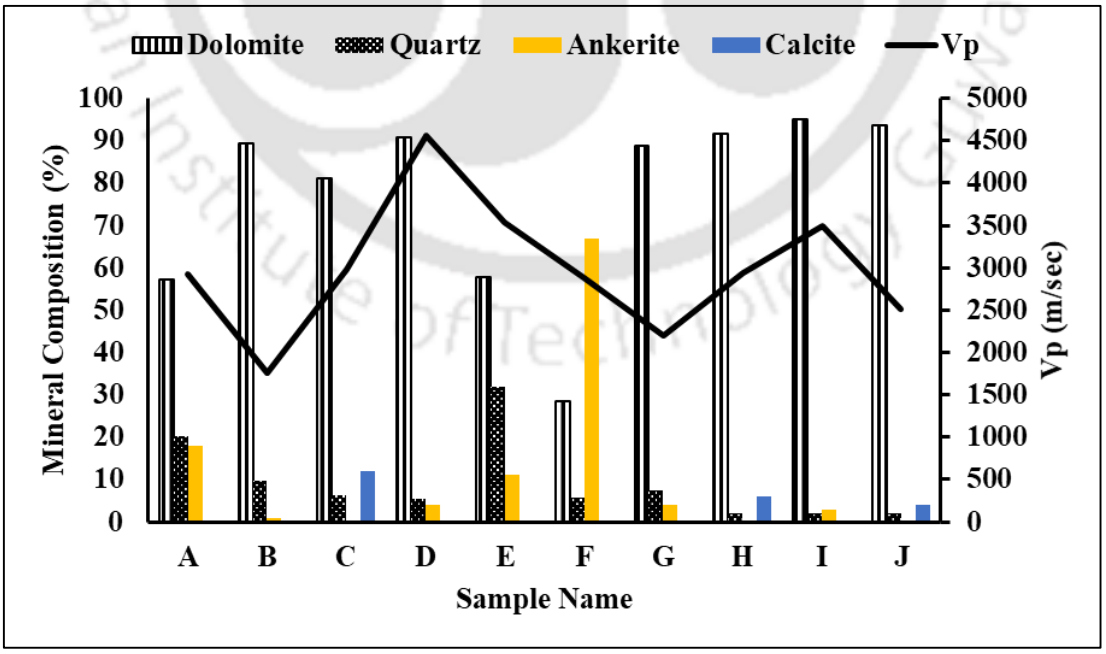


Figure 4.8 Cross-plot illustrating an analogy between mineral composition and $V_p$ for carbonates

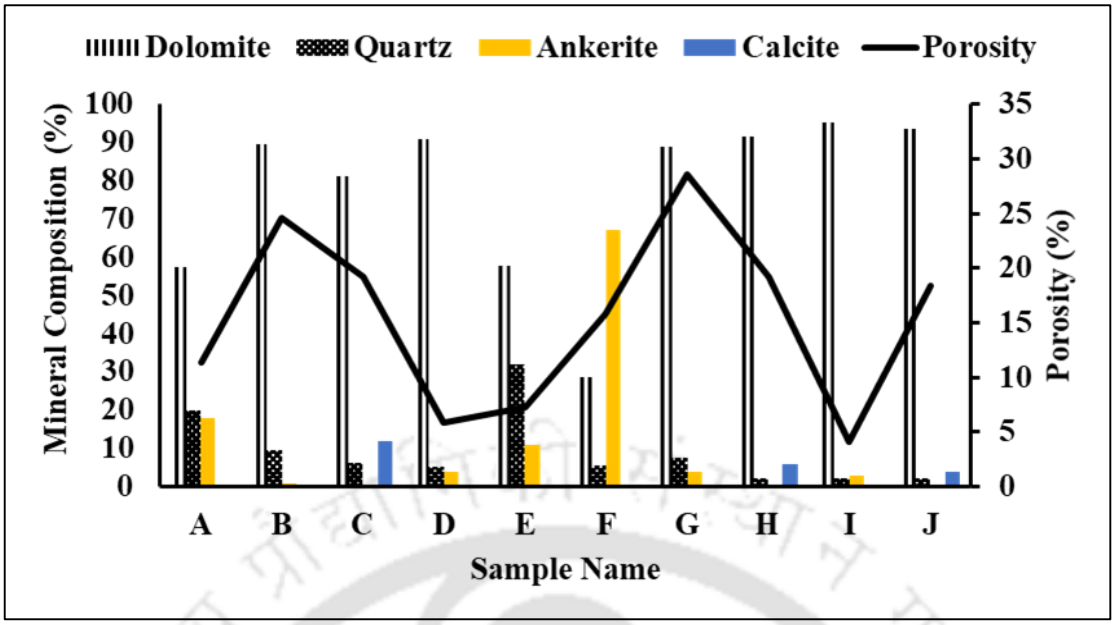


Figure 4.9 Cross-plot illustrating an analogy between mineral composition and porosity for carbonates

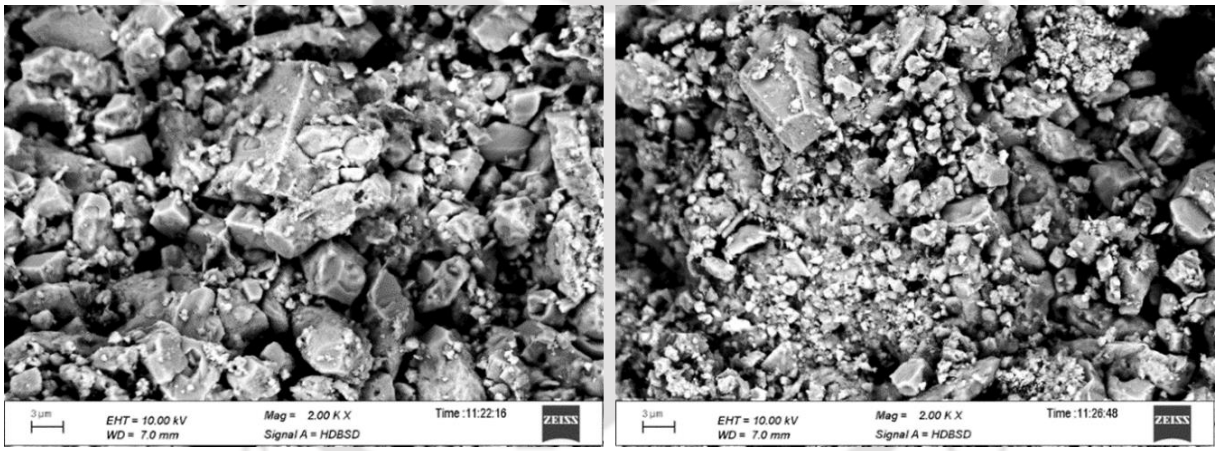


Figure 4.10 Representative FESEM images of carbonate A sample

The obtained pore diameters (mode values) were plotted with $V_p$ values, as shown in Figure 4.11, and it was observed that there exists an inverse relationship between the two. The low $R^2$= 0.34 indicates that with an increase in pore diameter (mode values), $V_p$ tends to decrease. This low correlation (when $V_p$ is depicted as a function of mode pore size only) was expected, and it can be attributed to the presence of a number of multiple parameters that have a coherent influence on $V_p$. A one-to-one correlation between $V_p$ and bulk density exists in the literature, where bulk density is a replica of grain density and porosity, or mineral content and porosity. It is to be highlighted here that there are several parameters such as bulk density, porosity that affect $V_p$ and the effectiveness of this correlation can be improved when these parameters, as discussed in the following sections, are also incorporated.

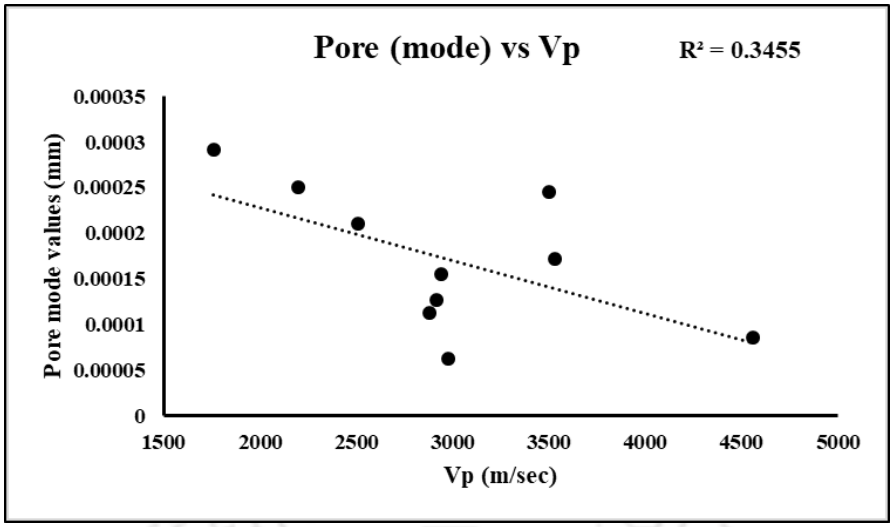


Figure 4.11 Pore diameter (mode values) obtained from digital image analysis and its variation with $V_p$ for carbonate rock core plugs

It is to be mentioned here that pore sizes derived here are from 2D images, and these derived values were correlated with the petrophysical properties of the 3D sample volume. Weger et al. (2009), in their study highlighted that directionality has a meagre effect on the geometrical parameter values.

#### 4.3.3.4 Porosity-Permeability Plot

The measured porosity and permeability for the carbonates were correlated with $R^2$= 0.87 as shown in Figure 4.12, and a direct relationship was obtained. This is applicable for samples with higher porosity and permeability values (CR_B_BO and CR_G_BO) as well as for samples with lower porosity and permeability above 0.01mD (CR_D_BO, CR_E_BO and CR_I_BO). However, for other samples with an appreciable amount of porosity, a similar trend is not followed (refer to Table 4.3). For instance, sample CR_F_BO porosity value is 15.77%, while the permeability is below the detectable limit (less than 0.01mD). Thus, it can be said that a sample with a high porosity value may not necessarily show a high permeability value, which is due to a complicated pore structure. This correlation between porosity and permeability may be found useful within one formation in understanding the fluid flow (Tiab and Donaldson, 2015). The carbonates D, E, I have a lower porosity value (5.9%, 7.25% and 4.09%, respectively), which may be the reason for their low permeability value (less than 0.01 mD). However, the association between porosity and permeability is qualitative and is not directly or indirectly quantitative. A plug may show high porosity without showing any permeability value at all, such as clays, shales. Similarly, a plug may also show high

permeability with a low porosity value in the case of micro fractured carbonates (Tiab and Donaldson, 2015).

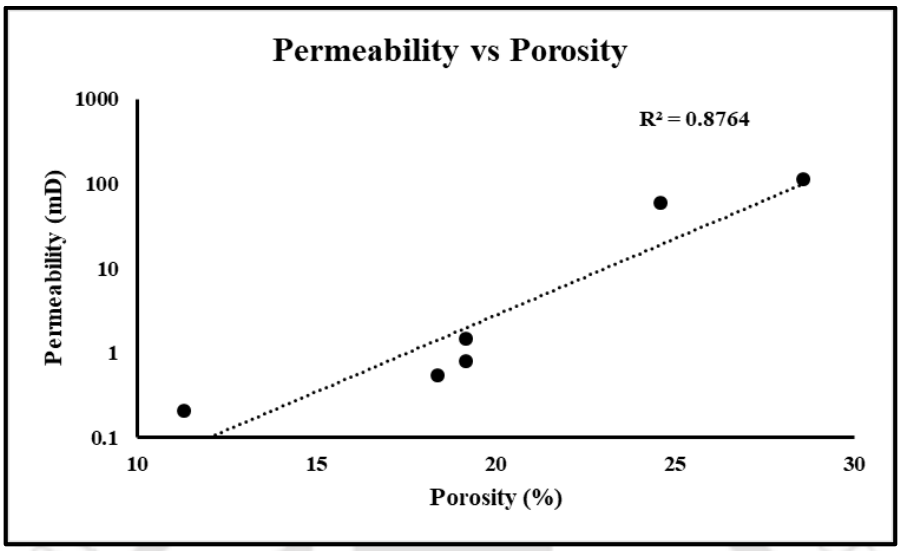


Figure 4.12 Porosity permeability crossplot for carbonates

The representative FESEM images of carbonate I is shown in Figure 4.13 under two different magnifications, 500X (upper two images) and 2KX (lower three images). From these FESEM images, it was noted that there was an absence of connected pores. There may be the presence of pores, however, they may be isolated pores. These isolated pores may contribute to porosity without showing any measurable permeability value.

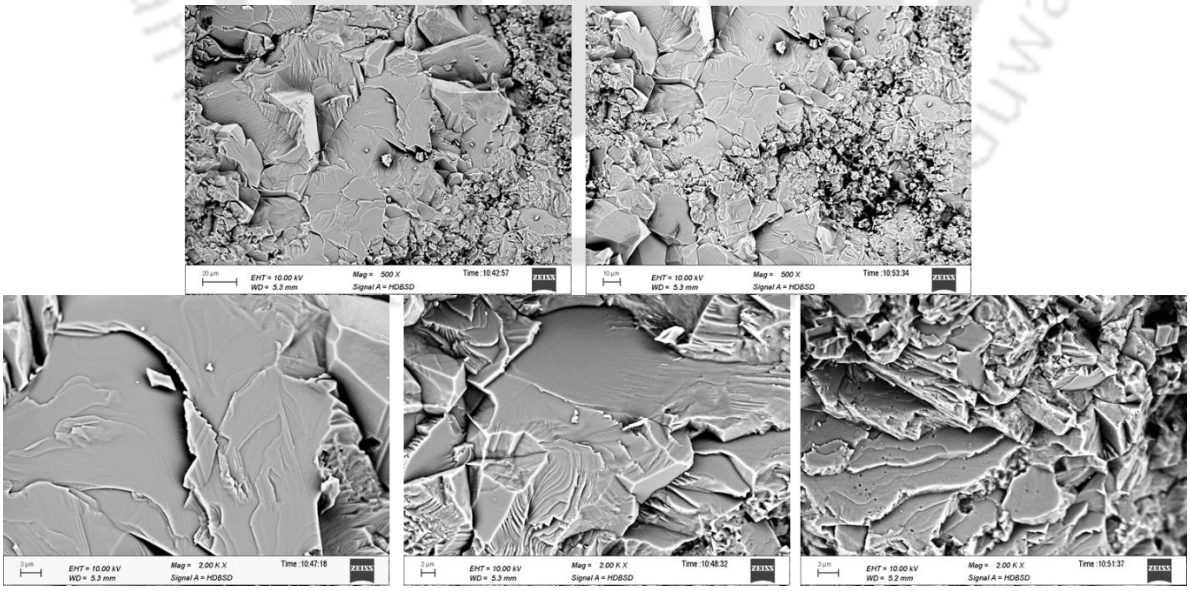

Figure 4.13 Representative FESEM images of carbonate I with different magnification (upper two images of 500X, lower three of 2KX magnification)

### 4.3.4 Multivariate Analysis

As observed in the previous sections, several factors have a combined effect on $V_p$. Thus, multivariate analysis was performed, and $V_p$ is modelled as a function of porosity, bulk density, aspect ratio and pore sizes (maximum, minimum, average and mode values).

#### 4.3.4.1 $V_p$ as a Function of Porosity and Others

$V_p$ was plotted as a function of porosity and other factors, including aspect ratio and pore sizes (max, min., average and mode). It was observed that there was a better correlation when $V_p$ was plotted as a function of porosity and mode pore values (Figure 4.14). Hence, it becomes evident that as the number of parameters increases, the effectiveness of the predictive velocity model also improves based on the increase in $R^2$ value. The maximum value of $R^2$ was observed to be 0.82 when $V_p$ was modelled as a function of porosity and mode pore size.

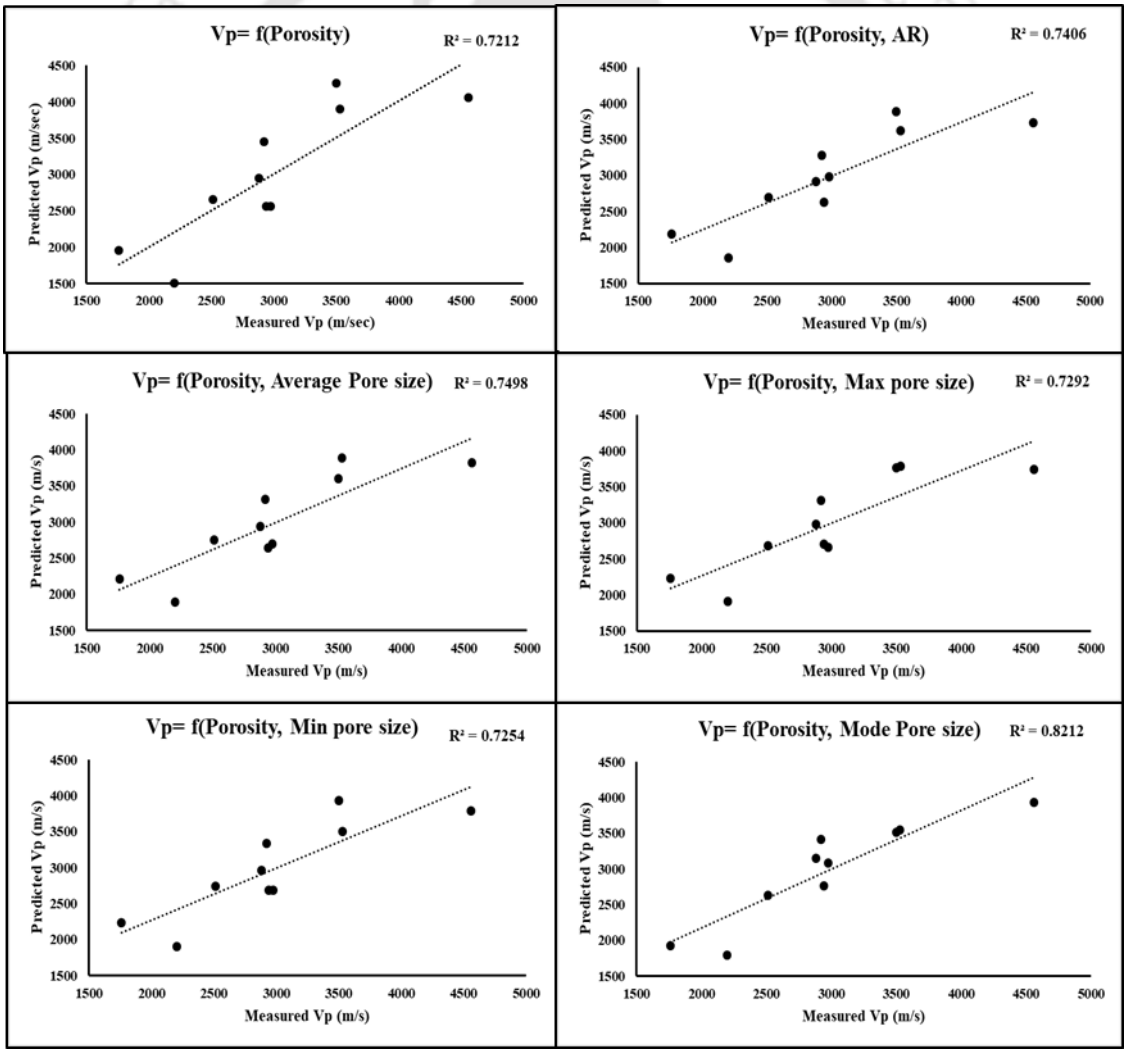


Figure 4.14 Predicted $V_p$ vs measured $V_p$ when $V_p$ presented as a function of porosity and others

### 4.3.4.2 $V_p$ as a Function of Porosity, Bulk Density and Others

Bulk density, apart from porosity, is also an important factor that leads to an alteration in $V_p$ value. To signify its importance, $V_p$ was depicted as a function of bulk density, porosity and other factors, including aspect ratio and pore sizes (max, min., average and mode). It was observed that the correlation improved when $V_p$ was depicted as a function of bulk density, porosity and mode pore values (Figure 4.15). Hence, it becomes evident that as the number of parameters increases, the effectiveness of the predictive velocity model also improves. The maximum value of $R^2$ was observed to be 0.83 when $V_p$ was modelled as a function of bulk density, porosity and mode pore size.

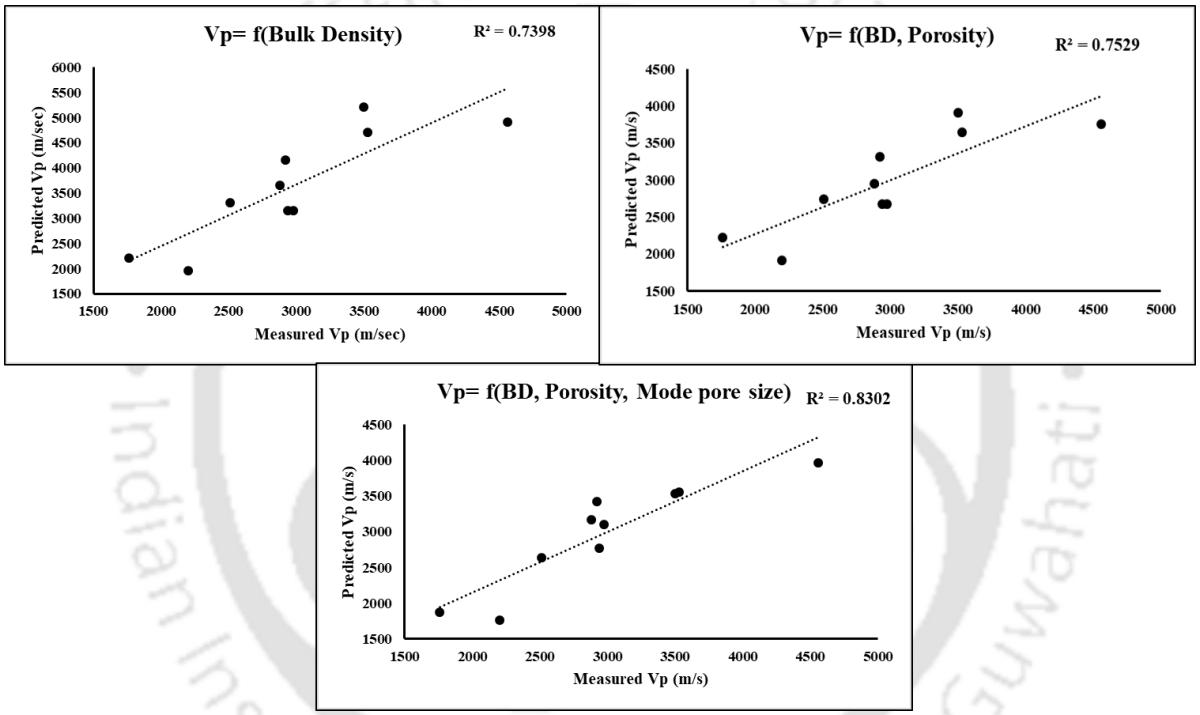


Figure 4.15 Predicted $V_p$ vs measured $V_p$ when $V_p$ presented as a function of bulk density, porosity and others

### 4.3.5 Effect of Saturation

The equation generated for the carbonate samples when $V_p$ is considered as a function of bulk density and mode pore size, obtained by multi-regression analysis, with $R^2$ =0.82, is shown below. Bulk density can be calculated based on the formulation of Bateman (1985). The fluid density value is taken from Table 4.4 (as specified by Schön (2015)). The grain density is varied by changing the proportions of major minerals, as shown in Table 4.5. Keeping these values in Bateman's equation, bulk density is obtained. Thereafter, keeping this obtained bulk density

value in the generated equation, $V_p$ obtained for different saturation conditions is plotted in Figure 4.16 for carbonate C with known mode pore size and porosity value 19.2%.

$V_P = f$ (Bulk density and mode pore size)

$V_p = 2619.2\rho - 3233656.3K - 2432.4$ $\qquad R^2 = 0.82$

$\rho = \phi$* fluid density + (1-$\phi$)* grain density (Bateman 1985)

where $\rho$ = bulk density, K= mode pore size, $\phi$ = porosity

$$GD_{mixture} = GD_{Calcite} * Proportion_{Calcite} + GD_{Dolomite} * Proportion_{Dolomite}$$

Table 4.4 $V_p$ and Density values for different fluids

| **Fluid** | **$V_p$ (m/s)** | **Density (g/cc)** |
|---|---|---|
| Hydrocarbon Gas | 600 | 0.35 |
| Oil | 1200 | 0.76 |
| Water | 1500 | 1 |
| Brine | 1635 | 1.05 |

The grain density of calcite mineral is 2.71 and the grain density of dolomite mineral is 2.87 (Simmons, 1965; Nur and Simmons, 1969; Domenico, 1984; Mavko et al., 2009).

Table 4.5 Varying proportions of major minerals in carbonates

| **Calcite (in fraction)** | **Dolomite (in fraction)** | **Grain density (Mix)** |
|---|---|---|
| 1 | 0 | 2.71 |
| 0.9 | 0.1 | 2.726 |
| 0.8 | 0.2 | 2.742 |
| 0.7 | 0.3 | 2.758 |
| 0.6 | 0.4 | 2.774 |
| 0.5 | 0.5 | 2.79 |
| 0.4 | 0.6 | 2.806 |

| | | |
|---|---|---|
| 0.3 | 0.7 | 2.822 |
| 0.2 | 0.8 | 2.838 |
| 0.1 | 0.9 | 2.854 |
| 0 | 1 | 2.87 |

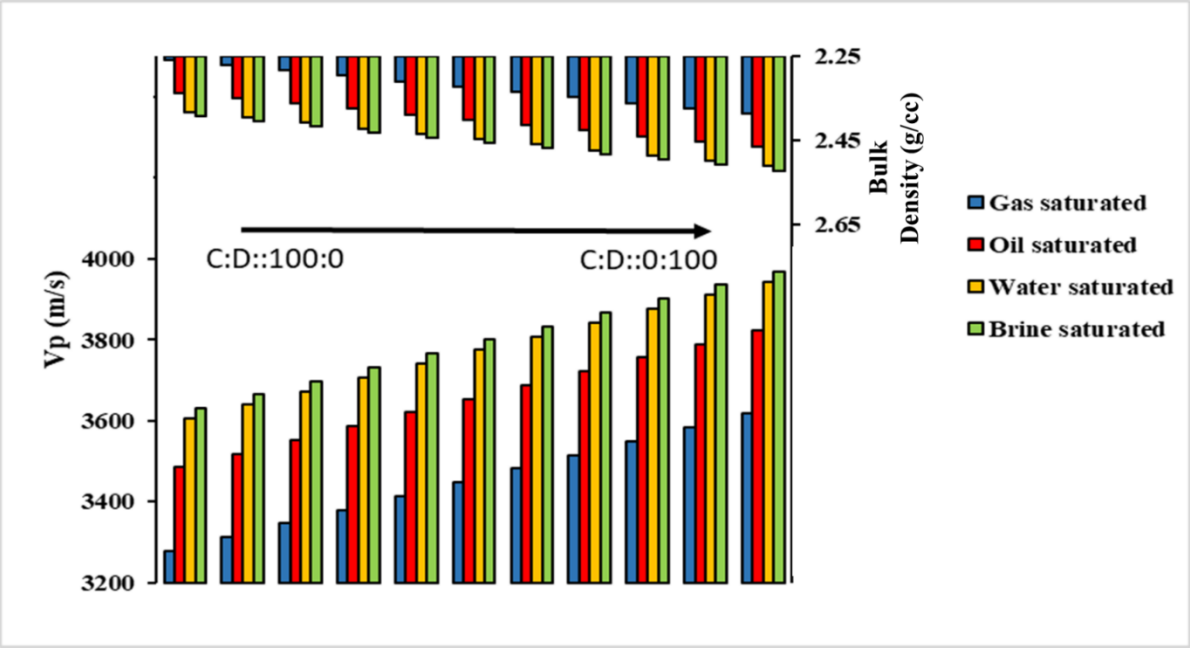


Figure 4.16 Saturation effects on $V_p$ considering variation in major mineral constituents for Carbonate C with porosity 19.2% (C:D means Calcite:Dolomite)

Keeping porosity constant and varying the major mineral composition for four different degrees of saturation, as shown in Figure 4.16, it was observed that as Dolomite content increases from 0 to 100%, $V_p$ also increases for all the four saturation conditions, respectively. This is because, as the calcite content decreases and dolomite content increases, there is an increase in the bulk density, which is again due to the higher grain density of Dolomite, resulting in an increase in $V_p$.

Now, keeping mineral composition fixed (Dolomite: Calcite:: 82:12) for carbonate C, porosity is varied from 2 to 40% (2%, 5%, 10%, 15%, 20%, 25%, 30%, 35%, 40%). Keeping these different porosity values in Bateman's equation, bulk density is obtained. Thereafter, keeping this obtained bulk density value in the generated equation, $V_p$ obtained for different saturation conditions is plotted in Figure 4.17.

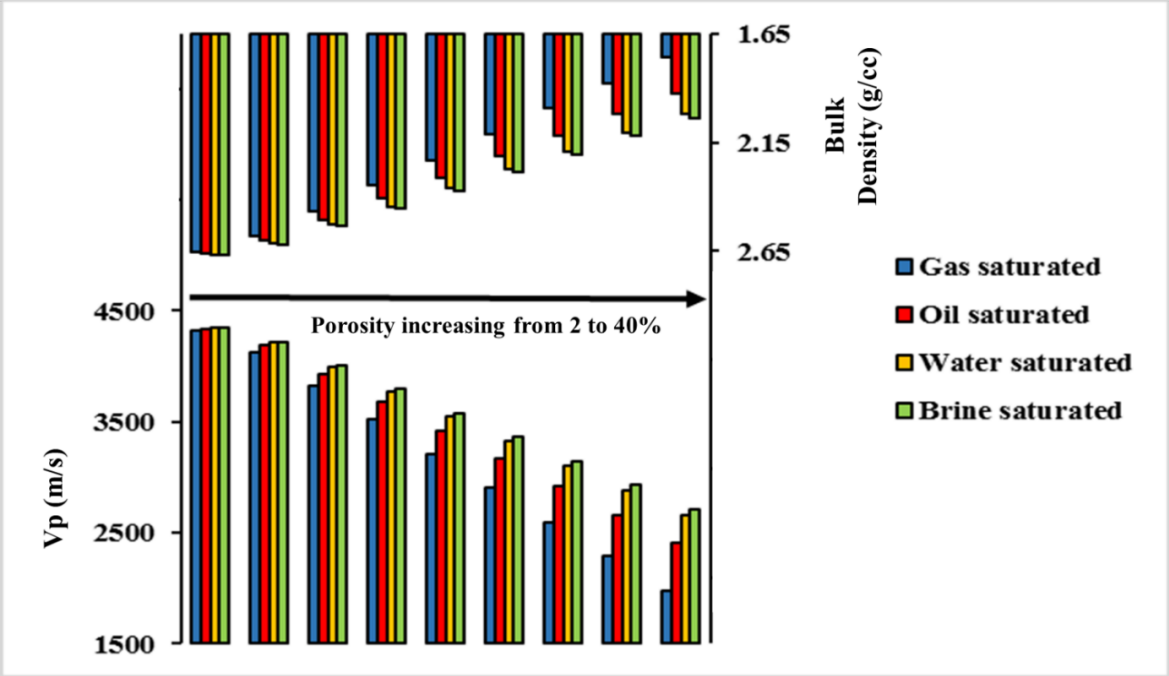


Figure 4.17 Saturation effects on $V_p$ considering variation in porosity for Carbonate C with fixed mineral composition % (Dolomite:Calcite::82:12)

Figure 4.17 highlights the alteration in the $V_p$ values when porosity is varied from 2 to 40% keeping major mineral composition constant. It is observed that there is an approximate 50% decrease in $V_p$ values when porosity varies from 2 to 40%. It can be said that porosity and mineral composition both have an effect on $V_p$, however, the porosity effect is more prominent, as observed from Figure 4.17.

It is to be noted that Gassmann's formulation is valid only at sufficiently low frequencies (Mavko et al., 2009), i.e., the formulation works well at low frequency seismic data (<100Hz) and may perform even less well as frequencies increase towards sonic logging ($10^4$ Hz) and laboratory ultrasonic measurements ($10^6$ Hz) (Mavko et al., 2009). The present study used transducers of frequency 54 kHz for the measurement of Vp in the laboratory. As a result, Gassmann's formulation was avoided and density, one of the prominent factors, was altered to observe the variations. The idea was to alter the mineral composition of the rock and thereafter observe the variations in Vp. This was done in a statistical way by changing the density (by varying the mineral composition) that would help in identifying the variations in Vp with the change in mineralogy. Additionally, for the wider applicability of the proposed model, we mathematically derived the variations in Vp due to change in fluid conditions for a set of rock types with predefined mineralogy and petrophysical properties. The variation in Vp indicates that the present methodology can be adapted as a generalized model for any reservoir.

Interpretation of reservoir characteristics away from the well-control or beyond the available data range is possible by capturing the fluctuations in Vp within the given geological constrains. Bulk mineralogy of rock may not be a standalone factor to correlate with Vp but has an effect on Vp along with density and porosity. However, there are several parameters that have a role to play in altering Vp while undertaking saturation studies. In other words, although density is one of the major factors, however, varying the density and keeping other factors constant may not entirely depict a true description, Hence, further complimentary studies may be carried out in the future on a larger dataset with different rock types under different geology setup.

## 4.4 Summary and Conclusions

This study attempts to bridge the gap between petrophysical, mineralogical and acoustic properties for carbonates that are known to possess a significant portion of the world's hydrocarbon reserves. The different properties were evaluated by conventional measurements and advanced techniques (digital image analysis). Ultrasonic measurement technique was used to model the compressional wave velocity ($V_p$) at the laboratory. For this, transducers of 54 kHz frequency were used to measure $V_p$ of carbonate core plugs by utilising the through transmission technique. The pore size (maximum, minimum, average and mode values) and aspect ratio were measured by employing the digital image analysis technique. Regression analysis was performed to understand how petrophysical properties, mineralogy affects $V_p$ and a generalized rock physics model is developed based on $V_p$. The effectiveness of the predictive velocity model improved on incorporating multiple parameters such as bulk density, porosity, pore size and aspect ratio collectively. In other words, $V_p$ estimates can be improved if the multivariate analysis is performed. A combination of bulk density, porosity and mode pore size was able to explain more than 83% of the deviation of $V_p$ ($R^2$=0.83). Thus, this study maximises the use of information obtained from laboratory analysis that is usually constrained by accurate geological details. Moreover, the effect of saturation on carbonates was statistically investigated by (i) keeping porosity constant and varying the major mineral constituents and (ii) keeping major mineral constituents constant and varying the porosity. Both these variations define the trend of velocity and provide key insight into how porosity and mineral composition play a fundamental role in altering $V_p$ values.

The results demonstrate the intimate relationships/correlations among different parameters and also highlight the need to incorporate an integrated analysis such as multi-regression analysis into the conventional physics-based transforms. The methodology/results presented in this

research article can be used by developers/users of rock physics laboratory pertaining to carbonates for future research use.

# Chapter 5
# A Multivariate Statistical Approach in Correlating the Acoustic Properties with Petrophysics and Mineralogy on Sandstones

## 5.1 Introduction

Sandstones result from a series of complicated geological and hydrodynamical processes, which induces heterogeneity in the pore spaces (Bakke and Oren, 1997). This heterogeneity, leading to a modification in the original structure, is largely responsible for altering the rock's petrophysical and geomechanical properties. Also, the prediction of the petrophysical properties of sandstone reservoirs is sensitive to the primary composition of the sediments (Bjørlykke and Jahren, 2010). Primary sediment composition is controlled by the mineralogical and textural composition of the depositional environment and by the diagenetic processes (Bjørlykke, 2014). The amalgamation of mineralogical and petrographical knowledge is essential for better approximation and analysis of rock behaviour (Ündül, 2016). However, little literature is available to systematically investigate how mineralogical composition controls the seismic properties and influence them (Dentith et al., 2020).

This study develops a multivariate statistical approach to understand the effects of all the parameters on $V_p$ in combination rather than separately. Multivariate regression analysis is a statistical method for predicting dependent variables based on changes in one or more or from a collection of independent variables (Johnson and Wichern, 2002). This method was applied in the present study to understand the undercovered trend and assess the influence of multiple parameters and their effects on the physical properties. Previous studies derived different relationships correlating $V_p$ with density, porosity and bulk mineralogy on a one to one basis for sandstones. However, bulk mineralogy of rock may not be a standalone factor to correlate with $V_p$ but has an effect on $V_p$ along with density and porosity. Therefore, this study intends to present a methodology for the interpretation of $V_p$ data from the laboratory measurements at ambient conditions for sandstone samples from the Upper Assam basin, India. For more than a century, the Upper Assam basin has been a prolific hydrocarbon producing basin (Mandal et al., 2011). An integrated analysis was conducted on the core samples by critically examining the associations of the mineralogical, petrographical and petrophysical properties with the ultrasonic measurements. Petrographic and mineralogical studies were conducted on all rock core plugs. Besides, this study proposes models in the form of equations relating ultrasonic compressional velocity with the petrophysical properties and the mineralogical content of the rocks under investigation by using a multivariate statistical approach. Several reliable

equations based on different petrophysical properties have been formulated to evaluate sonic velocity, which is important for identifying future prospective reservoirs or forecasting beyond the available data range. An effort is made to improve the predictivity of velocity behaviour related to the natural variability in porosity, density and mineralogy. The formulation so presented is derived from the laboratory data to help reduce the ambiguity when inferring variation in formation properties from acoustic properties. The developed models can be used in quantitative seismic interpretation to identify prospective reservoirs and for reservoir characterisation. Such methodology becomes crucial when seismic or sonic data are to be used to deduce petrophysical, geomechanical properties before embarking on a time-consuming and costly quantitative interpretation project, such that there is a maximum likelihood of attaining the desired outcome of the project. This approach of multi-parameter analysis has broader applications in modelling and analysing the experimental results in diverse fields such as engineering geology, rock engineering, rock and soil mechanics, mining-related issues (Jennrich, 1995; Grima and Babuska, 1999; Gokceoglu and Zorlu, 2004; Yilmaz and Yuksek, 2009; Monjezi et al., 2012; Kumar et al., 2013; Mishra and Basu, 2013; Heidari et al., 2018). The aim is to evaluate the dependency of the mineralogical parameters and petrophysical properties on the velocity and hence address the research gap in the literature regarding the influence of these parameters on the seismic properties.

## 5.2 Materials and Methods

### 5.2.1 Geology of the Study Area and Sample Description

The present study is based on the laboratory-based petrophysical and acoustic analysis of sandstone rock core plugs of one-inch diameter from the Upper Assam basin (Assam Arakan basin). The Upper Assam basin is a tertiary sub-basin (Mathur, 2014), and it is surrounded by the Himalayan orogenic belt in the north, Mishmi Thrust in the east, Schuppen Belt in the south (Mandal and Dasgupta, 2013). As per Bastia (2006), this basin is classified as a Category I sedimentary basin, and it is the first known hydrocarbon province (Pahari et al., 2008) in India. The sandstone core plugs belong to Tipam and Barail group; however, sample representation or identification from each group is confidential. As per the available literature (Wandrey, 2004b; Bharali and Borgohain, 2013), the bulk of gas and oil that was discovered in Upper Assam was found in Barail (Upper Eocene to Lower Oligocene age) and Tipam (Upper Miocene age) group. As per Mathur (2014), hydrocarbons were discovered in the Oligocene Barail Formation, Upper Miocene Girujan Formation, the Lakadong member of the Sylhet Formation (Lower Eocene) and the Langpar Formation (Upper Palaeocene). The location map

and stratigraphic succession of the Upper Assam basin are shown in Figure 5.1 and Figure 5.2 respectively.

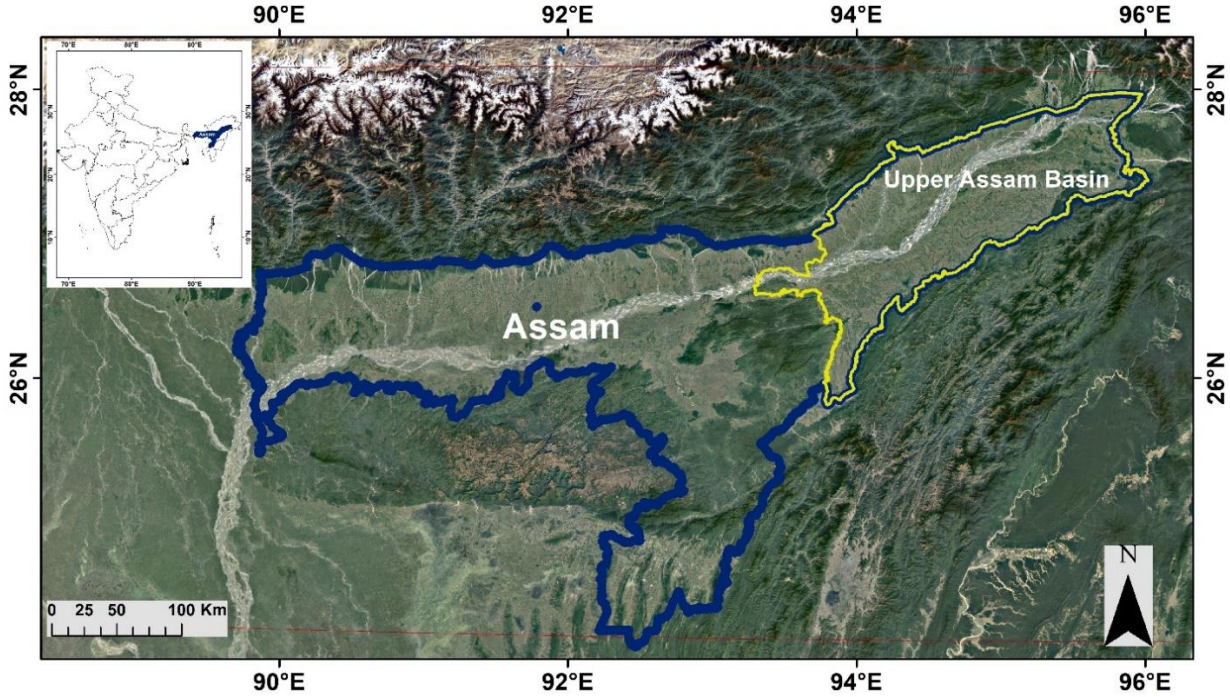


Figure 5.1 Study area location of the investigated sandstone rock core plugs from Upper Assam (UA) basin

### 5.2.2 Methodology

Sandstone rock core plugs, fifteen in number, were obtained from the Barail and Tipam formations of the Upper Assam basin, India, were used to measure parameters that include acoustic, petrophysical and mineralogical variables in the laboratory (Figure 5.3). Before carrying out any analysis, all the rock core plugs were cleaned using the soxhlet extractor apparatus to remove any organic content. The rock samples were then used for evaluating different parameters. Compressional wave velocity ($V_p$) was measured in the laboratory using piezoelectric transducers of 54 kHz by employing the ultrasonic-through transmission technique. Porosity was measured using a helium gas porosimeter, while permeability was measured using a nitrogen gas permeameter. The grain and pore diameters were calculated with the help of FESEM images. The petrographic analysis was carried out using optical microscopy. The mineral content of the rock core plugs was determined by XRD (X-ray Diffraction). The procedure of determining each parameter is discussed and elaborated in Chapter 3.

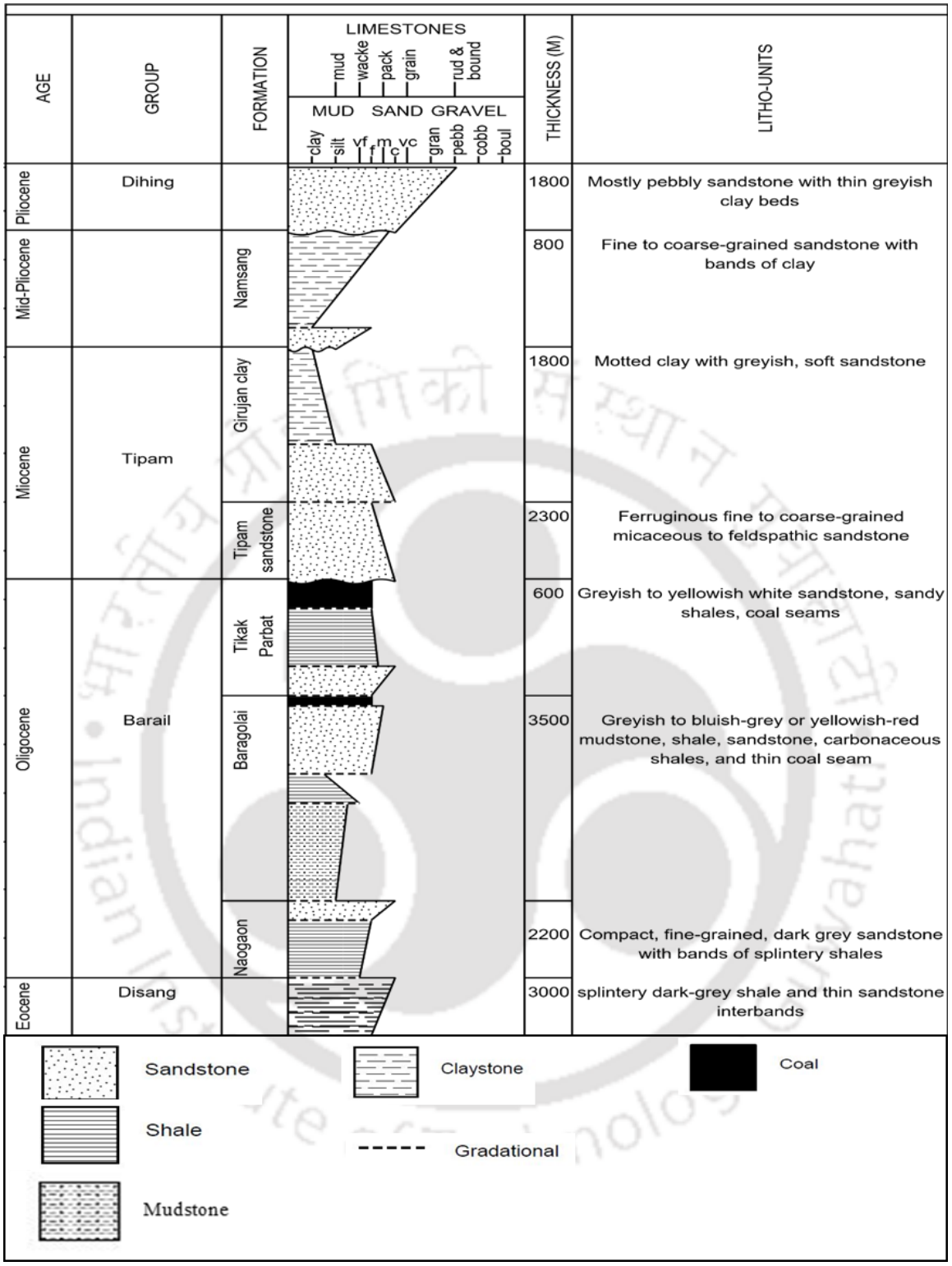


Figure 5.2 Stratigraphic column of Upper Assam (UA) basin (modified from Mishra and Ghosh, 1996)

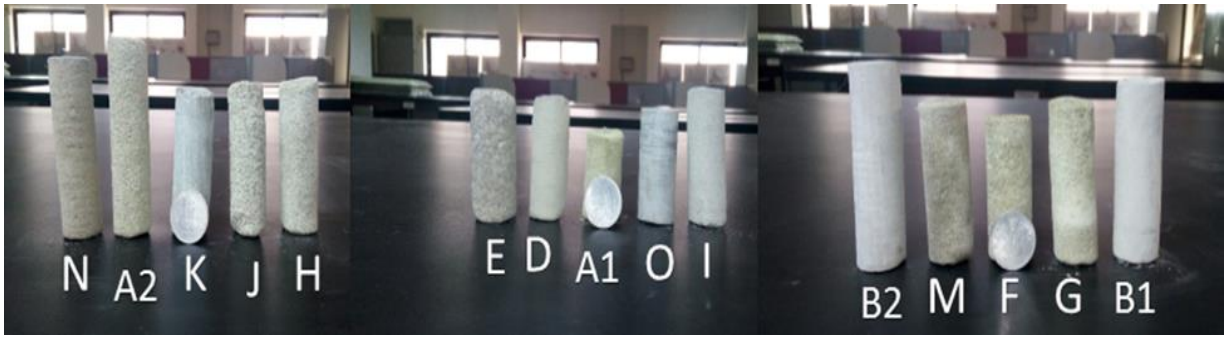


Figure 5.3 Sandstone rock samples considered in this study obtained from the Upper Assam basin

### 5.2.3 Statistical Analysis to Develop Mathematical Models for $V_p$

For the present study, multivariate regression analysis was applied to formulate correlations between $V_p$, the output or dependent variable and porosity, density, mineral composition (major mineral constituents, i.e., quartz and feldspar content), which are the inputs or independent variables. This was done to evaluate the dependency of the mineralogical parameters and petrophysical properties on the velocity and hence address the research gap in the literature on how these parameters influence the seismic properties (Dentith et al., 2020). By adopting this methodology, statistically derived rock physics equations (best-fit relationships) were developed. The coefficient of determination ($R^2$) was used to indicate the prediction efficacy of the model (between the measured and predicted values).

Additionally, the deviation in $V_p$ was investigated by varying the mineral content and porosity. The mineral content (in %) was varied from Quartz: Feldspar = 80:20 to 40:60 with an increment of 10% each for a set of porosity (5%, 10%, 20% and 30%) by using Bateman's equation (Bateman, 1985). This analysis was performed for different saturation conditions, i.e., water-saturated, gas saturated, oil-saturated and brine saturated. The statistically derived rock physics equation relating $V_p$ in terms of porosity and density was used to derive the variations in $V_p$.

Similarly keeping quartz content fixed (85%), the different feldspar contents (F1=Potassium Feldspar, F2=Sodium Feldspar, F3=Calcium Feldspar) were varied from 0% to 15% with an increment of 5% for different porosity ranges (5%, 10%, 20% and 30%) and the variations in $V_p$ were plotted for various saturation conditions.

## 5.3 Results and Discussion

### 5.3.1 Acoustic and Petrophysical Properties

The ranges obtained for $V_p$ and different petrophysical properties (porosity, bulk density, grain density and permeability) for the investigated sandstone plugs are summarised in tabular form along with the standard deviation (SD) in measurements (Table 5.1). The obtained ranges are also shown in histograms (Figure 5.4), along with the standard deviation in measurements of velocity, density and porosity in the form of an error bar. The nomenclature followed in naming the sample includes the type of sample (SS for sandstone), name (A, B1, B2 etc.) and the location (UA for Upper Assam basin).

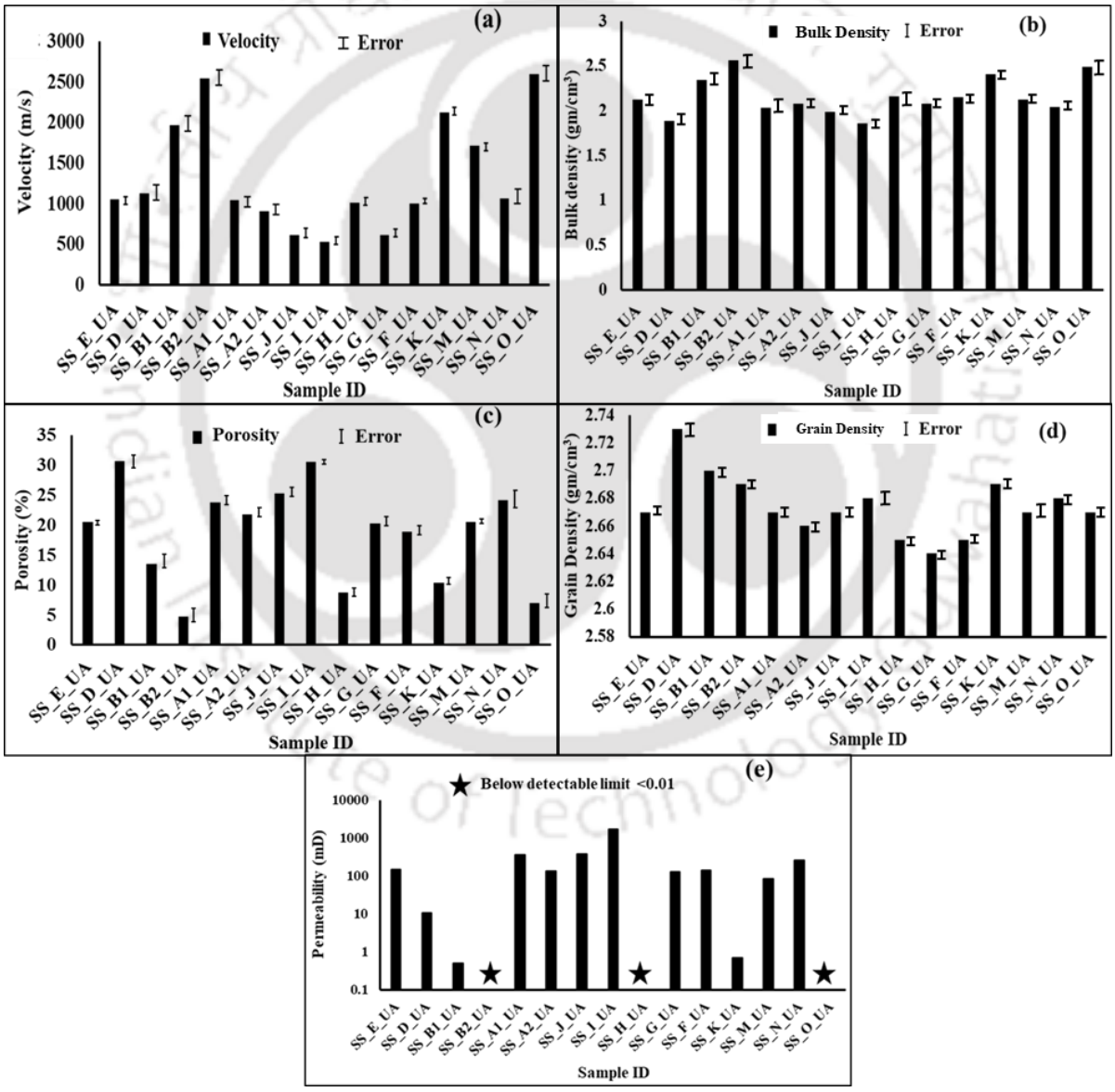


Figure 5.4 Histograms depicting the range of (a) P-wave velocity-$V_p$ and (b) petrophysical properties (bulk density, porosity, grain density and permeability) for the sandstone rock core plugs

Hydrocarbons are being produced for more than a century from the Upper Assam basin (Pahari et al., 2008; Mandal et al., 2011). As per Wandrey (2004b), the reservoir rocks are interbedded sandstones of the Kopili formation, sandstones of Barail, Surma and Tipam groups. Several researchers investigated the petrophysical and acoustic properties of this basin in the literature. Wandrey (2004b) reported a porosity range of 7-30% and a permeability range of 8-800 mD. Zaei and Rao (2019) reported average density as 2.40 g/cc and porosity as 13% for Tipam sandstones. The log derived porosity ranges from 27-30% (Ishwar and Bharadwaj, 2013) and 15-30% (Bharali and Borgohain, 2013). Similarly, Gogoi and Chatterjee (2019) reported log derived porosity for Tipam sandstones as 30-36% and for Barail sandstones as 18-30%. Mandal et al. (2011) reported a regional velocity trend in the range of 1600- 2900 m/s. Similarly, Gogoi and Chatterjee (2018), reported seismic velocity in the range of 2500-4000 m/s. Based on the variation in the range of these properties obtained from the literature, fifteen sandstone core plugs were examined to cover the maximal variability of the different parameters.

Table 5.1 Tabular summary of different measured properties along with the standard deviations (SD) for the sandstone plugs

| **Sample Name** | **Depth (m)** | **Velocity (m/s)** | | **Bulk Density (g/cc)** | | **Porosity (%)** | | | **Grain Density (g/cc)** | | **Permeability (mD)** |
|---|---|---|---|---|---|---|---|---|---|---|---|
| | | $V_p$ | **SD** | $\rho$ | **SD** | $\phi$ | **SD** | **% change** | **GD** | **SD** | $k$ |
| SS_E_UA | 2642-2648 | 1050 | 4.71 | 2.12 | 0.0006 | 20.55 | 0.021 | 0.103 | 2.67 | 0.001 | 142.75 |
| SS_D_UA | 2444-2452 | 1130 | 24.94 | 1.89 | 0.0003 | 30.73 | 0.085 | 0.276 | 2.73 | 0.007 | 10.44 |
| SS_B1_UA | 2420-2421 | 1970 | 29.43 | 2.34 | 0.0004 | 13.57 | 0.085 | 0.625 | 2.7 | 0.001 | 0.489 |
| SS_B2_UA | 2420-2421 | 2550 | 25.39 | 2.56 | 0.002 | 4.75 | 0.18 | 3.791 | 2.69 | 0.005 | <0.01 |
| SS_A1_UA | 2995-3000 | 1040 | 16.99 | 2.03 | 0.0011 | 23.87 | 0.014 | 0.059 | 2.67 | 0.001 | 354.53 |
| SS_A2_UA | 2995-3000 | 910 | 14.25 | 2.08 | 0.0008 | 21.84 | 0.015 | 0.07 | 2.66 | 0.001 | 135.061 |

| | | | | | | | | | | | |
|---|---|---|---|---|---|---|---|---|---|---|---|
| SS_J_UA | 2662-2671 | 610 | 9.42 | 1.99 | 0.0001 | 25.3 | 0.049 | 0.196 | 2.67 | 0.001 | 369.1 |
| SS_I_UA | 3018-3026 | 530 | 8.16 | 1.86 | 0.0005 | 30.55 | 0.026 | 0.087 | 2.68 | 0.001 | 1691.5 |
| SS_H_UA | 2963-2972 | 1013 | 9.42 | 2.16 | 0.0013 | 8.73 | 0.057 | 0.648 | 2.65 | 0.01 | <0.01 |
| SS_G_UA | 2832-2841 | 610 | 8.16 | 2.08 | 0.0008 | 20.32 | 0.057 | 0.278 | 2.64 | 0.001 | 125.38 |
| SS_F_UA | 2802-2810 | 1000 | 4.71 | 2.15 | 0.0003 | 18.9 | 0.028 | 0.15 | 2.65 | 0.001 | 137.31 |
| SS_K_UA | 3897-3904 | 2120 | 4.71 | 2.41 | 0.0001 | 10.45 | 0.064 | 0.609 | 2.69 | 0.007 | 0.673 |
| SS_M_UA | 3374-3381 | 1710 | 4.71 | 2.12 | 0.0006 | 20.49 | 0.007 | 0.035 | 2.67 | 0.007 | 83.81 |
| SS_N_UA | 3258-3267 | 1060 | 34.64 | 2.04 | 0.0002 | 24.13 | 0.28 | 1.162 | 2.68 | 0.013 | 259.58 |
| SS_O_UA | 3148-3156 | 2600 | 25.33 | 2.49 | 0.0013 | 6.98 | 0.231 | 3.307 | 2.67 | 0.007 | <0.01 |

### 5.3.2 Petrography

Sandstone plugs are of blackish-grey to light grey in colour and coarse to fine in texture. On thin section examination, the mineral phase present were quartz, feldspar and mica (Figure 5.5). The spectra obtained from XRD show the presence of quartz and feldspar (albite, potassium feldspar and anorthite) as major minerals present in sandstones (Figure 5.6). Table 5.2 summarizes the results of the semi-quantitative XRD analysis of sandstones. For sandstone A2, kaolinite mineral was present (24%), while in sandstone O, illite and kaolinite minerals, 12% each, were also present.

### 5.3.3 Image Analysis

Investigations on the representative rock core plugs under FESEM-backscattered electron mode revealed the presence of many pores of varying sizes (as highlighted in Figures 5.7 and 5.8). Such variability in the pores may be due to changes in the pore structure induced by a diagenetic process that probably would have influenced the petrophysical properties. Figures 5.7(a) and (b) shows the FESEM images for sandstone J and D, respectively, while Figures 5.8(a) and (b) shows the pore types of sandstone K and H, respectively. Three pore types were

recognised from the FESEM images, which are intergranular pore (pores between grains), intragranular pore (pores within individual grains) and microcracks.

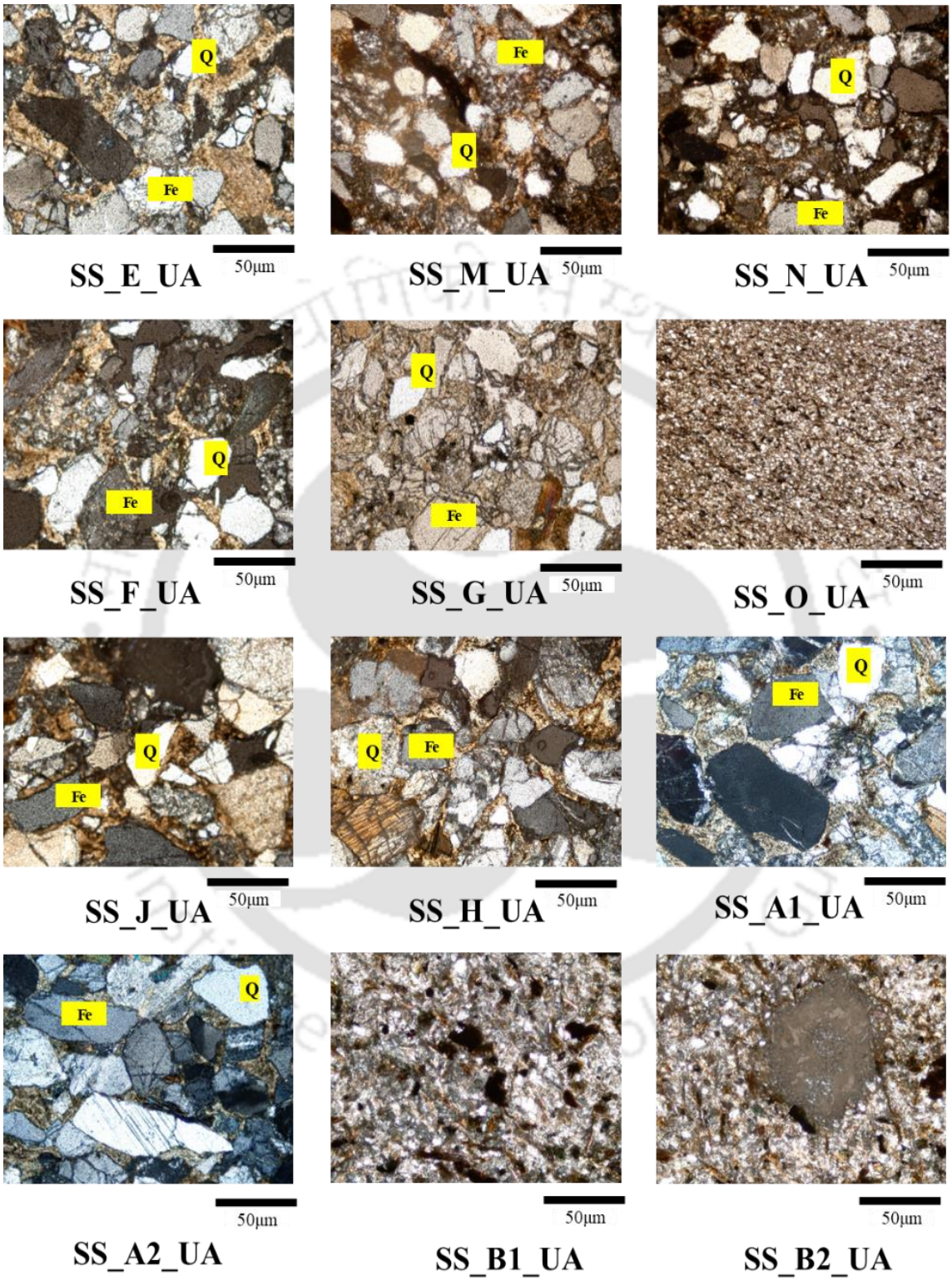


Figure 5.5 Thin section images of the sandstone samples (Magnification: 10X, Scale: 50µm) (Q stands for Quartz while Fe stands for Feldspar)

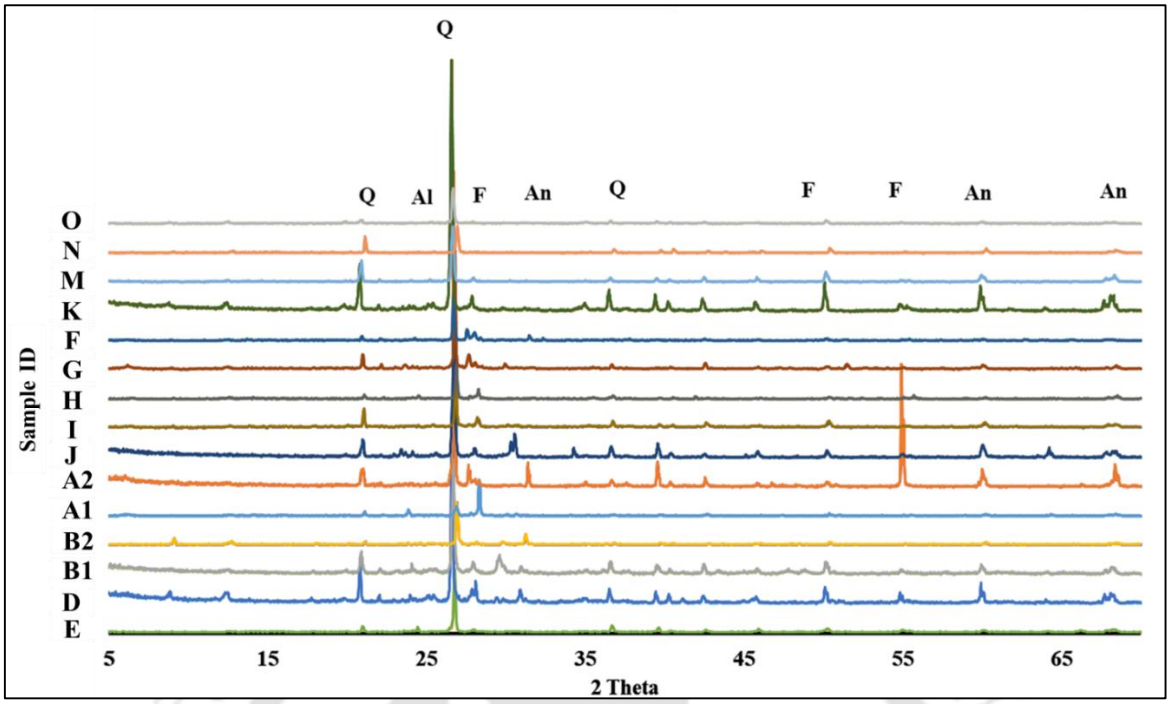


Figure 5.6 X-ray diffraction pattern of sandstone rock core plugs where Q- Quartz, Al- Albite, F- Feldspar, An- Anorthite (legends showing the sample ID)

Table 5.2 Mineral composition extracted from X-ray diffraction analysis for the selected sandstone rock core plugs

| Sample ID | Mineral Composition (%) | | | | | |
|---|---|---|---|---|---|---|
| | Quartz | Albite | K Feldspar | Anorthite | Biotite | Muscovite |
| SS_E_UA | 5 | 1 | 59 | 0 | 0 | 36 |
| SS_D_UA | 25 | 8 | 38 | 0 | 0 | 27 |
| SS_B1_UA | 66 | 0 | 10 | 22 | 3 | 0 |
| SS_B2_UA | 32 | 15 | 47 | 0 | 0 | 0 |
| SS_A1_UA | 44 | 32 | 10 | 14 | 0 | 0 |
| SS_A2_UA | 32 | 3 | 11 | 5 | 6 | 0 |
| SS_J_UA | 71 | 29 | 0 | 0 | 0 | 0 |
| SS_I_UA | 29 | 2 | 53 | 0 | 9 | 7 |
| SS_H_UA | 76 | 5 | 7 | 11 | 0 | 0 |
| SS_G_UA | 7 | 6 | 57 | 30 | 0 | 0 |
| SS_F_UA | 11 | 29 | 20 | 41 | 0 | 0 |
| SS_K_UA | 32 | 4 | 0 | 0 | 9 | 51 |
| SS_M_UA | 62 | 18 | 0 | 14 | 0 | 0 |

| | | | | | | |
|---|---|---|---|---|---|---|
| SS_N_UA | 68 | 0 | 31 | 0 | 0 | 0 |
| SS_O_UA | 69 | 0 | 0 | 0 | 7 | 0 |

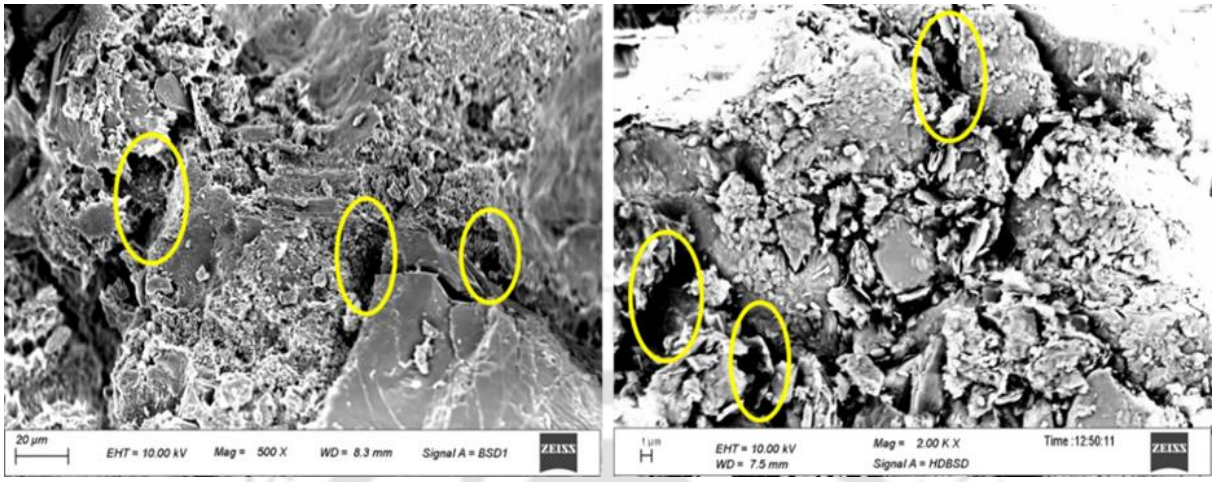


Figure 5.7 Details of the micropore were investigated with the help of FESEM in (a) SS_J_UA {Magnification: 500X}, (b) SS_D_UA {Magnification: 2KX} (Yellow circles represent pores)

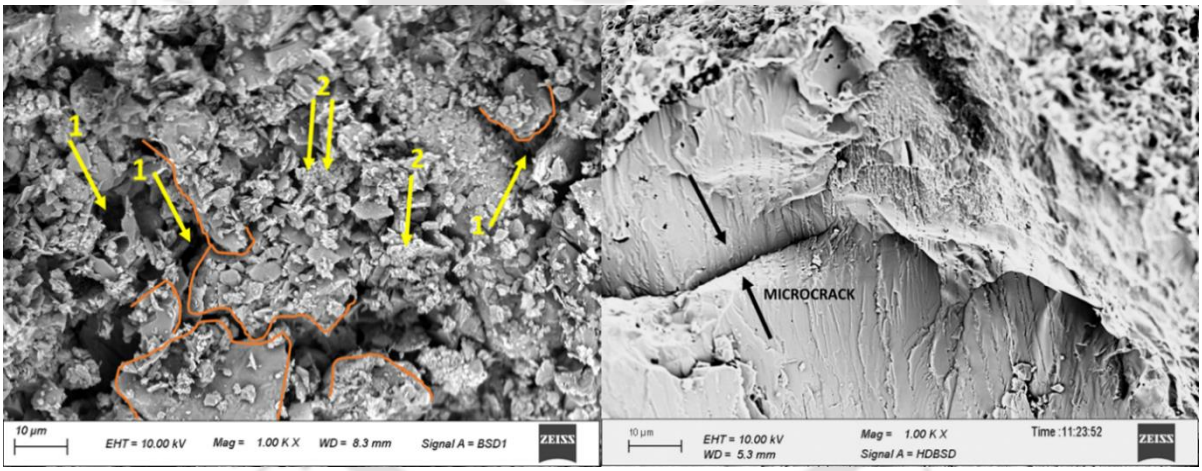


Figure 5.8 Pore types of sandstones by FESEM observations (a) intergranular (marked as 1) and intragranular (marked as 2) pore in SS_K_UA, (b) microcrack in SS_H_UA {Magnification: 1KX}

### 5.3.4 Regression Analysis

Interrelationships between various properties of sandstones are presented in Figure 5.9 (Figure 5.9(a) shows the variation of bulk density and porosity, Figure 5.9(b) shows the variation of bulk density and $V_p$, Figure 5.9(c) shows the variation of grain density and porosity, Figure 5.9(d) shows the variation of grain density and $V_p$, Figure 5.9(e) shows the variation of porosity and $V_p$ and Figure 5.9(f) shows the variation of permeability and $V_p$). The two critical properties of rocks, i.e., porosity and bulk density, impact the petrophysical and geomechanical

properties of sedimentary rocks (Seif, 2016). Bulk density reveals the composition of different minerals and porosity (Nabawy and Barakat, 2017). An inverse trend was observed between bulk density and porosity with $R^2$ = 0.879 (Figure 5.9(a)). The grain density values obtained for the sandstone rock core plugs in this study varies from 2.64 g/cc to 2.73 g/cc (Figure 5.4(d)). The observed variation in grain density values may be related to the changes in lithology since similar grain density values would signify homogeneous lithologies (Nabawy et al., 2015; Nabawy and David, 2016). The relationship between porosity and $V_p$ shows an inverse trend (Figure 5.9(e)). This is because seismic velocity in the pores is lower than that of the grains. The moderate correlation ($R^2$=0.596) can be attributed to the influence of bulk density. It is known that as bulk density increases, porosity decreases, and subsequently, $V_p$ increases. Bulk density and $V_p$ plot exhibit a direct correlation between the two, as shown in Figure 5.9(b). However, to address the low correlation in the porosity-$V_p$ plot, a multivariate analysis is performed in the following sections, and the interdependence among porosity, bulk density and $V_p$ is highlighted. An inverse trend was observed between permeability and $V_p$ with $R^2$= 0.727, as shown in Figure 5.9(f).

To investigate whether grain and pore size also has a role in altering $V_p$ in sandstones, the obtained grain and pore size (mode values) from FESEM analysis were plotted with $V_p$ (Figure 5.10), and no correlation was observed between them. However, in the case of carbonates, pore size plays a vital role in altering $V_p$, which complicates the relationship between $V_p$ and petrophysical properties (Assefa et al., 2003). Hence, for the present study, grain and pore size does not influence $V_p$, compared with other factors such as bulk density and porosity.

The variation of permeability with porosity for sandstones with the coefficient of determination 0.475 is shown in Figure 5.11. The three samples (along with their porosity values) for which permeability is less than 0.01 mD (below the detectable limit) were B2 (4.75%), H (8.73%) and O (6.98%). The low permeability for three sandstone samples, B2, H, O, may be due to lower porosity values. The correlation between porosity and permeability may help understand the fluid flow within one formation (Tiab and Donaldson, 2015). On the other hand, as per Tiab and Donaldson (2015), a core may also show higher porosity value without showing any permeability (clays, shales), while the reverse may also be true (micro fractured carbonates).

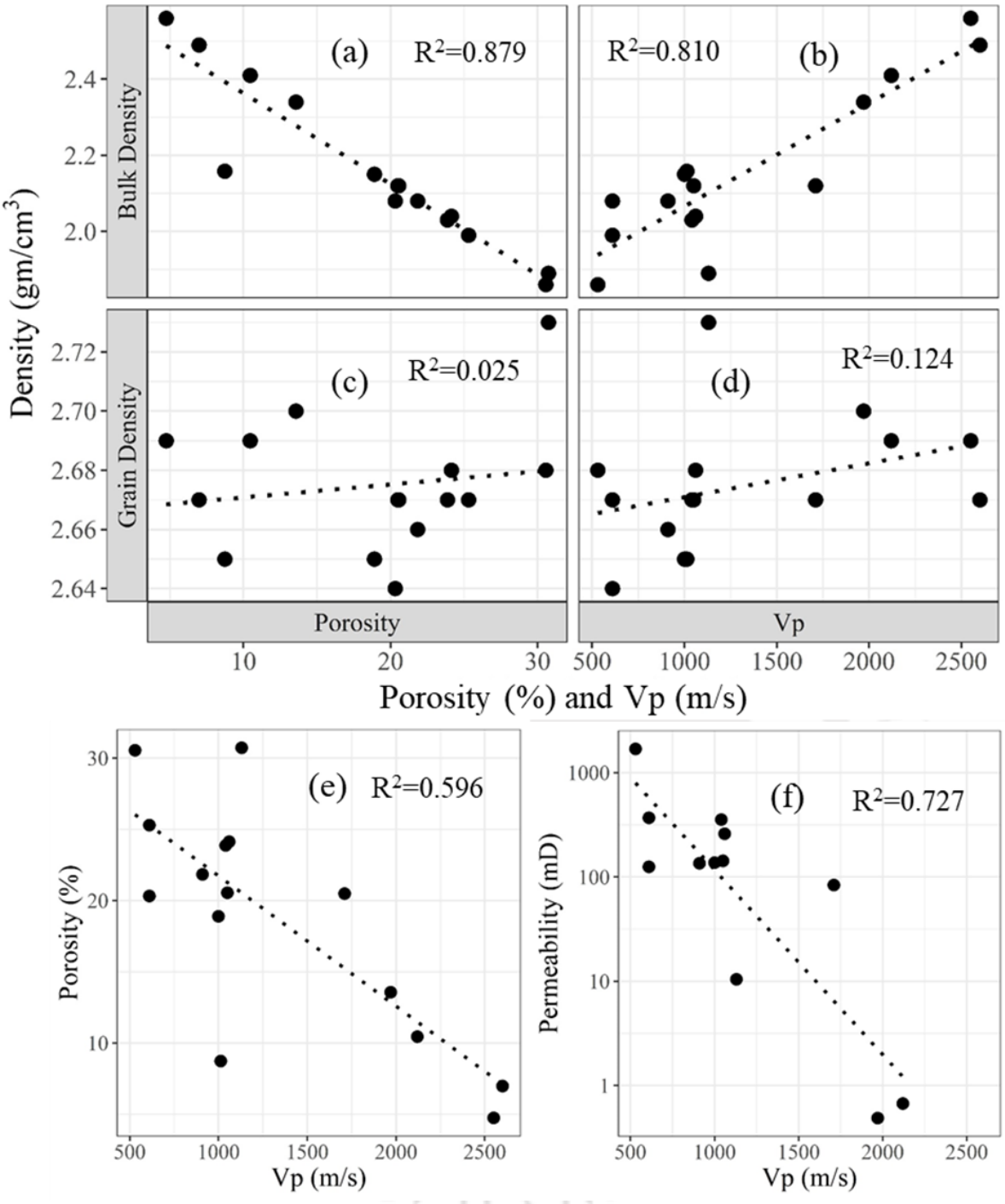


Figure 5.9 Correlations between different parameters for sandstones [(a) Bulk Density-Porosity, (b) Bulk Density-Velocity, (c) Grain Density-Porosity, (d) Grain Density-Velocity, (e) Porosity-Velocity, (f) Permeability-Velocity

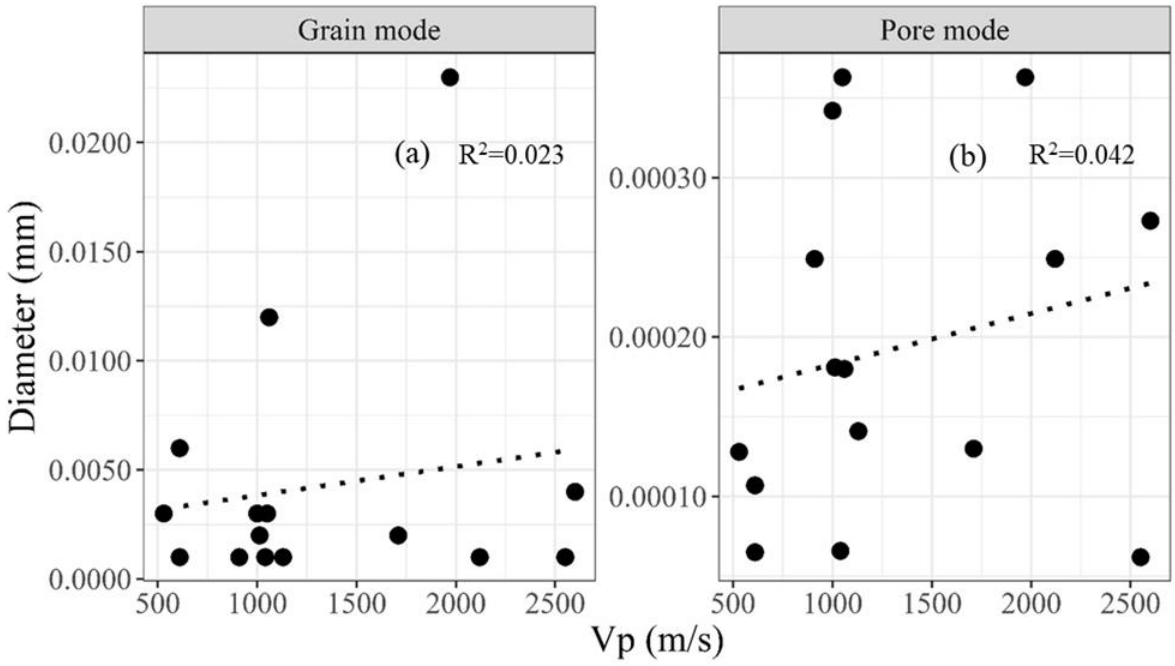


Figure 5.10 Variation of $V_p$ with (a) Grain size (mode values) and (b) Pore size (mode values) for sandstone rock core plugs

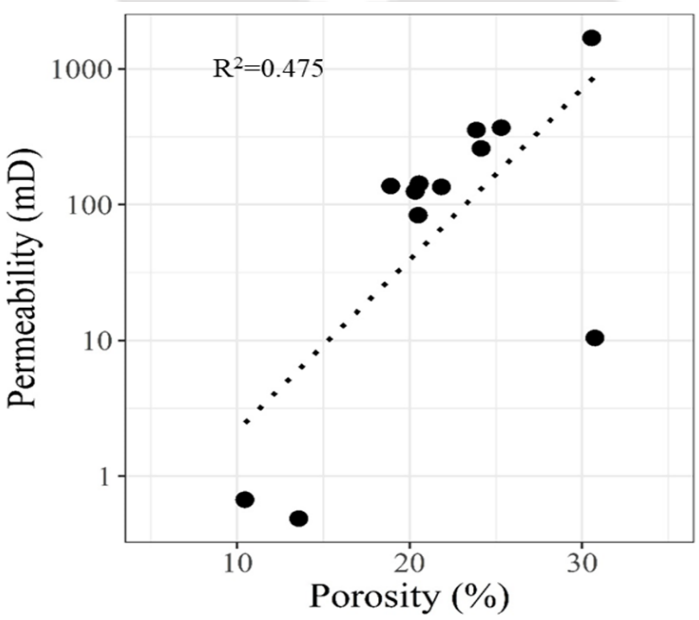


Figure 5.11 Porosity-permeability crossplot for sandstones

### 5.3.5 Multivariate Statistical Analysis

There are multiple factors that have coherent dominance on rock's petrophysical properties. With this knowledge, attempting to relate each property to all the factors will lead to ambiguity, which would be impractical and lead to under or overestimation. This can also be understood that several factors are interdependent. For example, considering major mineral constituents in

the case of clastic rocks, a subsequent increase in quartz content will certainly lead to a corresponding decrease in feldspar content. Thus, to understand the undercovered trend and assess the influence of multiple underlying parameters and their effects on the physical properties, multivariate analysis was performed in this study for sandstones.

It is evident from XRD analysis (Table 5.2) that the major minerals found in sandstones were quartz and feldspar (albite, potassium feldspar and anorthite). The cross-plot showing relationship between mineral composition and $V_p$ for sandstones is presented in Figure 5.12. It was observed that, for a higher quartz content in a sample, a corresponding increase in $V_p$ was observed. On the contrary, a higher feldspar content in a particular sandstone rock results in a correspondingly lower $V_p$ value. Thus, for a specific sandstone sample, keeping other petrophysical parameters constant, a more significant proportion of quartz content will be accompanied by a lower proportion of feldspar content, thereby leading to a higher $V_p$ value. However, if only the mineralogical composition and its relation with $V_p$ were to be considered for sandstones, establishing a direct relationship would be difficult since several parameters have a coherent effect. For instance, in sandstone O, illite and kaolinite minerals are also present (12% each). These clay minerals tend to reduce $V_p$ in sandstones (Han et al., 1986; Klimentos, 1991). Despite this, $V_p$ is 2600 m/s since the porosity is on the lower side (6.98%). Hence, it highlights that a one-to-one relationship may not depict a clear correlation, and an integrated analysis is required to understand the coherent effect.

As explained, porosity shows an inverse relation to $V_p$. Therefore, a change in porosity for the same proportion of mineral composition will result in a change in $V_p$ relative to the change in porosity. Therefore, any change in $V_p$ value will be reflected in porosity value proportionately. In other words, a rise in porosity will always lead to a decline in velocity.

The dependency of different variables on $V_p$ was investigated, and equations were proposed in this study. As observed from Figure 5.9(e), examining one to one relation between porosity-$V_p$ yielded a low correlation ($R^2$=0.596). Hence, an integrated analysis incorporating bulk density factor in porosity-$V_p$ relation was analysed. Equation (5.1) depicts the correlations between $V_p$, bulk density and porosity. Integrating bulk density factor in porosity-$V_p$ relation, $R^2$ improved from 0.596 to 0.852. This equation signals that the bulk density factor must also be included while assessing the correlation between $V_p$ and porosity. Thereafter, $V_p$ was presented in terms of porosity, bulk density, feldspar and quartz content and the following equations were proposed (equations (5.2), (5.3) and (5.4)). Equation (5.4) considers all the petrophysical and mineralogical variables that influence the acoustic properties. The proposed equations are

presented below (P-wave velocity $V_p$ in m/s, Bulk density ρ in g/cc, Porosity $\phi$ in %, Quartz content Q in %, Feldspar Content F in %):

- **Considering $V_p$, porosity and bulk density only**

$$V_p = 4743.62\rho + 51.43\phi - 9873.42 \qquad R^2 = 0.852 \qquad (5.1)$$

- **Considering $V_p$, porosity, bulk density and Feldspar content only**

$$V_p = 4467.70\rho + 49.34\phi - 4.89F - 9026.05 \qquad R^2 = 0.895 \qquad (5.2)$$

- **Considering $V_p$, porosity, bulk density and Quartz content only**

$$V_p = 4871.12\rho + 57.91\phi + 4.64Q - 10465.73 \qquad R^2 = 0.889 \qquad (5.3)$$

- **Considering $V_p$, porosity, bulk density, Quartz and Feldspar content only**

$$V_p = 4609.63\rho + 52.89\phi + 2.08Q - 3.39F - 9552.04 \qquad R^2 = 0.899 \qquad (5.4)$$

The crossplots between $V_p$, and Quartz, Feldspar content was plotted to investigate the multifaceted dependence. From the plots, as shown in Figure 5.12, the low value of $R^2$, i.e., $R^2$ =0.074 for $V_p$- Quartz plot and $R^2$ = 0.224 for $V_p$-Feldspar plot, were observed. This is due to the presence of outliers that is also dependent on porosity and bulk density. Hence, multiple parameters have a coherent influence, and an integrated approach should be adopted.

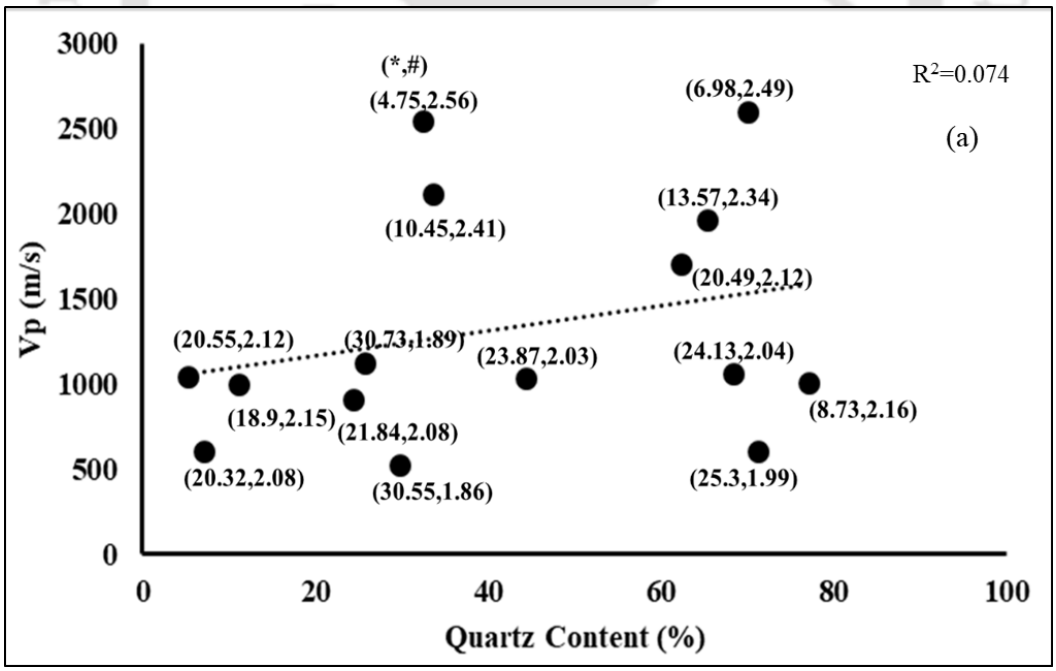

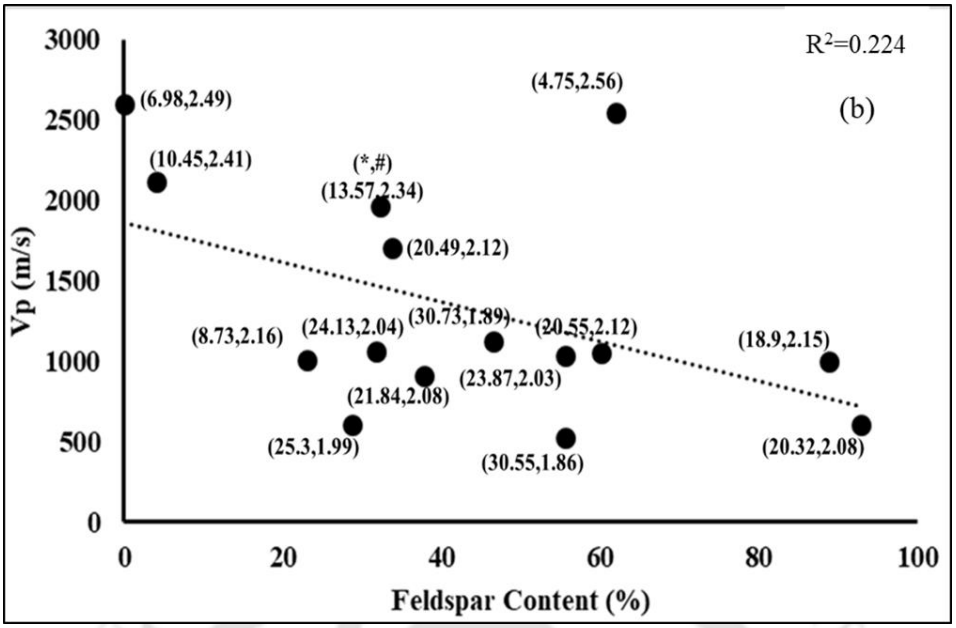


Figure 5.12 Cross-plot demonstrating a relationship between $V_p$ and mineral content for sandstones [(a) $V_p$-Quartz modelling, (b) $V_p$-Feldspar modelling] {* denotes porosity (in %) and # denotes bulk density (in g/cc)}

The applicability of the statistically derived equations (equations (5.1), (5.2), (5.3) and (5.4)) was checked by plotting the measured $V_p$ with the predicted $V_p$ from these equations (Figure 5.13). The obtained $R^2$ values provide conclusive evidence regarding the dependability of the relationships derived by using multivariate regression analysis. The obtained correlations in this study highlight that for sandstones, lithology and porosity impact the elastic properties.

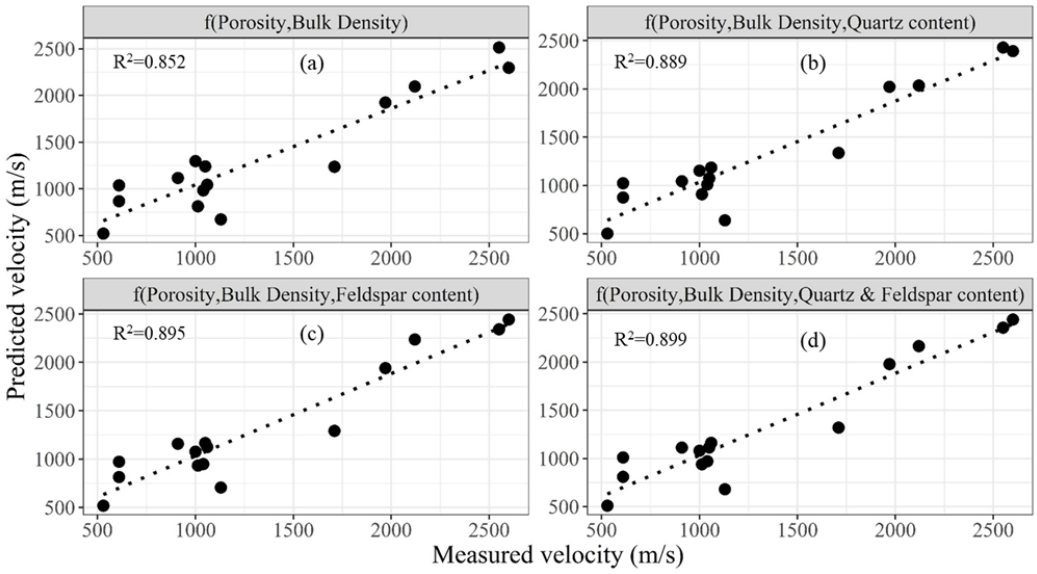


Figure 5.13 Cross-correlation between measured and predicted values of $V_p$ considering (a) $V_p$ in terms of porosity and bulk density only, (b) $V_p$ in terms of porosity, bulk density and Quartz content only, (c) $V_p$ in terms of porosity, bulk density and Feldspar content

### 5.3.6 Mathematical Models for $V_P$ to Study the Effect of Fluid Substitutions

The cumulative effect of porosity and mineral content on $V_p$ was investigated by varying the porosity and quartz, feldspar content for different saturation conditions. The statistically derived rock physics equation (5.1) was used to examine the variation of $V_p$. As per Bateman's equation (Bateman, 1985)-

$$\rho = \phi * \text{fluid density} + (1-\phi) * \text{grain density} \quad (5.5)$$

In this equation, grain density was varied as per-

$$(\text{Grain Density})_{\text{mixture}} = (\text{Grain Density})_{\text{Quartz}} * (\%\ \text{content})_{\text{Quartz}} + (\text{Grain Density})_{\text{Feldspar}} * (\%\ \text{content})_{\text{Feldspar}} \quad (5.6)$$

Where, grain density of quartz is 2.65 g/cc, and Feldspar is 2.56 g/cc (Yale, 1985). The grain density of the mixture was calculated using equation (5.6). The mineral content (in %) was varied from Quartz: Feldspar = 80:20 to 40:60 with an increment of 10%. Four different conditions of fluid substitutions with porosity 100% saturated with water with a fluid density as 1 g/cc, gas with a fluid density as 0.35 g/cc, oil with a fluid density as 0.76 g/cc and brine with a fluid density as 1.05 g/cc (Schön 2015) were considered for the analysis. On substituting these values in Bateman's equation (5.5), the respective bulk densities were obtained for the different saturation conditions. These obtained values and the set of porosity values (5%, 10%, 20% and 30%) were used in equation (5.1) to obtain the variations in $V_p$, as shown in Figure 5.14. For 5% porosity, $V_p$ varied from 2482 to 2320 m/s for water-saturated condition, 2328 to 2165 m/s for gas saturated conditions, 2425 to 2263 m/s for oil-saturated condition and 2494 to 2331 m/s for brine saturated condition. For 10% porosity, $V_p$ varied from 2352 to 2198 m/s for water-saturated condition, 2044 to 1890 m/s for gas saturated condition, 2238 to 2084 m/s for oil-saturated condition and 2376 to 2222 m/s for brine saturated condition. For 20% porosity, $V_p$ varied from 2092 to 1955 m/s for water-saturated condition, 1475 to 1339 m/s for gas saturated condition, 1854 to 1728 m/s for oil-saturated condition and 2140 to 2003 m/s for brine saturated condition. For 30% porosity, $V_p$ varied from 1832 to 1713 m/s for water-saturated condition, 907 to 788 m/s for gas saturated condition, 1491 to 1371 m/s for oil-saturated condition and 1903 to 1784 m/s for brine saturated condition.

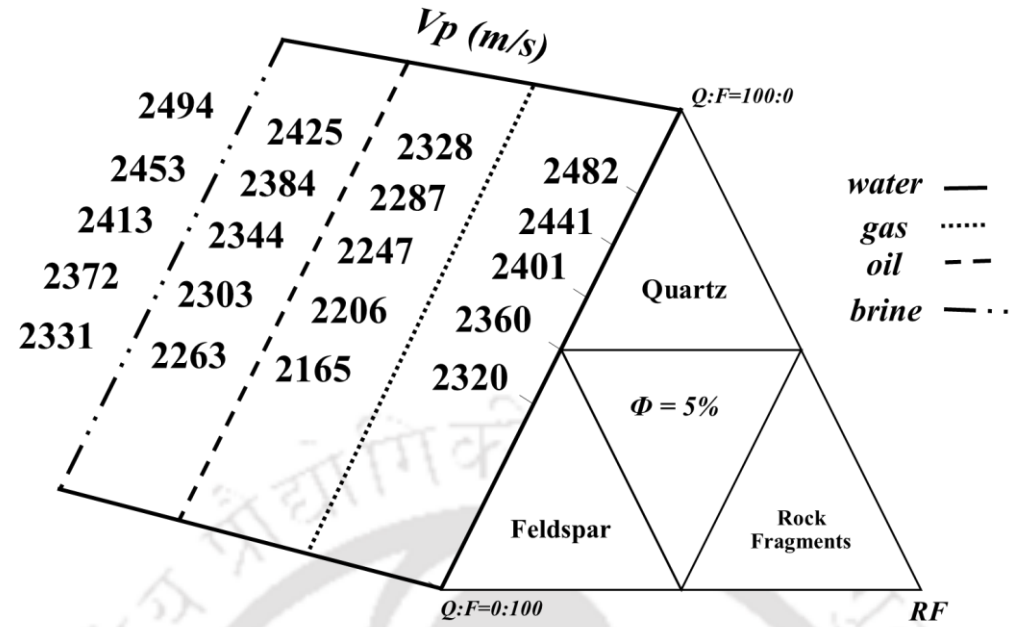


**(a)**

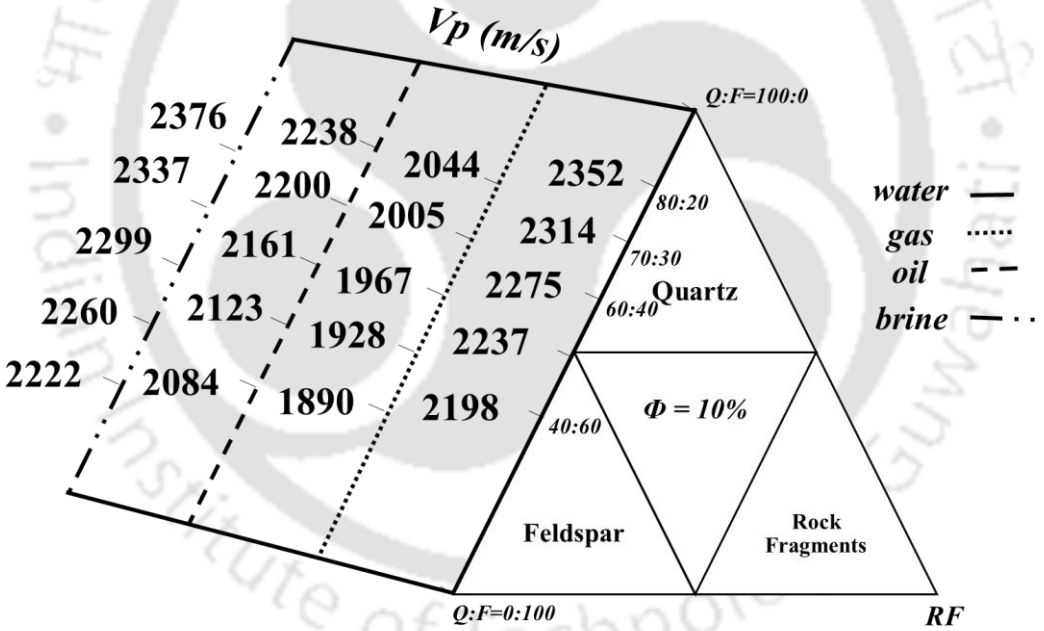


**(b)**

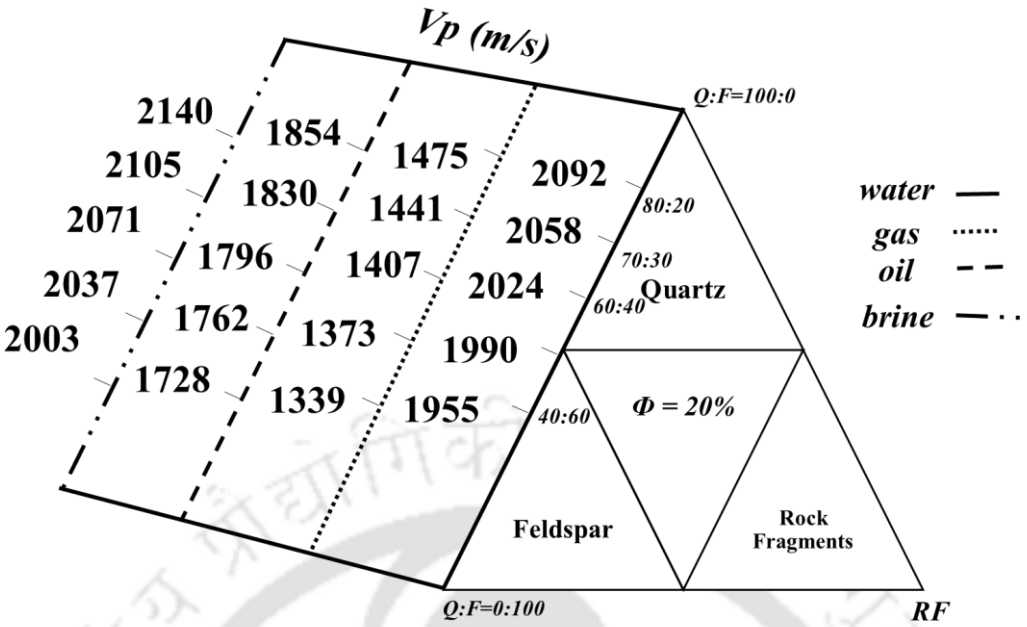


(c)

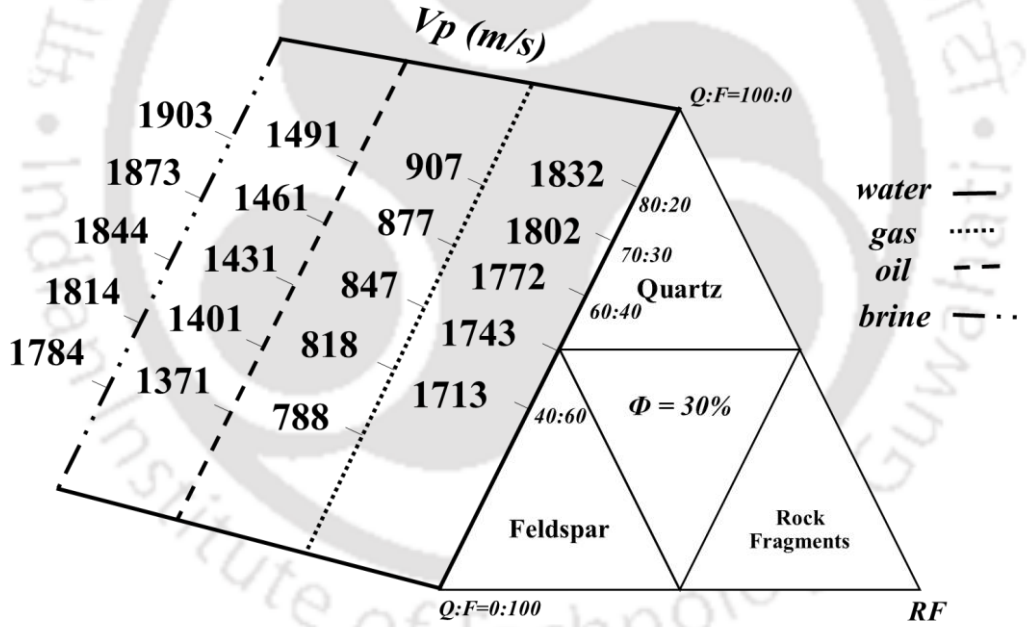


(d)

Figure 5.14 Pictorial representation of deviation in $V_p$ with change in major mineral content and porosity (a) 5%, (b) 10%, (c) 20%, (d) 30% for different saturation conditions

Now, keeping quartz content as fixed (85%) and altering the Feldspar content i.e., F1=K Feldspar (grain density = 2.56 g/cc), F2= Na Feldspar (grain density = 2.62 g/cc), F3=Ca Feldspar (grain density = 2.73 g/cc) (Yale, 1985) from 0% to 15%, the variation in $V_p$ was estimated using statistically derived rock physics equation (5.1). This analysis was performed

for different set of porosity (5%, 10%, 20% and 30%) for different saturation conditions as shown in Figure 5.15. For water saturated condition, $V_p$ varied from 2502 m/s to 2617 m/s for 5% porosity, 2371 m/s to 2480 m/s for 10% porosity, 2109 m/s to 2206 m/s for 20% porosity and 1847 m/s to 1932 m/s for 30% porosity (Figure 5.15(a)). For gas saturated condition, $V_p$ varied from 2348 m/s to 2463 m/s for 5% porosity, 2063 m/s to 2172 m/s for 10% porosity, 1492 m/s to 1589 m/s for 20% porosity and 922 m/s to 1007 m/s for 30% porosity (Figure 5.15(b)). For oil saturated condition, $V_p$ varied from 2445 m/s to 2560 m/s for 5% porosity, 2257 m/s to 2366 m/s for 10% porosity, 1881 m/s to 1978 m/s for 20% porosity and 1506 m/s to 1590 m/s for 30% porosity (Figure 5.15(c)). For brine saturated condition, $V_p$ varied from 2514 m/s to 2629 m/s for 5% porosity, 2395 m/s to 2504 m/s for 10% porosity, 2157 m/s to 2253 m/s for 20% porosity and 1918 m/s to 2003 m/s for 30% porosity (Figure 5.15(d)).

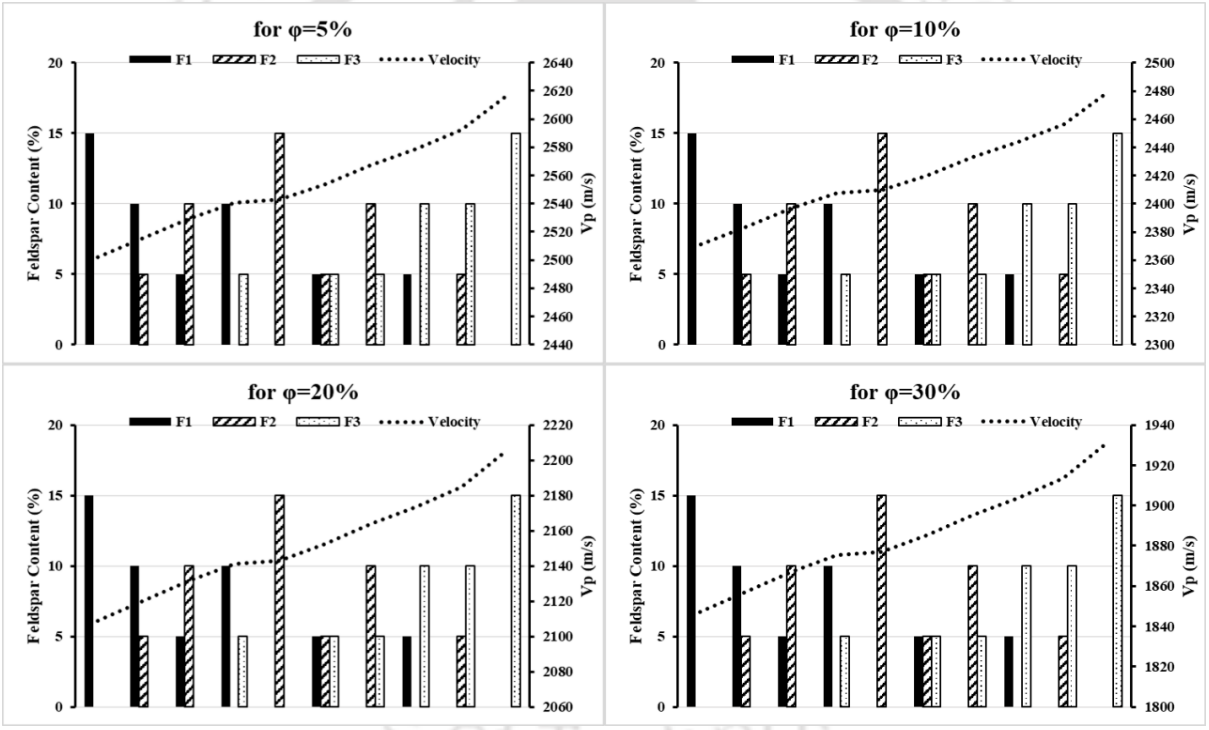


**(a)**

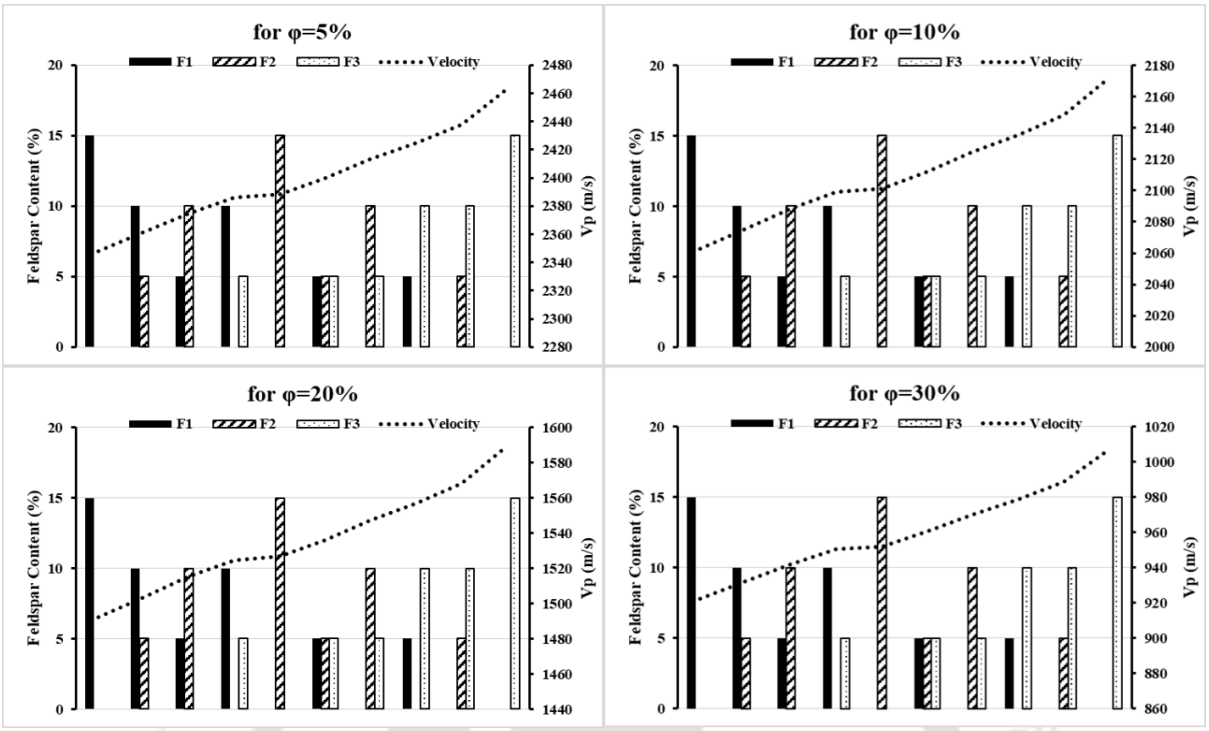


**(b)**

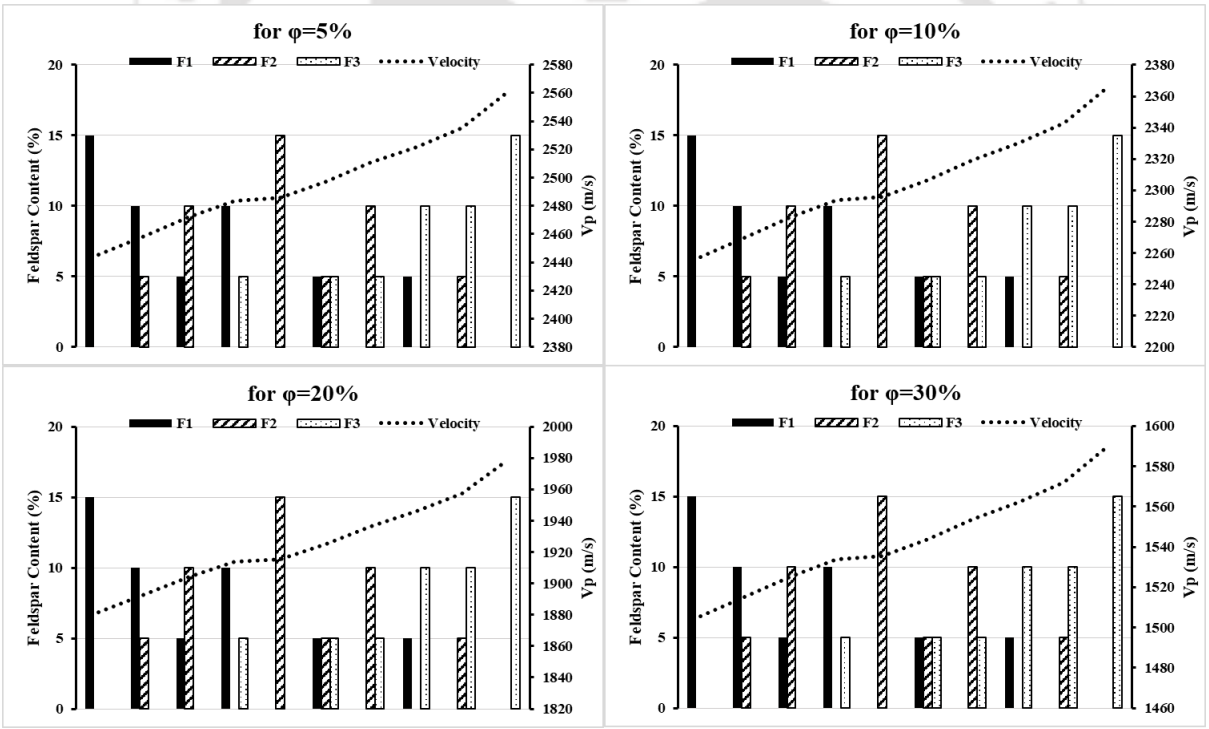


**(c)**

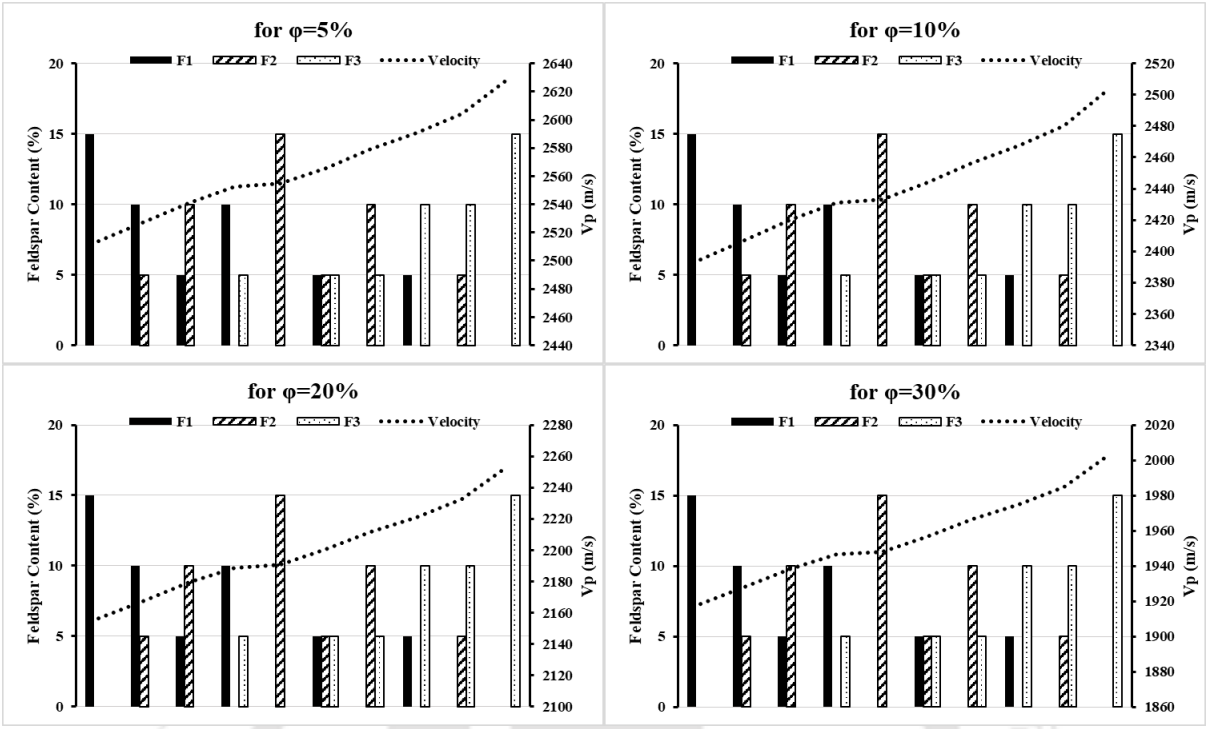


**(d)**

Figure 5.15 Variation of $V_p$ with change in Feldspar content (F1=K Feldspar, F2=Na Feldspar, F3=Ca Feldspar contents varying from 0% to 15%) for different porosity range (5%, 10%, 20%, 30%) keeping Quartz content as fixed (85%) for (a) water-saturated, (b) gas saturated, (c) oil-saturated and (d) brine saturated condition

The variations in $V_p$ (as observed from Figures 5.14 and 5.15) due to change in fluid conditions for a set of rock types with predefined mineralogy and petrophysical properties will help in the interpretation of reservoir characteristics away from the well-control. Hence, they can be adapted as a generalised model for any reservoir.

## 5.4 Summary and Conclusions

The present study investigates the sandstone core plugs of the Upper Assam Basin, India, and attempts to address the existing gap in the literature pertaining to the correlations between acoustic, mineralogical and petrophysical parameters. The different parameters of the sandstone core plugs investigated in the laboratory vary in the following range, i.e., $V_p$ ranges from 530 m/s to 2600 m/s, bulk density from 1.86 g/cc to 2.56 g/cc, grain density from 2.64 g/cc to 2.73 g/cc, porosity from 4.75% to 30.73% and permeability from 0.489 mD to 1691.5 mD. Positive correlations were observed between $V_p$-bulk density and negative correlation between $V_p$-porosity and $V_p$-permeability. On incorporating the effect of bulk density in the porosity-$V_p$ relationship, $R^2$ improved to 0.85 from 0.59. Grain and pore size did not show any correlation with $V_p$ when compared with other factors. The variation in $V_p$ with respect to the

mineralogy was investigated, considering the effect of significant minerals such as Quartz and Feldspar present in sandstones. On exclusive probing, a low correlation was observed with $V_p$-Quartz content and $V_p$-Feldspar content. The correlation improved on incorporating the collective (combined) influence of bulk density, porosity and mineral content on $V_p$ by using multivariate regression analysis. Therefore, a multivariate statistical approach was adopted integrating petrophysical and mineralogical data in rock physics-based models. The results highlight that it is imperative to consider the effect of mineralogy along with density, porosity, which was previously overlooked in the literature.

A simplified rock physics model for sandstones is proposed in the form of statistically derived equations. These equations may be systematically used for inferring the petrophysical properties based on acoustic properties. Cross-correlation of measured and predicted $V_p$, considering $V_p$ in terms of porosity, bulk density, and major minerals, show a strong coefficient of determination ($R^2 = 0.89$). These results are applicable for sandstones with varying mineral composition, and therefore can be considered a generalised model since it incorporates all the components that contribute to the variations in $V_p$. Another positive factor of this study is that all the parameters were measured in the laboratory, which requires a minimal number of assumptions with less uncertainty (Kelkar et al., 2002). Moreover, in the present study, the range of petrophysical properties and major mineral constituents in sandstones more or less falls within the broad spectrum that is expected for typical sandstones. For the broader applicability of the proposed model, we mathematically derived the variations in $V_p$ due to change in fluid conditions for a set of rock types with predefined mineralogy and petrophysical properties. The variation in $V_p$ indicates that the present methodology can be adapted as a generalised model for any reservoir. Interpretation of reservoir characteristics away from the well-control or beyond the available data range is possible by capturing the fluctuations in $V_p$ within the given geological constraints. Complementary studies may be carried out in the future with different rock types under different geology setups to further highlight the importance of the adopted methodology. This study strongly advocates incorporating petrophysical and mineralogical data in the quantitative interpretation of compressional wave velocity ($V_p$) to enhance the capability of rock physics models in characterising heterogeneous reservoirs. It is to be highlighted that one of the major aspects of statistically derived rock physics equations is that it integrates physical models with statistics to account for conditions that are beyond the available data range. The statistical trends developed may be utilised to effectively scale up core data to seismic data and thereby can facilitate accurate seismic interpretation. Future work

may focus on considering the effect of confining pressure on $V_p$ by following a similar workflow.

# Chapter 6
# Seismic Inversion using Rock Physics Models

## 6.1 Introduction

The integration of information obtained from diverse fields such as geology, petrophysics, and other earth science domains prove to be a key component in the technical success of an exploration project (Bosch, 2004). Interpretation of well log data provides an initial assessment of the hydrocarbon assets in the neighbourhood of the borehole (Grijalba-Cuenca et al., 2000). The spatial variability of petrophysical parameters is described using available borehole information and seismic data. In order to determine the variability of reservoir characteristics between two wells that are generally widely spaced, seismic imaging is a vital tool in interpreting the possible geological conditions between the wells. The inclusion of complementary information from petrophysics, geology and other fields is crucial for realistic seismic modelling.

Seismic modelling plays a crucial role in reservoir characterisation, making the results more effective and reliable (Sayers and Chopra, 2009). The inverted seismic section within the geological constraints will aid in interpreting possible reservoir parameters away from the well locations, facilitating extensive subsurface volume characterisation. The seismic reflections depend on the contrasts of the elastic properties, and each elastic property depends on several rock parameters such as density, porosity, mineralogy etc. Rock physics models are an essential component to predict subsurface properties from seismic image analysis (Payne et al., 2010). The rock physics models are mainly controlled by geological factors such as porosity, lithology, and fluid characteristics (Ali et al., 2020).

A typical reservoir characterisation requires quantitative mapping of the seismic reflection into the reservoir properties. This can be achieved by the integration of well and seismic data. Seismic data has high lateral coverage and resolution compared to well data. Well log provides a high-resolution information of the reservoir properties, however, this information is limited to the well from where it is derived (Feng et al., 2018). Additionally, the use of well log cross plots and petrophysical analysis of acoustic, elastic properties can be used as a tool to predict reservoir properties and help in distinguishing different lithologies and fluid contents (Anyiam et al., 2018). The well logs and derived parameters can be used as indicators of potential hydrocarbon zones in the study area. On the other hand, seismic data is smooth and available throughout the area i.e., it provides a continuous view of the subsurface information. The well logs define formation properties only in the vicinity of the borehole, hence seismic data is

generally used to complement the vertical resolution of the well log data (Grijalba-Cuenca et al., 2000). To correlate and calibrate seismic and well log data, seismic inversion is widely used as an effective technique in delineating the different properties that would help to revive potency, improve characterisation and increase production in case of mature fields.

For studies pertaining to reservoir characterisation, the different parameters should ideally be estimated from the inversion of geophysical observables, i.e., the inversion process should transform the seismically derived properties ($V_p$, Vs, acoustic and elastic impedance etc.) into parameters that define the reservoir conditions and lithology (such as porosity, permeability, saturation etc.). Various methods of deriving acoustic impedance from pre and post-stack seismic data have been established over the last decade for facilitating additional information related to reservoir characterisation (Leite and Vidal, 2011). This study attempts to transform post-stack seismic data into different properties that may aid in reservoir characterization. Different techniques of post-stack seismic inversion methods such as coloured inversion, sparse spike deconvolution, model-based analysis, geostatistical methods, multilayer linear calculator, probabilistic neural network, maximum likelihood inversion have been employed in the literature to predict and map the spatial variation of key parameters. For instance, sparse spike deconvolution was employed by Leite and Vidal (2011), Wang et al. (2013), Ali et al. (2018), Velis (2008), Broadhead and Tonellot, (2010), Maurya and Singh (2018), model-based inversion by Gogoi and Chatterjee (2019), Kumar et al. (2016), Kushwaha et al. (2021), Maurya and Singh (2019), Ali et al. (2018), Toqeer et al. (2021), Erryansyah et al. (2020), coloured inversion by Maurya and Singh (2019), Gupta and Gupta (2017), Ismail et al. (2020), Wydiabhakti (2012), Ansari (2014). The application of neural network (NN) has also acquired popularity more recently in geophysics (Maurya et al., 2020). NN methods hold superiority over the traditional methods owing to the different advantages such as their ability to establish non-linear relationships between input and output data; the increase in the computing power and interpretation of seismic data also lead to focus the research on the application of NN methods or machine learning (Farouk et al., 2021; Yasin et al., 2020). The wide application of NN methods includes the prediction of porosity, permeability, density, saturation, Young's modulus and brittleness index in reservoir characterisation (Russel, 2004; Gogoi and Chatterjee, 2019; Yasin et al., 2020). The two popular types of NN are multi-layer feed-forward neural network (MLFN) and probabilistic neural network (PNN). Studies conducted by Maurya and Singh (2019), Haris et al. (2017), Misra et al. (2010), Sun et al. (2013), Pramanik et al. (2004), Hampson et al. (2001), Abdulaziz et al. (2019) utilised PNN for estimation of different parameters, while Hampson et al. (2001), Singh et al. (2016), Yasin et al. (2020), Gogoi and

Chatterjee (2019) utilised MLFN to predict the various parameters. In general, these studies focus on the application of different techniques that is useful to predict reservoir properties and delineate facies in oil and gas exploration (Leite and Vidal, 2011; Yasin et al., 2020).

The main aim of this study is to use the seismic data inversion technique through which an elastic property such as acoustic impedance is estimated from the seismic response and predict petrophysical properties from elastic properties. For this purpose, reservoir characteristics will be delineated from well logs and thereafter, employ seismic inversion technique to spatially populate the different petrophysical properties across the seismic section of the Upper Assam basin, India. This study uses the coloured inversion method to obtain the acoustic impedance cube. It is described as a fast track technique (Lancaster and Whitcombe, 2000) that performs significantly better than traditional fast track routes (Campbell et al., 2015) and is useful in parameter interpretation beyond the well control. A multilayered feed-forward neural network was used to evaluate the different reservoir parameters such as density, porosity, saturation based on impedance. Other inversion algorithms may also be used to identify the merits or demerits (Cooke and Cant, 2010). After evaluating the parameters using well-modelled data, we propose a workflow to map the different petrophysical properties by integrating well data, laboratory-based and inversion analysis. The results were also compared with well log data for different formations of the Upper Assam basin. The proposed workflow provides a framework for reservoir characterisation using integrated seismic, well and laboratory-based analysis and focuses on developing a multidisciplinary approach that may aid future researchers in improving reservoir characterisation using seismic inversion.

## 6.2 Materials and Methods

### 6.2.1 Study Area

In this study, the analysis was performed on the seismic section of a small region in the south-west part of the Upper Assam basin, India (Figure 6.1). The geographical boundary of the seismic survey and the well locations are displayed in Figure 6.1(c).

The Upper Assam basin is one of the first discovered petroliferous regions in India (Raju, 1968; Mathur, 2014). This region is a tertiary sub-basin of the Assam-Arakan basin and has been one of the major onshore hydrocarbon producing regions (Raju and Mathur, 1995). Hydrocarbons were first discovered in the Oligocene Barail formation in the 1950s, thereafter in the Upper Miocene Girujan formation in the 1970s, followed by Lakdong member of the Sylhet formation (Lower Eocene) and the Langpar formation (Upper Palaeocene) in 1989 (Mathur, 2014). The source rocks are shales from Sylhet and Kopili formation, coals and shales of Barail group, and

Surma group shales in the south. The reservoir rocks are carbonates belonging to Sylhet formation, interbedded sandstones belonging to Kopili formation, and sandstones belonging to Barail, Surma and Tipam groups (Wandrey, 2004b; Gogoi and Chatterjee, 2019). Traps are primarily anticline and seals are shales and clays (Oligocene and Miocene), and the thick clays of Pliocene Gurjan group (Wandrey, 2004b). The stratigraphic succession of the Upper Assam basin is described in Table 6.1.

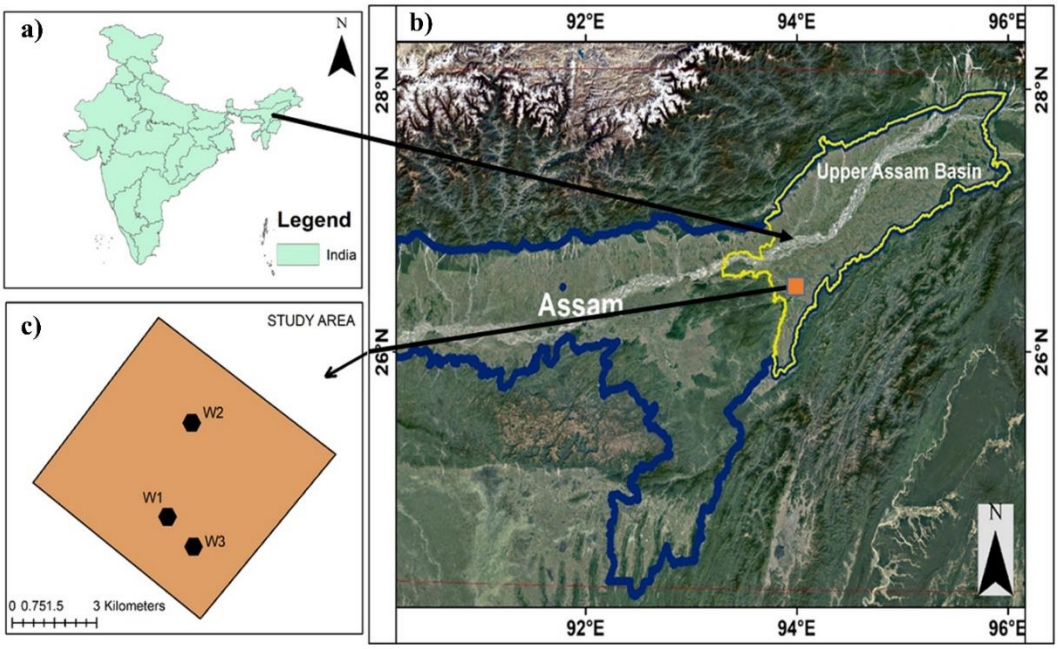


Figure 6.1 Geographical location of the study area (part of Upper Assam Basin) with the seismic survey boundary

Table 6.1 Stratigraphic succession of Upper Assam basin (modified after Murty, 1984; Deb and Barua, 2016)

| Depth (m) | Age | | Group | Formation | Litho-Units |
|---|---|---|---|---|---|
| 0 | PLEISTOCENE | | Alluvium | | |
| | TERTIARY | *Pliocene* | Dihing | Dhekiajuli | Sandstone with bands of clay |
| | | *Miocene* | Dupitila | Namsang | Motted clay with greyish, soft sandstone |
| | | | Tipam | Girujan | |
| | | | | Tipam | |
| 2500 | | *Oligocene* | Barail | Argillaceous | Mudstone, shale, sandstone with clay seams |
| | | *Eocene* | | Arenaceous | Dark grey shale with thin sandstone |
| | | | Jaintia | Kopili | |
| | | | | Sylhet | |
| | | *Palaeocene* | | Langpar | |
| 4200 | PRE CAMBRIAN | | Basement | | |

### 6.2.2 Dataset: Well Log

The different well log data analysed in this study include gamma-ray log (GR in API), density log (RHOB in g/cc), neutron porosity log (NPHI in v/v), resistivity log (HDRS in ohm-m) and sonic log (DT in microsec/ft). The different log responses of the wells W1, W2 and W3, along with lithology information and formation details, are shown in Figure 6.2(a), 6.2(b) and 6.2(c), respectively. The lithology information of the wells and the formation details, as shown in Figure 6.2, are based on well report made available along with the well logs.

As per the available well report, for well W1, Bokabil formation ranges from 1412 to 1694 m, Barail formation ranges from 1690 to 1737 m, Kopili formation ranges from 1737 to 2001 m and Sylhet formation ranges from 2001 to 2061 m. The generalised lithology of Bokabil formation consists of mainly clay/claystone with thin intercalations of sandstone and siltstone. Barail formation consists of mainly sandstone and siltstone with intercalations of claystone and marl and occasional coal bands. Kopili formation consists of dominantly shale with thin intercalations of sandstone, siltstone and clay in the upper part and limestone in the lower part. Sylhet formation consists of limestone with intercalations of thin bands of sandstone, shale and siltstone. In well W1, the Sylhet formation was found to be oil-bearing.

For well W2, Bokabil formation ranges from 1407 to 1766 m, Barail formation ranges from 1766 to 1820 m and Kopili formation ranges from 1820 to 2126.5 m. The generalised lithology of Bokabil formation consists of mainly alternations of sandstone, siltstone and claystone. Barail formation consists of alternate bands of shale, sandstone, siltstone and coal, limestone at the bottom. Kopili formation consists of mainly shale with thin bands of sandstone, siltstone and clay in the upper part and limestone in the bottom. No hydrocarbon shows were observed in well W2.

For well W3, Tipam formation ranges from 583 to 1575 m, Bokabil formation ranges from 1575 to 1946 m, Barail formation ranges from 1946 to 2059.5 and Kopili formation ranges from 2059.5 to 2318 m. The generalised lithology of Tipam formation consists of monotonous sand/sandstone with intercalations of thin layers of clay, siltstone and occasionally coal streaks. Bokabil formation consists of dominantly clay/claystone with intercalations of sand and siltstone. Barail formation consists of sandstone and siltstone with intercalations of claystone, shale and coal bands. Kopili formation consists of dominantly shale with thin intercalations of sandstone, clay and coal in the upper part and limestone in the lower part. No hydrocarbon shows were observed in the well W3.

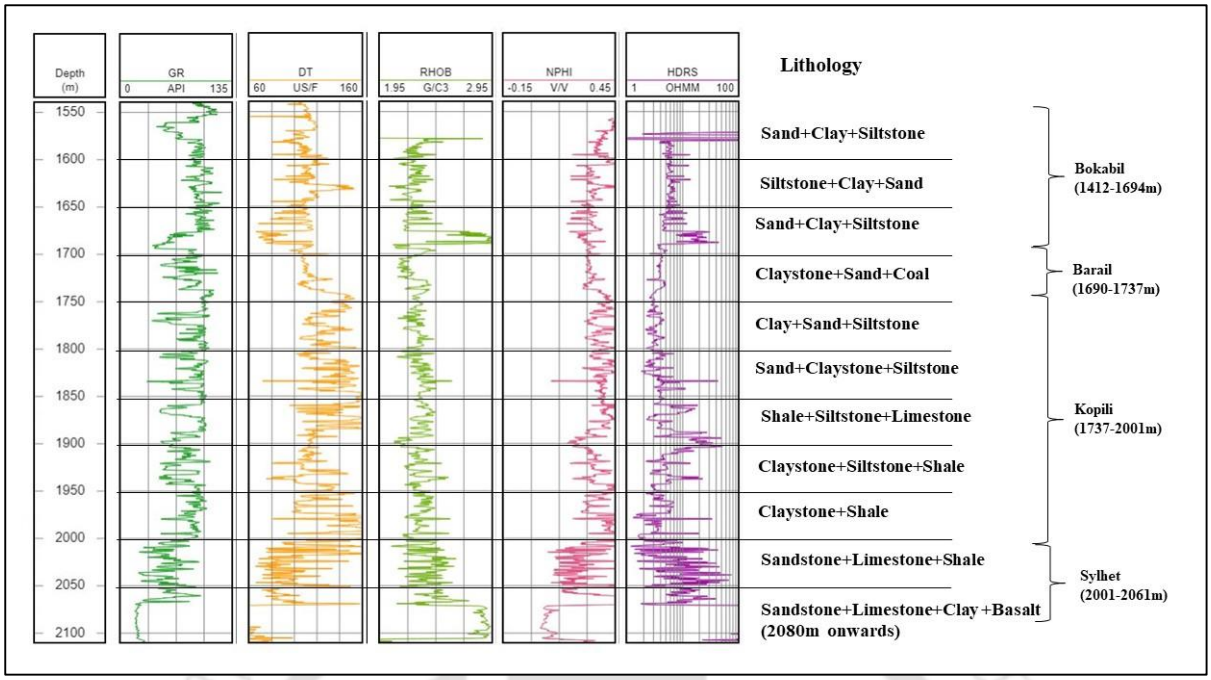


Figure 6.2(a) Log responses obtained for Well W1 along with lithology information and formation details

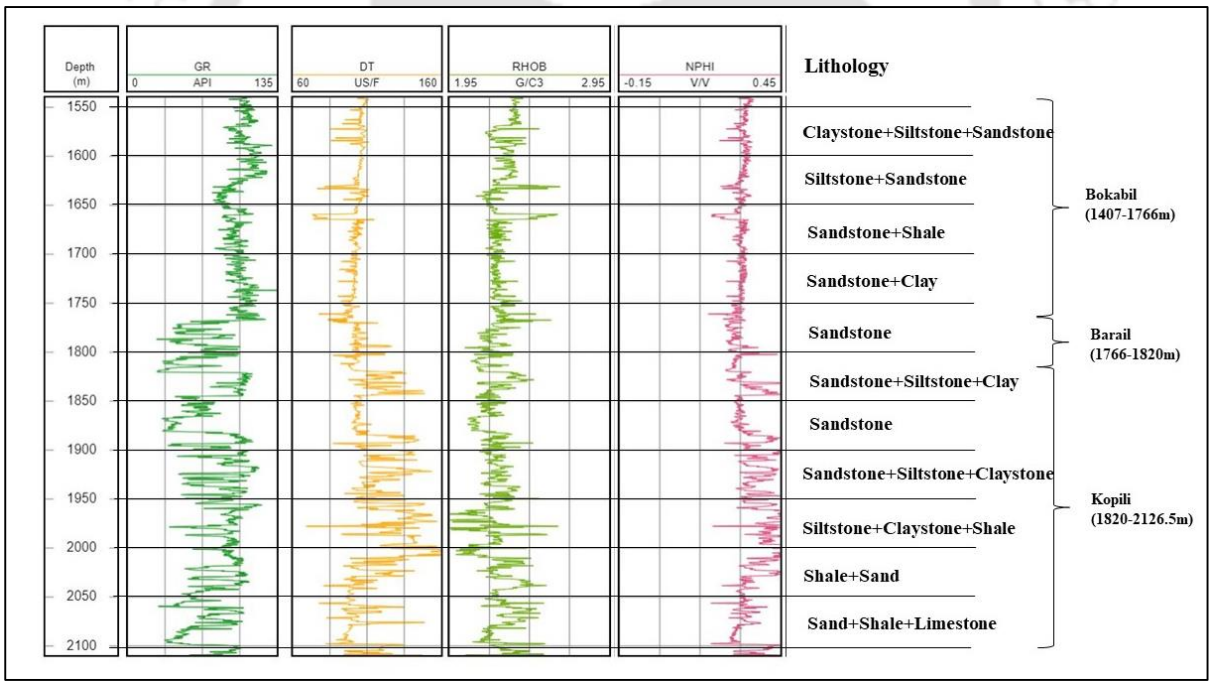


Figure 6.2(b) Log responses obtained for Well W2 along with lithology information and formation details

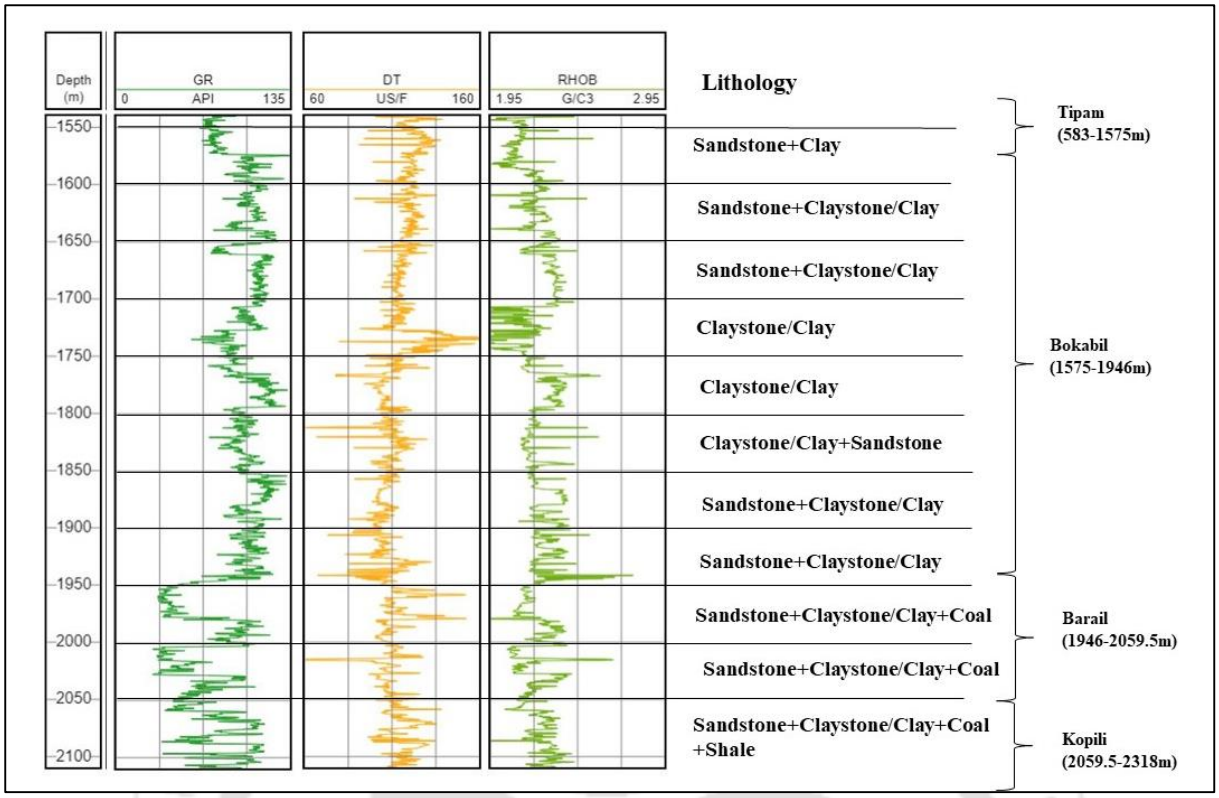


Figure 6.2(c) Log responses obtained for Well W3 along with lithology information and formation details

### 6.2.2.1 Derived Logs

For performing the inversion analysis, total porosity was estimated using density log, $\rho_b$ as per Bateman (1985) –

$$\phi = \frac{\rho_{ma} - \rho_b}{\rho_{ma} - \rho_f} \tag{6.1}$$

where $\rho_{ma}$ is the matrix density = 2.65 g/cc, $\rho_f$ is the fluid density = 1 g/cc

Total porosity was used instead of effective porosity for further analysis since effective porosity or neutron porosity may get unpredictably affected by gas (Darling, 2005). In most cases the density porosity, with an appropriate choice of fluid density, is still recommended (Darling, 2005).

As per the available well report, Well W1 was reported to be oil bearing for a few metres in the interval 2044.5 - 2042.5m (2m) and no hydrocarbon shows were observed in wells W2 and W3. Apart from this oil bearing zone, all the three wells were found to be water bearing. Hence, the fluid density was used as 1g/cc in Equation 6.1, so as not to complicate things. Additionally, from the available literature pertaining to Upper Assam basin, most of the researchers considered the fluid density as 1g/cc in their respective analysis (Gogoi and Chatterjee, 2021; Rai et al., 2021).

Water saturation was determined by using Archie's equation (Archie, 1942) –

$$S_w^n = \frac{a * R_w}{\phi^m * R_t} \quad (6.2)$$

where n is the saturation exponent, a is the tortuosity factor, m is the cementation exponent, $R_w$ is the resistivity of formation water, $R_t$ is the true resistivity of formation obtained from deep resistivity (HDRS) log response. The values of different exponents, i.e. n =2, a = 0.9, m =1.85, $R_w$ =0.5 ohm-m, were obtained from the literature for the Upper Assam basin (Kumar et al., 2018; Ishwar and Bhardwaj, 2013).

The rock physics formula- water saturation using Archie's equation was only available in the software, hence Archie's equation was used in the present study for the determination of water saturation. However, studies available in the literature such as Kumar et al., 2018; Ishwar and Bharadwaj, 2013, related to Upper Assam basin have used the Poupon–Leveaux Indonesian model (Poupon and Leveaux, 1971), also known as the Indonesian model.

The volume of shale was obtained from the gamma-ray log based on the following equation (Crain, 2002):

$$V_{shale} = \frac{GR_{\log} - GR_{\min}}{GR_{\max} - GR_{\min}} \quad (6.3)$$

### 6.2.3 Dataset: Seismic

In the present study, the seismic section of the Upper Assam Basin was used for analysis. The seismic survey consists of approximately 50 $km^2$ area with inline ranging from 1756-1895 and crossline ranging from 1224-1511. Both 2D and 3D survey was performed with inline orientation 129.22 degrees from north. In the post-stack seismic data, the two way travel time (TWT) range varies from 1000-2500 ms with step size 2 ms. Inline 1794 and crossline 1392 intersects well W1, inline 1820 and crossline 1389 intersects well W2 and inline 1790 and crossline 1444 intersects well W3. Figure 6.3 shows the seismic section along with the three wells W1, W2 and W3.

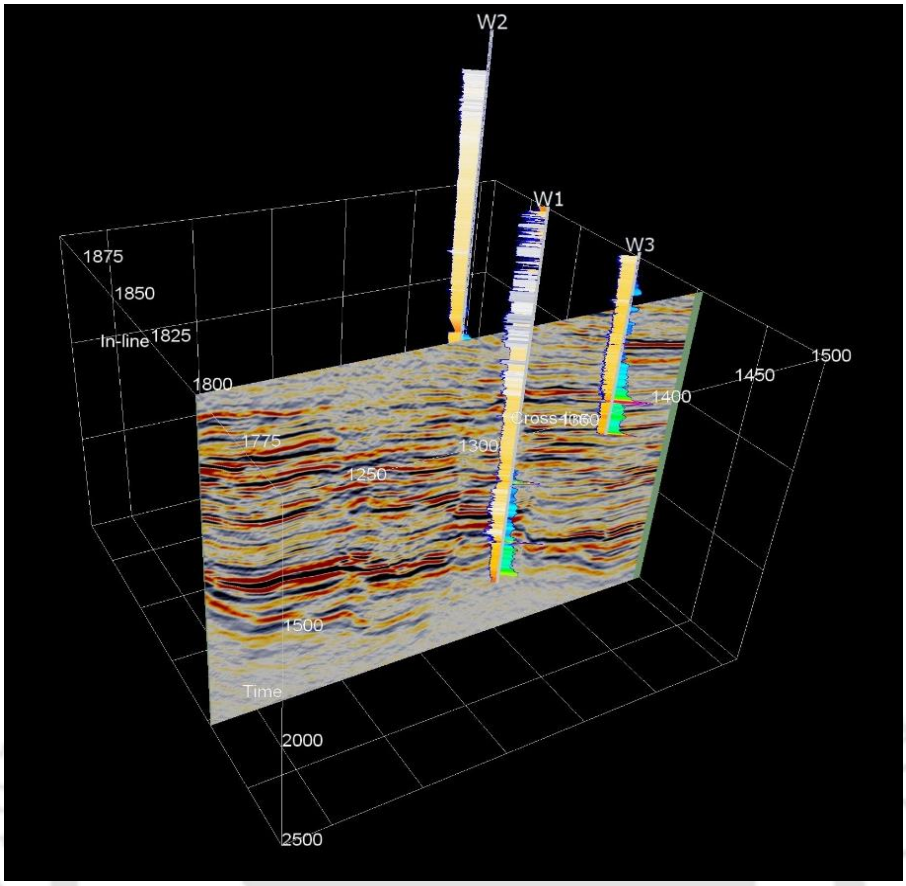


Figure 6.3 Seismic section along with the three wells (W1, W2 and W3) with logs

### 6.2.4 Seismic Data Processing

Seismic data processing, visualization and interpretation was performed using OpendTect software, which is an open-source, graphical user interface-based software (Aziz et al., 2017). For the present study, this software was used to visualise and inspect the data. The different plugins such as coloured inversion, neural network and horizon cube were used in the present study for interpretation and modelling.

### 6.2.5 Check Shot Data

The well logs are in the depth domain, while seismic data is in the time domain. As a result, a check shot data was applied before correlation to convert well data in the time domain (Dubey, 2012). For the present study, check shot data of well W1 was used, and it shows a good match to the seismic, as shown in Figure 6.4.

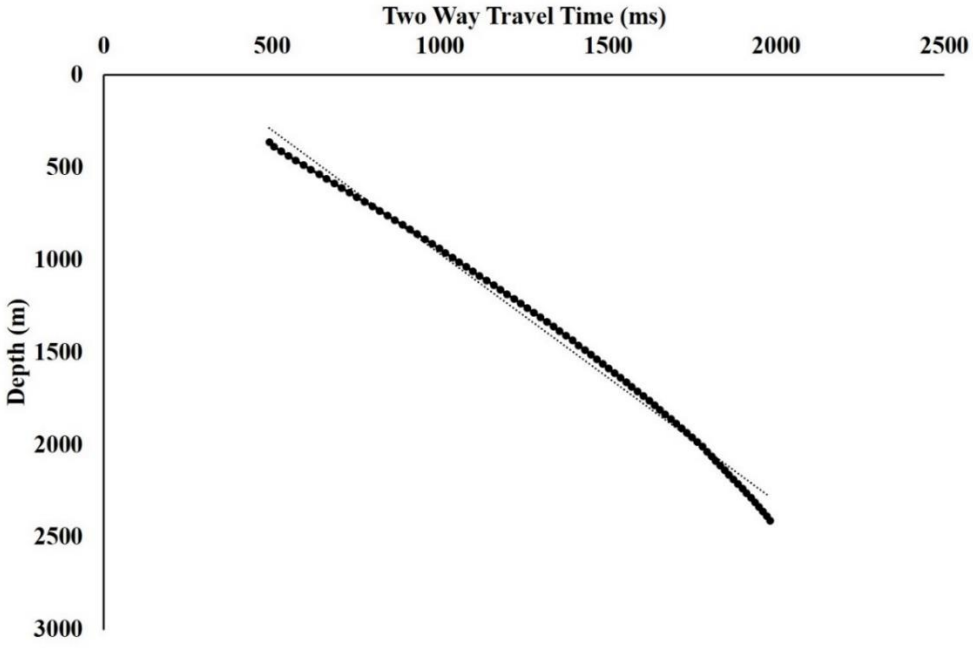


Figure 6.4 Check shot plot of well W1 used for well to seismic tie

### 6.2.6 Synthetic Seismic

A synthetic seismogram is constructed to identify seismic reflections and is the fundamental link between well data and seismic data. It is the main tool that allows geology picks to be associated with reflection in the seismic data (Herron, 2014).

### 6.2.7 Well Seismic Tie

The often observed mismatch between the synthetic and real seismic data has given rise to well to seismic tie (Dvorkin et al., 2014). Suitable selection of seismic wavelet and establishment of time-depth relationship with the use of seismic well tie can increase the accuracy of seismic inversion (Zhang et al., 2020b). The check shot data for well W1 was used for the well-to-seismic tie. The three main steps of seismic well tie include computation of coefficient of reflectivity from acoustic impedance (AI) curve, where AI (the product of the acoustic wave velocity and density log) is a layer property. The second step includes convolution between reflectivity and wavelet to generate synthetic wavelet. The final step involves the matching of synthetic to original wavelet near the well location with the help of process like manual shifting, stretching and squeezing (Zhang et al., 2020b). Figure 6.5 shows the well to seismic tie window using well W1 with a correlation of 0.66 within time interval 1150-2059 ms. Other different approaches such as semi-automatic and automatic methods may also be referred for seismic to well tying (Herrera et al., 2014; Herrera and Baan, 2014).

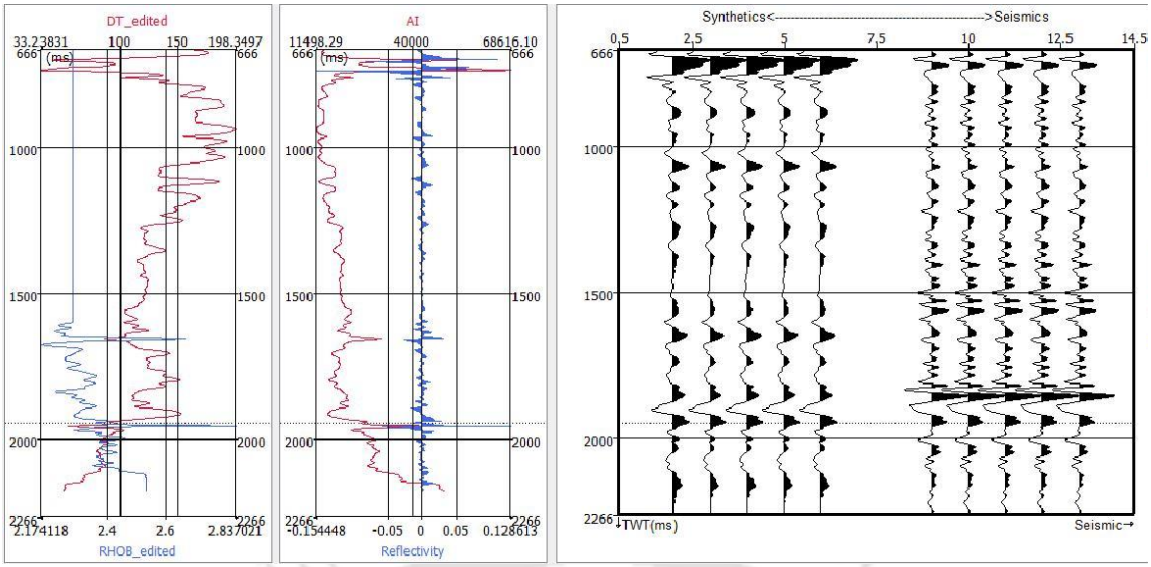


Figure 6.5 Correlation of well log data to seismic data (seismic well tie window) using well W1

Seismic data interpretation is performed on the basis of horizons. These horizons are important in seismic inversion as these horizons serve as a guide to interpolate well log properties between the wells (Maurya et al., 2020). There are different approaches, such as manual picking, interpolation and auto picking, available for picking seismic horizons in 3D seismic volumes. For the present study, a manual picking approach was adopted and Figure 6.6 depicts the interpreted seismic section showing (a) picked horizon seeds and (b) horizon surfaces.

### 6.2.8 Seismic Attribute

The seismic attribute is any measure of seismic data that helps us visually enhance or quantify features of interpretation interest (Brown, 2011; Simm & Bacon, 2014). One such attribute used in the present study to delineate faults is the thin fault likelihood attribute (Figure 6.7(a)). This attribute aims to capture and delineate faults and fractures, produces accurate, sharp faults. For the present seismic section, the different faults were identified, and major faults are marked as shown in Figure 6.7(b).

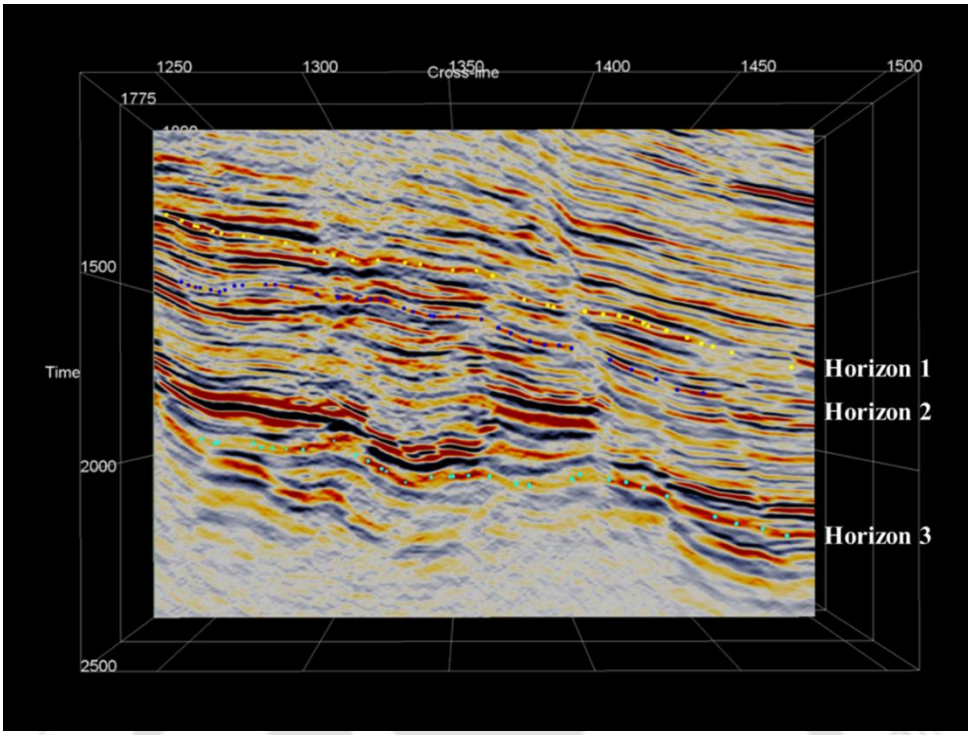


Figure 6.6(a) Interpreted seismic section showing picked horizon seeds (Horizon 1 by yellow colour, Horizon 2 by blue colour, Horizon 3 by cyan colour)

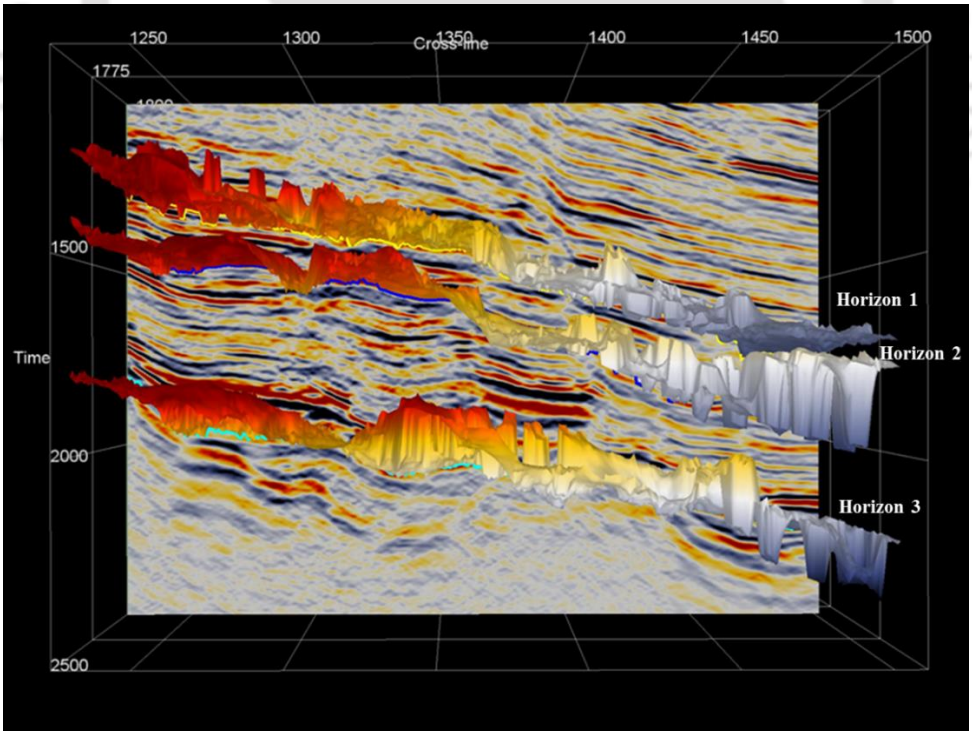


Figure 6.6(b) Interpreted seismic section showing horizon surfaces

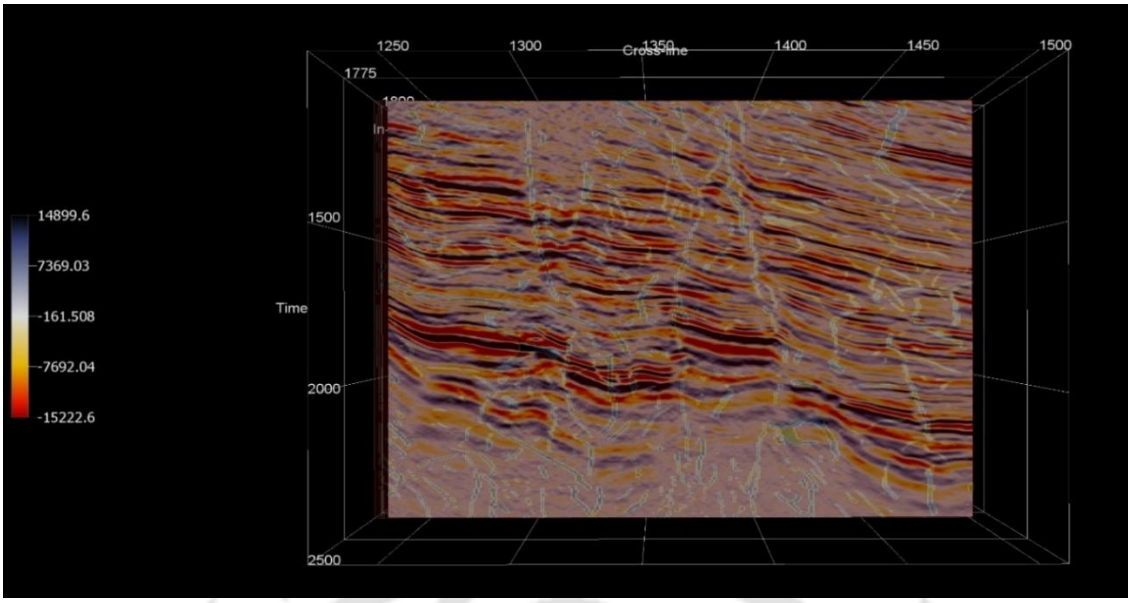


Figure 6.7(a) Interpreted seismic section showing attribute for imaging faults

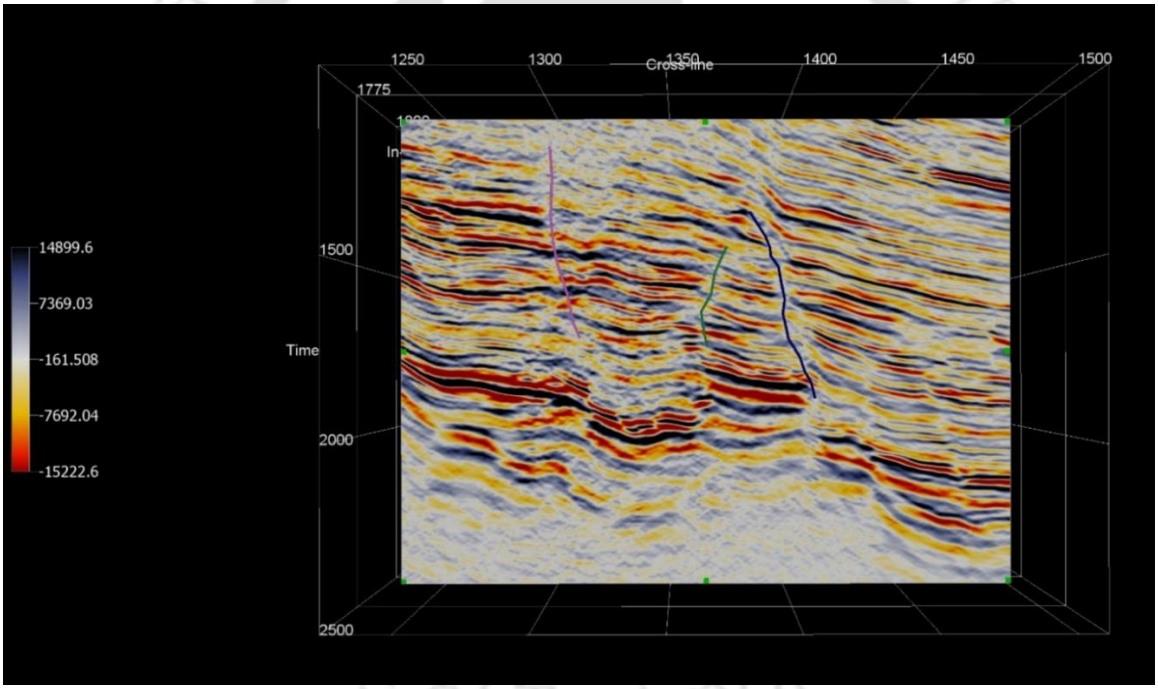


Figure 6.7(b) Interpreted seismic section showing marked major faults

### 6.2.9 Seismic Coloured Inversion

The inversion procedure first involves generating an operator (O) in the frequency domain. It is used for the transformation of seismic traces (S) into impedance (Z), i.e., Z= O*S (Lancaster and Whitcombe, 2000). The spectrum of the operator is derived based on the spectra of the AI log calculated from wells in the same area. To generate impedance from the reflectivity information of seismic data, the phase of the operator (O) is shifted 90 degree (Ansari, 2014). Figure 6.8 depicts the process of estimation of the coloured operator. Figure 6.9 depicts the

flowchart that displays the various steps followed in the prediction of petrophysical properties from AI.

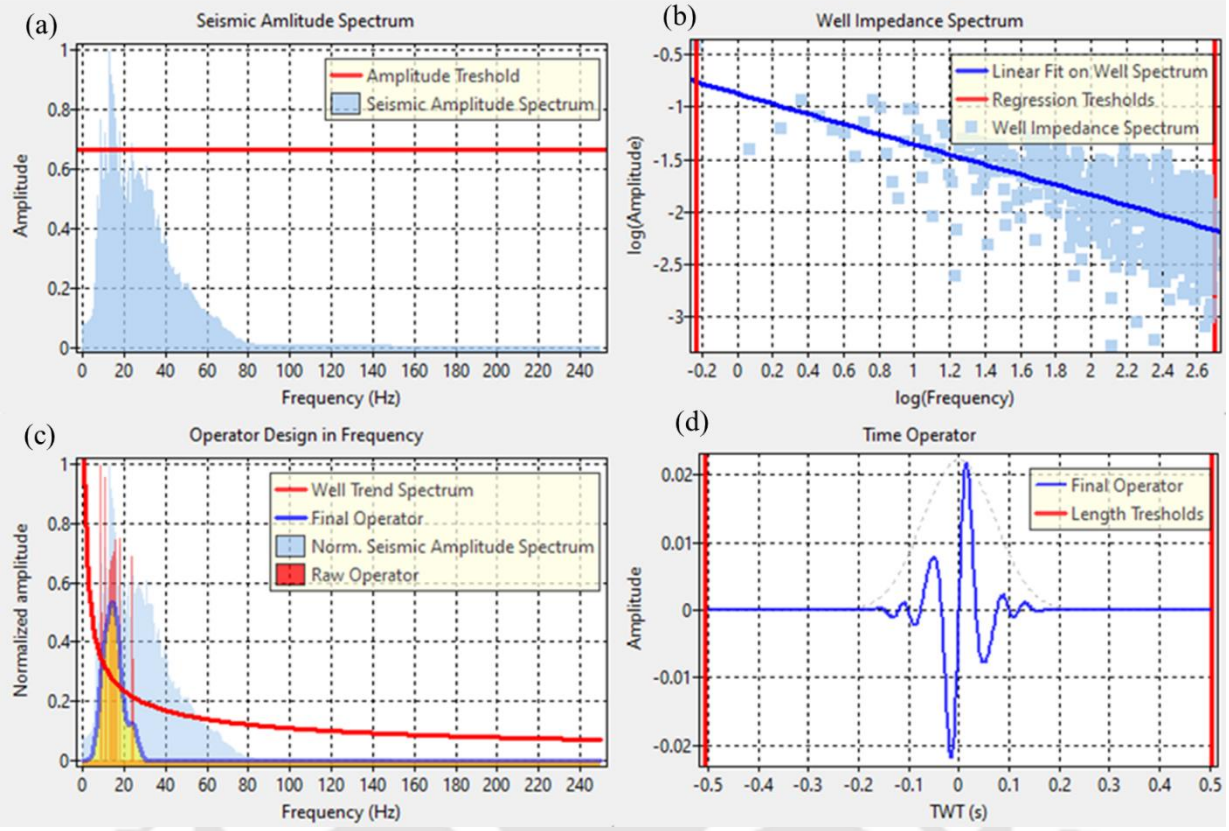


Figure 6.8 Process of estimation of coloured operator (a) using seismic amplitude spectrum, (b) using well impedance spectrum, (c) operator in frequency domain and (d) operator in time domain

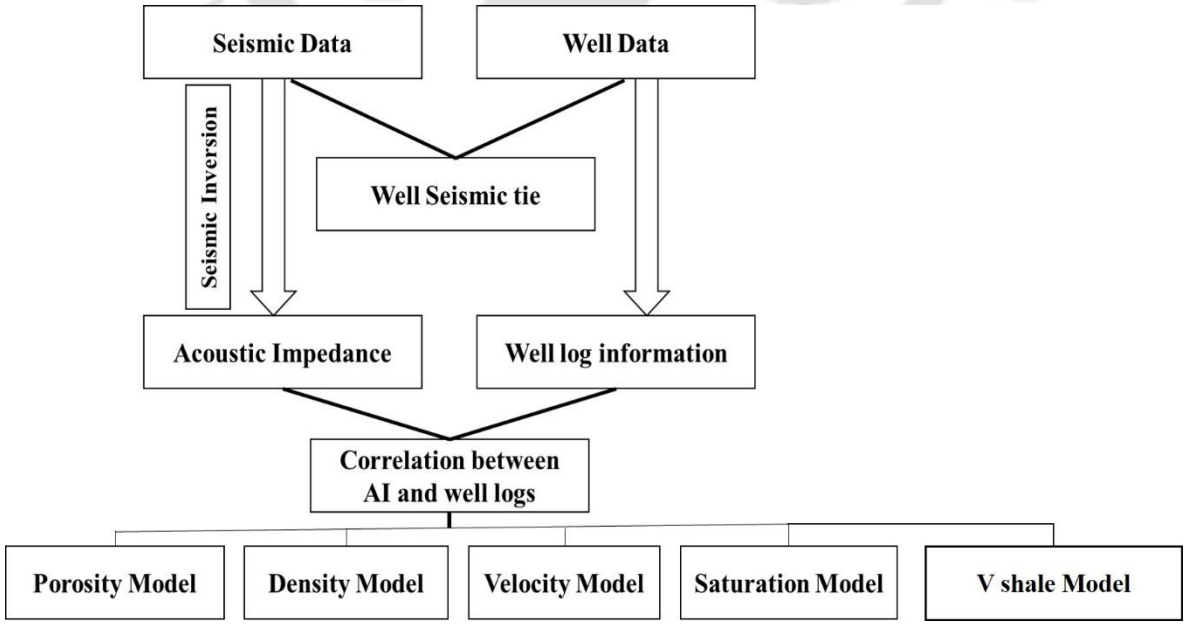


Figure 6.9 Steps followed in the prediction of petrophysical properties from seismic section

### 6.2.10 Machine Learning-Based Neural Network

In this study, a machine learning based neural network (NN) algorithm was used to extract the different petrophysical properties such as density, porosity, volume of shale, saturation from the acoustic impedance generated by performing seismic inversion on the seismic section of the Upper Assam basin. Well log data has both the frequency components, i.e. high and low frequency (Maurya et al., 2020), and hence the low-frequency model was computed from the well logs to compensate for the missing low frequency in seismic data (Mahgoub et al., 2017). Figure 6.10 presents a flowchart that shows the procedure involved for the prediction of different properties by a machine learning based neural network algorithm.

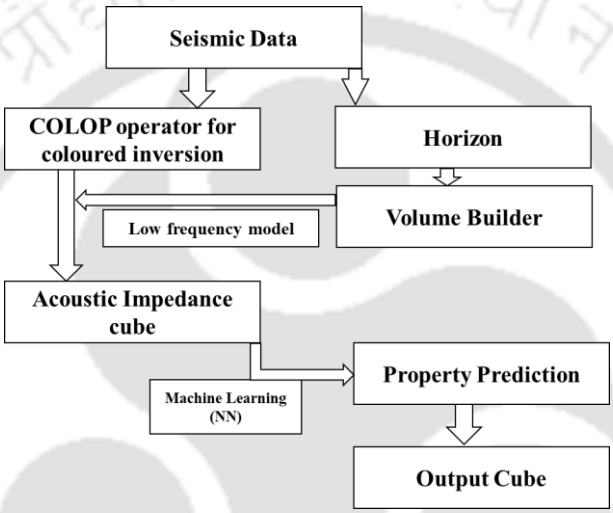


Figure 6.10 Flowchart displaying the steps followed in machine learning based NN for petrophysical property prediction

The NN algorithm consists of a fully connected network of three layers, the input layer, hidden layer and the output layer, where all the nodes are connected. There are two data sets, i.e. training set and test set. During training, the random dataset is selected and this is passed through the NN that would provide some output based on the weights assigned in the network. In the training set, the features of the dataset are known, so accordingly, the weights are updated. All the weights are multiplied by the respective amplitudes and this sum is passed through a sigmoidal type function. The sigmoidal type function is commonly used to avoid the blowup of the extrapolated outputs. Moreover, the actual non-linear operation takes place in the sigmoidal function. The errors are fed back through back propagation, the errors are compared and subsequently updated. This process is repeated several times. The test set is used for validation and subsequently stopped on overfitting. Figure 6.11 shows the neural network training window for prediction of different parameters, where the normalised RMSE curve

indicates the overall error on the train and test sets, in red and blue, respectively on a scale from 0 (no error) to 1 (maximum error). A scatter plot shows the actual target data on the horizontal axis and the predicted target data by the neural network. Figure 6.11 can be used to note the performance. The error rates can be compared on the basis of these training window of different properties. Hence, from the figure, it can be seen that NN performs equally well for density, porosity and velocity, while less well for Vshale and water saturation. The machine learning based neural network approach is adopted owing to its several advantages. The neural network can model any arbitrary dependency. These are universal approximators, and overfitting can be avoided (Acharyya and Dey, 2019).

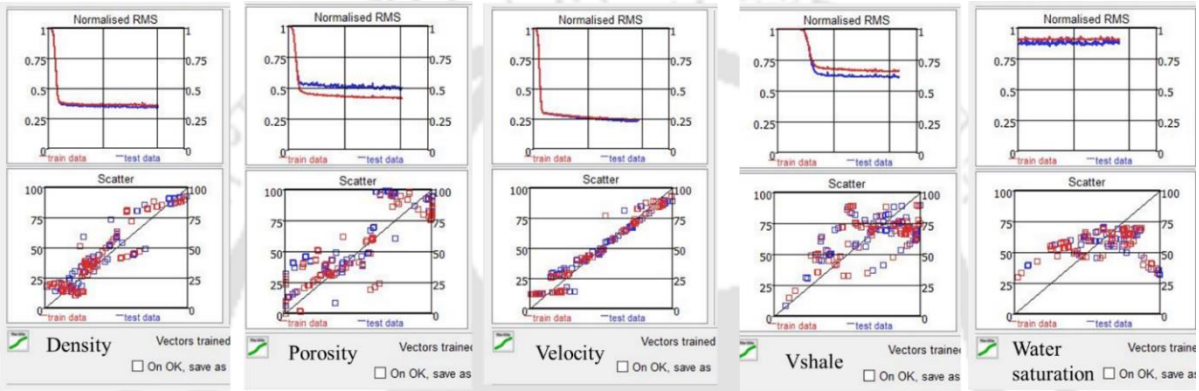


Figure 6.11 Neural network training window showing normalised RMSE and scatter plot for different properties

The interpretations are based on training one NN with well log data. The representation of seismic data in 3D cube is build up from three elements: the inline section, crossline section and time slice section (Aziz et al., 2017). The dimensions of inputs and outputs of the NN are of the matrix form: [two-way travel time * number of crossline/inline]. The two-way travel time (TWT) range varies from 1000-2500 ms with step size 2 ms, inline ranges from 1756-1895 and crossline ranges from 1224-1511.

### 6.2.11 Laboratory-Based Model

The laboratory model was developed based on experimental measurements conducted on core samples from Tipam and Barail formation of the Upper Assam basin, India (as elaborated in Chapter 5). The model includes statistically derived rock physics equations that relate to the different parameters such as velocity, porosity, density. A one-to-one relationship between AI, bulk density and porosity is shown in Figure 6.12. These correlations were used to populate bulk density and porosity from AI cube generated from inversion analysis. The obtained

density and porosity were cross-plotted with density and porosity obtained from AI cube when well log data were used as inputs.

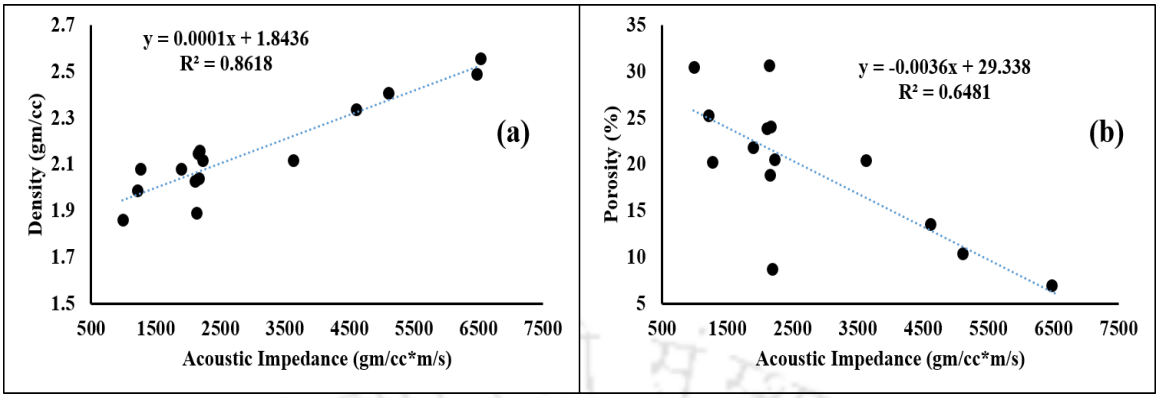


Figure 6.12 Cross plot between acoustic impedance (AI) and (a) density and (b) porosity estimated in the laboratory for sandstone core plugs from Upper Assam basin

The correlation between $V_p$, density and porosity obtained from multivariate analysis from examination of core plugs in the laboratory (as elaborated in chapter 5) is shown below.

$$V_p = 4743.62\rho + 51.43\phi - 9873.42 \qquad R^2 = 0.852 \qquad (6.4)$$

This equation was used to estimate $V_p$ by application of NN derived density and porosity at the well location (inline 1794, crossline 1392). Figure 6.13 presents a flowchart displaying the application of a laboratory-based model for petrophysical property prediction.

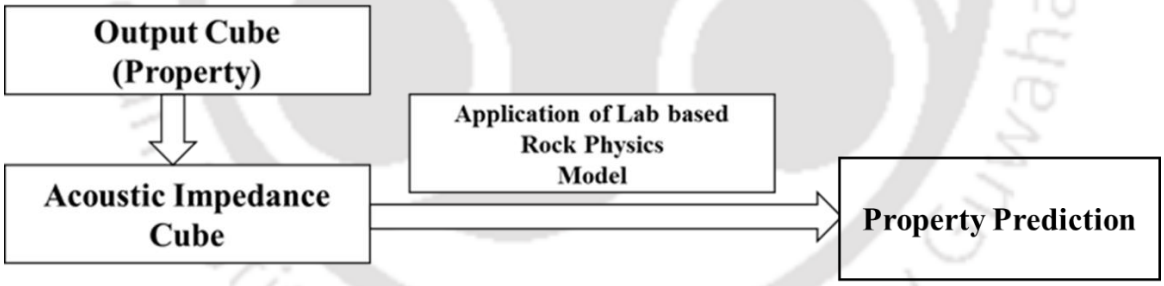


Figure 6.13 Flowchart displaying application of the laboratory-based model in petrophysical property prediction

## 6.3 Results and Discussion

Lithology identification was done based on analysis on a combination of different well logs. Thereafter, seismic inversion was performed on the seismic section with the help of coloured inversion operator (method) to generate the acoustic impedance. Subsequently, well logs were used as targets to populate the different properties. The laboratory-derived rock physics model was also used to populate the different parameters. Finally, the obtained results were cross

correlated with the well-modelled data to measure the prediction efficacy of the different parameters.

### 6.3.1 Lithology Interpretation Using a Combination of Well Logs

The lithological interpretation of the study area was performed on the basis of analysis on different plots, namely NPHI, RHOB, HDRS, GR and DT, as shown in Figure 6.15(a). NPHI-GR cross plot (Figure 6.14) indicates a combination of clean sandstones (low GR upto 45 API), shaly sandstones (intermediate GR varying between 45-75 API), sandy shale (GR varying between 75-90 API) and shales (GR>90 API). This classification was done based on studies conducted by El-Din et al. (2013) and Hakimi et al. (2017).

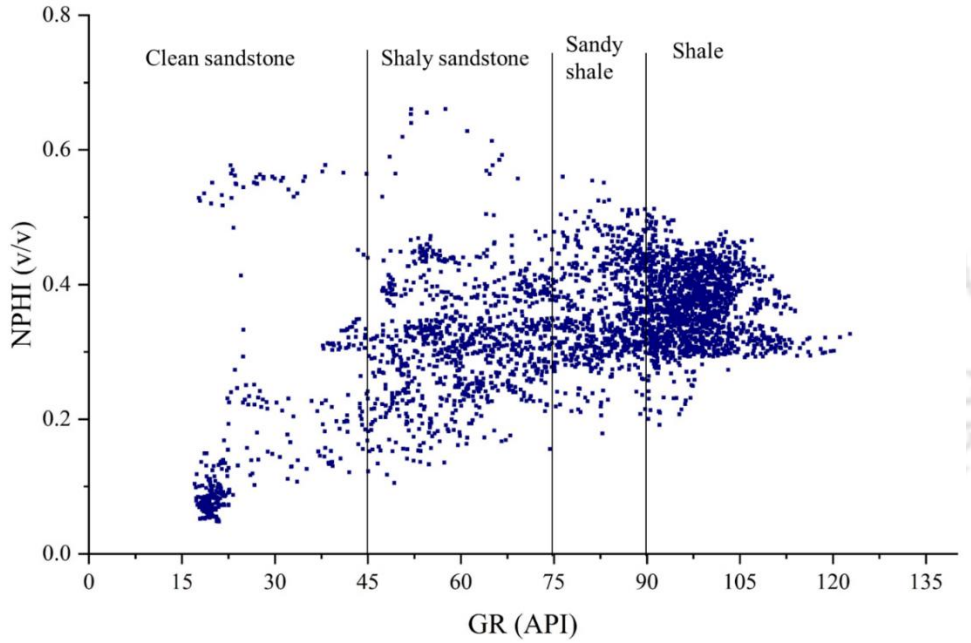


Figure 6.14 Cross plot between NPHI (v/v) and GR (API) displaying the variation in lithology for Well W1

Different sandstone layers with water, gas and hydrocarbon-bearing zones were identified on the basis of analysing in combination the different well log responses for well W1, as shown in Figure 6.15(a). Sandstone layers were interpreted in the intervals 1555-1570m, 1675-1690m, 1690-1737m, 1760-1774m, 1804-1810m, 1888-1910m. The sandstone layers in the interval 1675-1690m is characterised by high resistivity 15 to 30 ohm-m, and high density (>2.8 g/cc). The sandstone layer in the interval 1888-1910m appears to be gas bearing with a higher resistivity value in the order 15-40 ohm-m and also supported by cross over in density-porosity log response. The other sandstone layers were interpreted as water-bearing with resistivity in the order 5-8 ohm-m. The depth zone in the interval 1950-2060m was analysed,

as shown in Figure 6.15(b). The sandstone layers in the interval 2035-2039m and 2042-2046m show a variation in resistivity from 8-60 ohm-m, porosity 10-25% and hence, can be interpreted to be hydrocarbon (oil) bearing.

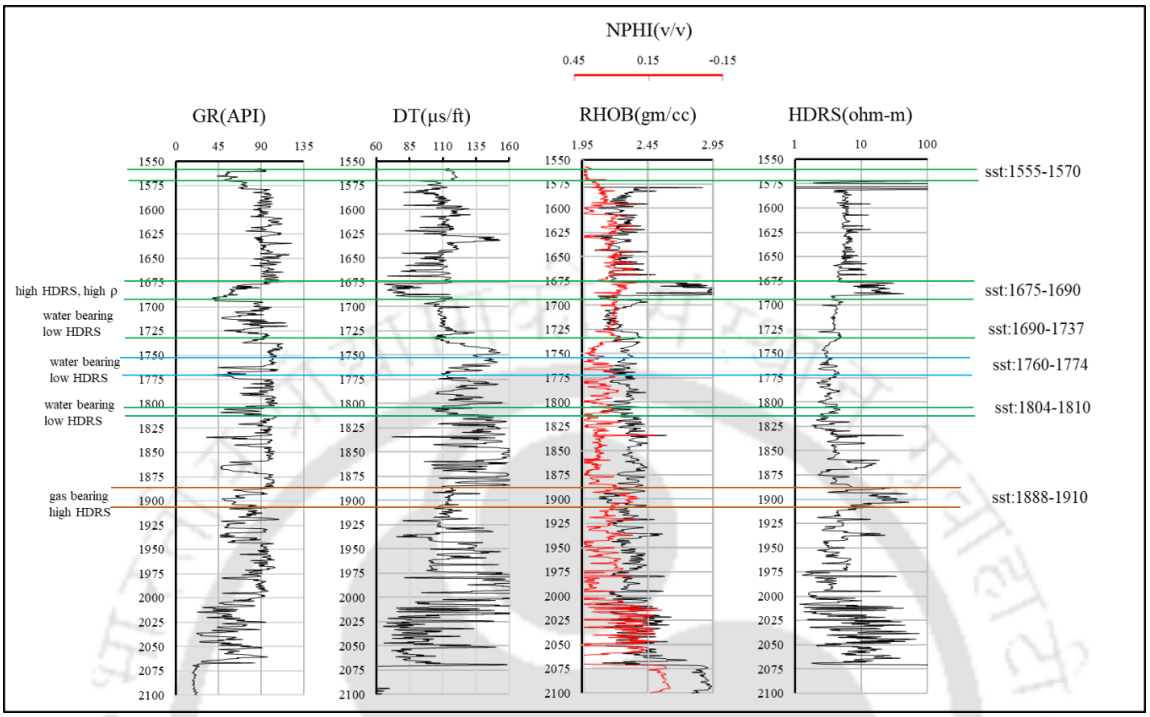


Figure 6.15(a) Different layers of sandstone and saturation zone identification using combination of conventional well log responses for well W1

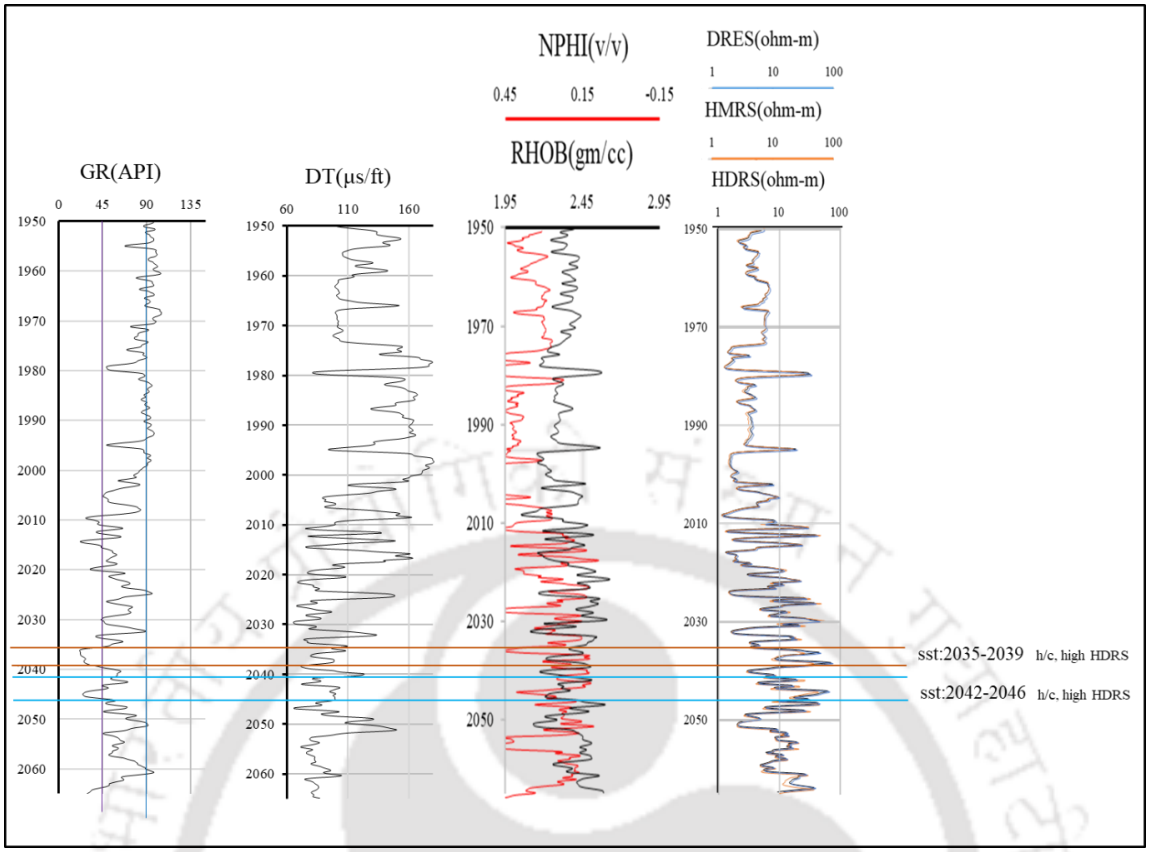


Figure 6.15(b) Different layers of sandstone and saturation zone identification using combination of conventional well log responses for well W1 for hydrocarbon bearing zones (Sylhet formation)

### 6.3.2 AI and Prediction of Properties by Well Logs

With the help of a coloured inversion operator (method), impedance was generated from the seismic section through inversion. The impedance values obtained from the neural network considering well W1 as target varies from 4603 to 14155 (g/cc) * (m/s), as shown in Figure 6.16.

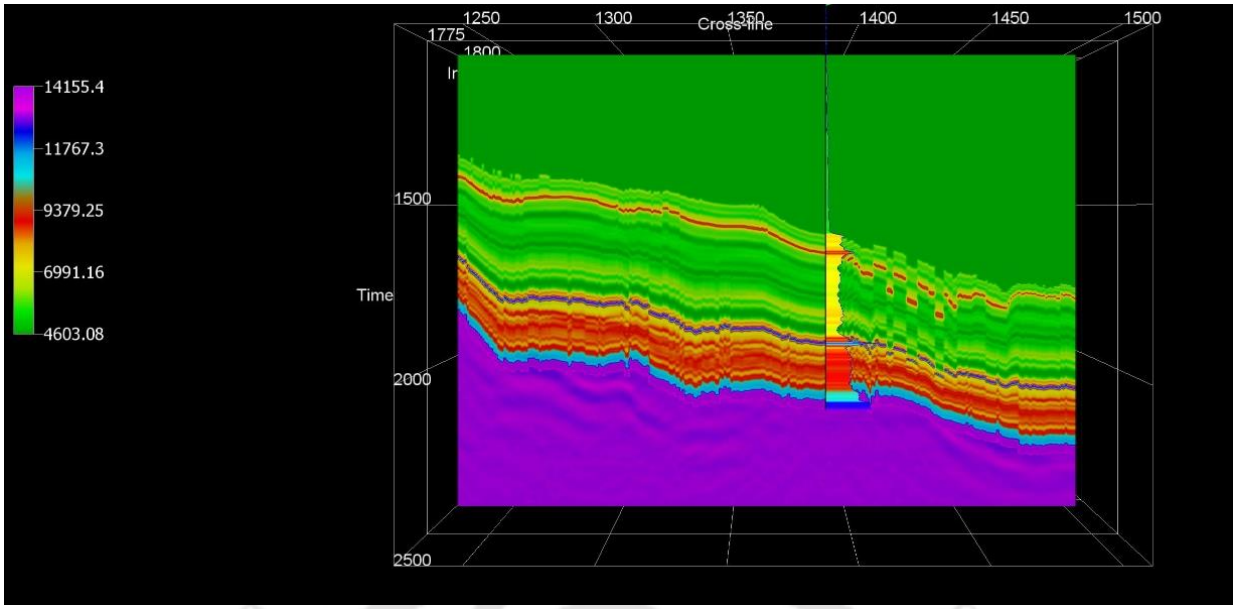


Figure 6.16 Impedance (in m/s*g/cc) generated through inversion analysis considering W1 as target

Based on this AI cube, the different petrophysical properties were evaluated by considering well W1 logs as target. The density log of well W1 was used as target to spatially populate across the survey area. The density values obtained from the neural network varies from 2.14 to 2.72 g/cc, as shown in Figure 6.17(a). Similarly, for obtaining the porosity across the survey area, PHID log obtained from the density log of well W1 was used. The porosity values obtained from the neural network varies from 6 to 29%, as shown in Figure 6.17(b). Subsequently, the velocity (from slowness DT values) obtained from neural network considering well 1 DT log as the target was populated and it varies from 2136 to 5050 m/s, as shown in Figure 6.17(c). Also, the volume of shale varies from 0 to 48%, as shown in Figure 6.17(d).

Similarly, slices of the petrophysical parameters that include density (in g/cc), porosity (in fraction), velocity (in m/s) and volume of shale (in fraction) are also shown for different formations, i.e., at Barail formation top (z=1660 ms), Barail formation bottom (z=1695 ms) and at Sylhet formation top (z=1925 ms) and Sylhet formation bottom (z=1951 ms), as shown in Figures 6.18 to 6.25.

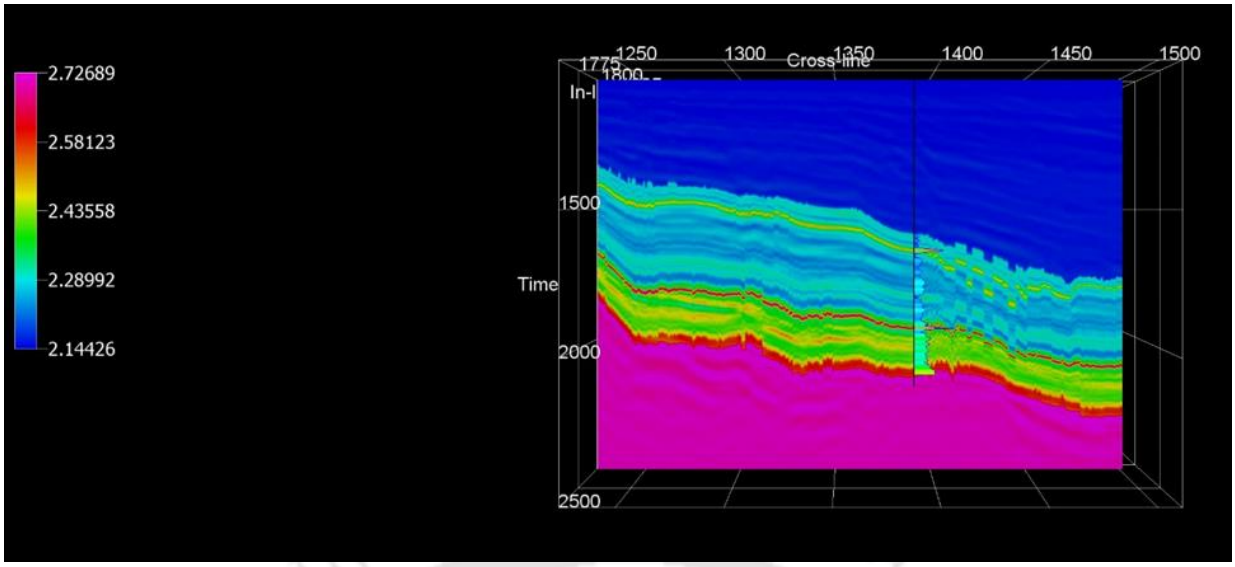


Figure 6.17(a) Density (in g/cc) generated from neural network analysis considering W1 as the target

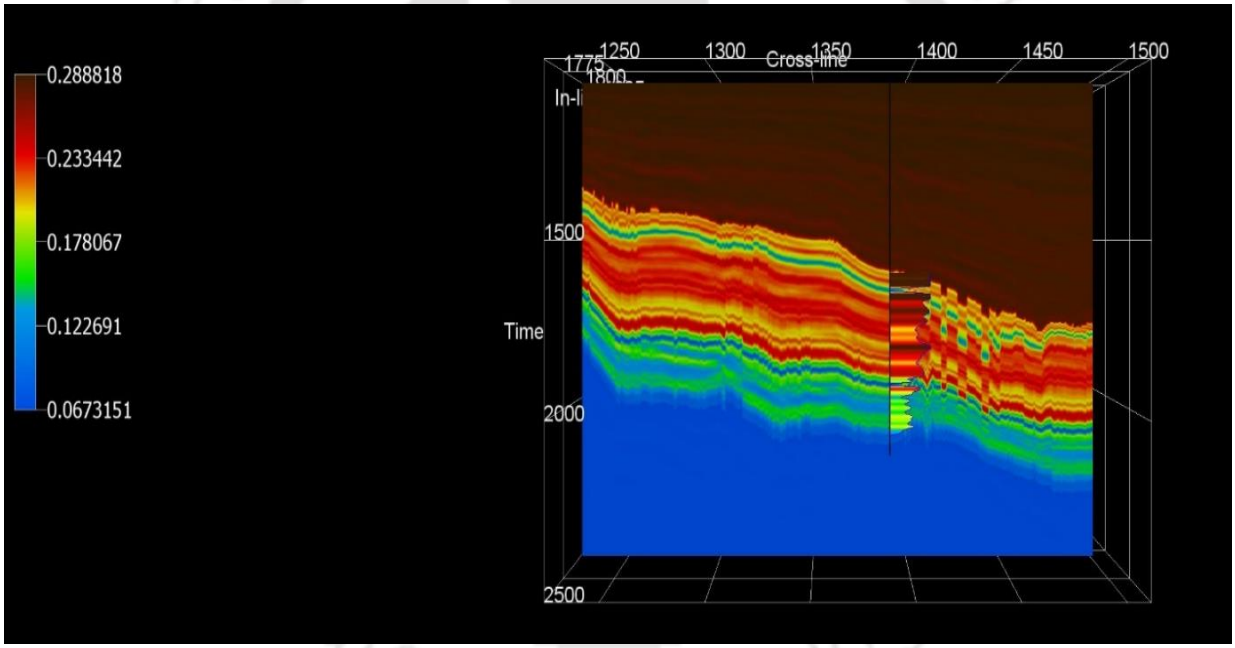


Figure 6.17(b) Porosity (in fraction) generated from neural network analysis considering W1 as the target

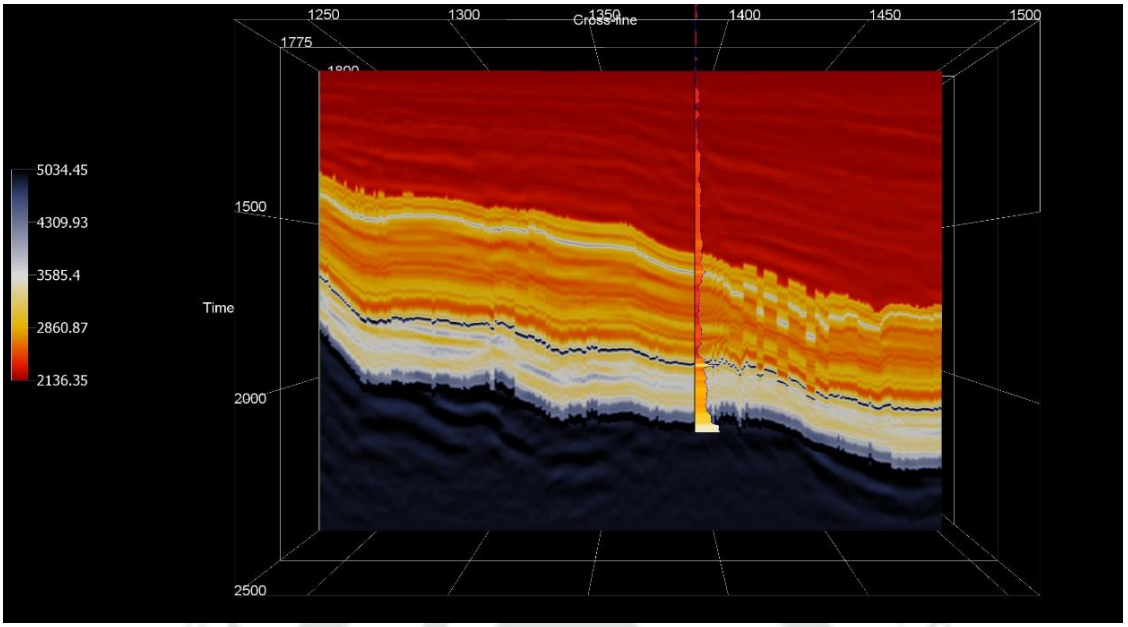


Figure 6.17(c) Velocity (in m/s) generated from neural network analysis considering W1 as the target

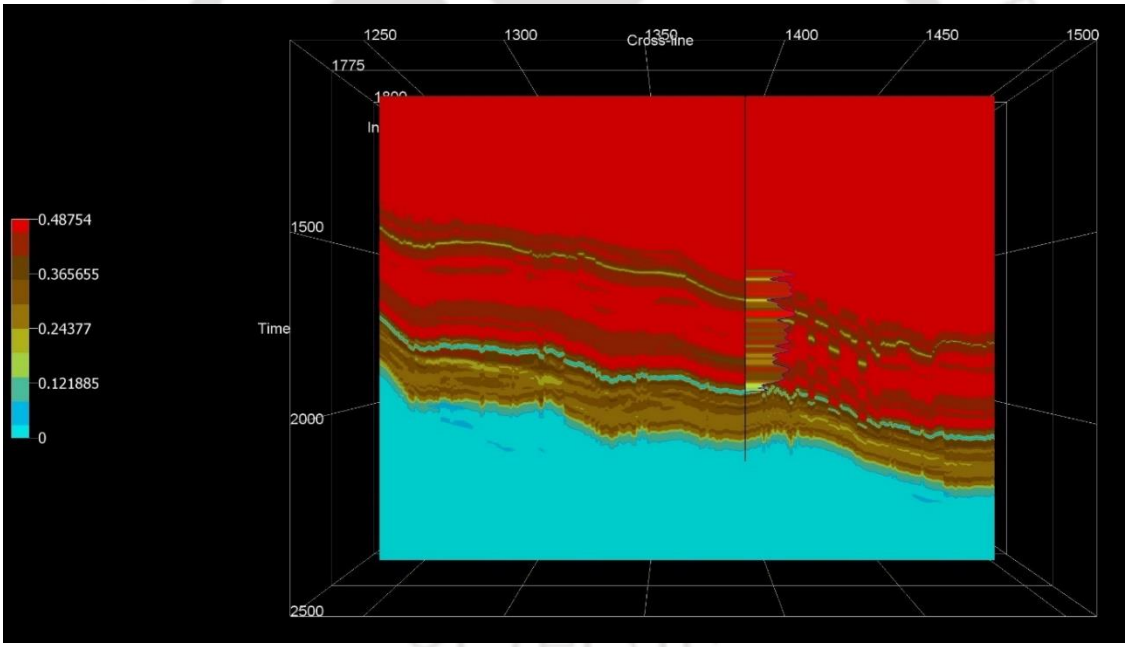


Figure 6.17(d) Volume of shale generated from neural network analysis considering W1 as the target

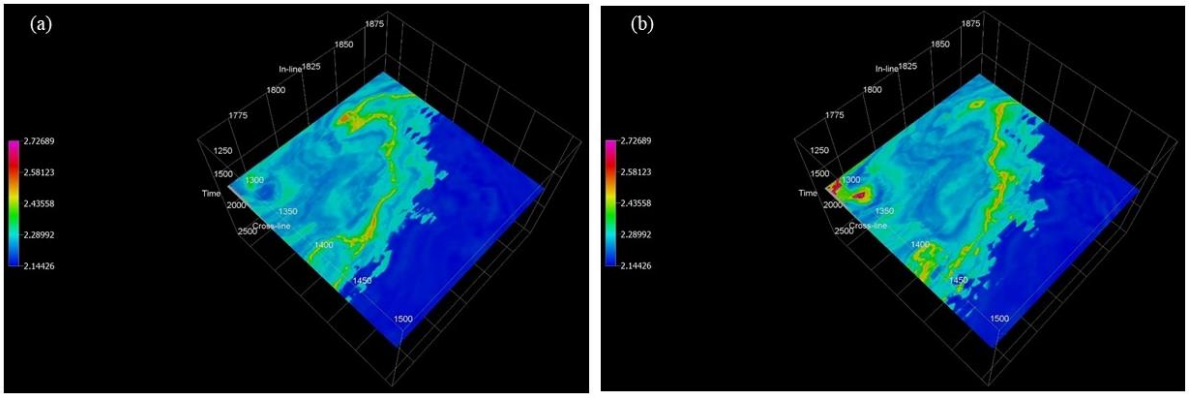


Figure 6.18 Density (in g/cc) slice for (a) Barail formation top, and (b) Barail formation bottom generated from neural network analysis considering W1 as target

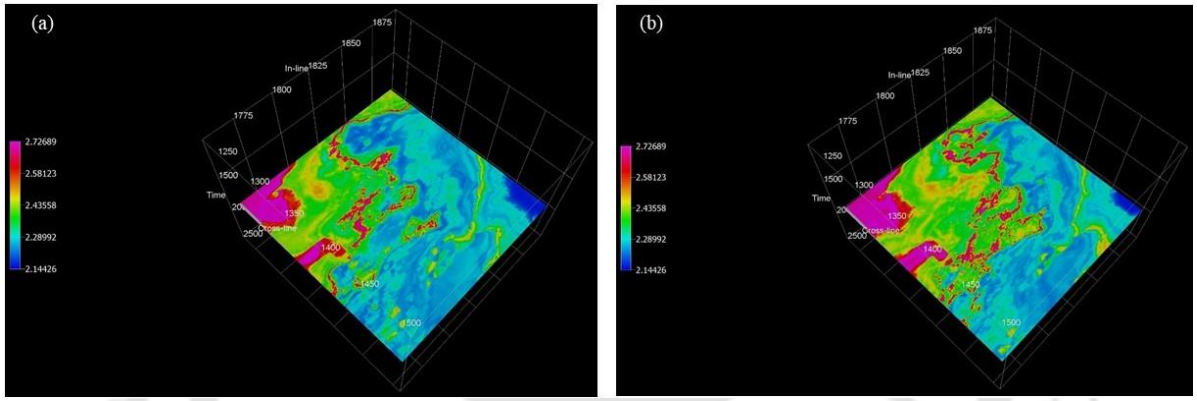


Figure 6.19 Density (in g/cc) slice for (a) Sylhet formation top, and (b) Sylhet formation bottom generated from neural network analysis considering W1 as target

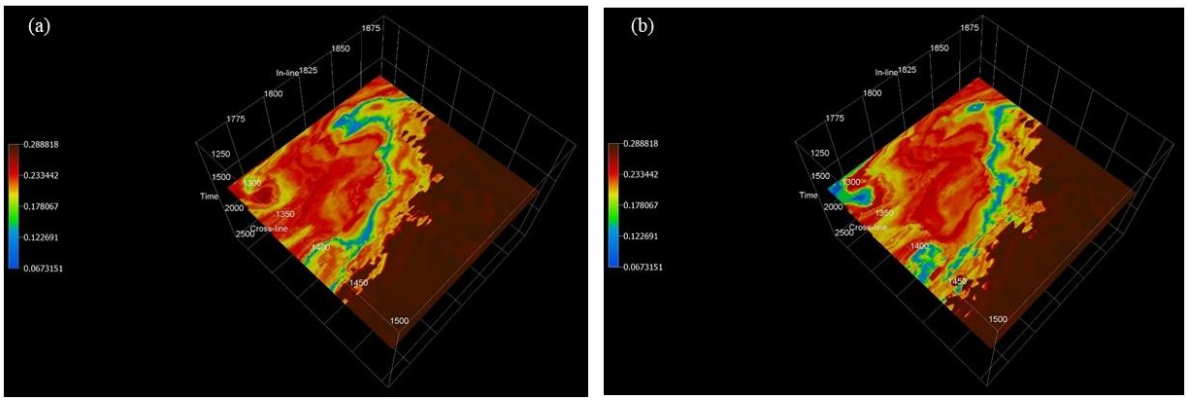


Figure 6.20 Porosity (in fraction) slice for (a) Barail formation top, and (b) Barail formation bottom generated from neural network analysis considering W1 as target

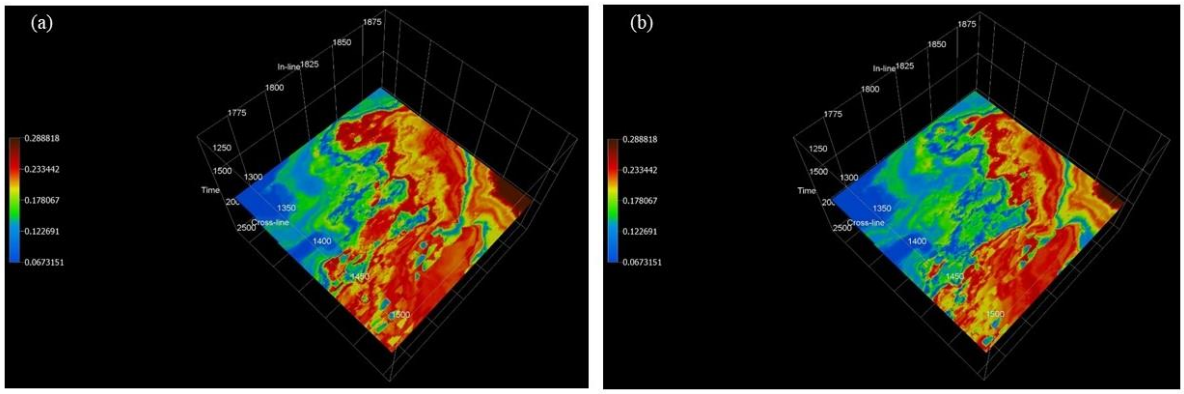


Figure 6.21 Porosity (in fraction) slice for (a) Sylhet formation top, and (b) Sylhet formation bottom generated from neural network analysis considering W1 as target

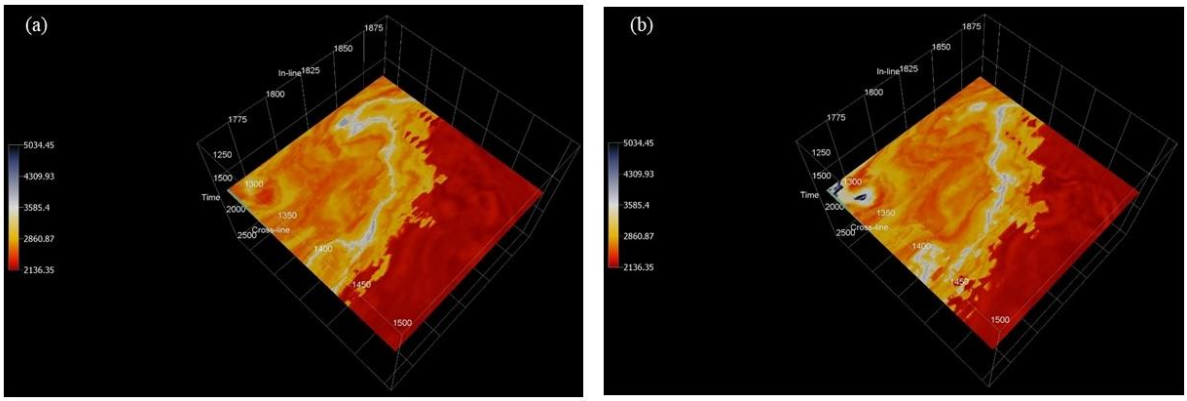


Figure 6.22 Velocity (in m/s) slice for (a) Barail formation top, and (b) Barail formation bottom generated from neural network analysis considering W1 as target

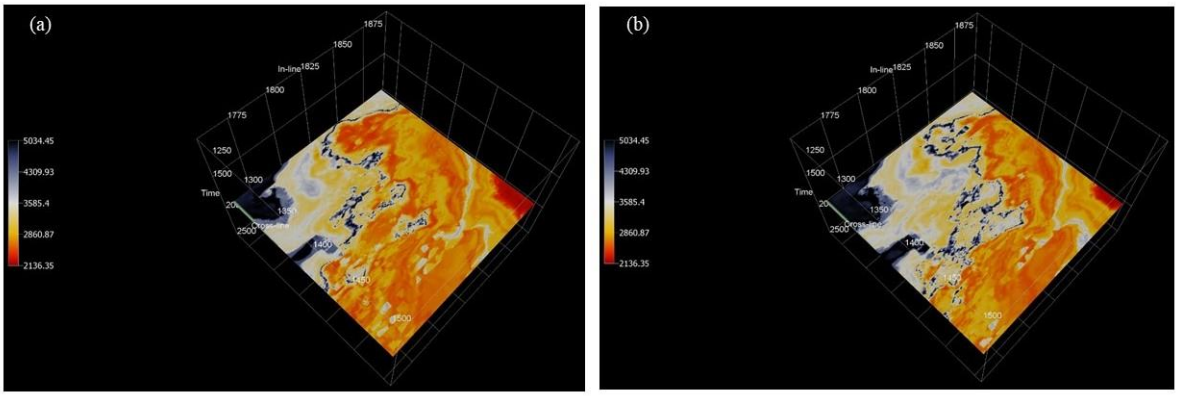


Figure 6.23 Velocity (in m/s) slice for (a) Sylhet formation top, and (b) Sylhet formation bottom generated from neural network analysis considering W1 as target

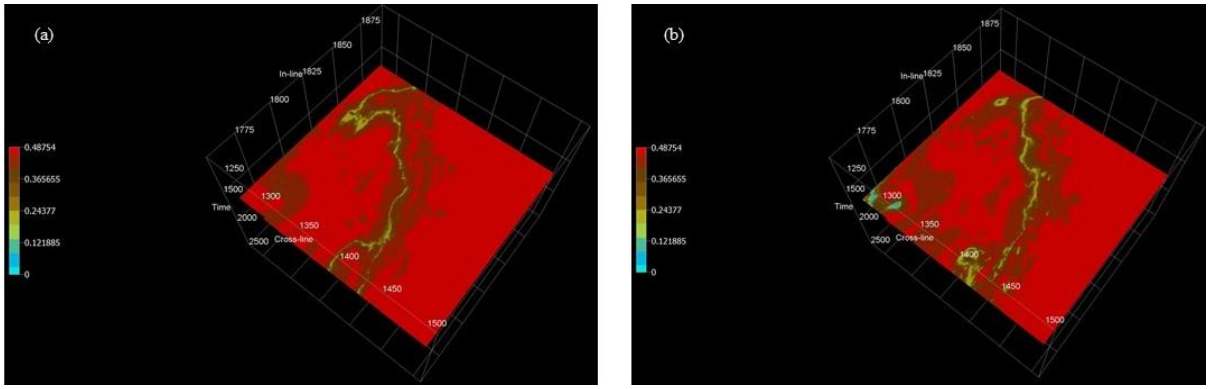


Figure 6.24 Volume of shale slice for (a) Barail formation top, and (b) Barail formation bottom generated from neural network analysis considering W1 as target

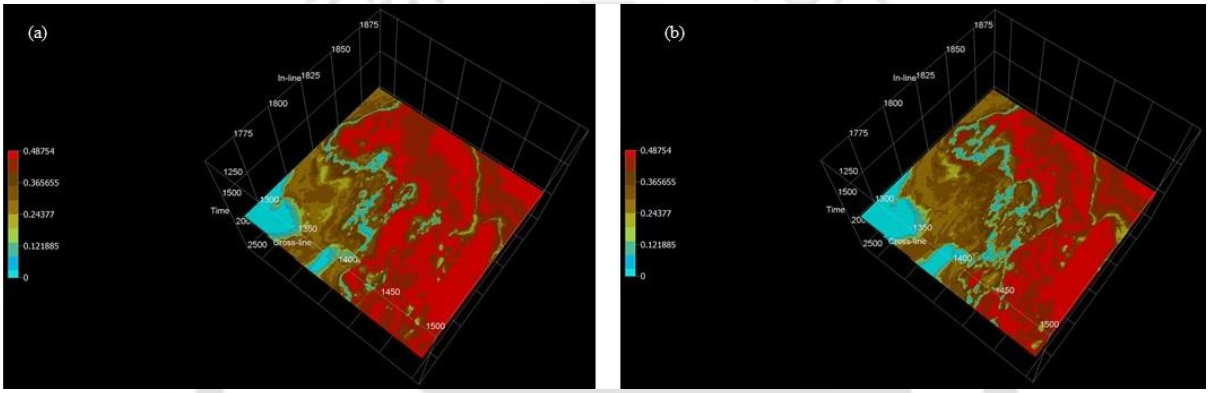


Figure 6.25 Volume of shale slice for (a) Sylhet formation top, and (b) Sylhet formation bottom generated from neural network analysis considering W1 as target

Water saturation was determined by considering well W1 (saturation log derived from Archie's relation - equation 6.2) as the target. The water saturation values obtained from the neural network considering well 1 as target varies from 9 to 27%, as shown in Figure 6.26.

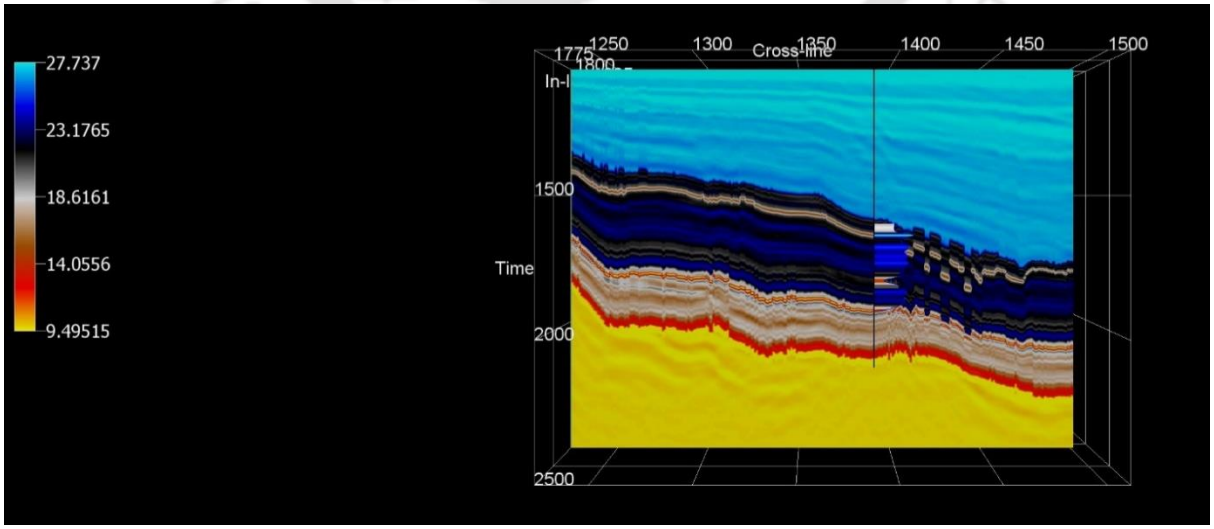


Figure 6.26 Water saturation (in %) generated from neural network analysis considering W1 as target

Figures 6.27 and 6.28 shows water saturation slices generated from neural network analysis considering W1 as the target for different formations, i.e., at Barail formation top (z=1660ms), Barail formation bottom (z=1695 ms) and at Sylhet formation top (z=1925 ms) and Sylhet formation bottom (z=1951 ms).

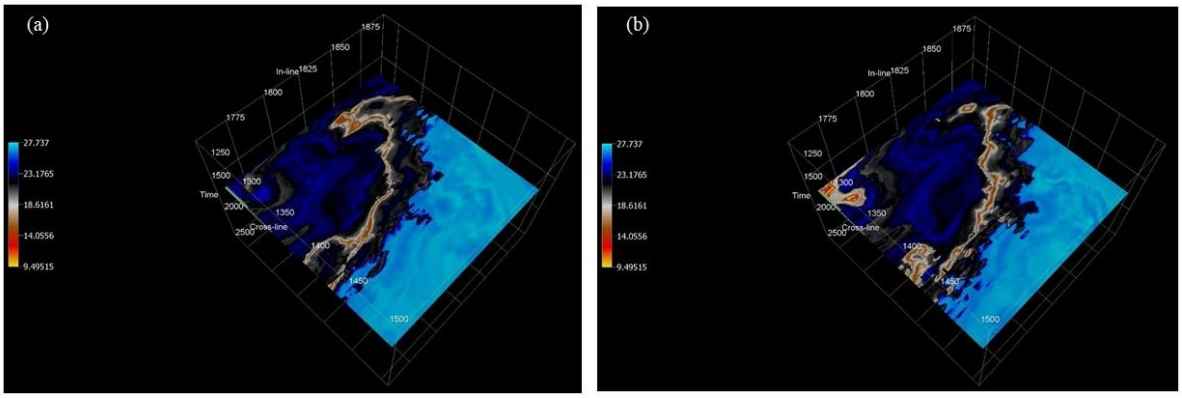


Figure 6.27 Water saturation slice for (a) Barail formation top, and (b) Barail formation bottom generated from neural network analysis considering W1 as target

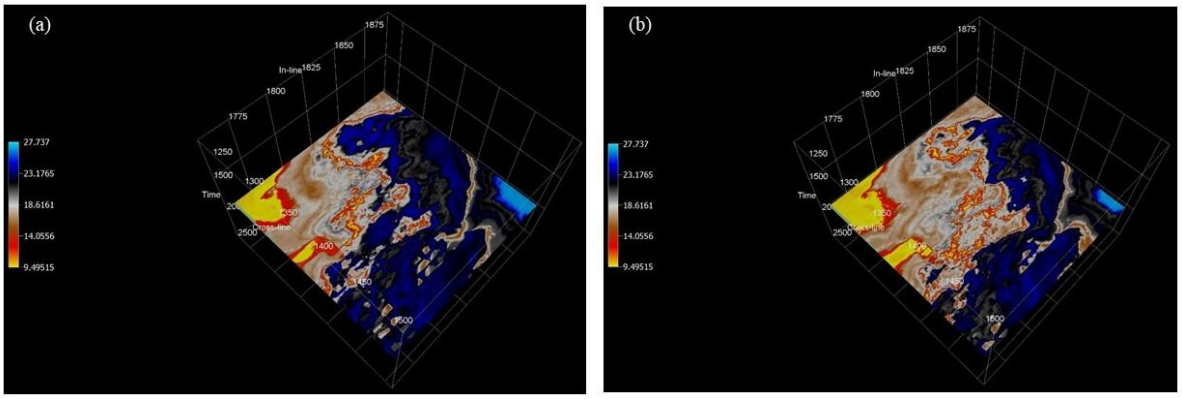


Figure 6.28 Water saturation slice for (a) Sylhet formation top, and (b) Sylhet formation bottom generated from neural network analysis considering W1 as target

From the results, as shown in Figure 6.17, it can be observed that the thickness of the hydrocarbon-bearing zone increases on approaching towards the northwestern part of the study area. Additionally, two hydrocarbon-bearing layers were interpreted at the bottom while analysing well log responses (Figure 6.15b). Combining these two important observations and assuming continuity in the sequence, it can be concluded that high exploration potential and development opportunities exist in the northwestern part of the study area if the effect of structural geology is not taken into consideration. The saturation plots (Figure 6.26) derived using inversion also support the findings.

Figure 6.29 shows the variation of different parameters across the survey area, i.e., from one end to the other end. The spatial distribution in density varies from 2.14 to 2.72 g/cc across W1

to W2 (Figure 6.29(a)). Similarly, the spatial distribution in density varies from 2.14 to 2.72 g/cc across W1 to W3 (Figure 6.29(a)). The spatial distribution in porosity varies from 6 to 28% across W1 to W2 (Figure 6.29(b)). Similarly, the spatial distribution in porosity varies from 6 to 28% across W1 to W3 (Figure 6.29(b)).

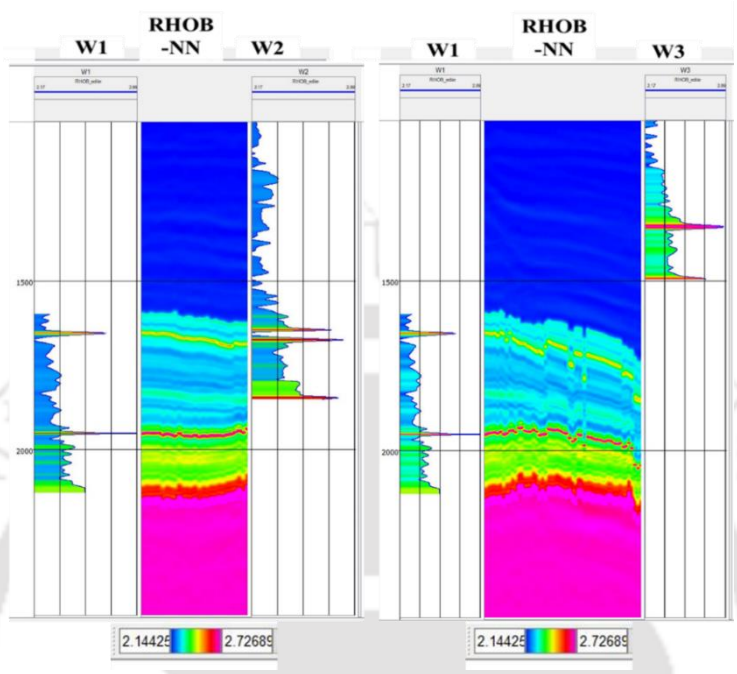


Figure 6.29(a) Spatial variation of density (in g/cc) predicted from neural network analysis across wells

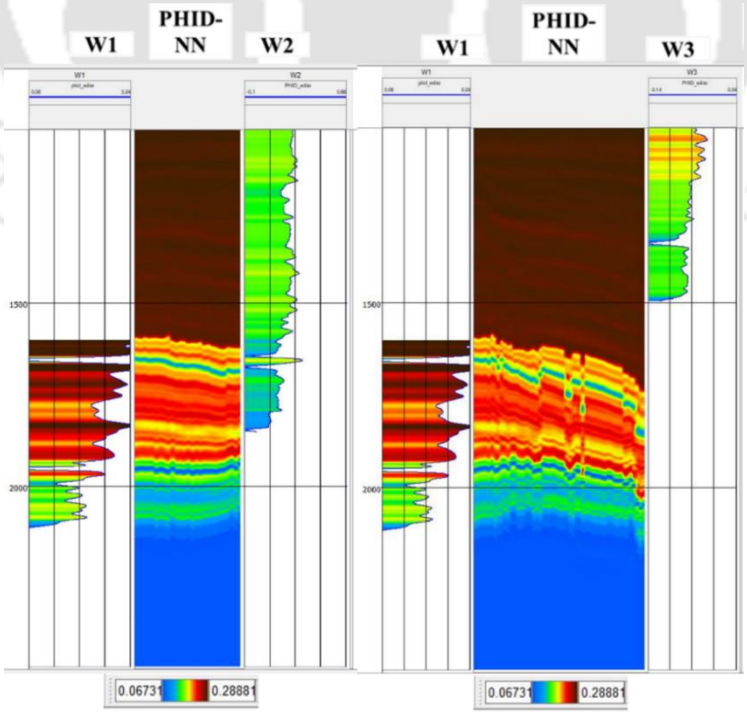


Figure 6.29(b) Spatial variation of porosity (in fraction) predicted from neural network analysis across wells

The values obtained by performing NN analysis were cross plotted against the well log values to inspect the correlation between them as shown in Figure 6.30. The cross plots between density from well and density generated through NN is shown in Figure 6.30(a) with r=0.9. Similarly, the cross plots between porosity from well and porosity generated through NN is shown in Figure 6.30(b) with r=0.89.

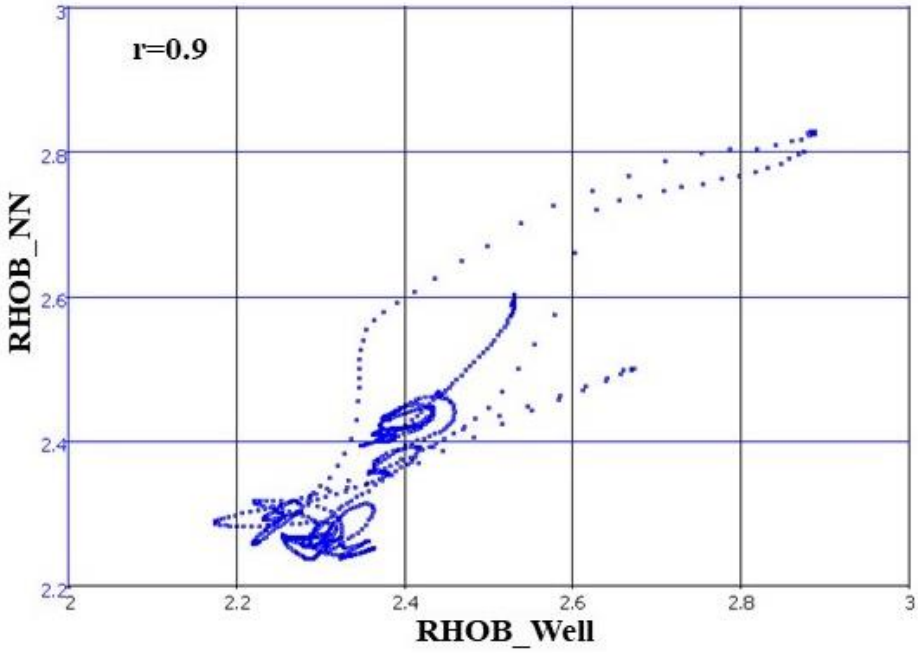


Figure 6.30(a) Plot showing correlation between density derived from well log and density derived from neural network analysis

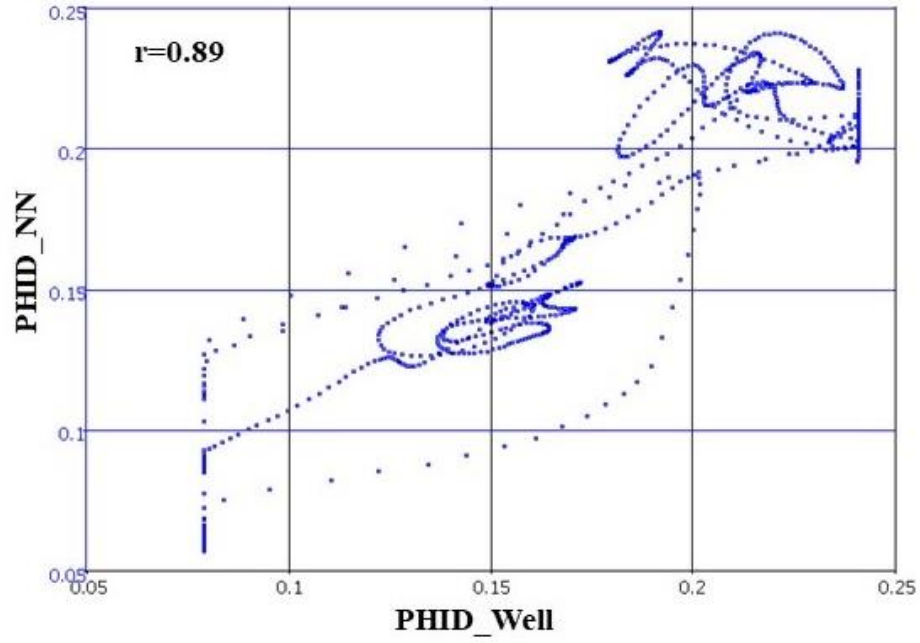


Figure 6.30(b) Plot showing a correlation between porosity derived from well log and porosity derived from neural network analysis

Well W1 was used as target since it is the only producing well amongst all the three wells and hence, the match between the seismic properties and the log properties of the other two wells W2, W3 were not shown. The value of correlation coefficient (r), displays the degree of match between the seismic properties and the log properties of the other two wells, based on the model that was generated. Considering Well W2, r=0.62 for density, r=0.62 for porosity; while considering Well W3, r=0.44 for density, r=0.46 for porosity.

## 6.4 Prediction of Petrophysical Properties using Laboratory Model

The results presented in this section utilise the rock physics model derived from experimental measurements conducted on sandstone core plugs of Tipam and Barail formation (as elaborated in chapter 5).

### 6.4.1 Using a One to One Correlation

The laboratory-based statistically derived trends (equations), as explained earlier, were used to spatially populate the different petrophysical and acoustic properties across the seismic survey. On application of a laboratory-based model (one to one correlation), the range of bulk density obtained from AI varies from 2.02 to 3.15 g/cc (Figure 6.31(a)). Similarly, on the application of a laboratory-based model, the range of porosity obtained from AI varies from 0 to 22.9% (Figure 6.31(b)).

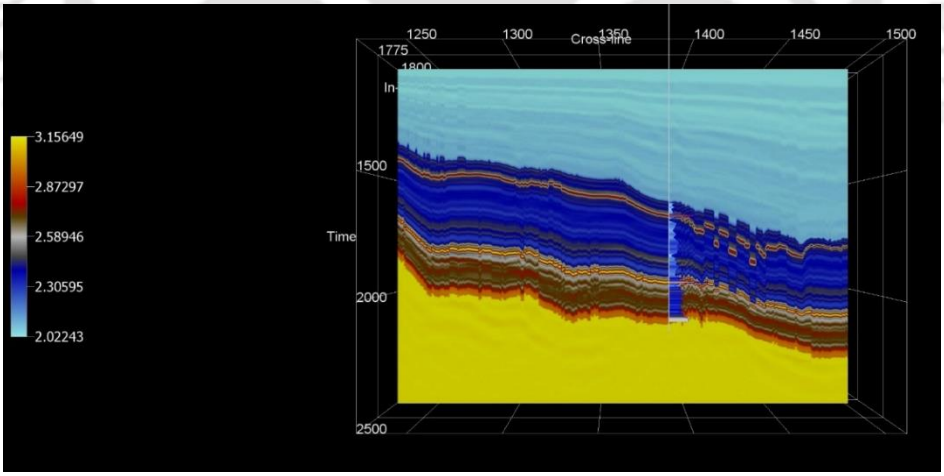


Figure 6.31(a) Variation of density (in g/cc) generated from impedance considering laboratory-based rock physics model

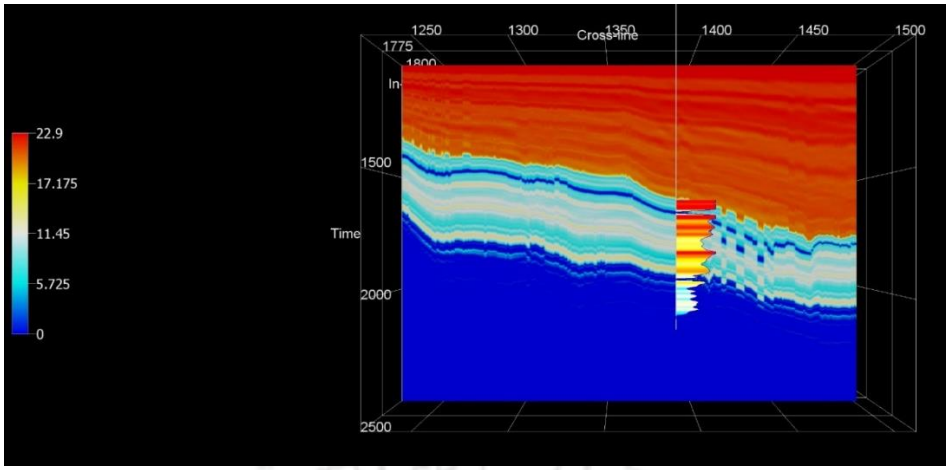


Figure 6.31(b) Variation of porosity (in %) generated from impedance considering laboratory-based rock physics model

To investigate any correlation between the applicability of NN derived results and laboratory-based results, the different parameters were cross-plotted together, as shown in Figure 6.32. The cross plots between density derived on the application of the laboratory-based model and NN derived is shown in Figure 6.32(a) with r= 0.88. The cross plots between porosity derived on the application of the laboratory-based model and NN derived is shown in Figure 6.32(b) with r= 0.86.

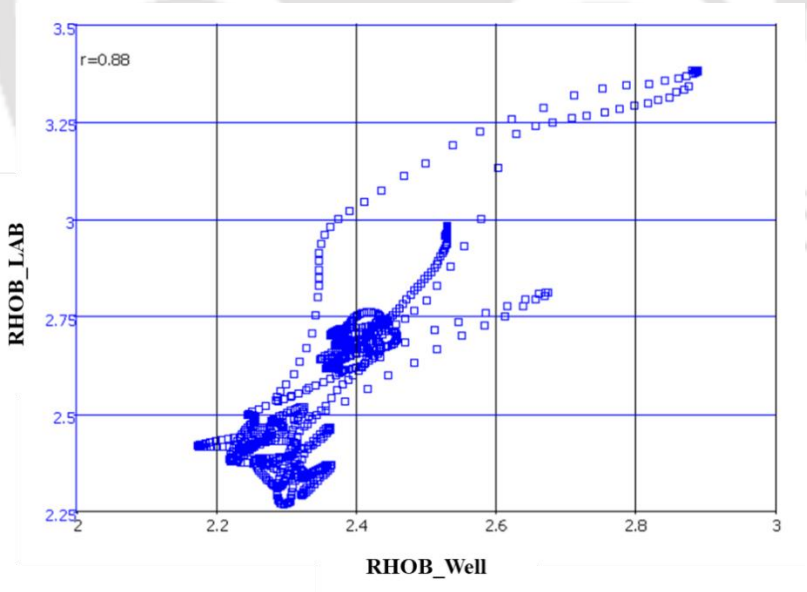


Figure 6.32(a) Cross-plot between density from laboratory results to the density obtained from neural network

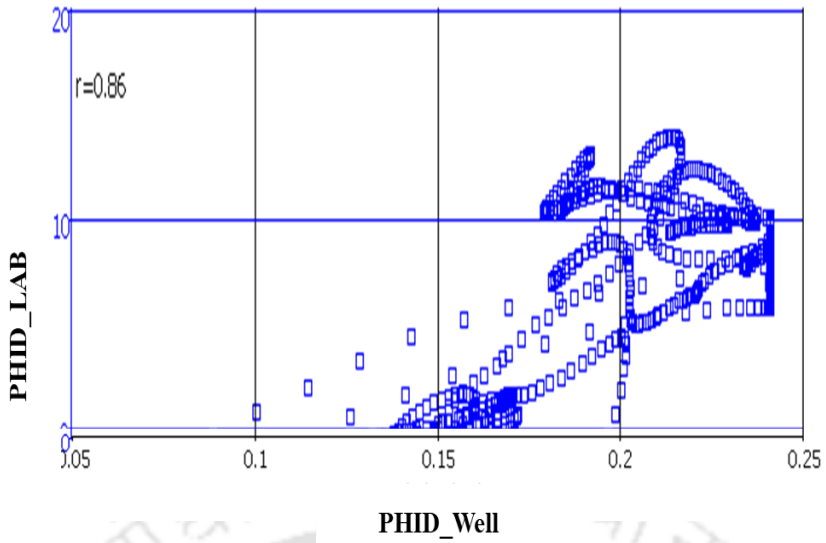


Figure 6.32(b) Cross-plot between porosity from laboratory results to the porosity obtained from neural network analysis

### 6.4.2 Using Multivariate Regression Equation

Using equation (6.4), $V_p$ was calculated by using density and porosity derived from neural network analysis. This obtained $V_p$ from equation (6.4) was cross plotted with the velocity derived from neural network analysis, and a strong correlation was obtained, as shown in Figure 6.33. However, neural network derived velocity values were found to be on a higher side when compared with laboratory-derived velocity, i.e., $V_p$ (from NN) = c * $V_p$ (from the lab), where c varies from 1.34 to 1.48 for Barail, 1.29 to 1.38 for Kopili and 1.33 to 1.48 for Sylhet formation.

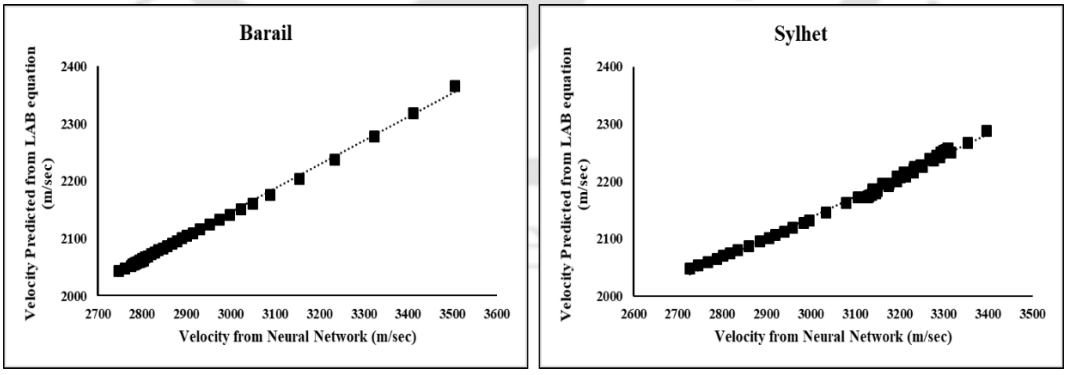


Figure 6.33 Cross-plot between velocity from laboratory results to the velocity obtained from the neural network for (a) Barail (b) Sylhet formation

The velocity obtained from equation (6.4) were transformed to AI (by using neural network derived density) and thereafter trained with the modelled well log to generate density and

porosity across the seismic section (Figure 6.34(a) and Figure 6.34(b)). It was observed that density varied from 2.23 g/cc to 2.73 g/cc, while porosity varied from 7 to 27%.

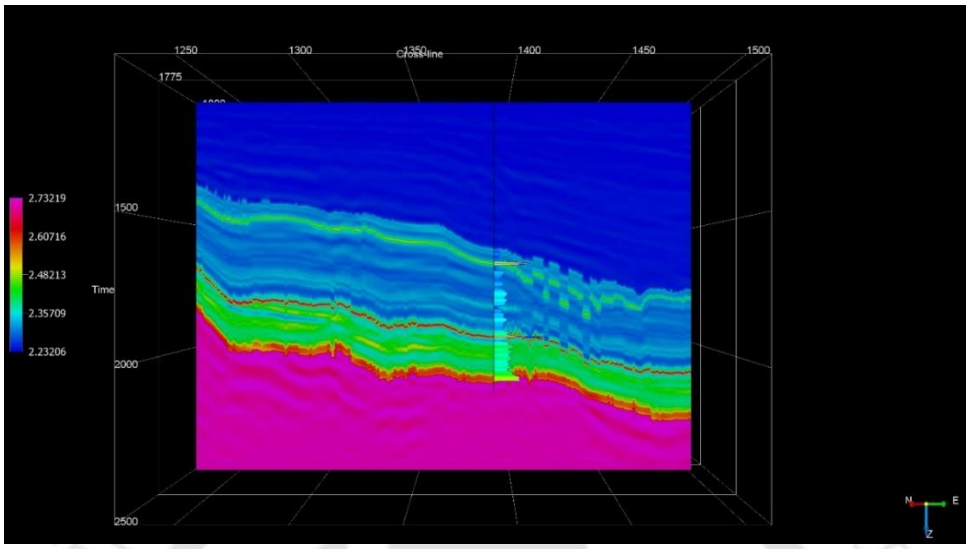


Figure 6.34(a) Density (in g/cc) results obtained after incorporating well log derived rock physics model and laboratory-generated rock physics model

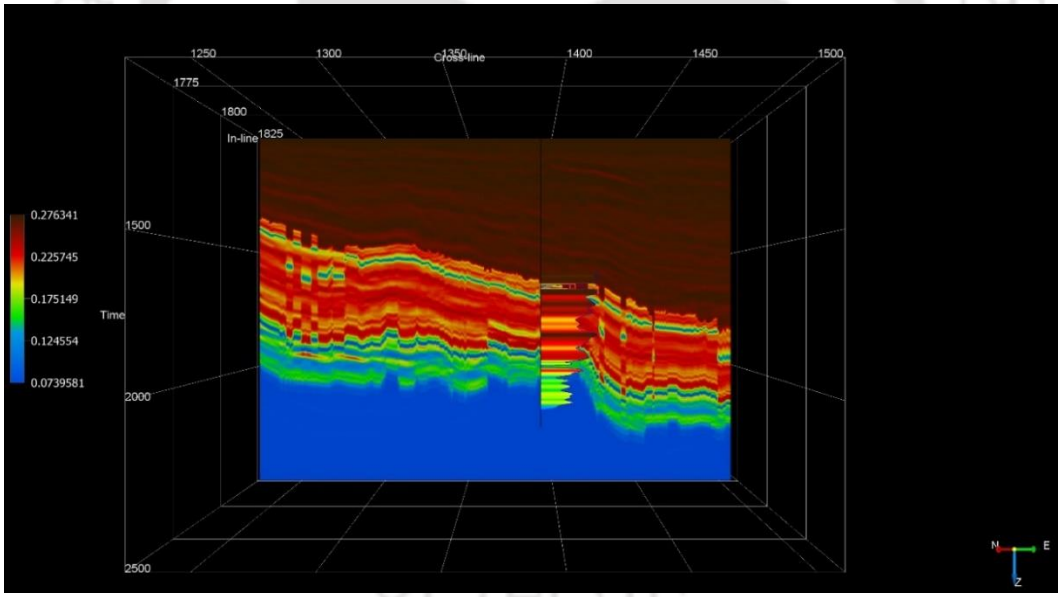


Figure 6.34(b) Porosity (in fraction) results obtained after incorporating well log derived rock physics model and laboratory-generated rock physics model

Similarly, density (in g/cc) and porosity (in fraction) slices are also shown considering laboratory-based rock physics model for different formations, i.e., at Barail formation top (z=1660 ms), Barail formation bottom (z=1695 ms), and at Sylhet formation top (z=1925 ms) and Sylhet formation bottom (z=1951 ms), as shown in Figures 6.34 to 6.37.

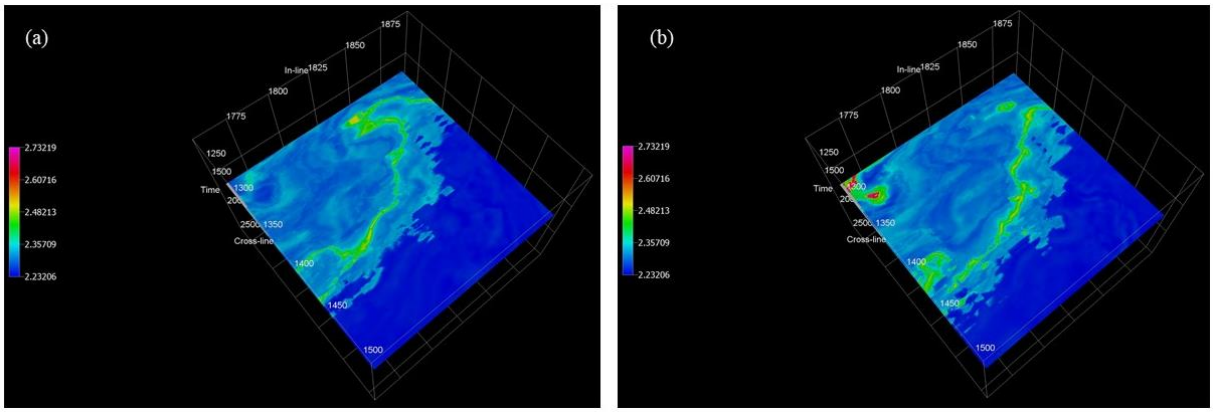


Figure 6.35 Density (in g/cc) slice for (a) Barail formation top and (b) Barail formation bottom generated from neural network analysis obtained after incorporating well log derived rock physics model and laboratory-generated rock physics model

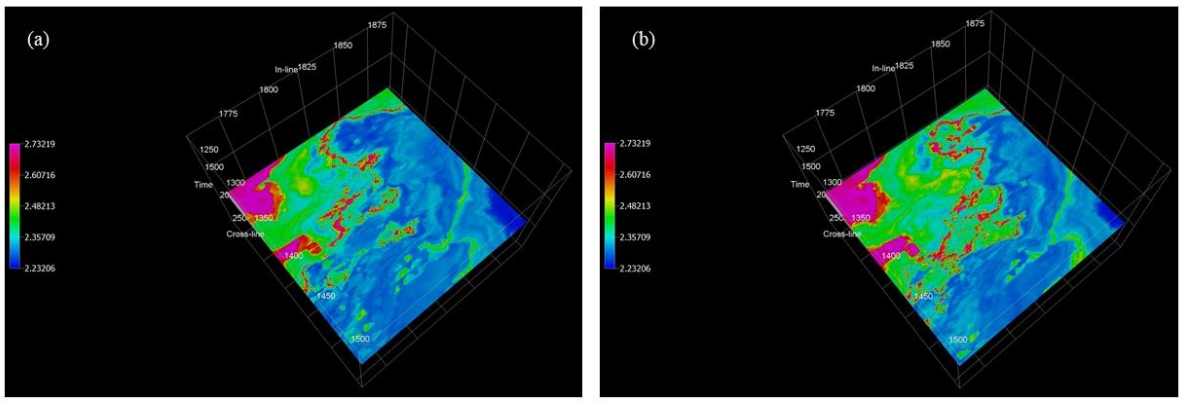


Figure 6.36 Density (in g/cc) slice for (a) Sylhet formation top and (b) Sylhet formation bottom generated from neural network analysis obtained after incorporating well log derived rock physics model and laboratory-generated rock physics model

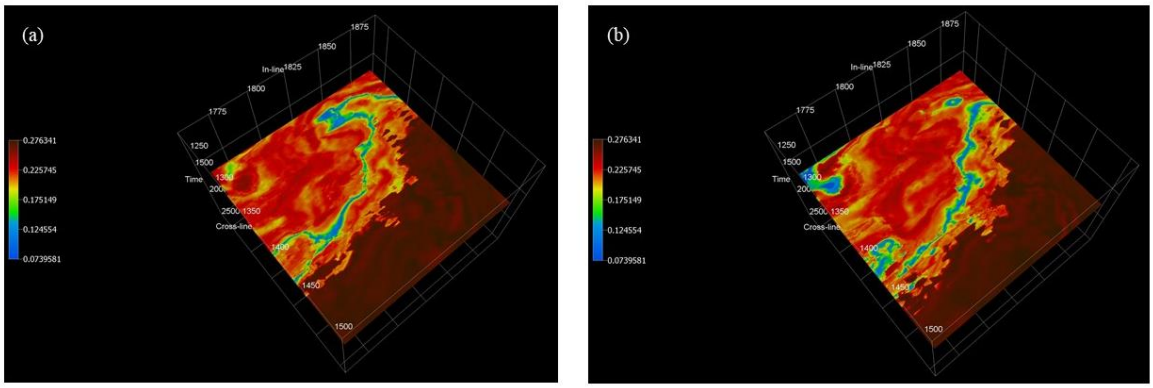


Figure 6.37 Porosity (in fraction) slice for (a) Barail formation top and (b) Barail formation bottom generated from neural network analysis obtained after incorporating well log derived rock physics model and laboratory-generated rock physics model

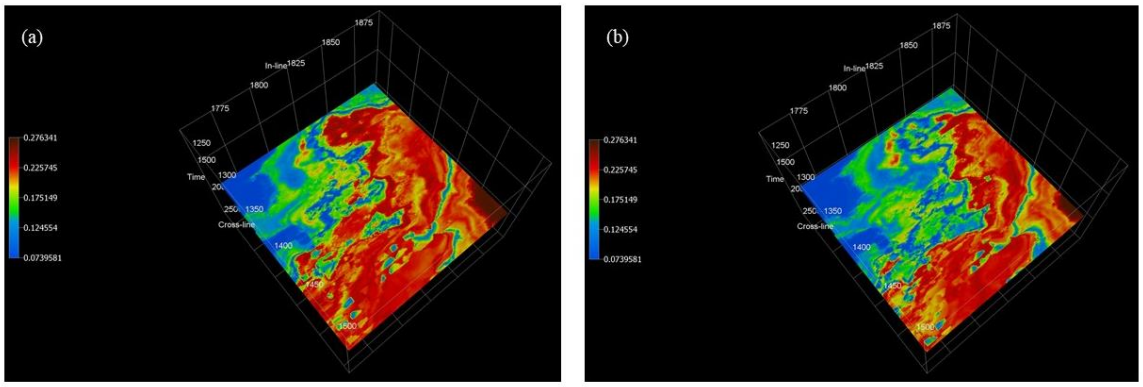


Figure 6.38 Porosity (in fraction) slice for (a) Sylhet formation top and (b) Sylhet formation bottom generated from neural network analysis obtained after incorporating well log derived rock physics model and laboratory-generated rock physics model

These generated density and porosity models were compared and plotted with the well-modelled logs. It was found that there was a reasonable match between the two parameters, i.e., r = 0.78 and r = 0.95 for density for Barail and Sylhet formation, while r = 0.91 and r = 0.94 for porosity for Barail and Sylhet formation as shown in Figure 6.39. These modelled parameters constitute of an amalgamation or integration of laboratory and well-modelled components that may be useful in enhancing the seismic reservoir characterisation.

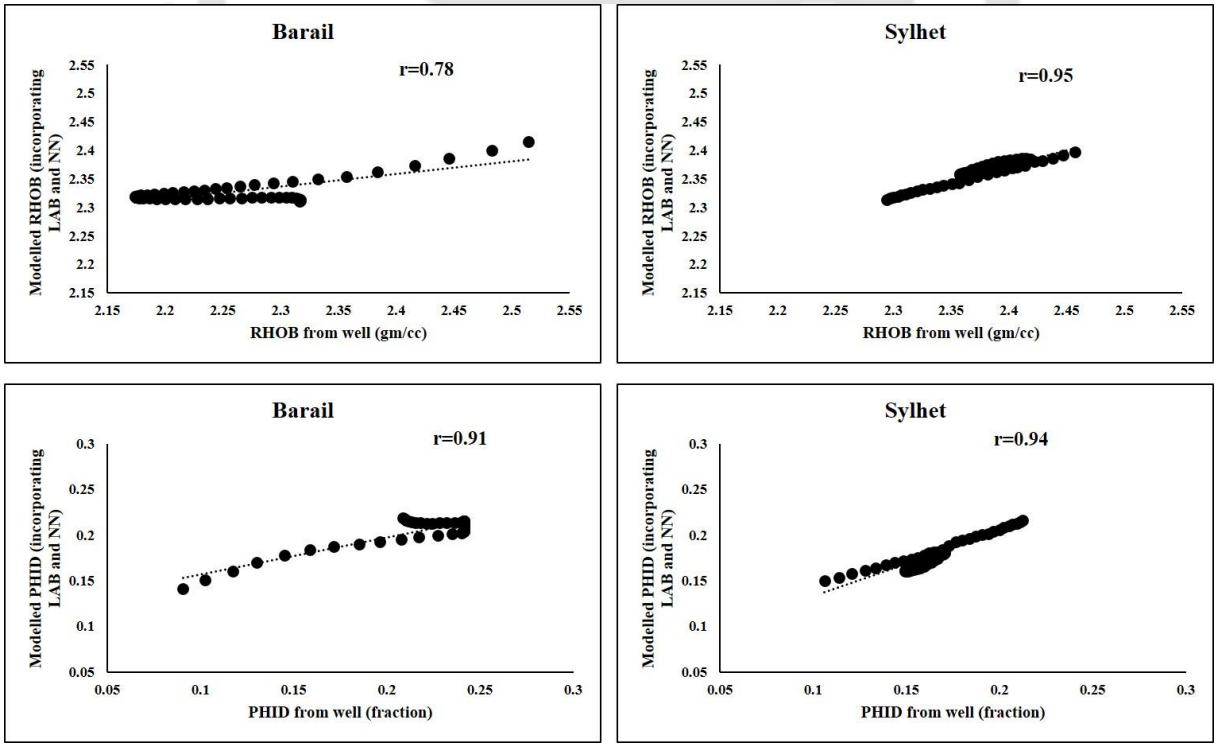


Figure 6.39 Cross plot between well log density, porosity with modelled density and porosity results obtained after incorporating laboratory and neural network derived density and porosity for Barail and Sylhet formation

Laboratory based estimation of petrophysical, geomechanical and mineralogical parameters is essential to corroborate data obtained from the well logs (Ambati et al., 2021). Although the well log data have a higher vertical resolution, but this information is limited in the vicinity of the well from where it is measured. On the other hand, analysis on the core plugs in the laboratory, collected from multiple wells of the same basin, tend to be more representative of a broader lithological unit, especially in case of clastic reservoirs, that offer relatively less heterogeneity as compared to carbonate reservoirs (Zhang et al., 2020). The choice of inclusion of information is motivated by primarily two reasons – (i) the trends can be said to be representative of the reservoir conditions and (ii) trends captured through petrophysical analysis can easily be extended for inversion based property prediction. The statistical derived models used for trend or pattern recognition may help to reduce uncertainty, ambiguity related to the most likely interpretation in case of reservoir characterization (Mukerji et al., 2001). Hence, we attempted to integrate different scales of study in order to capture the heterogeneity, i.e., application of laboratory and well log data to interpret seismic inversions in terms of petrophysical properties. Such a generalized predictive model will behave more realistic since it contains all the components that capture Vp variations. Integrating different methods may lead to the development of realistic models, thereby being a guiding force for quantitative decision analysis (Bosch 2004). This methodology may also find it application in detecting the expected small-scale variability that is noticeable in laboratory data, but indistinct in seismic data. Although the presented results correlate with the well log derived parameters, further complementary studies involving the influence or effect of other factors such as overburden pressure, fluid content, pore pressure etc. may also be required to validate the efficacy of the presented results.

Furthermore, the laboratory measurements are made on core samples a few mm in size at kHz frequencies, while seismic data are at a few 10's of Hz. Regarding the use of a particular frequency of transducer (54 kHz) in the present study, this scaling effect will always be a subject for further investigation/research, since the laboratory measurements are made on core samples a few mm in size at kHz frequencies, while seismic data are at a few 10's of Hz. In other words, frequency ranges pertaining to different scales of study are: seismic data in <100 Hz, sonic logging in $10^4$ Hz and laboratory ultrasonic measurements in $10^6$ Hz (Mavko et al., 2009). Additionally, to analyze the effect of frequency on laboratory based measurements, different sets of transducer along with sufficient number of rock types will be required for a comparative study to arrive at a conclusion.

## 6.5 Summary and Conclusions

The present study attempts to interpret the hydrocarbon-bearing zones from the well log analysis and thereafter populates the different parameters such as porosity, density, the volume of shale and water saturation with the help of seismic inversion for the Upper Assam basin, India. Different sandstone intervals were identified and the effect of water, gas and hydrocarbon zones in the sandstone layers were interpreted from the conventional well log responses. The gas-bearing zones showed cross over in density-porosity well log response and was also supported by high resistivity values of 15-40 ohm-m. Hydrocarbon (oil) bearing zone was identified in the interval 2035-2039 m and 2042-2046 m and these show a variation in resistivity from 8-60 ohm-m with porosity10-25%. For deriving the different properties through the help of inversion, a multilayered feed-forward network model was developed and the errors were fed back through back propagation. The range of different parameters vary in the following range: porosity between 6 to 29%, density between 2.14 g/cc to 2.72 g/cc, velocity between 2136 to 5034 m/s, $V_{shale}$ between 0 to 49% and water saturation between 9 to 28%. Based on the analysis, it was observed that the inversion derived parameters were in agreement with the well log data, and the hydrocarbon-bearing zones were being reflected in the saturation plot obtained after inversion analysis. Additionally, the modelled log results were compared with the inverted results and it shows a reasonable match with a correlation coefficient of 0.9 for density and 0.89 for porosity. The spatial variation of the different parameters was also populated, indicating prospective exploration potential in the northwestern region of the study area due to the increasing thickness of the hydrocarbon-bearing zone. However, incorporating the effect of structural geology in the present study may further help to facilitate the presence of exploration opportunity in the northwestern part of the study area. Laboratory-based trends between velocity, density and porosity, obtained by investigation on sandstone core plugs of the same basin were utilised and incorporated in the inversion analysis. On using a one to one laboratory-derived correlation, the range of density varied from 2 to 3.15 g/cc while porosity varied from 0 to 23%. Thereafter, the velocity obtained from the laboratory-derived rock physics model ($V_p$ as a function of density and porosity) was transformed to AI (by using neural network derived density) and subsequently trained with the modelled well log to generate density and porosity across the seismic section. On using laboratory-derived rock physics model, the different parameters varied as: density between 2.23 to 2.73 g/cc and porosity between 7 to 27%. These generated density and porosity models were compared and plotted with the well-modelled logs. It was found that there was a reasonable match between

the two parameters, i.e., r = 0.78 and r = 0.95 for density for Barail and Sylhet formation, while r = 0.91 and r = 0.94 for porosity for Barail and Sylhet formation. These modelled parameters constitute of an amalgamation or integration of laboratory and well-modelled components that may be useful in enhancing the seismic reservoir characterisation. Integrating different methods may lead to the development of realistic models, thereby being a guiding force for quantitative decision analysis.

# Chapter 7
# Summary and Conclusions

The aim of this study is the incorporation of laboratory-derived petrophysical and mineralogical data in the quantitative interpretation of compressional wave velocity ($V_p$) to enhance the capability of rock physics models in reservoir characterisation. All parameters were evaluated in the laboratory using recognised standard laboratory methods. The brief highlights and major conclusions of this study can be summarised as follows:

## 7.1 Conclusions

- The seismic wave propagation was reproduced in the laboratory using the ultrasonic velocity measurement technique to measure the $V_p$ of different rocks. Ultrasonic transducers of 54 kHz frequency were used to measure $V_p$ utilising the through transmission technique.
- For porosity measurement, an in-house helium gas porosimeter was developed. The fabricated setup is capable of performing measurements on rocks of known volumes of different dimensions up to NX (54 mm) core size. The obtained results were compared with an industry-based commercial porosimeter, and a strong $R^2$ =0.98 for carbonates, $R^2$ =0.95 for sandstones were obtained.
- A laboratory-based rock physics model for carbonates was developed by integrating petrophysical properties estimated from laboratory-based measurements along with the digital image analysis (DIA) technique. A multivariate statistical approach was adopted to understand the effects of bulk density, porosity, pore size and aspect ratio collectively on $V_p$. It was inferred that the effectiveness of the predictive velocity model improved by incorporating multiple parameters in combination. Approximately 50% decrease in $V_p$ was observed when porosity varied from 2 to 40% for different saturation conditions.
- The effects of petrophysical and mineralogical variables on the acoustic properties of sandstones were investigated using laboratory generated data. Single parameter correlations among petrophysical properties and mineralogy with $V_p$ showed that $V_p$ correlated inversely with porosity, permeability and feldspar content and directly with bulk density and quartz content. The collective influence of bulk density, porosity and mineral content on $V_p$ was incorporated to derive a simplified rock physics model for sandstones in the form of statistically derived equations. A generalised model was derived by varying the

major mineral fractions of sandstone rock type, i.e., quartz and feldspar, with porosity and varying saturation conditions to determine the range in $V_p$.

- Seismic inversion was carried out using the coloured inversion method across the seismic section of the Upper Assam Basin, using a well log derived rock physics model and laboratory-generated rock physics model. On using a well log derived rock physics model, the different parameters varied as: density between 2.14 to 2.72 g/cc, porosity between 6 to 29%, velocity between 2136 to 5034 m/s, volume of shale between 0 to 49% and water saturation between 9 to 27%. The inversion model was validated for density and porosity values by comparing the log derived observed value with the modelled derived values. The correlation coefficient 'r' was 0.90 for density and 0.89 for porosity with well log-based rock physics model. Based on the analysis, it was observed that prospective exploration potential exists in the northwestern region of the study area due to the increasing thickness as well as reservoir quality of the hydrocarbon-bearing zone. However, incorporating the effect of structural geology in the present study may further help to facilitate the presence of exploration opportunities in the northwestern part of the study area.
- Laboratory-based trends between velocity, density and porosity, obtained by investigation on sandstone core plugs of the same basin were utilised and applied on acoustic impedance obtained through inversion analysis. The velocity obtained from the laboratory-derived rock physics model was transformed to acoustic impedance by using neural network derived density and thereafter trained with the modelled well log to generate density and porosity across the seismic section. On using laboratory-derived rock physics model, the different parameters varied as: density between 2.23 to 2.73 g/cc and porosity between 7 to 27%. These generated density and porosity models were compared with well log derived density and porosity values. The correlation coefficient 'r' obtained for density in Barail is 0.78 and Sylhet formation is 0.95, while for porosity in Barail is 0.91 and Sylhet formation is 0.94. These modelled parameters are derived by the integration of laboratory and well-modelled components.

## 7.2 Limitations of the present work

The limitations of the work done are as follows:

- $V_p$ measurements were conducted in the laboratory under ambient conditions.
- $V_p$ measurements were conducted for a particular frequency transducer.

## 7.3 Recommendations for future work

The future scope of the work is as follows:

- Addition of shear wave velocity information
  - Aid in fluid identification
  - Estimation of geomechanical properties of rocks on the basis of $V_p$/Vs ratio
- Comparative Vp data analysis for a number of frequencies ranging from 54 kHz to 1 MHz
- Vp measurements under stressed conditions
- Implementation and comparison of other seismic inversion techniques
- Role of faults in hydrocarbon entrapment
- Applicability of Rock Physics in Unconventional Reservoirs

## List of Publications

## Research articles published from this thesis work

- **Garia, S.**, Pal, A. K., Ravi, K., & Nair, A. M. (2019). A comprehensive analysis on the relationships between elastic wave velocities and petrophysical properties of sedimentary rocks based on laboratory measurements. **Journal of Petroleum Exploration and Production Technology, SPRINGER**, 9(3), 1869-1881. https://doi.org/10.1007/s13202-019-0675-0
- **Garia, S.**, Pal, A. K., Nair, A. M., & Ravi, K. (2020). Elastic wave velocities as indicators of lithology-based geomechanical behaviour of sedimentary rocks: an overview. **SN Applied Sciences, SPRINGER**, 2(9), 1-21. https://doi.org/10.1007/s42452-020-03300-1
- **Garia, S.**, Pal, A. K., Ravi, K., & Nair, A. M. (2021). Laboratory assessment on factors controlling the acoustic properties of carbonates: A case study from Bombay offshore. **Journal of Petroleum Science and Engineering, ELSEVIER**, 203, 108607. https://doi.org/10.1016/j.petrol.2021.108607
- **Garia, S.**, Pal, A. K., Ravi, K., & Nair, A. M. (2022). A multivariate statistical approach in correlating the acoustic properties with petrophysics and mineralogy on sandstones. **Geophysical Journal International, OXFORD University Press,** ggac061. https://doi.org/10.1093/gji/ggac061
- Pal, A. K., **Garia, S.**, Ravi, K., & Nair, A. M. (2022). Pore scale image analysis for petrophysical modelling. **Micron**, **ELSEVIER,** *154*, 103195. https://doi.org/10.1016/j.micron.2021.103195
- Pal A. K., **Garia S.**, Ravi K., Nair A. M. (2018). Porosity Estimation by Digital Image Analysis. **ONGC Bulletin**, 53(2), 59.

## Research articles to-be-submitted from this thesis work

- **Garia**, **S.**, Pal, A. K., Devi, A.B., Ravi, K., & Nair, A. M. Fabrication, Optimization and Development of an in-house Helium gas Porosimeter (to be submitted)
- **Garia, S.**, Pal, A. K., Ravi, K., & Nair, A. M. Integrating Well and Seismic Data for Reservoir Characterisation: A Study from an oil field in Upper Assam basin, India (to be submitted)

- **Garia, S**., Pal, A. K., Ravi, K., & Nair, A. M. Application of laboratory derived rock physics model for property estimation using inversion in Upper Assam basin (to be submitted)

## Conferences from this thesis work

- Investigating Relationship of Acoustic Properties with Petrophysical Properties of Carbonates: From Nanoscale to Laboratory." **AGU Fall Meeting 2019**. AGU, 2019.
- Calibration and standardization of in house fabricated Helium Gas Porosimeter – **NCUPE 2019** (National Conference on Upstream Petroleum Engineering 2019).
- Ultrasonic p-wave velocity measurement of sedimentary rocks in lab and its dependency on different parameters by using multivariate regression analysis – **7ICRAGEE 2020** (7th International Conference on Recent Advances in Geotechnical Earthquake Engineering and Soil Dynamics)
- Prediction of Petrophysical Properties from Seismic Inversion and Neural Network: A case study. In **EGU General Assembly** Conference Abstracts (pp. EGU21-11824)

## Book Chapters from this thesis work

- Ultrasonic p-wave velocity measurement of sedimentary rocks in lab and its dependency on different parameters by using multivariate regression analysis. In: Sitharam T.G., Kolathayar S., Sharma M.L. (eds) Seismic Hazards and Risk. **Lecture Notes in Civil Engineering**, vol 116. **Springer**, Singapore.

## References


Abdulaziz, A. M., Mahdi, H. A., & Sayyouh, M. H. (2019). Prediction of reservoir quality using well logs and seismic attributes analysis with an artificial neural network: A case study from Farrud Reservoir, Al-Ghani Field, Libya. Journal of Applied Geophysics, 161, 239-254.

Abouelresh, M. O. (2017). An integrated characterization of the porosity in Qusaiba Shale, Saudi Arabia. Journal of Petroleum Science and Engineering, 149, 75-87.

Acharyya, R., & Dey, A. (2019). Assessment of bearing capacity for strip footing located near sloping surface considering ANN model. Neural Computing and Applications, 31(11), 8087-8100.

Al-Dousari, M., Garrouch, A. A., & Al-Omair, O. (2016). Investigating the dependence of shear wave velocity on petrophysical parameters. Journal of Petroleum Science and Engineering, 146, 286-296.

Aleardi M (2018). Estimating petrophysical reservoir properties through extended elastic impedance inversion: applications to off-shore and on-shore reflection seismic data. Journal of Geophysics and Engineering, 15(5), 2079-2090.

Ali, A., Alves, T. M., Saad, F. A., Ullah, M., Toqeer, M., & Hussain, M. (2018). Resource potential of gas reservoirs in South Pakistan and adjacent Indian subcontinent revealed by post-stack inversion techniques. Journal of Natural Gas Science and Engineering, 49, 41-55.

Ali, M., Ma, H., Pan, H., Ashraf, U., & Jiang, R. (2020). Building a rock physics model for the formation evaluation of the Lower Goru sand reservoir of the Southern Indus Basin in Pakistan. Journal of Petroleum Science and Engineering, 194, 107461.

Al-Thyabat, S., & Miles, N. J. (2006). An improved estimation of size distribution from particle profile measurements. Powder Technology, 166(3), 152-160.

Amann-Hildenbrand, A., Bertier, P., Busch, A., & Krooss, B. M. (2013). Experimental investigation of the sealing capacity of generic clay-rich caprocks. International Journal of Greenhouse Gas Control, 19, 620-641.

Amann-Hildenbrand, A., Ghanizadeh, A., & Krooss, B. M. (2012). Transport properties of unconventional gas systems. Marine and Petroleum Geology, 31(1), 90-99.

Ambati, V., Sharma, S., Babu, M. N., & Nair, R. R. (2021). Laboratory measurements of ultrasonic wave velocities of rock samples and their relation to log data: A case study from Mumbai offshore. Journal of Earth System Science, 130(3), 1-18.

Anovitz, L. M., & Cole, D. R. (2015). Characterization and analysis of porosity and pore structures. Reviews in Mineralogy and geochemistry, 80(1), 61-164.

Ansari, H. R. (2014). Use seismic colored inversion and power law committee machine based on imperial competitive algorithm for improving porosity prediction in a heterogeneous reservoir. Journal of Applied Geophysics, 108, 61-68.

Anselmetti, F. S., & Eberli, G. P. (1993). Controls on sonic velocity in carbonates. Pure and Applied geophysics, 141(2-4), 287-323.

Anyiam, O. A., Mode, A. W., & Okara, E. S. (2018). The use of cross-plots in lithology delineation and petrophysical evaluation of some wells in the western Coastal Swamp, Niger Delta. Journal of Petroleum Exploration and Production Technology, 8(1), 61-71.

Archie, G. E. (1942). The electrical resistivity log as an aid in determining some reservoir characteristics. Transactions of the AIME, 146(01), 54-62.

Archilha, N. L., Missagia, R. M., Hollis, C., de Ceia, M. A., McDonald, S. A., Neto, I. A. L., ... & Lee, P. (2015, October). 3D experimental investigation of velocity-permeability controlling factors in carbonates rocks. In 2015 SEG Annual Meeting. OnePetro.

Assefa, S., McCann, C. and Sothcott, J., 2003. Velocities of compressional and shear waves in limestones. Geophysical prospecting, 51(1), pp.1-13.

ASTM D 2845-08, (2005). Standard test method for laboratory determination of pulse velocities and ultrasonic elastic constants of rock,

ASTM D 5731-08, (2008). Standard test method for determination of the point load strength index of rock and application to rock strength classifications,

ASTM D 7012-10, (2010). Standard test method for compressive strength and elastic moduli of intact rock core specimens under varying states of stress and temperatures,

Avseth, P., Mukerji, T. and Mavko, G. (2010). Quantitative seismic interpretation: Applying rock physics tools to reduce interpretation risk. Cambridge university press.

Aziz, I. A., Jaafar, J., & Gilal, A. R. (2017). The Study of OpenDtect Seismic Data Interpretation and Visualization Package in Relation to Seismic Interpretation and Visualization Models. IJCSNS, 17(10), 124.

Babasafari, A. A., Rezaei, S., Salim, A. M. A., Kazemeini, S. H., & Ghosh, D. P. (2021). Petrophysical seismic inversion based on lithofacies classification to enhance reservoir properties estimation: a machine learning approach. Journal of Petroleum Exploration and Production, 11(2), 673-684.

Bachrach, R. (2006). Joint estimation of porosity and saturation using stochastic rock-physics modelling. Geophysics, 71(5), pp.O53-O63.

Baechle, G. T., Eberli, G. P., Weger, R. J., & Massaferro, J. L. (2009). Changes in dynamic shear moduli of carbonate rocks with fluid substitution. Geophysics, 74(3), E135-E147.

Baechle, G. T., Weger, R. J., Eberli, G. P., Massaferro, J. L., & Sun, Y. F. (2005). Changes of shear moduli in carbonate rocks: Implications for Gassmann applicability. The Leading Edge, 24(5), 507-510.

Bakke S, Øren PE (1997). 3-D pore-scale modelling of sandstones and flow simulations in the pore networks. Spe Journal, 2(02), 136-149.

Balan, B., Mohaghegh, S., & Ameri, S. (1995, September). State-of-the-art in permeability determination from well log data: Part 1-A comparative study, model development. In SPE Eastern Regional Meeting. Society of Petroleum Engineers.

Bastia, R. (2006). An overview of Indian sedimentary basins with special focus on emerging east coast deepwater frontiers. The Leading Edge, 25(7), 818-829.

Basu, D. N., Banerjee, A., & Tamhane, D. M. (1980). Source areas and migration trends of oil and gas in Bombay offshore basin, India. AAPG Bulletin, 64(2), 209-220.

Basu, D. N., Banerjee, A., & Tamhane, D. M. (1982). Facies distribution and petroleum geology of the Bombay offshore basin, India. Journal of Petroleum Geology, 5(1), 51-75.

Bateman, R. M. (1985). Open-hole log analysis and formation evaluation: International Human Resources Development Corporation. Boston, MA, 647.

Beeson, C. M. (1950). The Kobe porosimeter and the oil well research porosimeter. Journal of Petroleum Technology, 2(11), 313-318.

Bell, F.G. (1978). The physical and mechanical properties of the fell sandstones, Northumberland, England. Engineering Geology, 12, pp.1-29.

Berryman, J. G. (1995). Mixture theories for rock properties. Rock physics and phase relations: A handbook of physical constants, 3, 205-228.

Bharali, B. and Borgohain, P. (2013). Few characteristics of tipam sandstone formation within oilfield areas of upper assam–a study based on wireline log data. J. Earth Sci, pp.36-45.

Bjørlykke, K. (2014). Relationships between depositional environments, burial history and rock properties. Some principal aspects of diagenetic process in sedimentary basins. Sedimentary Geology, 301, 1-14.

Bjørlykke, K., & Jahren, J. (2010). Sandstones and sandstone reservoirs. In Petroleum geoscience (pp. 113-140). Springer, Berlin, Heidelberg.

Bosch, M. (2004). The optimization approach to lithological tomography: Combining seismic data and petrophysics for porosity prediction. Geophysics, 69(5), 1272-1282.

Bredesen, K. (2012). Use of inverse rock physics modeling in reservoir characterization (Master's thesis, The University of Bergen).

Broadhead, M. K., & Tonellot, T. L. (2010). Sparse seismic deconvolution by method of orthogonal matching pursuit. EAGE Expanded Abstracts.

Brocher, T. M. (2005). Empirical relations between elastic wavespeeds and density in the Earth's crust. Bulletin of the seismological Society of America, 95(6), 2081-2092.

Brotons, V., Tomas, R., Ivorra, S., Grediaga, A.,Martınez, J., Benavente, D., Gomez, M. (2016). Improved correlation between the static and dynamic elastic modulus of different types of rocks, Materials and structures, 49:3021-3037.

Brown, A. R. (2011). Interpretation of Three-Dimensional Seismic Data: AAPG Memoir 42, /SEG Investigation in Geophysics, No. 9 (Vol. 42). AAPG.

Burchette, T. P. (2012). Carbonate rocks and petroleum reservoirs: a geological perspective from the industry. Geological Society, London, Special Publications, 370(1), 17-37.

Campbell, T. J., Richards, F. B., Silva, R. L., Wach, G., & Eliuk, L. (2015). Interpretation of the Penobscot 3D seismic volume using constrained sparse spike inversion, Sable sub-Basin, offshore Nova Scotia. Marine and Petroleum Geology, 68, 73-93.

Castagna, P., Batzle, M.L., and Eastwood, R.L. (1985). Relationships between compressional-wave and shear-wave velocities in clastic silicate rocks, Geophysics, 50(4): 571–581.

Chaki, S., Takarli, M., Agbodjan, W.P., (2008). Influence of thermal damage on physical properties of a granite rock: Porosity, permeability and ultrasonic wave evolutions, Construction and Building materials, 22, 1456–1461.

Chandrasekhar, E., & Rao, V. E. (2012). Wavelet analysis of geophysical well-log data of Bombay offshore basin, India. Mathematical Geosciences, 44(8), 901-928.

Chang, C., Zoback, M.D., and Khaksar, A. (2006). Empirical relations between rock strength and physical properties in sedimentary rocks, J. Petrol. Sci. Eng. 51, 223–237.

Chen, X., & Xu, Z. (2017). The ultrasonic P-wave velocity-stress relationship of rocks and its application. Bulletin of Engineering Geology and the Environment, 76(2), 661-669.

Choquette, P. W., & Pray, L. C. (1970). Geologic nomenclature and classification of porosity in sedimentary carbonates. AAPG bulletin, 54(2), 207-250.

Çobanoğlu, İ., & Çelik, S. B. (2008). Estimation of uniaxial compressive strength from point load strength, Schmidt hardness and P-wave velocity. Bulletin of Engineering Geology and the Environment, 67(4), 491-498.

Cooke, D., & Cant, J. (2010). Model-based seismic inversion: Comparing deterministic and probabilistic approaches. CSEG Recorder, 35(4), 29-39.

Crain, E. R. (2002). Crain's petrophysical handbook. Spectrum 2000 Mindware Limited.

D'Andrea, D. V., Fischer, R. L., & Fogelson, D. E. (1965). Prediction of compressive strength from other rock properties (Vol. 6702). US Department of the Interior, Bureau of Mines.

Darling, T. (2005). Well logging and formation evaluation. Elsevier.

de Ceia, M. A., Misságia, R. M., Neto, I. L., & Archilha, N. (2015). Relationship between the consolidation parameter, porosity and aspect ratio in microporous carbonate rocks. Journal of Applied Geophysics, 122, 111-121.

de Oliveira, G. L. P., Ceia, M. A., Missagia, R. M., Archilha, N. L., Figueiredo, L., Santos, V. H., & Neto, I. L. (2016). Pore volume compressibilities of sandstones and carbonates from Helium porosimetry measurements. Journal of Petroleum Science and Engineering, 137, 185-201.

Deb, S. S., & Barua, I. (2016, March). Depositional environment, reservoir characteristics and extent of sediments of Langpar and Lakadong+ Therria in Chabua area of upper Assam basin. In 8th Biennial international conference and exposition on petroleum geophysics, Hyderabad, India: P-177 https://www. spgin dia. org/2010/177. pdf. Accessed (Vol. 14).

Dentith, M., Enkin, R.J., Morris, W., Adams, C. and Bourne, B. (2020). Petrophysics and mineral exploration: a workflow for data analysis and a new interpretation framework. Geophysical Prospecting, 68(1-Cost- Effective and Innovative Mineral Exploration Solutions), pp.178-199.

Desbois, G., Urai, J. L., Kukla, P. A., Konstanty, J., Baerle, C. (2011). High-resolution 3D fabric and porosity model in a tight gas sandstone reservoir: A new approach to investigate microstructures from mm-to nm-scale combining argon beam cross-sectioning and SEM imaging. Journal of Petroleum Science and Engineering, 78(2), 243-257.

Domenico, S. N. (1984). Rock lithology and porosity determination from shear and compressional wave velocity. Geophysics, 49(8), 1188–1195.

Dotson, B. J., Slobod, R. L., McCreery, P. N., Spurlock, J. W. (1951). Porosity-measurement comparisons by five laboratories. Journal of Petroleum Technology, 3(12), 341-346.

Du, Q., Yasin, Q., Ismail, A., & Sohail, G. M. (2019). Combining classification and regression for improving shear wave velocity estimation from well logs data. Journal of Petroleum Science and Engineering, 182, 106260.

Dubey, A. K. (2012). Reservoir characterization using AVO and seismic inversion techniques. In The 9th Biennial International Conference & Exposition on Petroleum.

Dunn, M. L., & Ledbetter, H. (1995). Poisson's ratio of porous and microcracked solids: theory and application to oxide superconductors. Journal of materials research, 10(11), 2715-2722.

Dvorkin, J., Gutierrez, M. A., & Grana, D. (2014). Seismic reflections of rock properties. Cambridge University Press.

Eberhart-Phillips, D., Han, D. H., Zoback, M. D. (1989). Empirical relationships among seismic velocity, effective pressure, porosity, and clay content in sandstone. Geophysics, 54(1), 82-89.

Eberli, G. P., Baechle, G. T., Anselmetti, F. S., & Incze, M. L. (2003). Factors controlling elastic properties in carbonate sediments and rocks. The Leading Edge, 22(7), 654-660.

Ehrenberg, S. N., & Nadeau, P. H. (2005). Sandstone vs. carbonate petroleum reservoirs: A global perspective on porosity-depth and porosity-permeability relationships. AAPG bulletin, 89(4), 435-445.

El Husseiny, A., & Vanorio, T. (2015). The effect of micrite content on the acoustic velocity of carbonate rocks. Geophysics, 80(4), L45-L55.

El Husseiny, A., & Vanorio, T. (2017). Porosity-permeability relationship in dual-porosity carbonate analogs. Geophysics, 82(1), MR65-MR74.

El Sayed, N. A., Abuseda, H., & Kassab, M. A. (2015). Acoustic wave velocity behaviour for some Jurassic carbonate samples, north Sinai, Egypt. Journal of African Earth Sciences, 111, 14-25.

El-Din, E. S., Mesbah, M. A., Kassab, M. A., Mohamed, I. F., Cheadle, B. A., & Teama, M. A. (2013). Assessment of petrophysical parameters of clastics using well logs: The Upper Miocene in El-Wastani gas field, onshore Nile Delta, Egypt. Petroleum Exploration and Development, 40(4), 488-494.

Entwisle, D. C., Hobbs, P. R. N., Jones, L. D., Gunn, D., and Raines, M. G. (2005). The relationships between effective porosity, uniaxial compressive strength and sonic velocity of intact Borrowdale Volcanic Group core samples from Sellafield, Geotech. Geol. Eng. 23:793–809.

Erryansyah, M., Nainggolan, T. B., & Manik, H. M. (2020). Acoustic impedance model-based inversion to identify target reservoir: a case study Nias Waters. In IOP Conference Series: Earth and Environmental Science (Vol. 429, No. 1, p. 012033). IOP Publishing.

Farouk, S., Sen, S., Ganguli, S. S., Abuseda, H., & Debnath, A. (2021). Petrophysical assessment and permeability modeling utilizing core data and machine learning approaches–A study from the Badr El Din-1 field, Egypt. Marine and Petroleum Geology, 133, 105265.

Fener, M. (2011). The effect of rock sample dimension on the P-wave velocity. Journal of Nondestructive Evaluation, 30(2), 99-105.

Feng, R. (2020). Estimation of reservoir porosity based on seismic inversion results using deep learning methods. Journal of Natural Gas Science and Engineering, 77, 103270.

Feng, R., Luthi, S. M., Gisolf, D., & Angerer, E. (2018). Reservoir lithology classification based on seismic inversion results by hidden Markov models: Applying prior geological information. Marine and Petroleum Geology, 93, 218-229.

Fereidooni, D. (2018). Assessing the effects of mineral content and porosity on ultrasonic wave velocity. Geomechanics and Engineering, 14(4), 399-406.

Fjaer, E., (1999). Static and dynamic moduli of weak sandstone, Rock Mechanics for industry. Balkema, pp. 675-681.

Fjeldstad, T., & Grana, D. (2018). Joint probabilistic petrophysics-seismic inversion based on Gaussian mixture and Markov chain prior models Probabilistic petroelastic prediction. Geophysics, 83(1), R31-R42.

Freyburg, E. (1972). Der Untere und mittlere Buntsandstein SW-Thuringen in seinen gesteinstechnicschen Eigenschaften. Deustche Gesellschaft Geologische Wissenschaften. A; Berlin, 176, 911-919.

Fusi, N., Martinez-Martinez, J. (2013). Mercury porosimetry as a tool for improving quality of micro-CT images in low porosity carbonate rocks. Engineering Geology, 166, 272-282.

Gaboreau, S., Robinet, J. C., Prêt, D. (2016). Optimization of pore-network characterization of a compacted clay material by TEM and FIB/SEM imaging. Microporous and Mesoporous Materials, 224, 116-128.

Gardner, G. H. F., Gardner, L. W. and Gregory, A. R. (1974). Formation velocity and density—The diagnostic basics for stratigraphic traps. Geophysics, 39(6), pp.770-780.

Garia, S., Pal, A. K., Nair, A. M., & Ravi, K. (2020). Elastic wave velocities as indicators of lithology-based geomechanical behaviour of sedimentary rocks: an overview. SN Applied Sciences, 2(9), 1-21.

Garia, S., Pal, A. K., Ravi, K., & Nair, A. M. (2019). A comprehensive analysis on the relationships between elastic wave velocities and petrophysical properties of sedimentary rocks based on laboratory measurements. Journal of Petroleum Exploration and Production Technology, 1-13.

Garia, S., Pal, A. K., Ravi, K., & Nair, A. M. (2021). Laboratory assessment on factors controlling the acoustic properties of carbonates: A case study from Bombay offshore. Journal of Petroleum Science and Engineering, 108607.

Gassmann, F. (1951). Elastic waves through a packing of spheres. Geophysics, 16(4), 673-685.

Gaviglio, P., (1989). Longitudinal waves propagation in a limestone: the relationship between velocity and density, Rock Mech. Rock Engng., 22(4), 29-306.

Gegenhuber, N. (2016). Interpretation of elastic properties for magmatic and metamorphic rock types, International Journal of Rock Mechanics and Mining Sciences, 88, 44–48. Elsevier.

Gercek, H.A. (2007). Poisson's ratio values for rocks, Int. J. Rock Mech. Min. Sci. 44, 1–13.

Ghafoori, M., Rastegarnia, A., & Lashkaripour, G. R. (2018). Estimation of static parameters based on dynamical and physical properties in limestone rocks. Journal of African Earth Sciences, 137, 22-31.

Gogoi, T. and Chatterjee, R. (2018). Neural network analysis and seismic-velocity model building in Upper Assam Basin, India: An aid to reservoir-characterisation study. In SEG Technical Program Expanded Abstracts 2018 (pp. 3161-3165). Society of Exploration Geophysicists.

Gogoi, T. and Chatterjee, R. (2019). Estimation of petrophysical parameters using seismic inversion and neural network modelling in Upper Assam basin, India. Geoscience Frontiers, 10(3), pp.1113-1124.

Gokceoglu, C., & Zorlu, K. (2004). A fuzzy model to predict the uniaxial compressive strength and the modulus of elasticity of a problematic rock. Engineering Applications of Artificial Intelligence, 17(1), 61-72.

González, E. F., Mukerji, T., & Mavko, G. (2008). Seismic inversion combining rock physics and multiple-point geostatistics. Geophysics, 73(1), R11-R21.

Grana, D. (2014). Probabilistic approach to rock physics modeling. Geophysics, 79(2), D123-D143.

Grana, D., & Della Rossa, E. (2010). Probabilistic petrophysical-properties estimation integrating statistical rock physics with seismic inversion. Geophysics, 75(3), O21-O37.

Grana, D., & Della Rossa, E. (2010). Probabilistic petrophysical-properties estimation integrating statistical rock physics with seismic inversion. Geophysics, 75(3), O21-O37.

Greenberg, M.L. and Castagna, J.P. (1992). Shear- wave velocity estimation in porous rocks: theoretical formulation, preliminary verification and applications1. Geophysical prospecting, 40(2), pp.195-209.

Grijalba-Cuenca, A., Torres-Verdin, C., & van der Made, P. (2000, October). Geostatistical inversion of 3D seismic data to extrapolate wireline petrophysical variables laterally away from the well. In SPE Annual Technical Conference and Exhibition. OnePetro.

Grima, M. A., & Babuška, R. (1999). Fuzzy model for the prediction of unconfined compressive strength of rock samples. International Journal of Rock Mechanics and Mining Sciences, 36(3), 339-349.

Guha, D. K. and Pandey, J. (1974). Stratigraphy of Bombay Offshore Region. Special Micropaleontological Reports, ONGC, unpubl.

Gupta, S. D., & Gupta, R. (2017). Importance of coloured inversion technique for thin hydrocarbon sand reservoir detection–A case in mid Cambay basin. Journal of the Geological Society of India, 90(4), 485-494.

Haines, T. J., Neilson, J. E., Healy, D., Michie, E. A., Aplin, A. C. (2015). The impact of carbonate texture on the quantification of total porosity by image analysis. Computers & Geosciences, 85, 112-125.

Hakimi, M. H., Al Qadasi, B. A., Al Sharrabi, Y., Al Sorore, O. T., & Al Samet, N. G. (2017). Petrophysical properties of Cretaceous clastic rocks (Qishn Formation) in the Sharyoof oilfield, onshore Masila Basin, Yemen. Egyptian journal of petroleum, 26(2), 439-455.

Hampson, D. P., Schuelke, J. S., & Quirein, J. A. (2001). Use of multiattribute transforms to predict log properties from seismic data. Geophysics, 66(1), 220-236.

Han, D. H., Nur, A., & Morgan, D. (1986). Effects of porosity and clay content on wave velocities in sandstones. Geophysics, 51(11), 2093-2107.

Haris, A., Sitorus, R. J., & Riyanto, A. (2017, April). Pore pressure prediction using probabilistic neural network: case study of South Sumatra Basin. In IOP Conference Series: Earth and Environmental Science (Vol. 62, No. 1, p. 012021). IOP Publishing.

Heidari, M., Mohseni, H., & Jalali, S. H. (2018). Prediction of uniaxial compressive strength of some sedimentary rocks by fuzzy and regression models. Geotechnical and Geological Engineering, 36(1), 401-412.

Heidari, M., Momeni, A.A. and Naseri, F. (2013). New weathering classifications for granitic rocks based on geomechanical parameters. Engineering geology, 166, pp.65-73.

Hemes, S., Desbois, G., Urai, J. L., Schröppel, B., Schwarz, J. O. (2015). Multi-scale characterization of porosity in Boom Clay (HADES-level, Mol, Belgium) using a combination of X-ray μ-CT, 2D BIB-SEM and FIB-SEM tomography. Microporous and mesoporous materials, 208, 1-20.

Herrera, R. H., & van der Baan, M. (2014). A semiautomatic method to tie well logs to seismic data. Geophysics, 79(3), V47-V54.

Herrera, R. H., Fomel, S., & van der Baan, M. (2014). Automatic approaches for seismic to well tying. Interpretation, 2(2), SD9-SD17.

Herron, D. A. (2014). Tutorial: Tying a well to seismic using a blocked sonic log. Interpretation, 2(2), SD1-SD7.

Huuse, M., & Feary, D. A. (2005). Seismic inversion for acoustic impedance and porosity of Cenozoic cool-water carbonates on the upper continental slope of the Great Australian Bight. Marine Geology, 215(3-4), 123-134.

Igathinathane, C., Melin, S., Sokhansanj, S., Bi, X., Lim, C. J., Pordesimo, L. O., & Columbus, E. P. (2009). Machine vision based particle size and size distribution determination of airborne dust particles of wood and bark pellets. Powder Technology, 196(2), 202-212.

Ishwar, N. B., & Bhardwaj, A. (2013). Petrophysical well log analysis for hydrocarbon exploration in parts of Assam Arakan Basin, India. In 10 th Biennial International Conference and Exposition, Kochi, Kerala, India.

Ismail, A., Ewida, H. F., Al-Ibiary, M. G., & Zollo, A. (2020). Integrated prediction of deep-water gas channels using seismic coloured inversion and spectral decomposition attribute, West offshore, Nile Delta, Egypt. NRIAG Journal of Astronomy and Geophysics, 9(1), 459-470.

ISRM (1977) Suggested Methods for Determining Water Content, Porosity, Density, Absorption and Related Properties and Swelling and Slake-Durability Index Properties, Int. J. Rock Mech. Min. Sci.Geomech. Abstr. 16,141-156.

ISRM (1978) Suggested Method for determining sound velocity, Int. J. Rock Mech. Min. Sci. Geomech. Abstr. 15,53-58.

ISRM (1978) Suggested Method for determining uniaxial compressive strength and deformability of rock materials, Int. J. Rock Mech. Min. Sci. Geomech. 16: 135-140.

ISRM (1981) Rock characterisation testing and monitoring. In: Brown ET (ed) Pergamon press, Oxford, 211pp.

ISRM (1985) Suggested Method for determining point load strength, Int. J. Rock Mech. Min. Sci. 22: 53-60.

Jelavić, S., Nielsen, A. R., Blazanovic, M., Bovet, N., Bechgaard, K., & Stipp, S. L. S. (2018). Effects of Cleaning Treatments on the Surface Composition of Porous Materials. Energy & fuels, 32(4), 4655-4661.

Jennrich R. I. (1995). An introduction to computational statistics regression analysis. Prentice-Hall, Englewood Cliffs, NJ

Ji, S. (2004). A generalized mixture rule for estimating the viscosity of solid- liquid suspensions and mechanical properties of polyphase rocks and composite materials. Journal of Geophysical Research: Solid Earth, 109(B10).

Ji, S., Gu, Q., & Xia, B. (2006). Porosity dependence of mechanical properties of solid materials. Journal of Materials Science, 41(6), 1757-1768.

Ji, S., Li, L., Motra, H. B., Wuttke, F., Sun, S., Michibayashi, K., & Salisbury, M. H. (2018). Poisson's ratio and auxetic properties of natural rocks. Journal of Geophysical Research: Solid Earth, 123(2), 1161-1185.

Ji, S., Sun, S., Wang, Q., & Marcotte, D. (2010). Lamé parameters of common rocks in the Earth's crust and upper mantle. Journal of Geophysical Research: Solid Earth, 115(B6).

Ji, S., Wang, Q., & Xia, B. (2003). P-wave velocities of polymineralic rocks: comparison of theory and experiment and test of elastic mixture rules. Tectonophysics, 366(3-4), 165-185.

Ji, S., Wang, Q., Marcotte, D., Salisbury, M. H., & Xu, Z. (2007). P wave velocities, anisotropy and hysteresis in ultrahigh- pressure metamorphic rocks as a function of confining pressure. Journal of Geophysical Research: Solid Earth, 112(B9).

Ji, S., Wang, Q., Xia, B., & Marcotte, D. (2004). Mechanical properties of multiphase materials and rocks: a phenomenological approach using generalized means. Journal of Structural Geology, 26(8), 1377-1390.

Jiang, R., Liu, C., Zhang, J., Zeng, Q., He, P., Huang, J., Du, B., He, W., Hao, T. and Zhang, J. (2020). Quantitative Reservoir Characterization of Tight Sandstone Using Extended Elastic Impedance. Natural Resources Research, pp.1-15.

Jin, X., Dou, Q., Hou, J., Huang, Q., Sun, Y., Jiang, Y., Li, T., Sun, P., Sullivan, C., Adersokan, H., Zhang, Z. (2017). Rock-physics-model-based pore type characterization and its implication for porosity and permeability qualification in a deeply-buried carbonate reservoir, Changxing formation, Lower Permian, Sichuan Bain, China. Journal of Petroleum Science and Engineering, 153, 223-233.

Johnson, R. A., & Wichern, D. W. (2002). Applied multivariate statistical analysis (Vol. 5, No. 8). Upper Saddle River, NJ: Prentice hall.

Johnston, D. H., & Toksöz, M. N. (1980). Ultrasonic P and S wave attenuation in dry and saturated rocks under pressure. Journal of Geophysical Research: Solid Earth, 85(B2), 925-936.

Johnston, J. E., & Christensen, N. I. (1993, December) Compressional to shear velocity ratios in sedimentary rocks. In International journal of rock mechanics and mining sciences & geomechanics abstracts (Vol. 30, No. 7, pp. 751-754). Pergamon.

Kadkhodaie-Ilkhchi, R., Moussavi-Harami, R., Rezaee, R., Nabi-Bidhendi, M., & Kadkhodaie-Ilkhchi, A. (2014). Seismic inversion and attributes analysis for porosity evaluation of the tight gas sandstones of the Whicher Range field in the Perth Basin, Western Australia. Journal of Natural Gas Science and Engineering, 21, 1073-1083.

Kahraman, S. (2001). A correlation between P-wave velocity, number of joints and Schmidt hammer rebound number. International Journal of Rock Mechanics and Mining Sciences, 38(5), 729-733.

Kahraman, S. (2007). The correlations between the saturated and dry P-wave velocity of rocks, Ultrasonics 46 (4) 341–348.

Kahraman, S., & Yeken, T. (2008). Determination of physical properties of carbonate rocks from P-wave velocity. Bulletin of Engineering Geology and the Environment, 67(2), 277-281.

Karakul, H., & Ulusay, R. (2013). Empirical correlations for predicting strength properties of rocks from P-wave velocity under different degrees of saturation. Rock mechanics and rock engineering, 46(5), 981-999.

Karaman, K., Kaya, A., & Kesimal, A. (2015). Effect of the specimen length on ultrasonic P-wave velocity in some volcanic rocks and limestones. Journal of African Earth Sciences, 112, 142-149.

Kassab, M. A., & Weller, A. (2015). Study on P-wave and S-wave velocity in dry and wet sandstones of Tushka region, Egypt. Egyptian Journal of Petroleum, 24(1), 1-11.

Kelkar, M., Perez, G., & Chopra, A. (2002). Applied geostatistics for reservoir characterisation (p. 264). Richardson, TX: Society of Petroleum Engineers.

Khandelwal, M., & Ranjith, P. G. (2010). Correlating index properties of rocks with P-wave measurements. Journal of Applied Geophysics, 71(1), 1-5.

Kılıç, A., & Teymen, A. (2008). Determination of mechanical properties of rocks using simple methods. Bulletin of Engineering Geology and the Environment, 67(2), 237.

King, M. S. (1970). Static and dynamic moduli of rocks under pressure. In: SOMERTON, W. H. (ed.), Proceedings of the 11th Symposium on Rock Mechanics, California. American Institute of Mining Engineers, New York, 329-351.

Klimentos, T. (1991). The effects of porosity-permeability-clay content on the velocity of compressional waves, Geophysics 56: 1930–1939.

Korte, D., Kaukler, D., Fanetti, M., Cabrera, H., Daubront, E., & Franko, M. (2017). Determination of petrophysical properties of sedimentary rocks by optical methods. Sedimentary Geology, 350, 72-79.

Kuila, U. (2013). Measurement and interpretation of porosity and pore-size distribution in mudrocks: The hole story of shales (Doctoral dissertation, Colorado School of Mines).

Kumar D., Ahmed I. (2011) Seismic Noise. In: Gupta H.K. (eds) Encyclopedia of Solid Earth Geophysics. Encyclopedia of Earth Sciences Series. Springer, Dordrecht. https://doi.org/10.1007/978-90-481-8702-7_146

Kumar, B. R., Vardhan, H., Govindaraj, M., & Vijay, G. S. (2013). Regression analysis and ANN models to predict rock properties from sound levels produced during drilling. International Journal of Rock Mechanics and Mining Sciences, 58, 61-72.

Kumar, M., & Han, D. H. (2005). Pore shape effect on elastic properties of carbonate rocks. In SEG Technical Program Expanded Abstracts 2005 (pp. 1477-1480). Society of Exploration Geophysicists.

Kumar, M., Dasgupta, R., Singha, D. K., & Singh, N. P. (2018). Petrophysical evaluation of well log data and rock physics modeling for characterization of Eocene reservoir in Chandmari oil field of Assam-Arakan basin, India. Journal of Petroleum Exploration and Production Technology, 8(2), 323-340.

Kumar, R., Das, B., Chatterjee, R., & Sain, K. (2016). A methodology of porosity estimation from inversion of post-stack seismic data. Journal of Natural Gas Science and Engineering, 28, 356-364.

Kurtulus C, CakIr S, & Yoğurtcuoğlu A. C. (2016). Ultrasound study of limestone rock physical and mechanical properties. Soil Mechanics and Foundation Engineering, 52(6), 348-354.

Kushwaha, P. K., Maurya, S. P., Rai, P., & Singh, N. P. (2021). Estimation of subsurface rock properties from seismic inversion and geo-statistical methods over F3-block, Netherland. Exploration Geophysics, 52(3), 258-272.

Kuster, G. T., & Toksöz, M. N. (1974). Velocity and attenuation of seismic waves in two-phase media: Part I. Theoretical formulations. Geophysics, 39(5), 587-606.

Kuva, J., Siitari-Kauppi, M., Lindberg, A., Aaltonen, I., Turpeinen, T., Myllys, M., & Timonen, J. (2012). Microstructure, porosity and mineralogy around fractures in Olkiluoto bedrock. Engineering geology, 139, 28-37.

Lancaster, S., & Whitcombe, D. (2000). Fast-track 'coloured'inversion. In SEG Technical Program Expanded Abstracts 2000 (pp. 1572-1575). Society of Exploration Geophysicists.

Leite, E. P., & Vidal, A. C. (2011). 3D porosity prediction from seismic inversion and neural networks. Computers & Geosciences, 37(8), 1174-1180.

Li, S., Dong, M., & Li, Z. (2009). Measurement and revised interpretation of gas flow behavior in tight reservoir cores. Journal of Petroleum Science and Engineering, 65(1-2), 81-88.

Li, Y. and Gu, H., (2015). The relationship between mineral content and acoustic velocity of sandstone reservoirs in Junggar basin. Journal of Geophysics and Engineering, 12(4), pp.629-637.

Ligtenberg, J. H. (2005). Detection of fluid migration pathways in seismic data: implications for fault seal analysis. Basin Research, 17(1), 141-153.

Liu, X, Wang, J., Ge L, Hu, F., Li, C., Li, X., Yu, J., Xu, H., Lu, S., Xue, Q (2017). Pore-scale characterization of tight sandstone in Yanchang Formation Ordos Basin China using micro-CT and SEM imaging from nm-to cm-scale. Fuel, 209, 254-264.

Love, J. C., Estroff, L. A., Kriebel, J. K., Nuzzo, R. G., & Whitesides, G. M. (2005). Self-assembled monolayers of thiolates on metals as a form of nanotechnology. Chemical reviews, 105(4), 1103-1170.

Lucia, F. J. (2007). Carbonate reservoir characterization: An integrated approach. Springer Science & Business Media.

Lumsden, D. N. (1979). Discrepancy between thin-section and X-ray estimates of dolomite in limestone. Journal of Sedimentary Research, 49(2), 429-435.

Madhubabu, N., Singh, P.K., Kainthola, A., Mahanta, B., Tripathy, A., and Singh, T.N. (2016), Prediction of compressive strength and elastic modulus of carbonate rocks. Measurement, 88: 202–213. Elsevier.

Mahgoub, M. I., Padmanabhan, E., & Abdullatif, O. M. (2017). Seismic inversion as a predictive tool for porosity and facies delineation in Paleocene fluvial/lacustrine reservoirs, Melut Basin, Sudan. Marine and Petroleum Geology, 86, 213-227.

Makarynska, D., Gurevich, B., Behura, J. and Batzle, M., 2010. Fluid substitution in rocks saturated with viscoelastic fluids. Geophysics, 75(2), pp.E115-E122.

Mandal, K., & Dasgupta, R. (2013). Upper Assam basin and its basinal depositional history. In SPG 10th Biennial international conference and exposition, Kochi, India.

Mandal, K.L., Chakraborty, S. and Dasgupta, R. (2011). Regional velocity trend in Upper Assam Basin and its relations with basinal depositional history. In SEG Technical Program Expanded Abstracts 2011 (pp. 1222-1226). Society of Exploration Geophysicists.

Mathur, N. (2014). Tertiary oils from Upper Assam Basin, India: A geochemical study using terrigenous biomarkers. Organic geochemistry, 76, 9-25.

Matthiesen, J., Bovet, N., Hilner, E., Andersson, M. P., Schmidt, D. A., Webb, K. J., and Stipp, S. L. S. (2014). How naturally adsorbed material on minerals affects low salinity enhanced oil recovery. Energy & Fuels, 28(8), 4849-4858.

Matthiesen, J., Hassenkam, T., Bovet, N., Dalby, K. N., & Stipp, S. L. S. (2017). Adsorbed organic material and its control on wettability. Energy & Fuels, 31(1), 55-64.

Maurya, S. P., & Singh, K. H. (2019). Predicting porosity by multivariate regression and probabilistic neural network using model-based and coloured inversion as external attributes: a quantitative comparison. Journal of the Geological Society of India, 93(2), 207-212.

Maurya, S. P., & Singh, N. P. (2018). Comparing pre-and post-stack seismic inversion methods-a case study from Scotian Shelf, Canada. J Ind Geophys Union, 22(6), 585-597.

Maurya, S. P., Singh, N. P., & Singh, K. H. (2020). Seismic Inversion Methods: A Practical Approach. Springer.

Mavko, G., & Mukerji, T. (1998). Bounds on low-frequency seismic velocities in partially saturated rocks. Geophysics, 63(3), 918-924.

Mavko, G., Mukerji, T., & Dvorkin, J. (2009). The rock physics handbook: Tools for seismic analysis of porous media. Cambridge university press.

Mazzoli, A., & Favoni, O. (2012). Particle size, size distribution and morphological evaluation of airborne dust particles of diverse woods by scanning electron microscopy and image processing program. Powder Technology, 225, 65-71.

McCann, D. M., Culshaw, M. G., & Northmore, K. J. (1990). Rock mass assessment from seismic measurements. Geological Society, London, Engineering Geology Special Publications, 6(1), 257-266.

McDowell, P.W., and Millett, N. (1984). Surface ultrasonic measurement of longitudinal and transverse wave velocities through rock samples, Int. J. Rock Mech. Min. Sci. Geomech. Abstr. 21:223-227.

Meldahl, P., Heggland, R., Bril, B., & de Groot, P. (2001). Identifying faults and gas chimneys using multiattributes and neural networks. The leading edge, 20(5), 474-482.

Mirkamali, M. S., Keshavarz Fk, N., & Bakhtiari, M. R. (2013). Fault zone identification in the eastern part of the Persian Gulf based on combined seismic attributes. Journal of Geophysics and Engineering, 10(1), 015007.

Mirkamali, M.S., Javaherian, A., Hassani, H., Saberi, M.R. and Hosseini, S.A. (2020). Quantitative pore- type characterisation from well logs based on the seismic petrophysics in a carbonate reservoir. Geophysical Prospecting, 68(7), pp.2195-2216.

Misaghi, A., Negahban, S., Landrø, M., & Javaherian, A. (2010). A comparison of rock physics models for fluid substitution in carbonate rocks. Exploration Geophysics, 41(2), 146-154.

Mishra, D. A., & Basu, A. (2013). Estimation of uniaxial compressive strength of rock materials by index tests using regression analysis and fuzzy inference system. Engineering Geology, 160, 54-68.

Mishra, H. K., & Ghosh, R. K. (1996). Geology, petrology and utilisation potential of some Tertiary coals of the northeastern region of India. International Journal of Coal Geology, 30(1-2), 65-100.

Misra, S., Chopra, S., & Zhang, J. (2010). Neural network regression analysis and post-stack inversion-A comparison. In SEG Technical Program Expanded Abstracts 2010 (pp. 1473-1477). Society of Exploration Geophysicists.

Mohan, M. (1978). Biostratigraphy, biofacies, paleo-ecology and geological evolution of the Bombay Offshore basin. ONGC, unpubl.

Mohan, M. (1985). Geohistory analysis of Bombay High region. Marine and petroleum geology, 2(4), 350-360.

Monjezi, M., Khoshalan, H. A., & Razifard, M. (2012). A neuro-genetic network for predicting uniaxial compressive strength of rocks. Geotechnical and Geological Engineering, 30(4), 1053-1062.

Montgomery, D. C., Peck, E. A., & Vining, G. G. (2012). Introduction to linear regression analysis (Vol. 821). John Wiley & Sons.

Moore, C. H., & Wade, W. J. (2013). Carbonate reservoirs: Porosity and diagenesis in a sequence stratigraphic framework. Newnes.

Moos, A.V., & De Quervain, F. (1948). Technishe Gesteinkunde (in German), Verlag Birkhauser, Basel

Moos, D., Zoback, M. D., & Bailey, L. (2001). Feasibility study of the stability of openhole multilaterals, Cook Inlet, Alaska. SPE Drilling & Completion, 16(03), 140-145.

Moradian, Z.A., and Behnia, M. (2009). Predicting the Uniaxial Compressive Strength and Static Young's Modulus of Intact Sedimentary Rocks Using the ultrasonic test, Int. J. Geomech. 9 (1(14)).

Mousavi, M. A., Prodanovic, M., & Jacobi, D. (2012). New classification of carbonate rocks for process-based pore-scale modeling. SPE Journal, 18(02), 243-263.

Mueller, H.J. (2013). Measuring the elastic properties of natural rocks and mineral assemblages under Earth's deep crustal and mantle conditions. Journal of Geodynamics, 71: 25–42. Elsevier

Mukerji, T., Avseth, P., Mavko, G., Takahashi, I., & González, E. F. (2001). Statistical rock physics: Combining rock physics, information theory, and geostatistics to reduce uncertainty in seismic reservoir characterization. The Leading Edge, 20(3), 313-319.

Murty, K. N. (1984). Geology and hydrocarbon prospects of Assam Shelf-Recent advances and present status. Pet. Asia J.;(India), 6(4).

Nabawy, B.S. and Barakat, M.K., (2017). Formation evaluation using conventional and special core analyses: Belayim Formation as a case study, Gulf of Suez, Egypt. Arabian Journal of Geosciences, 10(2), pp.1-23.

Nabawy, B.S. and David, C., (2016). X-Ray CT scanning imaging for the Nubia sandstone as a tool for characterising its capillary properties. Geosciences Journal, 20(5), pp.691-704.

Nabawy, B.S., Sediek, K.N. and Nafee, S.A. (2015). Pore fabric assignment using electrical conductivity of some Albian–Cenomanian sequences in north Eastern Desert, Egypt. Arabian Journal of Geosciences, 8(8), pp.5601-5615.

Narongsirikul, S., Mondol, N.H. and Jahren, J. (2019). Acoustic and petrophysical properties of mechanically compacted overconsolidated sands: Part 2–Rock physics modelling and applications. Geophysical Prospecting, 67(1), pp.114-127.

Nefeslioglu, H. A. (2013). Evaluation of geo-mechanical properties of very weak and weak rock materials by using non-destructive techniques: Ultrasonic pulse velocity measurements and reflectance spectroscopy. Engineering geology, 160, 8-20.

Nikolakopoulos, K., Lampropoulou, P., Papoulis, D., Rogkala, A., Giannakopoulou, P., & Petrounias, P. (2018). Combined use of remote sensing data, mineralogical analyses, microstructure studies and geographic information system for geological mapping of Antiparos Island (Greece). Geosciences, 8(3), 96.

Nur, A., & Simmons, G. (1969). Stress- induced velocity anisotropy in rock: An experimental study. Journal of Geophysical Research, 74(27), 6667-6674.

Ødegaard, E. R. I. K., and Avseth, P. (2003, June). Interpretation of elastic inversion results using rock physics templates. In 65th EAGE Conference & Exhibition (pp. cp-6). European Association of Geoscientists & Engineers.

Oliver, D. S., Reynolds, A. C., & Liu, N. (2008). Inverse theory for petroleum reservoir characterization and history matching.

Onajite, E. (2021). Seismic petrophysics and petrophysical well curves analysis for quantitative seismic interpretation. Applied Techniques to Integrated Oil and Gas Reservoir Characterization: A Problem-Solution Discussion with Experts, 233.

Pahari, S., Singh, H., Prasad, I.V.S.V. and Singh, R.R. (2008). Petroleum systems of upper Assam Shelf, India. Society of Petroleum Geophysicist, India. Geo-Horizons, pp.14-21.

Pal, A. K., Garia, S., Ravi, K., & Nair, A. M. (2018). Porosity Estimation by Digital Image Analysis. ONGC Bulletin, 53(2), 59.

Pal, A. K., Garia, S., Ravi, K., & Nair, A. M. (2020). Influence of Packing of Grain Particles on Porosity. In Geotechnical Characterization and Modelling (pp. 991-996). Springer, Singapore.

Panizza, G. and Ravazzoli, C., (2019). An efficient rock-physics workflow for modelling and inversion in anisotropic organic-shales. Journal of Petroleum Science and Engineering, 180, pp.1101-1111.

Pappalardo, G., (2015), Correlation Between P-Wave Velocity and Physical–Mechanical Properties of Intensely Jointed Dolostones, Peloritani Mounts, NE Sicily, Rock Mech. Rock Eng., 48: 1711–1721.

Parent, T., Domede, N., Sellier, A., and Mouatt, L. (2015), Mechanical characterization of limestone from sound velocity measurement, International Journal of Rock Mechanics & Mining Sciences. 79: 149–156.

Payne, M. A., Zelewski, G., Huang, X., Liu, E., Xu, S., Toms, J., ... & Martinez, A. (2009, January). Carbonate Reservoir Characterization: Bridging the Gap Between Core and Seismic. In International Petroleum Technology Conference. International Petroleum Technology Conference.

Payne, S. S., Wild, P., & Lubbe, R. (2010). An integrated solution to rock physics modelling in fractured carbonate reservoirs. In SEG Technical Program Expanded Abstracts 2010 (pp. 358-362). Society of Exploration Geophysicists.

Perras, M. A., & Diederichs, M. S. (2014). A review of the tensile strength of rock: concepts and testing. Geotechnical and geological engineering, 32(2), 525-546.

Phan, S. D., Gogoi, T., Chatterjee, R., & Sen, M. K. (2022). Predicting porosity, water saturation, and shale volume with high-resolution seismic inversion using Hopfield network: Upper Assam Basin, India. AAPG Bulletin, 106(1), 103-118.

Pramanik, A. G., Singh, V., Vig, R., Srivastava, A. K., & Tiwary, D. N. (2004). Estimation of effective porosity using geostatistics and multiattribute transforms: A case study. Geophysics, 69(2), 352-372.

Přikryl, R. (2006). Assessment of rock geomechanical quality by quantitative rock fabric coefficients: limitations and possible source of misinterpretations. Engineering Geology, 87(3-4), pp.149-162.

R Core Team (2013). R: A language and environment for statistical computing. R Foundation for Statistical Computing, Vienna, Austria.

Rafik, B., & Kamel, B. (2017). Prediction of permeability and porosity from well log data using the nonparametric regression with multivariate analysis and neural network, Hassi R'Mel Field, Algeria. Egyptian journal of petroleum, 26(3), 763-778.

Rai, N., Singha, D. K., & Chatterjee, R. (2021). Assessment of Paleocene to lower Oligocene formations and basement to estimate the potential hydrocarbon reservoirs using seismic inversion: a case study in the Upper Assam Shelf, India. Journal of Petroleum Exploration and Production Technology, 1-17.

Raju, A. T. R. (1968). Geological evolution of Assam and Cambay Tertiary basins of India. AAPG Bulletin, 52(12), 2422-2437.

Raju, S. V., & Mathur, N. (1995). Petroleum geochemistry of a part of Upper Assam Basin, India: a brief overview. Organic Geochemistry, 23(1), 55-70.

Rao R. P., Talukdar SN (1980). Petroleum geology of Bombay high field, India. 487-506.

Regnet, J. B., Robion, P., David, C., Fortin, J., Brigaud, B., & Yven, B. (2015). Acoustic and reservoir properties of microporous carbonate rocks: Implication of micrite particle size and morphology. Journal of Geophysical Research: Solid Earth, 120(2), 790-811.

Roy, A., & Chatterjee, R. (2020). Lithology Identification Using Lithology Impedance in Mumbai Offshore. In Petro-physics and Rock Physics of Carbonate Reservoirs (pp. 105-113). Springer, Singapore.

Russell, B.H. (2004). The application of multivariate statistics and neural networks to the prediction of reservoir parameters using seismic attributes. Ph.D. Dissertation. University of Calgary, Alberta. 392pp.

Sander, R., Pan, Z., & Connell, L. D. (2017). Laboratory measurement of low permeability unconventional gas reservoir rocks: A review of experimental methods. Journal of Natural Gas Science and Engineering, 37, 248-279.

Sang*, L. and Sun, Y. (2014). Rock physics modelling of clay-bearing formations: The pore structure effect. In SEG Technical Program Expanded Abstracts 2014 (pp. 2845-2849). Society of Exploration Geophysicists.

Sarkar, K., Vishal, V., Singh, T. N., (2012), An Empirical Correlation of Index Geomechanical Parameters with the Compressional Wave Velocity, Geotech. Geol. Eng., 30: 469–479.

Sayers, C. M. (2008). The elastic properties of carbonates. The Leading Edge, 27 (8), 1020-1024.

Sayers, C., & Chopra, S. (2009). Introduction to this special section: Seismic modeling. The Leading Edge, 28(5), 528-529.

Schön, J. H. (2015). Physical properties of rocks: Fundamentals and principles of petrophysics (Vol. 65). Elsevier.

Seif, E. S. S. A., (2016). Evaluation of geotechnical properties of Cretaceous sandstone, Western Desert, Egypt. Arabian Journal of Geosciences, 9(4), p.299.

Seyyedattar, M., Zendehboudi, S. and Butt, S. (2020). Technical and non-technical challenges of development of offshore petroleum reservoirs: Characterisation and production. Natural Resources Research, 29(3), pp.2147-2189.

Shahri, A.A., Gheirati, A., and Espersson, M. (2014). Prediction of Rock Mechanical Parameters as a Function of P-Wave Velocity, Int. Res. J. Earth Sci. 2(9): 7–14.

Shakoor, A. and Bonelli, R.E. (1991). Relationship between petrographic characteristics, engineering index properties and mechanical properties of selected sandstones. Bulletin of the Association of Engineering Geolologists, 28: 55-71.

Sharma, M., Singh, K. H., Pandit, S., Kumar, A., & Soni, A. (2020). Petrophysical Modelling of Carbonate Reservoir from Bombay Offshore Basin. In Petro-physics and Rock Physics of Carbonate Reservoirs (pp. 55-69). Springer, Singapore.

Sharma, P. K., Singh, T. N., (2008), A correlation between P-wave velocity, impact strength index, slake durability index and uniaxial compressive strength, Bull Eng.Geol. Envirol., 67:17–22.

Shen, W. J., Wan, J. M., Kim, Y., & Li, X. Z. (2015). Porosity calculation, pore size distribution and mineral analysis within shale rocks: Application of scanning electron microscopy. Electron. J. Geotech. Eng, 20, 11477-11490.

Simm, R., Bacon, M., & Bacon, M. (2014). Seismic Amplitude: An interpreter's handbook. Cambridge University Press.

Simmons, G. (1965). Single crystal elastic constants and calculated aggregate properties. Southern Methodist Univ Dallas Tex.

Sing, K. S. (1985). Reporting physisorption data for gas/solid systems with special reference to the determination of surface area and porosity (Recommendations 1984). Pure and applied chemistry, 57(4), 603-619.

Singh, T. N., Verma, A. K., Singh, V., & Sahu, A. (2005). Slake durability study of shaly rock and its predictions. Environmental Geology, 47(2), 246-253.

Singh, Y., Nair, R. R., Singh, H., Datta, P., Jaiswal, P., Dewangan, P., & Ramaprasad, T. (2016). Prediction of gas hydrate saturation throughout the seismic section in Krishna Godavari basin using multivariate linear regression and multi-layer feed forward neural network approach. Arabian Journal of Geosciences, 9(5), 415.

Soroush, H., Qutob, H., Oil, W., and Me, T. (2011), Evaluation of rock properties using ultrasonic pulse technique and correlating static to dynamic elastic constants. 2nd south Asian geoscience conference and exhibition, GEOIndia 2011, Greater Noida, New Delhi, India.

Stipp, S.L. and Hochella Jr, M.F., 1991. Structure and bonding environments at the calcite surface as observed with X-ray photoelectron spectroscopy (XPS) and low energy electron diffraction (LEED). Geochimica et Cosmochimica Acta, 55(6), pp.1723-1736.

Suicmez, V. S., & Touati, M. (2007, January). Pore Network Modeling: A new Technology for SCAL predictions and interpretations. In SPE Saudi Arabia Section Technical Symposium. Society of Petroleum Engineers.

Sun, H., Vega, S., & Tao, G. (2017). Analysis of heterogeneity and permeability anisotropy in carbonate rock samples using digital rock physics. Journal of Petroleum Science and Engineering, 156, 419-429.

Sun, X., Sun, S. Z., Jiang, S., Yang, H., Luo, C., & Pan, W. (2013, March). Application of Probabilistic Neural Network on Complex Carbonate Reservoir Prediction. In IPTC 2013: International Petroleum Technology Conference (pp. cp-350). European Association of Geoscientists & Engineers.

Tiab, D. and Donaldson, E.C. (2015). Petrophysics: theory and practice of measuring reservoir rock and fluid transport properties. Gulf professional publishing.

Toikka, G. and Hayes, R.A. (1997). Direct measurement of colloidal forces between mica and silica in aqueous electrolyte. Journal of colloid and interface science, 191(1), pp.102-109.

Toksoz, M.N., Cheng, C.H., and Timur, A., (1976), Velocities of seismic waves in porous rocks: Geophysics, 41, 621-645.

Toqeer, M., Ali, A., Alves, T. M., Khan, A., & Hussain, M. (2021). Application of model based post-stack inversion in the characterization of reservoir sands containing porous, tight and mixed facies: A case study from the Central Indus Basin, Pakistan. Journal of Earth System Science, 130(2), 1-21.

Torskaya, T., Shabro, V., Torres-Verdín, C., Salazar-Tio, R., & Revil, A. (2014). Grain shape effects on permeability, formation factor, and capillary pressure from pore-scale modeling. Transport in porous media, 102(1), 71-90.

Tuğrul, A. and Zarif, I.H. (1999). Correlation of mineralogical and textural characteristics with engineering properties of selected granitic rocks from Turkey. Engineering geology, 51(4), pp.303-317.

Ulusay, R., Türeli, K. and Ider, M.H. (1994). Prediction of engineering properties of a selected litharenite sandstone from its petrographic characteristics using correlation and multivariate statistical techniques. Engineering Geology, 38(1-2), pp.135-157.

Ündül, Ö. (2016). Assessment of mineralogical and petrographic factors affecting petro-physical properties, strength and cracking processes of volcanic rocks. Engineering geology, 210, pp.10-22.

Vanorio, T., Scotellaro, C., & Mavko, G. (2008). The effect of chemical and physical processes on the acoustic properties of carbonate rocks. The Leading Edge, 27(8), 1040-1048.

Velis, D. R. (2008). Stochastic sparse-spike deconvolution. Geophysics, 73(1), R1-R9.

Vernik, L. (1994). Predicting lithology and transport properties from acoustic velocities based on petrophysical classification of siliciclastics. Geophysics, 59(3), 420-427.

Vernik, L., Bruno, M., & Bovberg, C. (1993, December). Empirical relations between compressive strength and porosity of siliciclastic rocks. In International journal of rock mechanics and mining sciences & geomechanics abstracts (Vol. 30, No. 7, pp. 677-680). Pergamon.

Vilhelm, J., Ivankina, T., Lokají, T., and Rudajev, V. (2016), Comparison of laboratory and field measurements of P and S wave velocities of a periodite rock, International Journal of Rock Mechanics & Mining Sciences, 88:235-241.

Walpole, L. J. (1966). On bounds for the overall elastic moduli of inhomogeneous systems—I. Journal of the Mechanics and Physics of Solids, 14(3), 151-162.

Walton, W. H. (1948). Feret's statistical diameter as a measure of particle size. Nature, 162(4113), 329-330.

Wandrey, C. J. (2004a). Bombay geologic province Eocene to Miocene composite total petroleum system, India (Vol. 2208). US Department of the Interior, US Geological Survey.

Wandrey, C. J. (2004b). Sylhet-Kopili/Barail-Tipam composite total petroleum system, Assam geologic province, India. US Department of the Interior, US Geological Survey.

Wang, H., Sun, S. Z., Yang, H., Gao, H., Xiao, Y., & Hu, H. (2011). The influence of pore structure on P-& S-wave velocities in complex carbonate reservoirs with secondary storage space. Petroleum Science, 8(4), 394-405.

Wang, Q., & Ji, S. (2009). Poisson's ratios of crystalline rocks as a function of hydrostatic confining pressure. Journal of Geophysical Research: Solid Earth, 114(B9).

Wang, Q., Ji, S., Sun, S., & Marcotte, D. (2009). Correlations between compressional and shear wave velocities and corresponding Poisson's ratios for some common rocks and sulfide ores. Tectonophysics, 469(1-4), 61-72.

Wang, X., Sain, K., Satyavani, N., Wang, J., Ojha, M., & Wu, S. (2013). Gas hydrates saturation using geostatistical inversion in a fractured reservoir in the Krishna–Godavari basin, offshore eastern India. Marine and Petroleum Geology, 45, 224-235.

Ward, C. R., Taylor, J. C., & Cohen, D. R. (1999). Quantitative mineralogy of sandstones by X-ray diffractometry and normative analysis. Journal of Sedimentary Research, 69(5), 1050-1062.

Weger, R. J., Eberli, G. P., Baechle, G. T., Massaferro, J. L., & Sun, Y. F. (2009). Quantification of pore structure and its effect on sonic velocity and permeability in carbonates. AAPG bulletin, 93(10), 1297-1317.

Wei M, Xiong Y, Zhang L, Li J (2016). The effect of sample particle size on the determination of pore structure parameters in shales. International Journal of Coal Geology, 163, 177-185.

Wen, L., quan Luo, Z., jiao Yang, S., guang Qin, Y., & Wang, W. (2019). Correlation of geo-mechanics parameters with uniaxial compressive strength and P-wave velocity on dolomitic limestone using a statistical method. Geotechnical and Geological Engineering, 37(2), 1079-1094.

White, R. E., & Simm, R. (2003). Tutorial: Good practice in well ties. first break, 21(10).

Wildenschild, D., & Sheppard, A. P. (2013). X-ray imaging and analysis techniques for quantifying pore-scale structure and processes in subsurface porous medium systems. Advances in Water Resources, 51, 217-246.

Wydiabhakti, T. (2012, November). Mapping The Distribution of Gas Hydrates Using Coloured Inversion and Rock Physics Modeling in Blake Ridges, USA. In First EAGE Integrated Reservoir Modelling Conference-Are we doing it right? (pp. cp-323). European Association of Geoscientists & Engineers.

Wyllie, M. R. J., Gregory, A. R., & Gardner, L. W. (1956). Elastic wave velocities in heterogeneous and porous media. Geophysics, 21(1), 41-70.

Xu, S., & Payne, M. A. (2009). Modeling elastic properties in carbonate rocks. The Leading Edge, 28(1), 66-74.

Yagiz, S. (2011). P-wave velocity test for assessment of geotechnical properties of some rock materials. Bulletin of Materials Science, 34(4), 947.

Yale, D. P. (1985). Recent advances in rock physics. Geophysics, 50(12), 2480-2491.

Yale, D.P., & Jamieson, W.H. (1994). Static and dynamic mechanical properties of carbonates, American Rock Mechanics Association.

Yasar, E., & Erdogan, Y. (2004). Correlating sound velocity with the density, compressive strength and Young's modulus of carbonate rocks. International Journal of Rock Mechanics and Mining Sciences, 41(5), 871-875.

Yasin, Q., Du, Q., Sohail, G. M., & Ismail, A. (2018). Fracturing index-based brittleness prediction from geophysical logging data: application to Longmaxi shale. Geomechanics and Geophysics for Geo-Energy and Geo-Resources, 4(4), 301-325.

Yasin, Q., Sohail, G. M., Ding, Y., Ismail, A., & Du, Q. (2020). Estimation of petrophysical parameters from seismic inversion by combining particle swarm optimization and multilayer linear calculator. Natural Resources Research, 29(5), 3291-3317.

Yilmaz, I., & Yuksek, G. (2009). Prediction of the strength and elasticity modulus of gypsum using multiple regression, ANN, and ANFIS models. International journal of rock mechanics and mining sciences (1997), 46(4), 803-810.

Yilmaz, Ö. (2001). Seismic data analysis: Processing, inversion, and interpretation of seismic data. Society of exploration geophysicists.

Yong, H., Xinghe, Y., Shengli, L. I., Gongyang, C., Yanli, Z. H. O. U., & Zhaopu, G. A. O. (2014). Improving the accuracy of geological model by using seismic forward and inverse techniques. Petroleum Exploration and Development, 41(2), 208-216.

Yu C, Ji S, Li Q (2016). Effects of porosity on seismic velocities, elastic moduli and Poisson's ratios of solid materials and rocks. Journal of Rock Mechanics and Geotechnical Engineering, 8(1), 35-49.

Zaei, M. E., & Rao, K. S. (2019, December). Characterisation of Tipam Sandstone from Digboi Oil Field, Upper Assam, India. Paper presented at Indian Geotechnical Conference (IGC 2019), Surat, India. Retrieved from http://www.igs.org.in:8080/portal/igc-proceedings/igc-2019-surat-proceedings/TH11/TH11-38.pdf

Zargari S, Canter KL, Prasad M (2015). Porosity evolution in oil-prone source rocks. Fuel, 153, 110-117.

Zhang, B., Yang, Y., Pan, Y., Wu, H., & Cao, D. (2020b). Seismic well tie by aligning impedance log with inverted impedance from seismic data. Interpretation, 8(4), T917-T925.

Zhang, J., Xingyao, Y. I. N., Zhang, G., Yipeng, G. U., & Xianggang, F. A. N. (2020a). Prediction method of physical parameters based on linearized rock physics inversion. Petroleum Exploration and Development, 47(1), 59-67.

Zhang, S., Huang, H., Li, H., Wang, G., Dong, Y., & Luo, Y. (2017). Prestack seismic facies-controlled joint inversion of reservoir elastic and petrophysical parameters for sweet spot prediction. Energy Exploration & Exploitation, 35(6), 767-791.

Zou Y, Malzbender J (2016). Development and optimization of porosity measurement techniques. Ceramics international, 42(2), 2861-2870.

# Annexure

Table S1: Range of datasets of E and $V_p$ obtained by varying the volume percentage of major minerals for sandstones and carbonates, with a porosity variation from 2% to 40% for different geological scenarios (fluid saturations - water, gas, brine and oil saturated)

Water Saturated Sandstone

| Fraction of Quartz | Fraction of feldspar | Porosity (fraction) | Lower Bound K (GPa) | Upper Bound K (GPa) | Lower Bound G (GPa) | Upper Bound G (GPa) | Vp (km/s) | Lower Bound E (GPa) | Upper Bound E (GPa) |
|---|---|---|---|---|---|---|---|---|---|
| 0.7 | 0.3 | 0.02 | 28.1917 | 36.0616 | 0 | 31.3823 | 5.34839 | 0 | 72.9775 |
| 0.7 | 0.3 | 0.05 | 20.7038 | 34.4754 | 0 | 29.7131 | 4.95892 | 0 | 69.2458 |
| 0.7 | 0.3 | 0.1 | 14.3510 | 31.9465 | 0 | 27.0975 | 4.42222 | 0 | 63.3741 |
| 0.7 | 0.3 | 0.15 | 10.9814 | 29.5513 | 0 | 24.6703 | 3.99034 | 0 | 57.8989 |
| 0.7 | 0.3 | 0.2 | 8.8933 | 27.2795 | 0 | 22.4118 | 3.63532 | 0 | 52.7811 |
| 0.7 | 0.3 | 0.25 | 7.4724 | 25.1217 | 0 | 20.3051 | 3.33830 | 0 | 47.9867 |
| 0.7 | 0.3 | 0.3 | 6.4430 | 23.0696 | 0 | 18.3354 | 3.08616 | 0 | 43.4856 |
| 0.7 | 0.3 | 0.35 | 5.6629 | 21.1157 | 0 | 16.4897 | 2.86942 | 0 | 39.2516 |
| 0.7 | 0.3 | 0.4 | 5.0513 | 19.2530 | 0 | 14.7567 | 2.68114 | 0 | 35.2612 |
| 0.75 | 0.25 | 0.02 | 28.1777 | 36.0377 | 0 | 32.9836 | 5.40893 | 0 | 75.8195 |
| 0.75 | 0.25 | 0.05 | 20.6965 | 34.4530 | 0 | 31.1922 | 5.00932 | 0 | 71.8832 |
| 0.75 | 0.25 | 0.1 | 14.3477 | 31.9264 | 0 | 28.3935 | 4.46012 | 0 | 65.7030 |
| 0.75 | 0.25 | 0.15 | 10.9796 | 29.5333 | 0 | 25.8058 | 4.01945 | 0 | 59.9547 |
| 0.75 | 0.25 | 0.2 | 8.8922 | 27.2634 | 0 | 23.4059 | 3.65803 | 0 | 54.5944 |
| 0.75 | 0.25 | 0.25 | 7.4717 | 25.1074 | 0 | 21.1742 | 3.35625 | 0 | 49.5839 |
| 0.75 | 0.25 | 0.3 | 6.4425 | 23.0569 | 0 | 19.0936 | 3.10046 | 0 | 44.8897 |
| 0.75 | 0.25 | 0.35 | 5.6625 | 21.1044 | 0 | 17.1493 | 2.88090 | 0 | 40.4826 |
| 0.75 | 0.25 | 0.4 | 5.0510 | 19.2431 | 0 | 15.3282 | 2.69038 | 0 | 36.3366 |
| 0.8 | 0.2 | 0.02 | 28.1636 | 36.0138 | 0 | 34.6581 | 5.46936 | 0 | 78.7215 |

| | | | | | | | | | |
|---|---|---|---|---|---|---|---|---|---|
| 0.8 | 0.2 | 0.05 | 20.6892 | 34.4306 | 0 | 32.7351 | 5.05951 | 0 | 74.5720 |
| 0.8 | 0.2 | 0.1 | 14.3443 | 31.9063 | 0 | 29.7404 | 4.49776 | 0 | 68.0711 |
| 0.8 | 0.2 | 0.15 | 10.9777 | 29.5153 | 0 | 26.9817 | 4.04829 | 0 | 62.0401 |
| 0.8 | 0.2 | 0.2 | 8.8910 | 27.2473 | 0 | 24.4320 | 3.68048 | 0 | 56.4297 |
| 0.8 | 0.2 | 0.25 | 7.4709 | 25.0931 | 0 | 22.0686 | 3.37395 | 0 | 51.1971 |
| 0.8 | 0.2 | 0.3 | 6.4420 | 23.0442 | 0 | 19.8717 | 3.11455 | 0 | 46.3051 |
| 0.8 | 0.2 | 0.35 | 5.6621 | 21.0932 | 0 | 17.8244 | 2.89219 | 0 | 41.7212 |
| 0.8 | 0.2 | 0.4 | 5.0507 | 19.2332 | 0 | 15.9118 | 2.69946 | 0 | 37.4168 |
| 0.85 | 0.15 | 0.02 | 28.1496 | 35.9900 | 0 | 36.4109 | 5.52969 | 0 | 81.6856 |
| 0.85 | 0.15 | 0.05 | 20.6818 | 34.4082 | 0 | 34.3461 | 5.10950 | 0 | 77.3136 |
| 0.85 | 0.15 | 0.1 | 14.3410 | 31.8863 | 0 | 31.1411 | 4.53513 | 0 | 70.4793 |
| 0.85 | 0.15 | 0.15 | 10.9759 | 29.4974 | 0 | 28.2001 | 4.07684 | 0 | 64.1557 |
| 0.85 | 0.15 | 0.2 | 8.8899 | 27.2313 | 0 | 25.4917 | 3.70268 | 0 | 58.2873 |
| 0.85 | 0.15 | 0.25 | 7.4702 | 25.0788 | 0 | 22.9894 | 3.39142 | 0 | 52.8264 |
| 0.85 | 0.15 | 0.3 | 6.4414 | 23.0315 | 0 | 20.6705 | 3.12843 | 0 | 47.7319 |
| 0.85 | 0.15 | 0.35 | 5.6618 | 21.0820 | 0 | 18.5155 | 2.90330 | 0 | 42.9675 |
| 0.85 | 0.15 | 0.4 | 5.0505 | 19.2233 | 0 | 16.5077 | 2.70839 | 0 | 38.5020 |
| 0.9 | 0.1 | 0.02 | 28.1357 | 35.9661 | 0 | 38.2476 | 5.58992 | 0 | 84.7137 |
| 0.9 | 0.1 | 0.05 | 20.6745 | 34.3859 | 0 | 36.0297 | 5.15929 | 0 | 80.1094 |
| 0.9 | 0.1 | 0.1 | 14.3376 | 31.8662 | 0 | 32.5991 | 4.57223 | 0 | 72.9286 |
| 0.9 | 0.1 | 0.15 | 10.9740 | 29.4794 | 0 | 29.4636 | 4.10512 | 0 | 66.3020 |
| 0.9 | 0.1 | 0.2 | 8.8887 | 27.2153 | 0 | 26.5868 | 3.72461 | 0 | 60.1676 |
| 0.9 | 0.1 | 0.25 | 7.4694 | 25.0645 | 0 | 23.9378 | 3.40866 | 0 | 54.4722 |
| 0.9 | 0.1 | 0.3 | 6.4409 | 23.0188 | 0 | 21.4907 | 3.14211 | 0 | 49.1702 |
| 0.9 | 0.1 | 0.35 | 5.6614 | 21.0707 | 0 | 19.2232 | 2.91423 | 0 | 44.2216 |
| 0.9 | 0.1 | 0.4 | 5.0502 | 19.2134 | 0 | 17.1163 | 2.71717 | 0 | 39.5921 |
| 0.95 | 0.05 | 0.02 | 28.1217 | 35.9423 | 0 | 40.1745 | 5.65004 | 0 | 87.8078 |

| | | | | | | | | | |
|---|---|---|---|---|---|---|---|---|---|
| 0.95 | 0.05 | 0.05 | 20.6672 | 34.3635 | 0 | 37.7911 | 5.20888 | 0 | 82.9612 |
| 0.95 | 0.05 | 0.1 | 14.3343 | 31.8462 | 0 | 34.1178 | 4.60907 | 0 | 75.4201 |
| 0.95 | 0.05 | 0.15 | 10.9722 | 29.4615 | 0 | 30.7745 | 4.13314 | 0 | 68.4797 |
| 0.95 | 0.05 | 0.2 | 8.8876 | 27.1992 | 0 | 27.7188 | 3.74629 | 0 | 62.0709 |
| 0.95 | 0.05 | 0.25 | 7.4686 | 25.0502 | 0 | 24.9151 | 3.42567 | 0 | 56.1346 |
| 0.95 | 0.05 | 0.3 | 6.4404 | 23.0061 | 0 | 22.3333 | 3.15559 | 0 | 50.6201 |
| 0.95 | 0.05 | 0.35 | 5.6610 | 21.0595 | 0 | 19.9483 | 2.92499 | 0 | 45.4836 |
| 0.95 | 0.05 | 0.4 | 5.0499 | 19.2035 | 0 | 17.7382 | 2.72580 | 0 | 40.6871 |
| 1 | 0 | 0.02 | 28.1077 | 35.9184 | 0 | 42.1983 | 5.71006 | 0 | 90.9700 |
| 1 | 0 | 0.05 | 20.6599 | 34.3412 | 0 | 39.6357 | 5.25827 | 0 | 85.8706 |
| 1 | 0 | 0.1 | 14.3310 | 31.8262 | 0 | 35.7011 | 4.64565 | 0 | 77.9547 |
| 1 | 0 | 0.15 | 10.9704 | 29.4436 | 0 | 32.1357 | 4.16088 | 0 | 70.6895 |
| 1 | 0 | 0.2 | 8.8865 | 27.1832 | 0 | 28.8899 | 3.76773 | 0 | 63.9977 |
| 1 | 0 | 0.25 | 7.4679 | 25.0359 | 0 | 25.9225 | 3.44246 | 0 | 57.8139 |
| 1 | 0 | 0.3 | 6.4399 | 22.9935 | 0 | 23.1993 | 3.16888 | 0 | 52.0818 |
| 1 | 0 | 0.35 | 5.6606 | 21.0483 | 0 | 20.6911 | 2.93559 | 0 | 46.7534 |
| 1 | 0 | 0.4 | 5.0496 | 19.1936 | 0 | 18.3737 | 2.73429 | 0 | 41.7870 |

Water Saturated Carbonate

| **Fraction of Calcite** | **Fraction of Dolomite** | **Porosity (fraction)** | **Lower Bound K (GPa)** | **Upper Bound K (GPa)** | **Lower Bound G (GPa)** | **Upper Bound G (GPa)** | **Total Vp (km/s)** | **Lower Bound E (GPa)** | **Upper Bound E (GPa)** |
|---|---|---|---|---|---|---|---|---|---|
| 0.7 | 0.3 | 0.02 | 45.7219 | 72.8447 | 0 | 35.4526 | 6.05954 | 0 | 91.5119 |
| 0.7 | 0.3 | 0.05 | 28.4766 | 67.5330 | 0 | 33.7102 | 5.54369 | 0 | 86.7039 |
| 0.7 | 0.3 | 0.1 | 17.4851 | 59.6885 | 0 | 30.9496 | 4.85486 | 0 | 79.1658 |
| 0.7 | 0.3 | 0.15 | 12.6156 | 52.8866 | 0 | 28.3544 | 4.31830 | 0 | 72.1663 |

| | | | | | | | | | |
|---|---|---|---|---|---|---|---|---|---|
| 0.7 | 0.3 | 0.2 | 9.8676 | 46.9324 | 0 | 25.9102 | 3.88853 | 0 | 65.6495 |
| 0.7 | 0.3 | 0.25 | 8.1026 | 41.6767 | 0 | 23.6042 | 3.53656 | 0 | 59.5671 |
| 0.7 | 0.3 | 0.3 | 6.8732 | 37.0034 | 0 | 21.4250 | 3.24302 | 0 | 53.8768 |
| 0.7 | 0.3 | 0.35 | 5.9677 | 32.8209 | 0 | 19.3624 | 2.99448 | 0 | 48.5416 |
| 0.7 | 0.3 | 0.4 | 5.2731 | 29.0555 | 0 | 17.4073 | 2.78132 | 0 | 43.5290 |
| 0.75 | 0.25 | 0.02 | 45.7289 | 72.8631 | 0 | 34.6797 | 6.03060 | 0 | 89.7931 |
| 0.75 | 0.25 | 0.05 | 28.4793 | 67.5492 | 0 | 32.9889 | 5.52020 | 0 | 85.1116 |
| 0.75 | 0.25 | 0.1 | 17.4860 | 59.7018 | 0 | 30.3075 | 4.83778 | 0 | 77.7635 |
| 0.75 | 0.25 | 0.15 | 12.6161 | 52.8975 | 0 | 27.7834 | 4.30553 | 0 | 70.9317 |
| 0.75 | 0.25 | 0.2 | 9.8678 | 46.9414 | 0 | 25.4033 | 3.87878 | 0 | 64.5634 |
| 0.75 | 0.25 | 0.25 | 8.1028 | 41.6842 | 0 | 23.1552 | 3.52900 | 0 | 58.6127 |
| 0.75 | 0.25 | 0.3 | 6.8733 | 37.0097 | 0 | 21.0285 | 3.23709 | 0 | 53.0398 |
| 0.75 | 0.25 | 0.35 | 5.9678 | 32.8261 | 0 | 19.0134 | 2.98978 | 0 | 47.8096 |
| 0.75 | 0.25 | 0.4 | 5.2731 | 29.0599 | 0 | 17.1016 | 2.77757 | 0 | 42.8910 |
| 0.8 | 0.2 | 0.02 | 45.7358 | 72.8815 | 0 | 33.9197 | 6.00164 | 0 | 88.0927 |
| 0.8 | 0.2 | 0.05 | 28.4819 | 67.5655 | 0 | 32.2793 | 5.49666 | 0 | 83.5349 |
| 0.8 | 0.2 | 0.1 | 17.4869 | 59.7150 | 0 | 29.6748 | 4.82064 | 0 | 76.3734 |
| 0.8 | 0.2 | 0.15 | 12.6165 | 52.9084 | 0 | 27.2201 | 4.29270 | 0 | 69.7062 |
| 0.8 | 0.2 | 0.2 | 9.8681 | 46.9505 | 0 | 24.9027 | 3.86898 | 0 | 63.4840 |
| 0.8 | 0.2 | 0.25 | 8.1029 | 41.6917 | 0 | 22.7113 | 3.52139 | 0 | 57.6633 |
| 0.8 | 0.2 | 0.3 | 6.8734 | 37.0159 | 0 | 20.6360 | 3.23111 | 0 | 52.2064 |

| | | | | | | | | | |
|---|---|---|---|---|---|---|---|---|---|
| 0.8 | 0.2 | 0.35 | 5.9679 | 32.8313 | 0 | 18.6677 | 2.98504 | 0 | 47.0800 |
| 0.8 | 0.2 | 0.4 | 5.2732 | 29.0642 | 0 | 16.7984 | 2.77380 | 0 | 42.2546 |
| 0.85 | 0.15 | 0.02 | 45.7428 | 72.8999 | 0 | 33.1724 | 5.97265 | 0 | 86.4105 |
| 0.85 | 0.15 | 0.05 | 28.4845 | 67.5817 | 0 | 31.5809 | 5.47308 | 0 | 81.9739 |
| 0.85 | 0.15 | 0.1 | 17.4879 | 59.7283 | 0 | 29.0513 | 4.80345 | 0 | 74.9951 |
| 0.85 | 0.15 | 0.15 | 12.6170 | 52.9194 | 0 | 26.6644 | 4.27981 | 0 | 68.4898 |
| 0.85 | 0.15 | 0.2 | 9.8684 | 46.9595 | 0 | 24.4082 | 3.85912 | 0 | 62.4113 |
| 0.85 | 0.15 | 0.25 | 8.1031 | 41.6992 | 0 | 22.2723 | 3.51373 | 0 | 56.7188 |
| 0.85 | 0.15 | 0.3 | 6.8735 | 37.0222 | 0 | 20.2475 | 3.22509 | 0 | 51.3765 |
| 0.85 | 0.15 | 0.35 | 5.9680 | 32.8365 | 0 | 18.3252 | 2.98027 | 0 | 46.3528 |
| 0.85 | 0.15 | 0.4 | 5.2732 | 29.0685 | 0 | 16.4978 | 2.77000 | 0 | 41.6197 |
| 0.9 | 0.1 | 0.02 | 45.7498 | 72.9183 | 0 | 32.4375 | 5.94364 | 0 | 84.7462 |
| 0.9 | 0.1 | 0.05 | 28.4872 | 67.5979 | 0 | 30.8935 | 5.44945 | 0 | 80.4281 |
| 0.9 | 0.1 | 0.1 | 17.4888 | 59.7416 | 0 | 28.4370 | 4.78619 | 0 | 73.6285 |
| 0.9 | 0.1 | 0.15 | 12.6174 | 52.9303 | 0 | 26.1160 | 4.26687 | 0 | 67.2822 |
| 0.9 | 0.1 | 0.2 | 9.8686 | 46.9685 | 0 | 23.9197 | 3.84921 | 0 | 61.3453 |
| 0.9 | 0.1 | 0.25 | 8.1033 | 41.7067 | 0 | 21.8383 | 3.50603 | 0 | 55.7792 |
| 0.9 | 0.1 | 0.3 | 6.8737 | 37.0284 | 0 | 19.8629 | 3.21903 | 0 | 50.5501 |
| 0.9 | 0.1 | 0.35 | 5.9681 | 32.8417 | 0 | 17.9858 | 2.97546 | 0 | 45.6280 |
| 0.9 | 0.1 | 0.4 | 5.2733 | 29.0729 | 0 | 16.1997 | 2.76616 | 0 | 40.9864 |
| 0.95 | 0.05 | 0.02 | 45.7568 | 72.9367 | 0 | 31.7147 | 5.91460 | 0 | 83.0994 |

| | | | | | | | | | |
|---|---|---|---|---|---|---|---|---|---|
| 0.95 | 0.05 | 0.05 | 28.4898 | 67.6142 | 0 | 30.2168 | 5.42577 | 0 | 78.8974 |
| 0.95 | 0.05 | 0.1 | 17.4897 | 59.7548 | 0 | 27.8314 | 4.76888 | 0 | 72.2735 |
| 0.95 | 0.05 | 0.15 | 12.6179 | 52.9412 | 0 | 25.5749 | 4.25386 | 0 | 66.0835 |
| 0.95 | 0.05 | 0.2 | 9.8689 | 46.9776 | 0 | 23.4372 | 3.83925 | 0 | 60.2859 |
| 0.95 | 0.05 | 0.25 | 8.1034 | 41.7142 | 0 | 21.4090 | 3.49827 | 0 | 54.8444 |
| 0.95 | 0.05 | 0.3 | 6.8738 | 37.0347 | 0 | 19.4823 | 3.21293 | 0 | 49.7271 |
| 0.95 | 0.05 | 0.35 | 5.9681 | 32.8469 | 0 | 17.6495 | 2.97062 | 0 | 44.9055 |
| 0.95 | 0.05 | 0.4 | 5.2734 | 29.0772 | 0 | 15.9040 | 2.76230 | 0 | 40.3546 |
| 1 | 0 | 0.02 | 45.7638 | 72.9551 | 0 | 31.0036 | 5.88554 | 0 | 81.4700 |
| 1 | 0 | 0.05 | 28.4924 | 67.6304 | 0 | 29.5507 | 5.40205 | 0 | 77.3816 |
| 1 | 0 | 0.1 | 17.4907 | 59.7681 | 0 | 27.2345 | 4.75151 | 0 | 70.9300 |
| 1 | 0 | 0.15 | 12.6184 | 52.9521 | 0 | 25.0409 | 4.24080 | 0 | 64.8935 |
| 1 | 0 | 0.2 | 9.8692 | 46.9866 | 0 | 22.9604 | 3.82923 | 0 | 59.2330 |
| 1 | 0 | 0.25 | 8.1036 | 41.7218 | 0 | 20.9845 | 3.49047 | 0 | 53.9145 |
| 1 | 0 | 0.3 | 6.8739 | 37.0409 | 0 | 19.1054 | 3.20678 | 0 | 48.9075 |
| 1 | 0 | 0.35 | 5.9682 | 32.8521 | 0 | 17.3163 | 2.96574 | 0 | 44.1854 |
| 1 | 0 | 0.4 | 5.2734 | 29.0816 | 0 | 15.6107 | 2.75840 | 0 | 39.7243 |

Gas Saturated Sandstone

| **Fraction of Quartz** | **Fraction of feldspar** | **Porosity (fraction)** | **Lower Bound K (GPa)** | **Upper Bound K (GPa)** | **Lower Bound G (GPa)** | **Upper Bound G (GPa)** | **Total Vp (km/s)** | **Lower Bound E (GPa)** | **Upper Bound E (GPa)** |
|---|---|---|---|---|---|---|---|---|---|
| 0.7 | 0.3 | 0.02 | 4.4173 | 35.9564 | 0 | 31.3823 | 4.8316 | 0 | 72.9295 |

| | | | | | | | | | |
|---|---|---|---|---|---|---|---|---|---|
| 0.7 | 0.3 | 0.05 | 1.9027 | 34.2214 | 0 | 29.7131 | 3.9737 | 0 | 69.1313 |
| 0.7 | 0.3 | 0.1 | 0.9763 | 31.4670 | 0 | 27.0975 | 3.0663 | 0 | 63.1620 |
| 0.7 | 0.3 | 0.15 | 0.6567 | 28.8712 | 0 | 24.6703 | 2.4962 | 0 | 57.6035 |
| 0.7 | 0.3 | 0.2 | 0.4947 | 26.4208 | 0 | 22.4118 | 2.1049 | 0 | 52.4149 |
| 0.7 | 0.3 | 0.25 | 0.3968 | 24.1038 | 0 | 20.3051 | 1.8197 | 0 | 47.5604 |
| 0.7 | 0.3 | 0.3 | 0.3313 | 21.9096 | 0 | 18.3354 | 1.6025 | 0 | 43.0087 |
| 0.7 | 0.3 | 0.35 | 0.2843 | 19.8288 | 0 | 16.4897 | 1.4316 | 0 | 38.7325 |
| 0.7 | 0.3 | 0.4 | 0.2490 | 17.8528 | 0 | 14.7567 | 1.2937 | 0 | 34.7073 |
| 0.75 | 0.25 | 0.02 | 4.4170 | 35.9325 | 0 | 32.9836 | 4.8809 | 0 | 75.7676 |
| 0.75 | 0.25 | 0.05 | 1.9026 | 34.1991 | 0 | 31.1922 | 4.0060 | 0 | 71.7598 |
| 0.75 | 0.25 | 0.1 | 0.9763 | 31.4471 | 0 | 28.3935 | 3.0844 | 0 | 65.4749 |
| 0.75 | 0.25 | 0.15 | 0.6566 | 28.8535 | 0 | 25.8058 | 2.5076 | 0 | 59.6378 |
| 0.75 | 0.25 | 0.2 | 0.4947 | 26.4050 | 0 | 23.4059 | 2.1125 | 0 | 54.2024 |
| 0.75 | 0.25 | 0.25 | 0.3968 | 24.0898 | 0 | 21.1742 | 1.8250 | 0 | 49.1285 |
| 0.75 | 0.25 | 0.3 | 0.3313 | 21.8973 | 0 | 19.0936 | 1.6063 | 0 | 44.3813 |
| 0.75 | 0.25 | 0.35 | 0.2843 | 19.8179 | 0 | 17.1493 | 1.4345 | 0 | 39.9301 |
| 0.75 | 0.25 | 0.4 | 0.2490 | 17.8432 | 0 | 15.3282 | 1.2958 | 0 | 35.7482 |
| 0.8 | 0.2 | 0.02 | 4.4167 | 35.9087 | 0 | 34.6581 | 4.9301 | 0 | 78.6656 |
| 0.8 | 0.2 | 0.05 | 1.9026 | 34.1769 | 0 | 32.7351 | 4.0380 | 0 | 74.4390 |
| 0.8 | 0.2 | 0.1 | 0.9763 | 31.4273 | 0 | 29.7404 | 3.1024 | 0 | 67.8260 |
| 0.8 | 0.2 | 0.15 | 0.6566 | 28.8358 | 0 | 26.9817 | 2.5188 | 0 | 61.7006 |
| 0.8 | 0.2 | 0.2 | 0.4947 | 26.3893 | 0 | 24.4320 | 2.1200 | 0 | 56.0106 |
| 0.8 | 0.2 | 0.25 | 0.3968 | 24.0759 | 0 | 22.0686 | 1.8302 | 0 | 50.7114 |
| 0.8 | 0.2 | 0.3 | 0.3312 | 21.8850 | 0 | 19.8717 | 1.6101 | 0 | 45.7638 |
| 0.8 | 0.2 | 0.35 | 0.2843 | 19.8071 | 0 | 17.8244 | 1.4373 | 0 | 41.1342 |
| 0.8 | 0.2 | 0.4 | 0.2490 | 17.8337 | 0 | 15.9118 | 1.2980 | 0 | 36.7927 |
| 0.85 | 0.15 | 0.02 | 4.4163 | 35.8849 | 0 | 36.4109 | 4.9790 | 0 | 81.6253 |

| | | | | | | | | | |
|---|---|---|---|---|---|---|---|---|---|
| 0.85 | 0.15 | 0.05 | 1.9025 | 34.1546 | 0 | 34.3461 | 4.0698 | 0 | 77.1705 |
| 0.85 | 0.15 | 0.1 | 0.9763 | 31.4074 | 0 | 31.1411 | 3.1201 | 0 | 70.2164 |
| 0.85 | 0.15 | 0.15 | 0.6566 | 28.8181 | 0 | 28.2001 | 2.5298 | 0 | 63.7923 |
| 0.85 | 0.15 | 0.2 | 0.4947 | 26.3736 | 0 | 25.4917 | 2.1273 | 0 | 57.8399 |
| 0.85 | 0.15 | 0.25 | 0.3968 | 24.0619 | 0 | 22.9894 | 1.8353 | 0 | 52.3091 |
| 0.85 | 0.15 | 0.3 | 0.3312 | 21.8726 | 0 | 20.6705 | 1.6138 | 0 | 47.1565 |
| 0.85 | 0.15 | 0.35 | 0.2843 | 19.7962 | 0 | 18.5155 | 1.4400 | 0 | 42.3447 |
| 0.85 | 0.15 | 0.4 | 0.2490 | 17.8241 | 0 | 16.5077 | 1.3000 | 0 | 37.8410 |
| 0.9 | 0.1 | 0.02 | 4.4160 | 35.8611 | 0 | 38.2476 | 5.0278 | 0 | 84.6488 |
| 0.9 | 0.1 | 0.05 | 1.9024 | 34.1324 | 0 | 36.0297 | 4.1013 | 0 | 79.9557 |
| 0.9 | 0.1 | 0.1 | 0.9763 | 31.3876 | 0 | 32.5991 | 3.1376 | 0 | 72.6469 |
| 0.9 | 0.1 | 0.15 | 0.6566 | 28.8005 | 0 | 29.4636 | 2.5407 | 0 | 65.9137 |
| 0.9 | 0.1 | 0.2 | 0.4947 | 26.3579 | 0 | 26.5868 | 2.1345 | 0 | 59.6906 |
| 0.9 | 0.1 | 0.25 | 0.3968 | 24.0480 | 0 | 23.9378 | 1.8404 | 0 | 53.9218 |
| 0.9 | 0.1 | 0.3 | 0.3312 | 21.8603 | 0 | 21.4907 | 1.6174 | 0 | 48.5593 |
| 0.9 | 0.1 | 0.35 | 0.2843 | 19.7853 | 0 | 19.2232 | 1.4427 | 0 | 43.5617 |
| 0.9 | 0.1 | 0.4 | 0.2490 | 17.8146 | 0 | 17.1163 | 1.3020 | 0 | 38.8929 |
| 0.95 | 0.05 | 0.02 | 4.4156 | 35.8373 | 0 | 40.1745 | 5.0764 | 0 | 87.7380 |
| 0.95 | 0.05 | 0.05 | 1.9024 | 34.1102 | 0 | 37.7911 | 4.1326 | 0 | 82.7963 |
| 0.95 | 0.05 | 0.1 | 0.9763 | 31.3677 | 0 | 34.1178 | 3.1549 | 0 | 75.1186 |
| 0.95 | 0.05 | 0.15 | 0.6566 | 28.7828 | 0 | 30.7745 | 2.5514 | 0 | 68.0652 |
| 0.95 | 0.05 | 0.2 | 0.4947 | 26.3422 | 0 | 27.7188 | 2.1416 | 0 | 61.5630 |
| 0.95 | 0.05 | 0.25 | 0.3968 | 24.0340 | 0 | 24.9151 | 1.8453 | 0 | 55.5498 |
| 0.95 | 0.05 | 0.3 | 0.3312 | 21.8479 | 0 | 22.3333 | 1.6210 | 0 | 49.9724 |
| 0.95 | 0.05 | 0.35 | 0.2843 | 19.7745 | 0 | 19.9483 | 1.4453 | 0 | 44.7852 |
| 0.95 | 0.05 | 0.4 | 0.2490 | 17.8051 | 0 | 17.7382 | 1.3040 | 0 | 39.9484 |
| 1 | 0 | 0.02 | 4.4153 | 35.8135 | 0 | 42.1983 | 5.1248 | 0 | 90.8950 |

| | | | | | | | | | |
|---|---|---|---|---|---|---|---|---|---|
| 1 | 0 | 0.05 | 1.9023 | 34.0879 | 0 | 39.6357 | 4.1636 | 0 | 85.6937 |
| 1 | 0 | 0.1 | 0.9763 | 31.3479 | 0 | 35.7011 | 3.1720 | 0 | 77.6323 |
| 1 | 0 | 0.15 | 0.6566 | 28.7651 | 0 | 32.1357 | 2.5619 | 0 | 70.2475 |
| 1 | 0 | 0.2 | 0.4947 | 26.3264 | 0 | 28.8899 | 2.1486 | 0 | 63.4575 |
| 1 | 0 | 0.25 | 0.3968 | 24.0201 | 0 | 25.9225 | 1.8502 | 0 | 57.1932 |
| 1 | 0 | 0.3 | 0.3312 | 21.8356 | 0 | 23.1993 | 1.6245 | 0 | 51.3959 |
| 1 | 0 | 0.35 | 0.2843 | 19.7636 | 0 | 20.6911 | 1.4479 | 0 | 46.0152 |
| 1 | 0 | 0.4 | 0.2490 | 17.7955 | 0 | 18.3737 | 1.3060 | 0 | 41.0077 |

Gas Saturated carbonate

| **Fraction of Calcite** | **Fraction of Dolomite** | **Porosity (fraction)** | **Lower Bound K (GPa)** | **Upper Bound K (GPa)** | **Lower Bound G (GPa)** | **Upper Bound G (GPa)** | **Total Vp (km/s)** | **Lower Bound E (GPa)** | **Upper Bound E (GPa)** |
|---|---|---|---|---|---|---|---|---|---|
| 0.7 | 0.3 | 0.02 | 4.4173 | 72.5534 | 0 | 35.4526 | 5.4046 | 0 | 91.4607 |
| 0.7 | 0.3 | 0.05 | 1.9027 | 66.8725 | 0 | 33.7102 | 4.3406 | 0 | 86.5819 |
| 0.7 | 0.3 | 0.1 | 0.9763 | 58.5546 | 0 | 30.9496 | 3.2682 | 0 | 78.9405 |
| 0.7 | 0.3 | 0.15 | 0.6567 | 51.4109 | 0 | 28.3544 | 2.6207 | 0 | 71.8535 |
| 0.7 | 0.3 | 0.2 | 0.4947 | 45.2090 | 0 | 25.9102 | 2.1874 | 0 | 65.2628 |
| 0.7 | 0.3 | 0.25 | 0.3968 | 39.7742 | 0 | 23.6042 | 1.8770 | 0 | 59.1180 |
| 0.7 | 0.3 | 0.3 | 0.3313 | 34.9725 | 0 | 21.4250 | 1.6438 | 0 | 53.3753 |
| 0.7 | 0.3 | 0.35 | 0.2843 | 30.6994 | 0 | 19.3624 | 1.4621 | 0 | 47.9965 |
| 0.7 | 0.3 | 0.4 | 0.2490 | 26.8721 | 0 | 17.4073 | 1.3166 | 0 | 42.9481 |
| 0.75 | 0.25 | 0.02 | 4.4170 | 72.5717 | 0 | 34.6797 | 5.3815 | 0 | 89.7438 |
| 0.75 | 0.25 | 0.05 | 1.9026 | 66.8885 | 0 | 32.9889 | 4.3261 | 0 | 84.9940 |
| 0.75 | 0.25 | 0.1 | 0.9763 | 58.5676 | 0 | 30.3075 | 3.2604 | 0 | 77.5462 |
| 0.75 | 0.25 | 0.15 | 0.6566 | 51.4214 | 0 | 27.7834 | 2.6160 | 0 | 70.6296 |
| 0.75 | 0.25 | 0.2 | 0.4947 | 45.2177 | 0 | 25.4033 | 2.1843 | 0 | 64.1894 |

| | | | | | | | | | |
|---|---|---|---|---|---|---|---|---|---|
| 0.75 | 0.25 | 0.25 | 0.3968 | 39.7814 | 0 | 23.1552 | 1.8749 | 0 | 58.1780 |
| 0.75 | 0.25 | 0.3 | 0.3313 | 34.9785 | 0 | 21.0285 | 1.6423 | 0 | 52.5539 |
| 0.75 | 0.25 | 0.35 | 0.2843 | 30.7043 | 0 | 19.0134 | 1.4610 | 0 | 47.2808 |
| 0.75 | 0.25 | 0.4 | 0.2490 | 26.8762 | 0 | 17.1016 | 1.3157 | 0 | 42.3270 |
| 0.8 | 0.2 | 0.02 | 4.4167 | 72.5900 | 0 | 33.9197 | 5.3584 | 0 | 88.0452 |
| 0.8 | 0.2 | 0.05 | 1.9026 | 66.9045 | 0 | 32.2793 | 4.3117 | 0 | 83.4217 |
| 0.8 | 0.2 | 0.1 | 0.9763 | 58.5806 | 0 | 29.6748 | 3.2527 | 0 | 76.1637 |
| 0.8 | 0.2 | 0.15 | 0.6566 | 51.4320 | 0 | 27.2201 | 2.6113 | 0 | 69.4146 |
| 0.8 | 0.2 | 0.2 | 0.4947 | 45.2264 | 0 | 24.9027 | 2.1812 | 0 | 63.1225 |
| 0.8 | 0.2 | 0.25 | 0.3968 | 39.7886 | 0 | 22.7113 | 1.8727 | 0 | 57.2426 |
| 0.8 | 0.2 | 0.3 | 0.3312 | 34.9844 | 0 | 20.6360 | 1.6407 | 0 | 51.7356 |
| 0.8 | 0.2 | 0.35 | 0.2843 | 30.7093 | 0 | 18.6677 | 1.4598 | 0 | 46.5673 |
| 0.8 | 0.2 | 0.4 | 0.2490 | 26.8803 | 0 | 16.7984 | 1.3149 | 0 | 41.7072 |
| 0.85 | 0.15 | 0.02 | 4.4163 | 72.6083 | 0 | 33.1724 | 5.3353 | 0 | 86.3648 |
| 0.85 | 0.15 | 0.05 | 1.9025 | 66.9206 | 0 | 31.5809 | 4.2971 | 0 | 81.8649 |
| 0.85 | 0.15 | 0.1 | 0.9763 | 58.5935 | 0 | 29.0513 | 3.2448 | 0 | 74.7930 |
| 0.85 | 0.15 | 0.15 | 0.6566 | 51.4426 | 0 | 26.6644 | 2.6065 | 0 | 68.2082 |
| 0.85 | 0.15 | 0.2 | 0.4947 | 45.2350 | 0 | 24.4082 | 2.1780 | 0 | 62.0619 |
| 0.85 | 0.15 | 0.25 | 0.3968 | 39.7957 | 0 | 22.2723 | 1.8706 | 0 | 56.3118 |
| 0.85 | 0.15 | 0.3 | 0.3312 | 34.9903 | 0 | 20.2475 | 1.6392 | 0 | 50.9206 |
| 0.85 | 0.15 | 0.35 | 0.2843 | 30.7142 | 0 | 18.3252 | 1.4587 | 0 | 45.8558 |
| 0.85 | 0.15 | 0.4 | 0.2490 | 26.8844 | 0 | 16.4978 | 1.3140 | 0 | 41.0886 |
| 0.9 | 0.1 | 0.02 | 4.4160 | 72.6266 | 0 | 32.4375 | 5.3122 | 0 | 84.7022 |
| 0.9 | 0.1 | 0.05 | 1.9024 | 66.9366 | 0 | 30.8935 | 4.2826 | 0 | 80.3232 |
| 0.9 | 0.1 | 0.1 | 0.9763 | 58.6065 | 0 | 28.4370 | 3.2369 | 0 | 73.4337 |
| 0.9 | 0.1 | 0.15 | 0.6566 | 51.4532 | 0 | 26.1160 | 2.6017 | 0 | 67.0105 |
| 0.9 | 0.1 | 0.2 | 0.4947 | 45.2437 | 0 | 23.9197 | 2.1749 | 0 | 61.0078 |

| | | | | | | | | | |
|---|---|---|---|---|---|---|---|---|---|
| 0.9 | 0.1 | 0.25 | 0.3968 | 39.8029 | 0 | 21.8383 | 1.8684 | 0 | 55.3855 |
| 0.9 | 0.1 | 0.3 | 0.3312 | 34.9963 | 0 | 19.8629 | 1.6376 | 0 | 50.1087 |
| 0.9 | 0.1 | 0.35 | 0.2843 | 30.7191 | 0 | 17.9858 | 1.4576 | 0 | 45.1464 |
| 0.9 | 0.1 | 0.4 | 0.2490 | 26.8885 | 0 | 16.1997 | 1.3132 | 0 | 40.4713 |
| 0.95 | 0.05 | 0.02 | 4.4156 | 72.6449 | 0 | 31.7147 | 5.2890 | 0 | 83.0572 |
| 0.95 | 0.05 | 0.05 | 1.9024 | 66.9527 | 0 | 30.2168 | 4.2679 | 0 | 78.7965 |
| 0.95 | 0.05 | 0.1 | 0.9763 | 58.6195 | 0 | 27.8314 | 3.2290 | 0 | 72.0859 |
| 0.95 | 0.05 | 0.15 | 0.6566 | 51.4638 | 0 | 25.5749 | 2.5969 | 0 | 65.8214 |
| 0.95 | 0.05 | 0.2 | 0.4947 | 45.2524 | 0 | 23.4372 | 2.1717 | 0 | 59.9600 |
| 0.95 | 0.05 | 0.25 | 0.3968 | 39.8101 | 0 | 21.4090 | 1.8662 | 0 | 54.4639 |
| 0.95 | 0.05 | 0.3 | 0.3312 | 35.0022 | 0 | 19.4823 | 1.6360 | 0 | 49.3000 |
| 0.95 | 0.05 | 0.35 | 0.2843 | 30.7240 | 0 | 17.6495 | 1.4564 | 0 | 44.4391 |
| 0.95 | 0.05 | 0.4 | 0.2490 | 26.8925 | 0 | 15.9040 | 1.3123 | 0 | 39.8553 |
| 1 | 0 | 0.02 | 4.4153 | 72.6632 | 0 | 31.0036 | 5.2657 | 0 | 81.4294 |
| 1 | 0 | 0.05 | 1.9023 | 66.9687 | 0 | 29.5507 | 4.2532 | 0 | 77.2845 |
| 1 | 0 | 0.1 | 0.9763 | 58.6325 | 0 | 27.2345 | 3.2210 | 0 | 70.7493 |
| 1 | 0 | 0.15 | 0.6566 | 51.4744 | 0 | 25.0409 | 2.5920 | 0 | 64.6408 |
| 1 | 0 | 0.2 | 0.4947 | 45.2611 | 0 | 22.9604 | 2.1685 | 0 | 58.9184 |
| 1 | 0 | 0.25 | 0.3968 | 39.8172 | 0 | 20.9845 | 1.8640 | 0 | 53.5467 |
| 1 | 0 | 0.3 | 0.3312 | 35.0082 | 0 | 19.1054 | 1.6344 | 0 | 48.4944 |
| 1 | 0 | 0.35 | 0.2843 | 30.7289 | 0 | 17.3163 | 1.4552 | 0 | 43.7339 |
| 1 | 0 | 0.4 | 0.2490 | 26.8966 | 0 | 15.6107 | 1.3114 | 0 | 39.2405 |

Brine Saturated sandstone

| **Fraction of Quartz** | **Fraction of feldspar** | **Porosity (fraction)** | **Lower Bound K (GPa)** | **Upper Bound K (GPa)** | **Lower Bound G (GPa)** | **Upper Bound G (GPa)** | **Total Vp (km/s)** | **Lower Bound E (GPa)** | **Upper Bound E (GPa)** |
|---|---|---|---|---|---|---|---|---|---|

| | | | | | | | | | |
|---|---|---|---|---|---|---|---|---|---|
| 0.7 | 0.3 | 0.02 | 29.3489 | 36.0809 | 0 | 31.3823 | 5.3801 | 0 | 72.9863 |
| 0.7 | 0.3 | 0.05 | 22.3196 | 34.5219 | 0 | 29.7131 | 5.0275 | 0 | 69.2667 |
| 0.7 | 0.3 | 0.1 | 15.9519 | 32.0346 | 0 | 27.0975 | 4.5326 | 0 | 63.4126 |
| 0.7 | 0.3 | 0.15 | 12.4110 | 29.6767 | 0 | 24.6703 | 4.1263 | 0 | 57.9522 |
| 0.7 | 0.3 | 0.2 | 10.1566 | 27.4382 | 0 | 22.4118 | 3.7869 | 0 | 52.8468 |
| 0.7 | 0.3 | 0.25 | 8.5953 | 25.3104 | 0 | 20.3051 | 3.4990 | 0 | 48.0627 |
| 0.7 | 0.3 | 0.3 | 7.4500 | 23.2852 | 0 | 18.3354 | 3.2519 | 0 | 43.5701 |
| 0.7 | 0.3 | 0.35 | 6.5741 | 21.3554 | 0 | 16.4897 | 3.0373 | 0 | 39.3428 |
| 0.7 | 0.3 | 0.4 | 5.8824 | 19.5143 | 0 | 14.7567 | 2.8493 | 0 | 35.3576 |
| 0.75 | 0.25 | 0.02 | 29.3337 | 36.0570 | 0 | 32.9836 | 5.4413 | 0 | 75.8289 |
| 0.75 | 0.25 | 0.05 | 22.3110 | 34.4995 | 0 | 31.1922 | 5.0793 | 0 | 71.9057 |
| 0.75 | 0.25 | 0.1 | 15.9477 | 32.0145 | 0 | 28.3935 | 4.5724 | 0 | 65.7444 |
| 0.75 | 0.25 | 0.15 | 12.4087 | 29.6587 | 0 | 25.8058 | 4.1574 | 0 | 60.0120 |
| 0.75 | 0.25 | 0.2 | 10.1551 | 27.4221 | 0 | 23.4059 | 3.8115 | 0 | 54.6648 |
| 0.75 | 0.25 | 0.25 | 8.5943 | 25.2960 | 0 | 21.1742 | 3.5188 | 0 | 49.6651 |
| 0.75 | 0.25 | 0.3 | 7.4493 | 23.2724 | 0 | 19.0936 | 3.2678 | 0 | 44.9798 |
| 0.75 | 0.25 | 0.35 | 6.5736 | 21.3441 | 0 | 17.1493 | 3.0502 | 0 | 40.5797 |
| 0.75 | 0.25 | 0.4 | 5.8821 | 19.5044 | 0 | 15.3282 | 2.8598 | 0 | 36.4390 |
| 0.8 | 0.2 | 0.02 | 29.3185 | 36.0331 | 0 | 34.6581 | 5.5025 | 0 | 78.7317 |
| 0.8 | 0.2 | 0.05 | 22.3025 | 34.4771 | 0 | 32.7351 | 5.1310 | 0 | 74.5962 |
| 0.8 | 0.2 | 0.1 | 15.9436 | 31.9944 | 0 | 29.7404 | 4.6119 | 0 | 68.1156 |
| 0.8 | 0.2 | 0.15 | 12.4063 | 29.6406 | 0 | 26.9817 | 4.1883 | 0 | 62.1015 |
| 0.8 | 0.2 | 0.2 | 10.1536 | 27.4060 | 0 | 24.4320 | 3.8359 | 0 | 56.5050 |
| 0.8 | 0.2 | 0.25 | 8.5933 | 25.2816 | 0 | 22.0686 | 3.5382 | 0 | 51.2838 |
| 0.8 | 0.2 | 0.3 | 7.4486 | 23.2596 | 0 | 19.8717 | 3.2834 | 0 | 46.4010 |
| 0.8 | 0.2 | 0.35 | 6.5731 | 21.3328 | 0 | 17.8244 | 3.0629 | 0 | 41.8244 |
| 0.8 | 0.2 | 0.4 | 5.8817 | 19.4944 | 0 | 15.9118 | 2.8701 | 0 | 37.5255 |

| | | | | | | | | | |
|---|---|---|---|---|---|---|---|---|---|
| 0.85 | 0.15 | 0.02 | 29.3033 | 36.0092 | 0 | 36.4109 | 5.5636 | 0 | 81.6966 |
| 0.85 | 0.15 | 0.05 | 22.2940 | 34.4547 | 0 | 34.3461 | 5.1824 | 0 | 77.3396 |
| 0.85 | 0.15 | 0.1 | 15.9395 | 31.9743 | 0 | 31.1411 | 4.6512 | 0 | 70.5270 |
| 0.85 | 0.15 | 0.15 | 12.4040 | 29.6226 | 0 | 28.2001 | 4.2189 | 0 | 64.2213 |
| 0.85 | 0.15 | 0.2 | 10.1521 | 27.3899 | 0 | 25.4917 | 3.8600 | 0 | 58.3677 |
| 0.85 | 0.15 | 0.25 | 8.5923 | 25.2673 | 0 | 22.9894 | 3.5574 | 0 | 52.9188 |
| 0.85 | 0.15 | 0.3 | 7.4479 | 23.2469 | 0 | 20.6705 | 3.2989 | 0 | 47.8339 |
| 0.85 | 0.15 | 0.35 | 6.5726 | 21.3214 | 0 | 18.5155 | 3.0753 | 0 | 43.0771 |
| 0.85 | 0.15 | 0.4 | 5.8813 | 19.4845 | 0 | 16.5077 | 2.8801 | 0 | 38.6172 |
| 0.9 | 0.1 | 0.02 | 29.2882 | 35.9853 | 0 | 38.2476 | 5.6245 | 0 | 84.7255 |
| 0.9 | 0.1 | 0.05 | 22.2855 | 34.4323 | 0 | 36.0297 | 5.2336 | 0 | 80.1374 |
| 0.9 | 0.1 | 0.1 | 15.9354 | 31.9542 | 0 | 32.5991 | 4.6903 | 0 | 72.9797 |
| 0.9 | 0.1 | 0.15 | 12.4016 | 29.6046 | 0 | 29.4636 | 4.2492 | 0 | 66.3721 |
| 0.9 | 0.1 | 0.2 | 10.1506 | 27.3738 | 0 | 26.5868 | 3.8839 | 0 | 60.2533 |
| 0.9 | 0.1 | 0.25 | 8.5913 | 25.2529 | 0 | 23.9378 | 3.5764 | 0 | 54.5705 |
| 0.9 | 0.1 | 0.3 | 7.4472 | 23.2341 | 0 | 21.4907 | 3.3141 | 0 | 49.2785 |
| 0.9 | 0.1 | 0.35 | 6.5720 | 21.3101 | 0 | 19.2232 | 3.0876 | 0 | 44.3378 |
| 0.9 | 0.1 | 0.4 | 5.8809 | 19.4745 | 0 | 17.1163 | 2.8901 | 0 | 39.7140 |
| 0.95 | 0.05 | 0.02 | 29.2730 | 35.9615 | 0 | 40.1745 | 5.6854 | 0 | 87.8205 |
| 0.95 | 0.05 | 0.05 | 22.2770 | 34.4100 | 0 | 37.7911 | 5.2846 | 0 | 82.9913 |
| 0.95 | 0.05 | 0.1 | 15.9313 | 31.9341 | 0 | 34.1178 | 4.7291 | 0 | 75.4748 |
| 0.95 | 0.05 | 0.15 | 12.3993 | 29.5866 | 0 | 30.7745 | 4.2792 | 0 | 68.5546 |
| 0.95 | 0.05 | 0.2 | 10.1492 | 27.3577 | 0 | 27.7188 | 3.9075 | 0 | 62.1622 |
| 0.95 | 0.05 | 0.25 | 8.5903 | 25.2386 | 0 | 24.9151 | 3.5951 | 0 | 56.2391 |
| 0.95 | 0.05 | 0.3 | 7.4465 | 23.2214 | 0 | 22.3333 | 3.3291 | 0 | 50.7350 |
| 0.95 | 0.05 | 0.35 | 6.5715 | 21.2989 | 0 | 19.9483 | 3.0997 | 0 | 45.6066 |
| 0.95 | 0.05 | 0.4 | 5.8806 | 19.4645 | 0 | 17.7382 | 2.8998 | 0 | 40.8159 |

| | | | | | | | | | |
|---|---|---|---|---|---|---|---|---|---|
| 1 | 0 | 0.02 | 29.2579 | 35.9376 | 0 | 42.1983 | 5.7462 | 0 | 90.9836 |
| 1 | 0 | 0.05 | 22.2685 | 34.3876 | 0 | 39.6357 | 5.3355 | 0 | 85.9028 |
| 1 | 0 | 0.1 | 15.9272 | 31.9141 | 0 | 35.7011 | 4.7676 | 0 | 78.0131 |
| 1 | 0 | 0.15 | 12.3969 | 29.5686 | 0 | 32.1357 | 4.3089 | 0 | 70.7693 |
| 1 | 0 | 0.2 | 10.1477 | 27.3416 | 0 | 28.8899 | 3.9308 | 0 | 64.0949 |
| 1 | 0 | 0.25 | 8.5893 | 25.2242 | 0 | 25.9225 | 3.6136 | 0 | 57.9248 |
| 1 | 0 | 0.3 | 7.4458 | 23.2086 | 0 | 23.1993 | 3.3439 | 0 | 52.2036 |
| 1 | 0 | 0.35 | 6.5710 | 21.2876 | 0 | 20.6911 | 3.1116 | 0 | 46.8835 |
| 1 | 0 | 0.4 | 5.8802 | 19.4546 | 0 | 18.3737 | 2.9095 | 0 | 41.9231 |

Brine Saturated Carbonate

| **Fraction of Calcite** | **Fraction of Dolomite** | **Porosity (fraction)** | **Lower Bound K (GPa)** | **Upper Bound K (GPa)** | **Lower Bound G (GPa)** | **Upper Bound G (GPa)** | **Total Vp (km/s)** | **Lower Bound E (GPa)** | **Upper Bound E (GPa)** |
|---|---|---|---|---|---|---|---|---|---|
| 0.7 | 0.3 | 0.02 | 29.3489 | 72.8973 | 0 | 35.4526 | 6.1002 | 0 | 91.5211 |
| 0.7 | 0.3 | 0.05 | 22.3196 | 67.6527 | 0 | 33.7102 | 5.6296 | 0 | 86.7258 |
| 0.7 | 0.3 | 0.1 | 15.9519 | 59.8953 | 0 | 30.9496 | 4.9882 | 0 | 79.2061 |
| 0.7 | 0.3 | 0.15 | 12.4110 | 53.1571 | 0 | 28.3544 | 4.4780 | 0 | 72.2220 |
| 0.7 | 0.3 | 0.2 | 10.1566 | 47.2497 | 0 | 25.9102 | 4.0624 | 0 | 65.7181 |
| 0.7 | 0.3 | 0.25 | 8.5953 | 42.0284 | 0 | 23.6042 | 3.7175 | 0 | 59.6464 |
| 0.7 | 0.3 | 0.3 | 7.4500 | 37.3803 | 0 | 21.4250 | 3.4265 | 0 | 53.9648 |
| 0.7 | 0.3 | 0.35 | 6.5741 | 33.2157 | 0 | 19.3624 | 3.1778 | 0 | 48.6366 |
| 0.7 | 0.3 | 0.4 | 5.8824 | 29.4631 | 0 | 17.4073 | 2.9628 | 0 | 43.6294 |
| 0.75 | 0.25 | 0.02 | 29.3337 | 72.9157 | 0 | 34.6797 | 6.0709 | 0 | 89.8020 |
| 0.75 | 0.25 | 0.05 | 22.3110 | 67.6690 | 0 | 32.9889 | 5.6054 | 0 | 85.1327 |
| 0.75 | 0.25 | 0.1 | 15.9477 | 59.9086 | 0 | 30.3075 | 4.9701 | 0 | 77.8024 |
| 0.75 | 0.25 | 0.15 | 12.4087 | 53.1681 | 0 | 27.7834 | 4.4642 | 0 | 70.9855 |

| | | | | | | | | | |
|---|---|---|---|---|---|---|---|---|---|
| 0.75 | 0.25 | 0.2 | 10.1551 | 47.2588 | 0 | 25.4033 | 4.0518 | 0 | 64.6297 |
| 0.75 | 0.25 | 0.25 | 8.5943 | 42.0360 | 0 | 23.1552 | 3.7091 | 0 | 58.6895 |
| 0.75 | 0.25 | 0.3 | 7.4493 | 37.3866 | 0 | 21.0285 | 3.4199 | 0 | 53.1251 |
| 0.75 | 0.25 | 0.35 | 6.5736 | 33.2210 | 0 | 19.0134 | 3.1725 | 0 | 47.9017 |
| 0.75 | 0.25 | 0.4 | 5.8821 | 29.4675 | 0 | 17.1016 | 2.9585 | 0 | 42.9885 |
| 0.8 | 0.2 | 0.02 | 29.3185 | 72.9341 | 0 | 33.9197 | 6.0416 | 0 | 88.1013 |
| 0.8 | 0.2 | 0.05 | 22.3025 | 67.6853 | 0 | 32.2793 | 5.5811 | 0 | 83.5553 |
| 0.8 | 0.2 | 0.1 | 15.9436 | 59.9219 | 0 | 29.6748 | 4.9520 | 0 | 76.4108 |
| 0.8 | 0.2 | 0.15 | 12.4063 | 53.1791 | 0 | 27.2201 | 4.4504 | 0 | 69.7582 |
| 0.8 | 0.2 | 0.2 | 10.1536 | 47.2679 | 0 | 24.9027 | 4.0411 | 0 | 63.5481 |
| 0.8 | 0.2 | 0.25 | 8.5933 | 42.0436 | 0 | 22.7113 | 3.7007 | 0 | 57.7376 |
| 0.8 | 0.2 | 0.3 | 7.4486 | 37.3929 | 0 | 20.6360 | 3.4132 | 0 | 52.2890 |
| 0.8 | 0.2 | 0.35 | 6.5731 | 33.2262 | 0 | 18.6677 | 3.1672 | 0 | 47.1693 |
| 0.8 | 0.2 | 0.4 | 5.8817 | 29.4718 | 0 | 16.7984 | 2.9542 | 0 | 42.3492 |
| 0.85 | 0.15 | 0.02 | 29.3033 | 72.9525 | 0 | 33.1724 | 6.0122 | 0 | 86.4187 |
| 0.85 | 0.15 | 0.05 | 22.2940 | 67.7015 | 0 | 31.5809 | 5.5568 | 0 | 81.9934 |
| 0.85 | 0.15 | 0.1 | 15.9395 | 59.9352 | 0 | 29.0513 | 4.9339 | 0 | 75.0312 |
| 0.85 | 0.15 | 0.15 | 12.4040 | 53.1900 | 0 | 26.6644 | 4.4366 | 0 | 68.5399 |
| 0.85 | 0.15 | 0.2 | 10.1521 | 47.2770 | 0 | 24.4082 | 4.0304 | 0 | 62.4733 |
| 0.85 | 0.15 | 0.25 | 8.5923 | 42.0511 | 0 | 22.2723 | 3.6923 | 0 | 56.7907 |
| 0.85 | 0.15 | 0.3 | 7.4479 | 37.3992 | 0 | 20.2475 | 3.4065 | 0 | 51.4565 |
| 0.85 | 0.15 | 0.35 | 6.5726 | 33.2315 | 0 | 18.3252 | 3.1618 | 0 | 46.4394 |
| 0.85 | 0.15 | 0.4 | 5.8813 | 29.4762 | 0 | 16.4978 | 2.9499 | 0 | 41.7115 |
| 0.9 | 0.1 | 0.02 | 29.2882 | 72.9709 | 0 | 32.4375 | 5.9828 | 0 | 84.7541 |
| 0.9 | 0.1 | 0.05 | 22.2855 | 67.7178 | 0 | 30.8935 | 5.5324 | 0 | 80.4469 |
| 0.9 | 0.1 | 0.1 | 15.9354 | 59.9485 | 0 | 28.4370 | 4.9157 | 0 | 73.6633 |
| 0.9 | 0.1 | 0.15 | 12.4016 | 53.2010 | 0 | 26.1160 | 4.4227 | 0 | 67.3306 |

| | | | | | | | | | |
|---|---|---|---|---|---|---|---|---|---|
| 0.9 | 0.1 | 0.2 | 10.1506 | 47.2861 | 0 | 23.9197 | 4.0195 | 0 | 61.4052 |
| 0.9 | 0.1 | 0.25 | 8.5913 | 42.0587 | 0 | 21.8383 | 3.6838 | 0 | 55.8487 |
| 0.9 | 0.1 | 0.3 | 7.4472 | 37.4055 | 0 | 19.8629 | 3.3998 | 0 | 50.6275 |
| 0.9 | 0.1 | 0.35 | 6.5720 | 33.2368 | 0 | 17.9858 | 3.1564 | 0 | 45.7118 |
| 0.9 | 0.1 | 0.4 | 5.8809 | 29.4806 | 0 | 16.1997 | 2.9456 | 0 | 41.0753 |
| 0.95 | 0.05 | 0.02 | 29.2730 | 72.9894 | 0 | 31.7147 | 5.9534 | 0 | 83.1070 |
| 0.95 | 0.05 | 0.05 | 22.2770 | 67.7341 | 0 | 30.2168 | 5.5080 | 0 | 78.9155 |
| 0.95 | 0.05 | 0.1 | 15.9313 | 59.9619 | 0 | 27.8314 | 4.8974 | 0 | 72.3071 |
| 0.95 | 0.05 | 0.15 | 12.3993 | 53.2120 | 0 | 25.5749 | 4.4087 | 0 | 66.1302 |
| 0.95 | 0.05 | 0.2 | 10.1492 | 47.2952 | 0 | 23.4372 | 4.0087 | 0 | 60.3437 |
| 0.95 | 0.05 | 0.25 | 8.5903 | 42.0663 | 0 | 21.4090 | 3.6752 | 0 | 54.9116 |
| 0.95 | 0.05 | 0.3 | 7.4465 | 37.4118 | 0 | 19.4823 | 3.3929 | 0 | 49.8020 |
| 0.95 | 0.05 | 0.35 | 6.5715 | 33.2420 | 0 | 17.6495 | 3.1510 | 0 | 44.9867 |
| 0.95 | 0.05 | 0.4 | 5.8806 | 29.4850 | 0 | 15.9040 | 2.9412 | 0 | 40.4408 |
| 1 | 0 | 0.02 | 29.2579 | 73.0078 | 0 | 31.0036 | 5.9239 | 0 | 81.4773 |
| 1 | 0 | 0.05 | 22.2685 | 67.7504 | 0 | 29.5507 | 5.4836 | 0 | 77.3990 |
| 1 | 0 | 0.1 | 15.9272 | 59.9752 | 0 | 27.2345 | 4.8791 | 0 | 70.9623 |
| 1 | 0 | 0.15 | 12.3969 | 53.2230 | 0 | 25.0409 | 4.3947 | 0 | 64.9385 |
| 1 | 0 | 0.2 | 10.1477 | 47.3043 | 0 | 22.9604 | 3.9978 | 0 | 59.2888 |
| 1 | 0 | 0.25 | 8.5893 | 42.0739 | 0 | 20.9845 | 3.6666 | 0 | 53.9793 |
| 1 | 0 | 0.3 | 7.4458 | 37.4181 | 0 | 19.1054 | 3.3861 | 0 | 48.9800 |
| 1 | 0 | 0.35 | 6.5710 | 33.2473 | 0 | 17.3163 | 3.1455 | 0 | 44.2641 |
| 1 | 0 | 0.4 | 5.8802 | 29.4894 | 0 | 15.6107 | 2.9368 | 0 | 39.8078 |

Oil Saturated Sandstone

| Fraction of Quartz | Fraction of feldspar | Porosity (fraction) | Lower Bound K (GPa) | Upper Bound K (GPa) | Lower Bound G (GPa) | Upper Bound G (GPa) | Total Vp (km/s) | Lower Bound E (GPa) | Upper Bound E (GPa) |
|---|---|---|---|---|---|---|---|---|---|
| 0.7 | 0.3 | 0.02 | 22.4405 | 36.0074 | 0 | 31.3823 | 5.2547 | 0 | 72.9528 |
| 0.7 | 0.3 | 0.05 | 14.0791 | 34.3444 | 0 | 29.7131 | 4.7621 | 0 | 69.1869 |
| 0.7 | 0.3 | 0.1 | 8.6854 | 31.6989 | 0 | 27.0975 | 4.1187 | 0 | 63.2652 |
| 0.7 | 0.3 | 0.15 | 6.2796 | 29.1997 | 0 | 24.6703 | 3.6284 | 0 | 57.7475 |
| 0.7 | 0.3 | 0.2 | 4.9175 | 26.8350 | 0 | 22.4118 | 3.2424 | 0 | 52.5938 |
| 0.7 | 0.3 | 0.25 | 4.0410 | 24.5943 | 0 | 20.3051 | 2.9307 | 0 | 47.7693 |
| 0.7 | 0.3 | 0.3 | 3.4297 | 22.4680 | 0 | 18.3354 | 2.6736 | 0 | 43.2431 |
| 0.7 | 0.3 | 0.35 | 2.9790 | 20.4477 | 0 | 16.4897 | 2.4580 | 0 | 38.9886 |
| 0.7 | 0.3 | 0.4 | 2.6330 | 18.5255 | 0 | 14.7567 | 2.2746 | 0 | 34.9817 |
| 0.75 | 0.25 | 0.02 | 22.4316 | 35.9835 | 0 | 32.9836 | 5.3131 | 0 | 75.7928 |
| 0.75 | 0.25 | 0.05 | 14.0757 | 34.3221 | 0 | 31.1922 | 4.8086 | 0 | 71.8197 |
| 0.75 | 0.25 | 0.1 | 8.6841 | 31.6789 | 0 | 28.3935 | 4.1515 | 0 | 65.5859 |
| 0.75 | 0.25 | 0.15 | 6.2790 | 29.1819 | 0 | 25.8058 | 3.6524 | 0 | 59.7923 |
| 0.75 | 0.25 | 0.2 | 4.9172 | 26.8192 | 0 | 23.4059 | 3.2605 | 0 | 54.3939 |
| 0.75 | 0.25 | 0.25 | 4.0408 | 24.5802 | 0 | 21.1742 | 2.9445 | 0 | 49.3516 |
| 0.75 | 0.25 | 0.3 | 3.4296 | 22.4555 | 0 | 19.0936 | 2.6843 | 0 | 44.6311 |
| 0.75 | 0.25 | 0.35 | 2.9789 | 20.4366 | 0 | 17.1493 | 2.4664 | 0 | 40.2026 |
| 0.75 | 0.25 | 0.4 | 2.6330 | 18.5158 | 0 | 15.3282 | 2.2812 | 0 | 36.0396 |
| 0.8 | 0.2 | 0.02 | 22.4227 | 35.9596 | 0 | 34.6581 | 5.3714 | 0 | 78.6927 |
| 0.8 | 0.2 | 0.05 | 14.0723 | 34.2997 | 0 | 32.7351 | 4.8548 | 0 | 74.5036 |
| 0.8 | 0.2 | 0.1 | 8.6829 | 31.6590 | 0 | 29.7404 | 4.1841 | 0 | 67.9453 |
| 0.8 | 0.2 | 0.15 | 6.2784 | 29.1641 | 0 | 26.9817 | 3.6762 | 0 | 61.8661 |
| 0.8 | 0.2 | 0.2 | 4.9169 | 26.8033 | 0 | 24.4320 | 3.2783 | 0 | 56.2154 |
| 0.8 | 0.2 | 0.25 | 4.0406 | 24.5661 | 0 | 22.0686 | 2.9581 | 0 | 50.9493 |

| | | | | | | | | | |
|---|---|---|---|---|---|---|---|---|---|
| 0.8 | 0.2 | 0.3 | 3.4294 | 22.4430 | 0 | 19.8717 | 2.6949 | 0 | 46.0298 |
| 0.8 | 0.2 | 0.35 | 2.9788 | 20.4256 | 0 | 17.8244 | 2.4747 | 0 | 41.4236 |
| 0.8 | 0.2 | 0.4 | 2.6329 | 18.5060 | 0 | 15.9118 | 2.2877 | 0 | 37.1017 |
| 0.85 | 0.15 | 0.02 | 22.4138 | 35.9358 | 0 | 36.4109 | 5.4296 | 0 | 81.6546 |
| 0.85 | 0.15 | 0.05 | 14.0689 | 34.2774 | 0 | 34.3461 | 4.9008 | 0 | 77.2400 |
| 0.85 | 0.15 | 0.1 | 8.6817 | 31.6390 | 0 | 31.1411 | 4.2164 | 0 | 70.3443 |
| 0.85 | 0.15 | 0.15 | 6.2778 | 29.1462 | 0 | 28.2001 | 3.6998 | 0 | 63.9694 |
| 0.85 | 0.15 | 0.2 | 4.9165 | 26.7874 | 0 | 25.4917 | 3.2959 | 0 | 58.0585 |
| 0.85 | 0.15 | 0.25 | 4.0404 | 24.5520 | 0 | 22.9894 | 2.9715 | 0 | 52.5625 |
| 0.85 | 0.15 | 0.3 | 3.4293 | 22.4305 | 0 | 20.6705 | 2.7053 | 0 | 47.4391 |
| 0.85 | 0.15 | 0.35 | 2.9787 | 20.4145 | 0 | 18.5155 | 2.4828 | 0 | 42.6517 |
| 0.85 | 0.15 | 0.4 | 2.6328 | 18.4963 | 0 | 16.5077 | 2.2942 | 0 | 38.1682 |
| 0.9 | 0.1 | 0.02 | 22.4050 | 35.9120 | 0 | 38.2476 | 5.4877 | 0 | 84.6803 |
| 0.9 | 0.1 | 0.05 | 14.0655 | 34.2551 | 0 | 36.0297 | 4.9466 | 0 | 80.0304 |
| 0.9 | 0.1 | 0.1 | 8.6805 | 31.6191 | 0 | 32.5991 | 4.2485 | 0 | 72.7840 |
| 0.9 | 0.1 | 0.15 | 6.2772 | 29.1284 | 0 | 29.4636 | 3.7230 | 0 | 66.1029 |
| 0.9 | 0.1 | 0.2 | 4.9162 | 26.7715 | 0 | 26.5868 | 3.3133 | 0 | 59.9236 |
| 0.9 | 0.1 | 0.25 | 4.0401 | 24.5378 | 0 | 23.9378 | 2.9847 | 0 | 54.1914 |
| 0.9 | 0.1 | 0.3 | 3.4291 | 22.4180 | 0 | 21.4907 | 2.7155 | 0 | 48.8593 |
| 0.9 | 0.1 | 0.35 | 2.9786 | 20.4035 | 0 | 19.2232 | 2.4908 | 0 | 43.8870 |
| 0.9 | 0.1 | 0.4 | 2.6328 | 18.4866 | 0 | 17.1163 | 2.3005 | 0 | 39.2389 |
| 0.95 | 0.05 | 0.02 | 22.3961 | 35.8882 | 0 | 40.1745 | 5.5456 | 0 | 87.7718 |
| 0.95 | 0.05 | 0.05 | 14.0621 | 34.2328 | 0 | 37.7911 | 4.9922 | 0 | 82.8764 |
| 0.95 | 0.05 | 0.1 | 8.6793 | 31.5991 | 0 | 34.1178 | 4.2803 | 0 | 75.2652 |
| 0.95 | 0.05 | 0.15 | 6.2766 | 29.1106 | 0 | 30.7745 | 3.7461 | 0 | 68.2672 |
| 0.95 | 0.05 | 0.2 | 4.9158 | 26.7557 | 0 | 27.7188 | 3.3304 | 0 | 61.8111 |
| 0.95 | 0.05 | 0.25 | 4.0399 | 24.5237 | 0 | 24.9151 | 2.9978 | 0 | 55.8362 |

| | | | | | | | | | |
|---|---|---|---|---|---|---|---|---|---|
| 0.95 | 0.05 | 0.3 | 3.4290 | 22.4055 | 0 | 22.3333 | 2.7256 | 0 | 50.2905 |
| 0.95 | 0.05 | 0.35 | 2.9785 | 20.3924 | 0 | 19.9483 | 2.4987 | 0 | 45.1293 |
| 0.95 | 0.05 | 0.4 | 2.6327 | 18.4769 | 0 | 17.7382 | 2.3066 | 0 | 40.3139 |
| 1 | 0 | 0.02 | 22.3872 | 35.8644 | 0 | 42.1983 | 5.6034 | 0 | 90.9314 |
| 1 | 0 | 0.05 | 14.0587 | 34.2106 | 0 | 39.6357 | 5.0375 | 0 | 85.7796 |
| 1 | 0 | 0.1 | 8.6780 | 31.5792 | 0 | 35.7011 | 4.3118 | 0 | 77.7891 |
| 1 | 0 | 0.15 | 6.2760 | 29.0928 | 0 | 32.1357 | 3.7688 | 0 | 70.4629 |
| 1 | 0 | 0.2 | 4.9155 | 26.7398 | 0 | 28.8899 | 3.3473 | 0 | 63.7213 |
| 1 | 0 | 0.25 | 4.0397 | 24.5096 | 0 | 25.9225 | 3.0106 | 0 | 57.4971 |
| 1 | 0 | 0.3 | 3.4288 | 22.3930 | 0 | 23.1993 | 2.7355 | 0 | 51.7327 |
| 1 | 0 | 0.35 | 2.9784 | 20.3814 | 0 | 20.6911 | 2.5064 | 0 | 46.3789 |
| 1 | 0 | 0.4 | 2.6326 | 18.4672 | 0 | 18.3737 | 2.3127 | 0 | 41.3932 |

Oil Saturated Carbonate

| **Fraction of Calcite** | **Fraction of Dolomite** | **Porosity (fraction)** | **Lower Bound K (GPa)** | **Upper Bound K (GPa)** | **Lower Bound G (GPa)** | **Upper Bound G (GPa)** | **Total Vp (km/s)** | **Lower Bound E (GPa)** | **Upper Bound E (GPa)** |
|---|---|---|---|---|---|---|---|---|---|
| 0.7 | 0.3 | 0.02 | 22.4405 | 72.6954 | 0 | 35.4526 | 5.9396 | 0 | 91.4857 |
| 0.7 | 0.3 | 0.05 | 14.0791 | 67.1939 | 0 | 33.7102 | 5.2989 | 0 | 86.6416 |
| 0.7 | 0.3 | 0.1 | 8.6854 | 59.1050 | 0 | 30.9496 | 4.4914 | 0 | 79.0508 |
| 0.7 | 0.3 | 0.15 | 6.2796 | 52.1255 | 0 | 28.3544 | 3.8975 | 0 | 72.0069 |
| 0.7 | 0.3 | 0.2 | 4.9175 | 46.0419 | 0 | 25.9102 | 3.4423 | 0 | 65.4528 |
| 0.7 | 0.3 | 0.25 | 4.0410 | 40.6921 | 0 | 23.6042 | 3.0824 | 0 | 59.3391 |
| 0.7 | 0.3 | 0.3 | 3.4297 | 35.9508 | 0 | 21.4250 | 2.7905 | 0 | 53.6228 |
| 0.7 | 0.3 | 0.35 | 2.9790 | 31.7199 | 0 | 19.3624 | 2.5492 | 0 | 48.2663 |
| 0.7 | 0.3 | 0.4 | 2.6330 | 27.9211 | 0 | 17.4073 | 2.3463 | 0 | 43.2366 |
| 0.75 | 0.25 | 0.02 | 22.4316 | 72.7137 | 0 | 34.6797 | 5.9118 | 0 | 89.7679 |

| | | | | | | | | | |
|---|---|---|---|---|---|---|---|---|---|
| 0.75 | 0.25 | 0.05 | 14.0757 | 67.2100 | 0 | 32.9889 | 5.2774 | 0 | 85.0515 |
| 0.75 | 0.25 | 0.1 | 8.6841 | 59.1181 | 0 | 30.3075 | 4.4768 | 0 | 77.6526 |
| 0.75 | 0.25 | 0.15 | 6.2790 | 52.1363 | 0 | 27.7834 | 3.8871 | 0 | 70.7777 |
| 0.75 | 0.25 | 0.2 | 4.9172 | 46.0508 | 0 | 25.4033 | 3.4347 | 0 | 64.3731 |
| 0.75 | 0.25 | 0.25 | 4.0408 | 40.6994 | 0 | 23.1552 | 3.0766 | 0 | 58.3920 |
| 0.75 | 0.25 | 0.3 | 3.4296 | 35.9569 | 0 | 21.0285 | 2.7861 | 0 | 52.7937 |
| 0.75 | 0.25 | 0.35 | 2.9789 | 31.7250 | 0 | 19.0134 | 2.5458 | 0 | 47.5425 |
| 0.75 | 0.25 | 0.4 | 2.6330 | 27.9253 | 0 | 17.1016 | 2.3436 | 0 | 42.6071 |
| 0.8 | 0.2 | 0.02 | 22.4227 | 72.7321 | 0 | 33.9197 | 5.8839 | 0 | 88.0684 |
| 0.8 | 0.2 | 0.05 | 14.0723 | 67.2262 | 0 | 32.2793 | 5.2559 | 0 | 83.4771 |
| 0.8 | 0.2 | 0.1 | 8.6829 | 59.1312 | 0 | 29.6748 | 4.4621 | 0 | 76.2663 |
| 0.8 | 0.2 | 0.15 | 6.2784 | 52.1470 | 0 | 27.2201 | 3.8767 | 0 | 69.5576 |
| 0.8 | 0.2 | 0.2 | 4.9169 | 46.0596 | 0 | 24.9027 | 3.4270 | 0 | 63.3001 |
| 0.8 | 0.2 | 0.25 | 4.0406 | 40.7068 | 0 | 22.7113 | 3.0708 | 0 | 57.4497 |
| 0.8 | 0.2 | 0.3 | 3.4294 | 35.9630 | 0 | 20.6360 | 2.7817 | 0 | 51.9680 |
| 0.8 | 0.2 | 0.35 | 2.9788 | 31.7300 | 0 | 18.6677 | 2.5423 | 0 | 46.8211 |
| 0.8 | 0.2 | 0.4 | 2.6329 | 27.9295 | 0 | 16.7984 | 2.3409 | 0 | 41.9791 |
| 0.85 | 0.15 | 0.02 | 22.4138 | 72.7504 | 0 | 33.1724 | 5.8561 | 0 | 86.3871 |
| 0.85 | 0.15 | 0.05 | 14.0689 | 67.2423 | 0 | 31.5809 | 5.2343 | 0 | 81.9181 |
| 0.85 | 0.15 | 0.1 | 8.6817 | 59.1443 | 0 | 29.0513 | 4.4474 | 0 | 74.8919 |
| 0.85 | 0.15 | 0.15 | 6.2778 | 52.1578 | 0 | 26.6644 | 3.8662 | 0 | 68.3463 |
| 0.85 | 0.15 | 0.2 | 4.9165 | 46.0685 | 0 | 24.4082 | 3.4193 | 0 | 62.2336 |
| 0.85 | 0.15 | 0.25 | 4.0404 | 40.7141 | 0 | 22.2723 | 3.0650 | 0 | 56.5122 |
| 0.85 | 0.15 | 0.3 | 3.4293 | 35.9691 | 0 | 20.2475 | 2.7772 | 0 | 51.1456 |
| 0.85 | 0.15 | 0.35 | 2.9787 | 31.7351 | 0 | 18.3252 | 2.5389 | 0 | 46.1018 |
| 0.85 | 0.15 | 0.4 | 2.6328 | 27.9337 | 0 | 16.4978 | 2.3382 | 0 | 41.3524 |
| 0.9 | 0.1 | 0.02 | 22.4050 | 72.7688 | 0 | 32.4375 | 5.8282 | 0 | 84.7237 |

| | | | | | | | | | |
|---|---|---|---|---|---|---|---|---|---|
| 0.9 | 0.1 | 0.05 | 14.0655 | 67.2584 | 0 | 30.8935 | 5.2127 | 0 | 80.3745 |
| 0.9 | 0.1 | 0.1 | 8.6805 | 59.1574 | 0 | 28.4370 | 4.4326 | 0 | 73.5291 |
| 0.9 | 0.1 | 0.15 | 6.2772 | 52.1685 | 0 | 26.1160 | 3.8556 | 0 | 67.1438 |
| 0.9 | 0.1 | 0.2 | 4.9162 | 46.0773 | 0 | 23.9197 | 3.4115 | 0 | 61.1736 |
| 0.9 | 0.1 | 0.25 | 4.0401 | 40.7214 | 0 | 21.8383 | 3.0591 | 0 | 55.5794 |
| 0.9 | 0.1 | 0.3 | 3.4291 | 35.9752 | 0 | 19.8629 | 2.7728 | 0 | 50.3266 |
| 0.9 | 0.1 | 0.35 | 2.9786 | 31.7401 | 0 | 17.9858 | 2.5354 | 0 | 45.3848 |
| 0.9 | 0.1 | 0.4 | 2.6328 | 27.9379 | 0 | 16.1997 | 2.3355 | 0 | 40.7272 |
| 0.95 | 0.05 | 0.02 | 22.3961 | 72.7872 | 0 | 31.7147 | 5.8002 | 0 | 83.0778 |
| 0.95 | 0.05 | 0.05 | 14.0621 | 67.2746 | 0 | 30.2168 | 5.1911 | 0 | 78.8458 |
| 0.95 | 0.05 | 0.1 | 8.6793 | 59.1706 | 0 | 27.8314 | 4.4177 | 0 | 72.1778 |
| 0.95 | 0.05 | 0.15 | 6.2766 | 52.1793 | 0 | 25.5749 | 3.8450 | 0 | 65.9499 |
| 0.95 | 0.05 | 0.2 | 4.9158 | 46.0862 | 0 | 23.4372 | 3.4037 | 0 | 60.1201 |
| 0.95 | 0.05 | 0.25 | 4.0399 | 40.7288 | 0 | 21.4090 | 3.0532 | 0 | 54.6513 |
| 0.95 | 0.05 | 0.3 | 3.4290 | 35.9813 | 0 | 19.4823 | 2.7682 | 0 | 49.5108 |
| 0.95 | 0.05 | 0.35 | 2.9785 | 31.7452 | 0 | 17.6495 | 2.5319 | 0 | 44.6700 |
| 0.95 | 0.05 | 0.4 | 2.6327 | 27.9421 | 0 | 15.9040 | 2.3327 | 0 | 40.1033 |
| 1 | 0 | 0.02 | 22.3872 | 72.8055 | 0 | 31.0036 | 5.7723 | 0 | 81.4493 |
| 1 | 0 | 0.05 | 14.0587 | 67.2907 | 0 | 29.5507 | 5.1693 | 0 | 77.3320 |
| 1 | 0 | 0.1 | 8.6780 | 59.1837 | 0 | 27.2345 | 4.4028 | 0 | 70.8378 |
| 1 | 0 | 0.15 | 6.2760 | 52.1900 | 0 | 25.0409 | 3.8343 | 0 | 64.7647 |
| 1 | 0 | 0.2 | 4.9155 | 46.0951 | 0 | 22.9604 | 3.3958 | 0 | 59.0730 |
| 1 | 0 | 0.25 | 4.0397 | 40.7361 | 0 | 20.9845 | 3.0473 | 0 | 53.7278 |
| 1 | 0 | 0.3 | 3.4288 | 35.9874 | 0 | 19.1054 | 2.7637 | 0 | 48.6984 |
| 1 | 0 | 0.35 | 2.9784 | 31.7503 | 0 | 17.3163 | 2.5283 | 0 | 43.9575 |
| 1 | 0 | 0.4 | 2.6326 | 27.9463 | 0 | 15.6107 | 2.3299 | 0 | 39.4809 |